GRAPHENE QUANTUM DOT AND METAL NANOCLUSTER-BASED NANO FUNCTIONAL MATERIALS FOR ELECTROCHEMICAL SENSING APPLICATIONS

A Thesis submitted
in partial fulfillment for the Degree of

Doctor of Philosophy

by

SAISREE S.

Department of Chemistry

INDIAN INSTITUTE OF SPACE SCIENCE AND TECHNOLOGY

THIRUVANANTHAPURAM

February, 2023

This thesis is dedicated to my beloved,

Appa, Achan, Amma, Husband, and Brother,

for being my strong pillars of support for all the adventures in my life.

A special dedication goes to

my research supervisor

for her trust and care throughout my research life.

"PhD cannot be the cup of tea for all
But once you take your own tea pot,
You can definitely finish it off.
Do a small thing, enjoy each sip."

-Saisree S

CERTIFICATE

This is to certify that the thesis entitled **Graphene Quantum Dot and Metal Nanocluster-based Nano Functional Materials for Electrochemical Sensing Applications** submitted by **Saisree S** to the Indian Institute of Space Science and Technology, Thiruvananthapuram, in partial fulfillment of the degree of Doctor of Philosophy is a *bonafide* record of research work carried out by her under my supervision. The contents of this thesis, in full or in parts, have not been submitted to any other Institution or University for the award of any degree or diploma.

Prof. K.Y. Sandhya
Supervisor
Department of Chemistry
IIST

Thiruvananthapuram – 695547
February, 2023

Counter signature of HOD with seal

DECLARATION

I declare that this thesis entitled **Graphene Quantum Dot and Metal Nanocluster-based Nano Functional Materials for Electrochemical Sensing Applications** submitted in partial fulfillment of the degree of **Doctor of Philosophy** is a record of original work carried out by me under the supervision of Prof. K.Y. Sandhya and has not formed the basis for the award of any other degree or diploma, in this or any other Institution or University. In keeping with the ethical practice in reporting scientific information, due acknowledgments have been made wherever the findings of others have been cited.

Saisree S

SC16D029

Thiruvananthaouram-695547

February, 2023

ACKNOWLEDGEMENTS

This moment is the formal occasion to convey my unending gratitude to all the divine spirits behind the successful completion of my doctoral thesis. There were many moments we felt gratitude towards our loved ones for their constant support and selfless effort for our happiness and success, but expressing formal gratitude to your pillars of success may look like a masquerade, or rather no amount of words can truly convey my gratitude. Now, I take this opportunity to acknowledge everyone who stood with me throughout my life in one way or another and for the successful completion of one of my biggest dreams, doing scientific research in a prestigious institution.

First and foremost, I am extremely obliged to the Almighty for His love and blessings that give me the courage, strength, inspiration, confidence, sturdiness, stubbornness, opportunities, and all achievements in my life. While looking back, I am feeling very happy and satisfied in my life and luckiest to be a part of the Indian Institute of Space Science and Technology and the Department of Chemistry. The past six years of my doctoral research life have been a colorful story with mixed emotions of passion, enthusiasm, cheerfulness, misfortune, and forbearance, along with new/unexpected experiences and exciting achievements. I am very thankful for my research journey, which influenced me in many ways to shape me into a strong human being to persevere and complete the dream satisfactorily.

I am fully beholden and grateful to the person who made me acquire the most momentous educational achievement in my life, my research supervisor, my mentor, Prof. K.Y. Sandhya. It was her trust in me that brought out my research aptitude, and without her strong support, it wouldn't have happened. She has never degraded me and patiently tolerated all my excuses and shortcomings. There were times when I thought that my Ph.D. would remain an abandoned dream. But at last, this has turned out to be one of the best things I have achieved, and I would not be able to complete it within the stipulated time without the support, guidance, and love showered by her. She has opened the door of the fine fortune of working in a field of significant impact, devotedly and patiently, and thereby enriched me with a great sense of satisfaction and happiness to get hold of the knowledge and power of

critical reasoning via these years of my research endeavor. Her intelligent ideas, thought-provoking discussions, healthy criticisms, comprehensive understanding, scientific discernment, eternal enthusiasm, and imperishable hard work inspired and influenced me to establish the overall direction of my research, to move forward with investigations in depth, and to grow as an independent researcher and a noble individual at the end of this ride. Thank you, ma'am, for instilling the confidence in me to become a successful professional without compromising family obligations.

I thank Dr. V.K Dhadhwal, former Director of IIST, for his timely support, in overcoming the challenges that arise amidst the journey to continue my research life successfully. I also thank Dr. S. Somanath, Dr. D. Sam Dayala Dev, former Directors of IIST, and Dr. S. Unnikrishnan Nair, Director of IIST, for allowing me to accomplish my research work in the excellent ambiance of IIST with the adequate facilities provided. It is my profound privilege to express my extreme sense of gratefulness to Prof. Kuruvilla Joseph, Dean of Student Activities, for his care, motivation, and support. He has generously spent his busy time offering me valuable comments on improving my working environment. I express my sincere gratitude to Prof. Nirmala Rachel James and Prof. K. Prabhakaran, former HODs Chemistry, for providing a healthy working atmosphere. I am immensely gratified to my doctoral committee members, Dr. K. P. Prathish, Dr. R. S. Rajeev, Dr. Kuntala Bhattacharjee, Dr. K. Prabhakaran, and Dr. J. Mary Gladis, for their constructive criticism and valuable suggestions at various phases of this research program and for lending me their expertise and intuition to investigate my scientific and technical problems. I openly express gratitude towards all the Faculty members of the Department of Chemistry for their boundless support during these years. I sincerely thank all the Faculty members of other Departments of IIST for their assistance and support during the course of my study. I am taking this opportunity to thank all the efforts undertaken by my dear teachers for inculcating a passion for knowledge right from the primary school level across my academic life, which spans nearly twenty-five years. Their immense encouragement, motivation, and blessings helped me grow with determination and patience, which paid a lot for what I am today in my professional and personal life.

I got a very special opportunity to get my dear friend as my senior group member. Words fail me to express my sincerest thanks to my beloved senior, Dr. Arya Nair J. S, who has been a constant energy booster, vibrant gossip partner, and legitimate critic who has been

there in all my ups and downs. She helped me a lot in my harder times and cheered me up with exciting notions, stimulating discussions, and satisfactory remedies. We shared moments of deep anxiety, great accomplishment, and slapstick humour. We could develop more esprit de corps by being in the same research group. I am thankful to all my senior group members, Dr. Mohammed Mukthar Ali and Dr. Aswathi R, for their significant contribution in making this journey worth pursuing. When I am gratefully mentioning Dr. Aswathi for all her prompt support, special care, and encouragement, it wouldn't be complete without adding the name Dr. Reshma C. They both were there with me for everything. Their sisterly affection, valuable advice, and enjoyable moments mean a lot to me. I am incredibly thankful to the unfading help of all the senior research fellows of our Department, Dr. Roymon Joseph, Dr. Manjunath, Dr. Praveen Wilson, Dr. Meegle.S.Mathew, Dr.Devi Renuka, Dr. Lavanya J, and Dr. Sujith Vijayan, offering their valuable time and suggestions. I sincerely admire the companionship of Dr. Haritha H and B. D. S. Deeraj, and the joyful moments we had to have together. My research life has become more exciting and livelier by the love and support of my friends and fellow researchers, which filled the brighter shades of the journey. I am expressing my gratitude and love to Dr. Neema P. M, Dr. Yogesh Choudhary, Mrs. Sreekala K, Ms. Bhasha Sathyan, Ms. Ann Mary Tomy, Mr. Sanu Xavier, Mr. Govind Kumar Sharma, Mrs. Chitra K.S and Ms. Varsha M V. A very special thanks goes to Ms. Raji S, Mrs. Farha S and Mrs. Athira K. S for adding more fun-filled moments to the latter times of my hostel life in Anuradha. I am delighted to have very obedient and loving junior group members, Mrs. Dhrishya V, Ms. Archana V. S, Arya. S. Nair and Elsa Dais. I am extending my gratitude towards them and also to Mr. Jithu Joseph, Ms. S. Krishnendhu, Ms. Rhiya Paul, Mr. Gaurav Banerjee, and for their contribution towards the happier environment in the department and also thanking all other friends of IIST. I wish to express my gratitude to all the friends who accompanied me so far in the happiest journey of my life.

I am deeply indebted to all staff members of the Department of Chemistry, especially Mrs. Jayashree L, Mrs. Jayashree R, Mrs. Bindu Prajeesh, Mrs. Bindu P C, Mrs. Ramya, Mr. Loveson Albert, Mr. Sreekumaran Nair, Mr. Muraleedharan, Mrs. S.H. Adheena and Mrs. M. Nazeema for their support and help. I must acknowledge the support of much selfless personnel who performed various characterization techniques during my research. Special thanks to Mr. Vijayaraghavan, PSG college of engineering, Coimbatore, Mr. Satheesh,

Aerospace Dept., IIST, Dr. Saju Pillai CSIR-NIIST Thiruvananthapuram, staff at IISc Bangalore and staff at CUSAT-STIC for patiently doing the analysis till satisfactory results were obtained. I thank the editors and reviewers of my publications, as the comments and input from them enhanced the quality of my thesis. I am taking a moment to thank CISF staffs, Mr. Meeraj, Gym trainer, Warden 'Chechimar and Chettanmar', and the cleaning staffs of IIST for all their supports, love and care.

I don't really understand how to thank somebody who always defeats me with their love and care. Yes, my family. The wholehearted support, constant inspiration, love, and confidence from my family are the real thrive of my journey. The great blessings of my Grandparents are always there with me in each of my footsteps. My grandfathers, Mr. G. Madhavakurup and Mr. Narayanapillai; my grandmothers, Mrs. L. Gouriamma and Mrs. Karthikakuttyamma be the proudest about this success of mine. My father, Mr. Sadasivakurup N, my superhero, nurtured, cared and led me through a fruitful life. He always bestowed me enough freedom to choose my ways. Thank you so much, Acha, for trusting me this much. My mother, Mrs. K. Radhamani, the innocent angel, has always been there for me. Her care, love, compassion, hope, and prayers always showered upon me as a boon. Thank you Amma, for keeping me always safe in your hands. The motherly affection from my appa, Mrs. G. Sathy, paved another strong pillar for my successful journey. Her evocative pieces of advice, philosophical chit-chats, and adequate suggestions have been there for me at all times. My little brother, Mr. Saijith, my 'Jerry' pair, has continually been there, shoulder to shoulder for everything and taught me that teasing and irritating are other ways to show the affection. I feel he has some healing mantra to make me happy and calm forever. Thank you, Appa and brother, for your unfailing endless support.

Well, this acknowledgment wouldn't be complete without remembering a jovial person who came amidst my research journey to expand my lovely family. Mr. Vishnu M. R, the partner in crime, always amazed me with his unceasing support and boundless freedom poured over me. He is a good friend, a sincere criticizer, a cheerful chatterbox, a patient listener, and a noble adviser who always holds my hands. His heightened encouragement helped me a lot in completing my research work in a fast and better way. He came into my life at a stage when I was mentally challenged. From there onwards, he succeeded in keeping me sane and eternally happy. I owe you everything for being my better half. A pretty special word of thanks goes to my in-laws, whose heart-warming kindness, care, and patience

surfaced a smooth and steady path to my research journey. Especially, my father-in-law, Mr. Mohanan Nair M, and mother-in-law, Mrs. Remadevi L, for all the sacrifices they have made on my behalf during this long ride. I am very fortunate to enjoy the playtime company of Arunya R, S. Harshan, Akshitha A, Arundev R, Nivaan Vijay, S. Dhakshith, and Anudhya; at that time, I am in a paradise of joy. Thank you, little ones, for the stress-free times we had to have together and for going to explore further!

Thank you all…

Saisree S.

ABSTRACT

Electrochemistry, the chapter of chemistry that deals with the relations between electrical and chemical phenomena, have an ever-increasing impact on everybody's daily life. Out of the myriad applications of electrochemistry, considerable attention has been devoted to the fields of electrochemical (EC) sensing in recent decades. The emergence of nanotechnology as an indispensable tool for great advancement in science and technology has generated great capability of controlling materials at the nanometer scale and has enabled exciting opportunities to design materials with desirable electronic, ionic, photonic, and mechanical properties. This development has also contributed to developing and fabricating new structures and devices for EC sensing applications in recent years. In this scenario, this thesis work aims to address the challenges in the fields of EC sensing by the rational design of nano-functional materials using graphene quantum dots (GQD) and metal nanoclusters (MNC).

The on-site monitoring of various analyte species in the diversity of fields by EC sensor requires considerable improvements in sensitivity, selectivity, and accuracy along with its inherently fast, accurate, compact, portable, and cost-effective properties. Herein, we are trying to meet the aforementioned needs by developing various nano-functional materials based on GQD and MNC. The various steps involved in the study are preparing different types of GQD and MNC-based materials, their characterization, developing modified electrodes using the prepared materials, studying their EC sensing properties, and examining the reasons/mechanisms behind the effective sensing behaviors.

The sensing capability of nitrogen-doped graphene quantum dots (N-GQDs) was explored for the first time towards hazardous heavy metal ions and found to be selectively detecting cadmium ions (Cd(II)). Cd(II) is one of the hazardous heavy metal ions in the World Health Organization's list of 10 chemicals of major public concern. The aromatic N-GQDs, synthesized through a hydrothermal route using a single precursor polyaniline, exhibited a 25-fold increase in the current response compared to that of a glassy carbon electrode (GCE). The LOD value of 1.0×10^{-5} ppb, i.e. in parts per trillion by N-GQDs is the lowest value ever reported, which is 3-4 magnitudes lower than the previously reported values. The effective N-doping, which is attributed to the synthesis procedure, seems to play a crucial role in the sensing performance of N-GQDs, which spontaneously reduces Cd(II), mostly through the N-sites (This work was published in *RSC New Journal of Chemistry, 2020*). A white emissive sulfur co-doped nitrogen-graphene quantum dots (S,N-GQDs) was synthesized from polyaniline using sulfuric acid as an acid catalyst and S-doping agent. The S,N-GQDs, for the first time, exhibited simultaneous sensing towards three of the top ten toxic metal ions: Cd(II), Pb(II), and Hg(II), with highly sharp peaks and adequate peak-to-peak separation. The limit of detection values of Cd(II), Pb(II), and Hg(II) on S,N-GQD were 1, 10, and 1 pM and is the lowest reported hitherto for the simultaneous sensing of the metal ions. The enhanced sensitivity and the simultaneous sensing capability of S, N-GQD is assigned to the co-doping with S, which enabled the sensing of Pb(II) and Hg(II) through the M(II)-S interactions and the enhanced electronic properties, respectively (This work is published in *ACS, Applied Nano Materials*).

Further, a highly stable copper (Cu) nanocluster (NC), which exhibited stability for more than one year, was synthesized using N-GQD as reducing and capping agents and smaller glutathione molecules as additional capping agents. The synthesized NC, CuNC@N-GQDs, successfully sensed three neurofunctional molecules, dopamine (DA), serotonin (SER), and nicotine (NIC), which are functionally correlated to each other, simultaneously with well-defined peaks and good peak-to-peak separation. The limits of detection obtained were 0.001, 1.00, and 0.01 nM for DA, SER, and NIC, respectively. The higher sensitivity and the simultaneous sensing are indicative of the synergistic effect of CuNCs and N-GQDs in the CuNC@N-GQDs (This work was published in *RSC Journal of Materials Chemistry B, 2022*). An ultra-stable gold-copper nanocluster on nitrogen-doped graphene quantum dot (AuCuNC@N-GQD), with a stability of more than one year, was achieved through a galvanic exchange process. The AuCuNC@N-GQD displayed intense solid- and solution-state near-infrared (NIR) emission. The NC exhibited selective and enhanced glycine (GLY) sensing through a (non-enzymatic) EC strategy. The detection limit obtained for GLY was 10 nM, which is the lowest in the detection limits reported hitherto. The enhanced and selective sensing of AuCuNC@N-GQD towards GLY is assigned to the preferential Au-GLY interaction and the improvement in the electronic and conductivity characteristics of the NC (This work is under review in *ACS, Applied Nano Materials*). The EC sensing capability of AuCuNC@N-GQD was further extended towards heavy metal ions and observed a highly selective sensing property towards Pb(II) with almost nil current response for all other interfering metal ions studied. Pb(II) is included in the top ten list of chemicals of major public health concern by the World Health Organization, and its prevalent usage in batteries and other industries makes the detection of Pb(II) in environmental samples decidedly significant. The LOD value obtained was 1 pM, the lowest reported hitherto for Pb(II) by any other material. The selective interaction between Au(I) and Pb(II) is attributed to the selective sensing of Pb(II) by AuCuNC@N-GQD. (Manuscript under preparation)

In conclusion, this thesis presents an understanding of, how the logical designing of nano-functional materials can meet the needs and conquer the challenges in the EC sensing of various analytes.

TABLE OF CONTENTS

LIST OF FIGURES

LIST OF TABLES

ABBREVATIONS

AA	Ascorbic acid
Ach	Acetylcholine
CE	Counter electrode
CA	Catechol/ caffeine
Cd(II)	Cadmium II ion
DA	Dopamine
DNP	2,4-dinitrophenol
DNT	2,4 dinitrotoluene
DPV	Differential pulse voltammetry
EC	Electrochemical
EIS	Electrochemical impedance spectroscopy
ESI	Electron Spray Ionisation
EPA	Environmental Protection Agency
eV	Electron volt
EP	Epinephrine
FESEM	Field emission scanning electron microscope
FTIR	Fourier transform infra-red
GCE	Glassy carbon electrode
GLY	Glycine
GQD	Graphene quantum dots
Gr	Graphene
GSH	Glutathione
Hg(II)	Mercury (II)
HRTEM	High resolution transmission electron microscopy
HIS	Histidine
LDR	Linear dynamic range

LSV	Linear - sweep voltammetry
μA	microampere
^{o}C	Degree Celsius
μL	microliter
μM	micromolar
2D	Two - dimensional
M	Molar
$mAhg^{-1}$	milliampere hour per gram
mg	milligram
min	Minutes
mL	milliliter
mm	millimeter
mM	millimolar
MNC	Metal nano cluster
mV	millivolt
NC	Nano cluster
nM	nanomolar
nm	nanometer
NIC	Nicotine
NMP	N-methyl pyrrolidone
DNP	2-nitrophenol
NP	nanoparticle
NEP	Norepinephrine
Pb(II)	Lead (II) ion
PBS	Phosphate buffer solution
ppb	parts per billion
ppm	parts per million
pM	picomolar
ppt	parts per trillion

Pt	Platinum
ppq	parts per quadrillion
1D	One dimensional
RE	Reference Electrode and Resorcinol
rGO	Reduced graphene oxide
RT	Room Temperature
%RSD	Relative standard deviations
SWCNT	single-walled carbon nanotubes
S/N	Signal-to-noise
SA	Surface Area
SER	Serotonin
TNP	2,4,6-trinitrophenol
UA	Uric Acid
UV	Ultra – violet
WE	Working electrode
XPS	X-ray photoelectron spectroscopy
XRD	X-ray diffraction
0D	Zero dimensional

NOTATIONS

C_{ox}	Concentration of the oxidized species
C_{red}	Concentration of the reduced species
E	Potential
E_o	Standard potential of the redox couple
E_p	Peak potential
E_{pa}	Anodic peak potentials
E_{pc}	Cathodic peak potential
F	Faraday's constant;
i	Current
I_p	Peak current
i_{pa}	Anodic peak current
i_{pc}	Cathodic peak current
k_s	Heterogeneous electron transfer rate constant
n	Number of electrons transferred
R	Universal gas constant
R_S	Solution resistance
T	Temperature (K)
t	Time
υ	Scan rate
α	Charge transfer coefficient
ΔE_p	Peak potential separation

NOMENCLATURE

Ag/AgCl	Silver/Silver chloride
$AgNO_3$	Silver nitrate
$AuCl_3$	Gold chloride
$CdCl_2$	Cadmium chloride
$Co(NO_3)_2$	Cobalt(II) nitrate
$CuSO_4$	Copper(II) sulfate
$FeCl_2$	Ferrous chloride
$FeCl_3$	Ferric chloride
H_2O_2	Hydrogen peroxide
H_2SO_4	Sulphuric acid
$HAuCl_4$	Hydrogen tetrachloroaurate (III)
HCl	Hydrochloric acid
Hg/Hg_2Cl_2	Mercury/Mercuric chloride
Hg_2Cl_2	Mercury(II) chloride
HNO_3	Nitric acid
$K_2Cr_2O_7$	Potassium dichromate
NaOH	Sodium hydroxide
$NiSO_4$	Nickel(II) sulfate
$PbNO_3$	Lead(II) nitrate
S	Sulfur
Si	Silicon

$SnCl_2$	Stannous chloride
$SnCl_4$	Stannic chloride
$Zn(NO_3)_2$	Zinc nitrate
-COOH	Carboxylic acid group
-OH	Hydroxyl group
-C=O	Carbonyl group
$-NO_2$	Nitro group
$-NH_2$	Amino group
-C-O-C	Ether group

CHAPTER 1

INTRODUCTION

This chapter briefs on sensors and the fundamental aspects of electrochemical (EC) sensors and various EC sensing methods such as voltammetric, amperometric, potentiometric, and electrode processes. On material front, the chapter provides a state-of-the-art literature survey on graphene quantum dot (GQD) and metal nanocluster (MNC) based materials in EC sensing and the properties of GQD and MNC. Finally, the chapter briefs about the motivation of our research work, research problem, objectives, and the expected outcomes of the proposed work. In addition, the outline of the thesis and a brief introduction of each chapter are provided at the end of the chapter.

1.1 Sensors

The capacity of humans to interact with the environment depends mainly on the depth of knowledge acquired about the processes (either human-induced or natural) that occur in the real world. Though the physical senses help humans understand and comprehend the environment, it is highly limited, and there exist many situations in various fields of technology that demand better sensing capability. By using a sensor, which is a device that receives signals and responds to a signal or stimulus for better understanding of the surrounding. That is, a sensor can be any technical component that independently detects certain physical or chemical variables and properties in the environment or of living and non-living things. An essential property of sensors is the conversion of the measured data into signals or visual displays that a human or an electronic device can meaningfully interpret. Sensors have peneterated in all walks of our life such as in our offices, gardens, shopping malls, homes, cars, toys which make our lives safer, easier and more comfortable, and helps us tackle many day-to-day chores with ease. Nowadays sensors are widely applied in medical devices for detecting patient's vital signs, including ECG, peripheral oxygen saturation, blood pressure, respiration, temperature, and blood glucose level(Karimi-maleh, Karimi, and Alizadeh 2020). Vital roles are played by sensors in modern military applications such as

flight controls, weaponry controls, indicators, communications, and battlefield surveillance systems. Sensors are found in various security systems, for instance, explosives detection systems, chemical warfare, crime detection systems, intrusion detection systems and civil establishments to mention a few.

1.2 Voyage of Sensors; antiquity to contemporary

The evidence of construction of various types of sensors can be traced back to the histories. Philo of Byzantium constructed a device in the third century BC that could show air's expansion and contraction in response to temperature changes. In the 17th century, the Italian astronomer and physicist Galileo Galilei built the first version of the glass thermometer, a 'thermoscope.' In 1938, Arthur Ruge and Edward Simmons created the first variable strain gauge used on electronic scales. This particular type of transducer converts mechanical force, such as stretching or compressing, into changes in electrical resistance. World War II saw the development of technologies, including radio frequency identification transponders and the forerunners of radio frequency identification chips(Simões and Xavier 2017). History has shown that materials science and engineering advancements have been essential drivers in developing sensor technologies. Ongoing developments in materials technology will permit better control of material properties and behavior, thereby offering possibilities for new sensors with advanced features, such as greater fidelity, lower cost, and enhanced efficiency. Recent advances in sensor technologies have been powered by high-speed and low-cost electronic circuits, novel signal processing methods, and advanced manufacturing technologies.

The sensor technologies have changed a lot in the last decade in terms of compactness, smartness and sensitivity and are embedded in all modern computing and navigation devices in compact forms and today a smartphone carries around 22 sensors on average. The traditional sensors such as photosensors, optical sensors, capacitive sensors and almost all sensors have been replaced by their integrated circuit forms such as microelectromechanical system (MEMS). The technologies of sensors have further advanced and has become smart sensors and are seen in smart watches, smart gadgets or in advanced applications such as self-driving cars where hundreds of smart sensors are involved for seamless and smooth driving in driver-less cars. The same can also be seen in robotics, medical diagnosis, brain–computer

interface and many more, where artificial intelligence has empowered the sensors with intelligence and smartness for emerging and modern applications such as industry, healthcare and sophisticated automation(Brett and Oliveira-brett 2011).

1.3 Classification of Sensors

The world of sensors is immensely explored these days because of their ability to make our day-to-day life much more accessible. A sensor has many forms of input properties and electrical output properties. All the sensors are categorized on the basis of their uses, applications, material used and some production technologies. A few classifications of sensors are as follows,

- The first classification of the sensors is divided into active and passive. Active sensors require an external excitation signal or a power signal. On the other hand, passive sensors do not require any external power signal and directly generate output response.
- The second type of classification is based on the means of detection used in the sensor. Some of the means of detection are Electric, Biological, Chemical, Radioactive, etc.
- The following classification is based on the conversion phenomenon, i.e., the input and the output. Some common conversion phenomena are Photoelectric, Thermoelectric, Electrochemical, Electromagnetic, Thermo-optic, etc.
- The final classification of the sensors is analog and digital sensors. Analog sensors produce an analog output, i.e., a continuous output signal concerning measured quantity. Digital sensors, in contrast to analog sensors, work with discrete or digital data.

1.4 Electrochemical Sensors

Electrochemical (EC) sensors represent the most rapidly growing class of chemical sensors. A chemical sensor is a device that provides a certain type of response directly related to the quantity of a specific species through a chemical reaction which leads to its qualitative and quantitative determination. A useful definition of a chemical sensor is that device that transforms chemical information (presence of a particular element or ion, concentration, chemical activity, etc.) into an analytically useful signal. All chemical sensors consist of two parts, a chemically selective layer (where the selective chemistry takes place), which isolates

the response of the analyte from its immediate environment, and a transducer, which transforms the response into a detectable signal using modern instrumentation. Depending on the transducer type, Chemical sensors can be categorized into EC, optical, mass, or thermal sensors and are designed to detect and respond to an analyte in the gaseous, liquid, or solid-state (Stradiotto et al., 2003). The schematic showing the working principle and operation of an EC sensor is given in Figure 1.1.

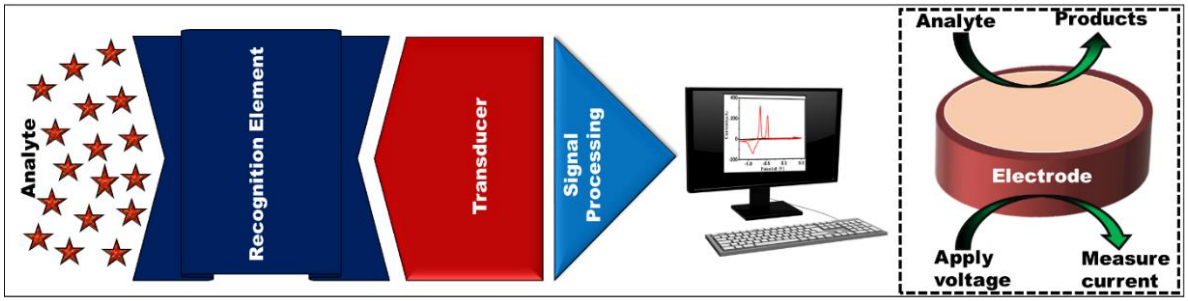

Figure 1.1. Schematic representation of an EC sensor, its working principle, and operation.

Historically, the use of electrochemical sensors began in the 1950s by monitoring industrial oxygen (Islam et al., 2010). Labor laws related to the health and safety of the workers required the monitoring of toxic gases and fuels in confined spaces, prompting a burst of research into electrochemical sensors that could exhibit good selectivity for the detection of different gases. Leland C. Clark proposed the oxygen sensor concept using two electrodes of a cell with an oxygen-permeable membrane separating the electrodes and the electrolyte solution. The oxygen diffused through the membrane and was reduced in the indicator electrode. This resulted in a current proportional to the oxygen concentration in the sample. The Clark oxygen sensor found wide application in medicine and environmental and industrial monitoring by developing the first glucose oxidase enzyme electrode in 1962. The glucose electrode was the first EC biosensor developed and was a real breakthrough in sensors and medical sciences. The first commercial glucose meters were available by the 1970s and have become the gold standard of the biosensor field. One of electrochemistry's greatest sensor achievements is the point-of-care monitoring of glucose which helps diabetic people who constitute ~5% of the world's population. This global, multi-billion-dollar market is based on modified disposable electrodes(Kadara and Tothill 2008). The extreme interest of researchers on efficient sensors and electrodes can be understandable from the current literature bloom in this area. A recent report on the comparison among the EC activity of

screen-printed electrodes from Alderon Biosciences, University of Florence and DropSens where it was observed that the electrodes from DropSens exhibited the best electrochemical performance(Kadara, Jenkinson, and Banks 2009). The manufacturing of disposable one shot usage strips are attractive due to the low cost, ability to mass produce, reproducibility and simplicity. Though intense research exists in the design and development of new reusable electrodes which can make the system much simpler and more cost effective.

Electrochemistry has become a powerful tool to probe reactions involving electron transfers (Kaifer & GómezKaifer, 1999). Electrochemistry relates the flow of electrons to chemical changes. For instance, in inorganic chemistry, the resulting chemical change is often the oxidation or reduction of a metal complex. EC sensors' attractive features, including remarkable sensitivity, experimental and instrumentation simplicity, portability, and low cost, make the EC sensors a potential candidate among other sensors such as optical, mass, and thermal (Stradiotto et al., 2003). The commercialization of the developed sensors become a necessity concerning the vast range of applicability in important fields such as clinical, industrial, environmental, and agricultural, which further demands considerable improvements in sensitivity, selectivity, and accuracy to meet the future needs in diverse fields (Faridbod et al., 2011).

So as a summary, the supremacy of EC sensing methods is owing to its:

- Experimental simplicity
- Portability
- Fast analysis
- Cost-effectiveness
- Low power consumption
- Lower detection limits
- Good selectivity and reproducibility
- Suitability for label-free detection

1.4.1 Electrochemical Methods

The signal from an EC sensor is usually derived from an electrical response given in the presence of an analyte. EC responses monitored by different methods are primarily based on potential, resistance, and electrical current. Thus, classification among the EC methods includes (see Figure 1.2),

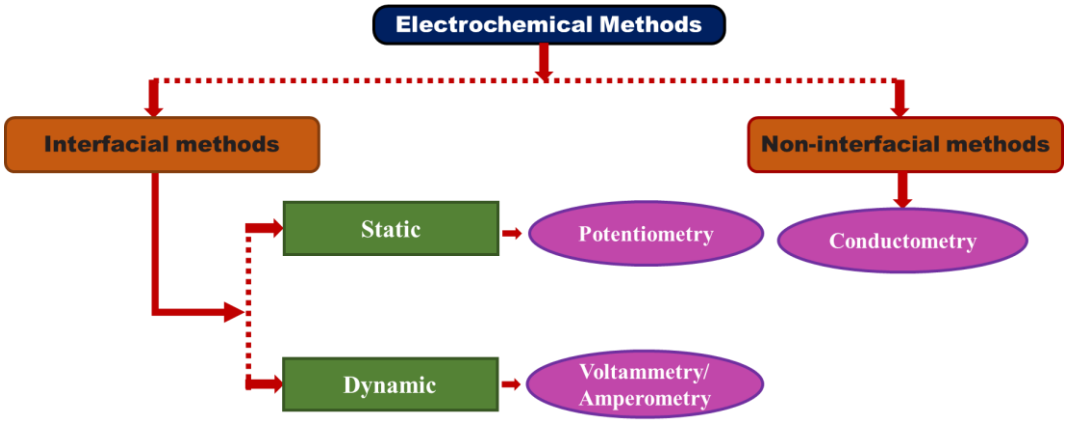

Figure 1.2. A schematic representation of the EC methods with their subdivisions

- The *Interfacial methods* are methods that respond directly or indirectly to the presence of the analyte on the electrode surface, resulting in a disturbance of an electric signal that can be measured. The *interfacial methods* can be further divided into two main groups: static and dynamic. The *static methods* are defined as those in which the electric current is zero ($i = 0$). In contrast, the *dynamic methods* include redox reactions, where electron transfer occurs between the electrode and the analyte. Therefore, the surface of the electrode receives an electric stimulus with a nonzero current ($i \neq 0$).
- The *non-interfacial method* is based essentially on a cell of known size, with two equidistant electrodes that measure the electrical conductance (essentially, the resistance) of a solution as a whole. When applying an alternating current signal, there is no electrode polarization, and the response is given in terms of the electric resistance of the solution as a function of the cell constant, which is based on the surface area of the electrodes, their spacing, and the solution volume in the electrochemical cell.
- *Potentiometry* is a *static interfacial method* based on measuring the potential of an EC cell. The measuring setup contains two electrodes, an indicator electrode (measuring electrode)

and a reference electrode, which, when placed in a solution together, produce a certain potential. *Potentiometric sensors* are those in which a local equilibrium is established at the sensor interface, where either the electrode or membrane potential is measured, and information about the composition/concentration of the sample(s) in the solution is obtained from the potential difference between the two electrodes.

- The *voltammetric methods* are, also known as potential sweep methods, consist of the application of a potential varying continuously with time on a working electrode, which leads to the occurrence of oxidation or reduction reactions of electroactive species in the solution, in accordance with the adsorption of species with the potential and a capacitive current due to the electrical double layer. The observed current is proportional to the electroactive species' concentration. The *amperometric sensor* is a special case of a voltammetric sensor in which the current is measured at a fixed operating potential. It measures the current flowing through the working electrode as a function of time as a constant potential is applied to the working electrode.
- *Conductometry* is a non-interfacial method, as it is based essentially on a cell of known size, with two equidistant electrodes that measure the electrical conductance of a solution as a whole. When applying an alternating current signal, there is no electrode polarization, and the response is given in terms of the electric resistance of the solution as a function of the cell constant, which is based on the surface area of the electrodes, their spacing, and the solution volume in the electrochemical cell.

We have majorly utilized voltammetric methods for sensing purposes in our work. Hence, a detailed view of the voltammetric methods and their general advantages are described comprehensively in the forthcoming sections.

1.4.2 Voltammetric sensors

As discussed in the previous section, voltammetric sensors are those in which the information about an analyte is obtained by measuring the current response as a function of the applied potential. To be more precise, all the voltammetric techniques involve the application of a potential (E) to an electrode in a varying manner from one preset value to another and then the resulting current (i) flowing through the EC cell is recorded and is monitored over a period of time (t). Thus, all the voltammetric techniques can be described

as function of E, i, and t. If this potential (or range) is conveniently chosen, it will force the electroactive species at the electrode surface to undergo either oxidation or reduction electrochemically and in turn, results in a current response proportional to the concentration, based on the conditions. The analytical advantages of the various voltammetric techniques include excellent sensitivity with a very large useful linear concentration range for both inorganic and organic species (10^{-12} to 10^{-1} M), a large number of useful solvents and electrolytes, a wide range of temperatures, rapid analysis times (seconds), simultaneous determination of several analytes, the ability to determine kinetic and mechanistic parameters, a well-developed theory and thus the ability to reasonably estimate the values of unknown parameters, and the ease with which different potential waveforms can be generated and small currents measured (Kounaves, 1997). The general uses of voltammetric techniques, to list a few, are,

- Quantitative determination of organic and inorganic compounds in aqueous and nonaqueous solutions
- Fundamental studies of oxidation and reduction processes in various media
- Determination of adsorption processes on surfaces
- Determination of electron transfer and reaction mechanisms
- Measurement of kinetic rates and constants
- Determination of thermodynamic properties of solvated species

The basic instrumentation of a voltammetric sensor comprises a controlled-potential equipment called the potentiostat and an EC cell that requires minimum two electrodes: WE and CE, immersed in a suitable electrolyte. The WE, which makes contact with the analyte, must apply the desired potential in a controlled way and facilitate the transfer of charge to and from the analyte resulting from the oxidation or reduction processes, and a second electrode, counter electrode (CE) which acts as the other half of the cell must have a known potential with which to gauge the potential of the WE; furthermore, it must balance the charge added or removed by the WE. However, it is challenging for an electrode to maintain a constant potential while passing current to counter redox events at the WE. Therefore, a better arrangement involves the use of a three-electrode system, where the roles of supplying electrons and providing a reference potential are divided between two separate electrodes, referred to as the CE and the RE, respectively, because it is necessary to avoid the passage of

current through the RE, which otherwise would alter its potential via changes in the activities of various electroactive species. So, a typical EC cell consists of the analyte sample dissolved in a solvent, an ionic electrolyte, in contact with the three electrodes: the RE, WE, and the CE (or secondary or auxiliary electrode). While the WE is the electrode at which the reaction of interest occurs, the RE (e.g., Ag/AgCl, Hg/Hg_2Cl_2) provides a stable potential with respect to the WE. An inert conducting material (e.g., platinum (Pt), graphite) is usually used as the CE/auxiliary electrode. While the applied potential is measured against the RE, the CE closes the electrical circuit for the current to flow. A potentiostat performs the experiments that effectively control the voltage between the RE and WE while measuring the current through the CE (the WE are connected to the ground). A supporting electrolyte is required in the controlled-potential experiments to eliminate electromigration effects, decrease the resistance of the solution and maintain the ionic strength constant (Stradiottoet al., 2003).

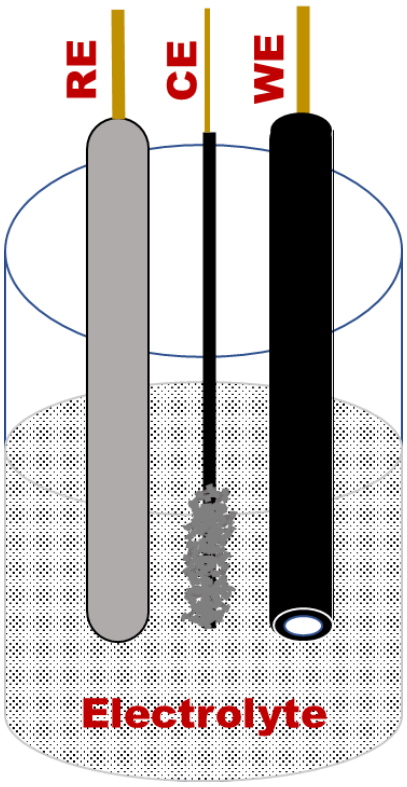

Figure 1.3. The basic instrumental set up of a voltammetric experiment: the three-electrode system

❖ **Working electrode (WE)**

The WE is the one on which the reaction of interest is occurring and often can be of inert metals such as gold, silver or Pt; carbon materials such as glassy carbon (GC), pyrolytic carbon or carbon paste; and mercury drop. The most widely used WE substrate is the GC which is an electrically conductive and gas impermeable material and is obtainable in pure state (Sindhu & Girish Kumar, 2011), because of its cited advantages such as, (i) high resistance to chemical attack (ii) low cost (iii) easy pre-treatment by polishing with metallographic paper (iii) larger overpotential for production of hydrogen and dissolved oxygen and (iv) increased reversibility for several redox couples and reactions that involve subsequent proton transfer.

- **Reference electrode (RE)**

A RE is the one with a fixed electrode potential value which is not varied with the external potential applied in the WE and must be insensitive to the composition of the analyte solution. The commonly used REs are, Silver-silver chloride electrode, Calomel electrode, to name a few.

- **Counter electrode (CE)**

The role of the CE is to supply the current required by the WE, without limiting the measured response of the cell. In voltammetric sensors, the current flows between the WE and the CE. The key condition for an electrode to act as a CE is that it should not dissolve in the medium of the EC cell and the reaction product at the CE should not react at the WE. It should have a large area compared to that of the WE to ensure that the area of the electrode does not control the limiting current. Most often the CE consists of a thin Pt wire or thin foil, although Au or graphite can be used.

- **Supporting electrolyte**

The supporting electrolyte is an inert soluble ionic salt added to the solvent; generally, in 10-fold or 100- fold excess over the concentration of the species being studied. Inert in the sense, the ability to avoid oxidation or reduction at the RE during the course of the EC measurements. The main function of the supporting electrolyte is that it carries most of the ionic current of the cell since its concentration is much larger than that of the other species in solution. Thus, it serves to complete the circuit of the EC cell and keep the cell resistance to a low value (Laina & Girish Kumar, 2013)

1.4.3 Faradaic and non-Faradaic Electrode Processes

Two types of processes occur at electrodes: One type involves a direct transfer of electrons via an oxidation reaction at one electrode and a reduction reaction at the other. Since such reactions are governed by Faraday's first law (i.e., the amount of chemical reaction caused by the flow of current is proportional to the amount of electricity passed), and are called Faradaic processes. Electrodes at which Faradaic processes occur are sometimes called the charge transfer electrodes. For a thermodynamically controlled reversible process the applied potential (E) of the electrode is given by the well-known Nernst equation, Eq. (1.1),

$$E = E^{\circ} + \frac{2.303RT}{nF} log \frac{C_O}{C_R} \qquad (1.1)$$

Where E° is the standard potential of the redox couple; R - universal gas constant; T - temperature (K); n - number of electrons transferred; F – Faraday's constant, which represents the amount of electric charge carried by one mole of electrons, i.e., Avogadro's number x charge of an electron; C_O is the concentration of the oxidized species; C_R is the concentration of the reduced species.

Under certain conditions, a range of voltages may be applied to a cell that does not produce Faradaic processes at one or both of the electrodes. Faradaic processes may be prevented either because electrons do not have sufficient energy to pass over the potential energy barrier at the electrode-solution interface (thermodynamic reasons) or because the electron-transfer reaction is not fast enough on the time scale of the experiment (kinetic reasons). However, the processes such as adsorption and desorption can occur, and the structure of the electrode-solution interface can change with changing potential or solution composition. These processes are called non-Faradaic processes. Under these circumstances, conduction of continuous alternating currents can still take place. With such currents, reversal of the charge relationship occurs with each half-cycle as first negative and then positive ions are attracted alternately to the electrode surface. Electrical energy from the external voltage source is consumed and converted to heat by friction associated with the motion of ions. In other terms, when the voltage changes, the ions in the double layer have to rearrange and

adjust to the new potential, and this rearrangement requires energy. Thus, each electrode surface behaves as a plate of a capacitor, whose capacitance is large (several hundred to several thousand microfarads per square centimeter). The capacitive current increases with frequency and with electrode area; by controlling these variables, it is possible to adjust conditions so that essentially all of the alternating current in a cell is carried across the electrode interface by this non-Faradaic process. The basic difference between a faradaic and a non-Faradaic current can be further understood by imagining an electron travelling down the external circuit to an electrode surface. When the electron reaches the solution interface, it can either remain at the electrode surface and increase the charge on the double layer, which constitutes a non-Faradaic current; or can leave the electrode surface and transfer to a species in the solution, thus becoming a part of the faradaic current (Skoog et al., 1998).

Therefore, the non-Faradaic current is a result of those processes that do not involve the transfer of electrons across the electrode–solution interface and they stem from the electrical capacitance present at the interface, which can be calculated using the equation, Eq. (1.2),

$$C = \frac{\mathrm{q}}{\mathrm{E}} \qquad (1.2)$$

Where q and E represent the charge and the potential, respectively.

The current in a voltammetric experiment measures the rate of the electrode process. Different strategies may occur when an electrode is placed in an electrolyte solution. The steps involved in an electrode reaction are:

1. Mass transfer of the species between the bulk solution and the electrode surface.
2. Heterogeneous electron transfer at the electrode/solution interface.
3. Chemical reactions, either preceding or following the electron transfer.
4. Surface reactions such as adsorption, desorption, and electrodeposition–dissolution

1.4.4 Different voltammetric techniques

This section discusses some of the more common forms of voltammetric techniques currently in use for a variety of analytical purposes. The uniqueness of each technique rests

on the subtle differences in the manner and the timing in which the potential is applied and the current is measured (Kounaves, 1997).

1.4.4.1 Linear-Sweep Voltammetry (LSV)

The LSV is the simplest among the voltammetric techniques in which the potential of the WE is altered linearly with time. LSV measures the current at the WE while the potential between the working and a RE is linearly swept in time. i.e., it involves an increase in the imposed potential linearly at a constant scanning rate from an initial potential to a defined upper potential limit. A measure of the current signal is denoted by a peak or trough that is formed at the potential where the species begins to be oxidized or reduced (Pillay, 2009).

1.4.4.2 Cyclic Voltammetry (CV)

The CV has become an important and most extensively used electroanalytical technique in many areas of chemistry. It is widely used for the study of redox processes, to provide information on the reversibility and kinetics of the reactions, and for understanding reaction intermediates. The CV is based on varying the applied potential at a WE in both the forward and backward/reverse directions while monitoring the current. i.e., the potential of WE is scanned linearly from an initial potential to a final potential and then back to the initial potential. The potential at which the peak current occurs is known as the peak potential (Ep). The important parameters in a cyclic voltammogram are the cathodic and the anodic peak potentials (Epc, Epa) and peak currents (ipc, ipa), respectively. The magnitude of the Faradaic current (ipc or ipa) gives an indication of the rate at which the electrons are being transferred between the redox species and the electrode. The cyclic voltammetric processes could be reversible, quasi-reversible or irreversible. If the electron transfer process is fast compared

with the other processes (such as diffusion), the reaction is said to be electrochemically reversible, where the electroactive oxidized (or reduced) species in the forward scan is in equilibrium with the electroactive reduced (oxidized) species in the reverse scan and the peak separation is given by Eq. (1.3),

$$\Delta E_p = E_{pa} - E_{pc} = \frac{2.303}{RT} = \frac{0.0592}{n}\ V \qquad (1.3)$$

ΔEp should be independent of the scan rate (υ) but in practice, ΔEp increases slightly with increasing υ, and this is due to the solution resistance (RS) between the reference and working electrodes. Theoretically, the potential difference between the oxidation and reduction peaks is 59 mV (eqn 3) for an one-electron reversible redox reactions. However, in practice, this value is difficult to attain and sometimes found in the 60-100 mV range, because of cell resistance. Thus, for a reversible redox reaction at 25 °C with "n" electrons, ΔEp should be 0.0592/n V or about 60 mV for a one-electron reaction.

The formal reduction potential (E_0) for a reversible couple is given by Eq. (1.4),

$$E_0 = \frac{E_{pa} + E_{pc}}{2} \qquad (1.4)$$

For a reversible reaction, the concentration is related to the peak current by the Randles–Sevcik expression (at 25 °C), Eq. (1.5):

$$i_p = (2.686 \times 10^5) n^{3/2} A D^{1/2} C \upsilon^{1/2} \qquad (1.5)$$

where i_p is the peak current in Amps, A is the electrode area (in cm^2), D is the diffusion coefficient ($cm^2\ s^{-1}$), C is the concentration in mol cm^{-3}, and υ is the scan rate in Vs^{-1}. A linear plot of i_p vs. $\upsilon^{1/2}$ indicates that the currents are controlled by planar diffusion to the electrode surface (***diffusion-controlled process***), and if there is a linear relationship between i_p and υ, that corresponds to an ***adsorption-controlled process***.

For an irreversible process, only forward oxidation (reduction) peak is observed, but at times, a weak reverse reduction (oxidation) peak as a result of slow electron exchange or slow chemical reactions at the electrode surface is possible. Irreversibility due to a slow electron transfer rate results in $\Delta E_p > 0.0592/n$ V, greater than, say, 70 mV for a one-electron reaction. Quasi-reversible processes are those in which, unlike the reversible process where the current is purely mass transport controlled, the current is controlled by a mixture of mass transport and charge transfer kinetics. The process occurs when the relative rate of electron transfer with respect to that of the mass transport is insufficient to maintain the Nernst equilibrium at the electrode surface. For the quasi-reversible process, i_p increases with $\upsilon^{1/2}$ but not in a linear relationship and $\Delta E_p > 0.059/n$ (Figure 1.4).

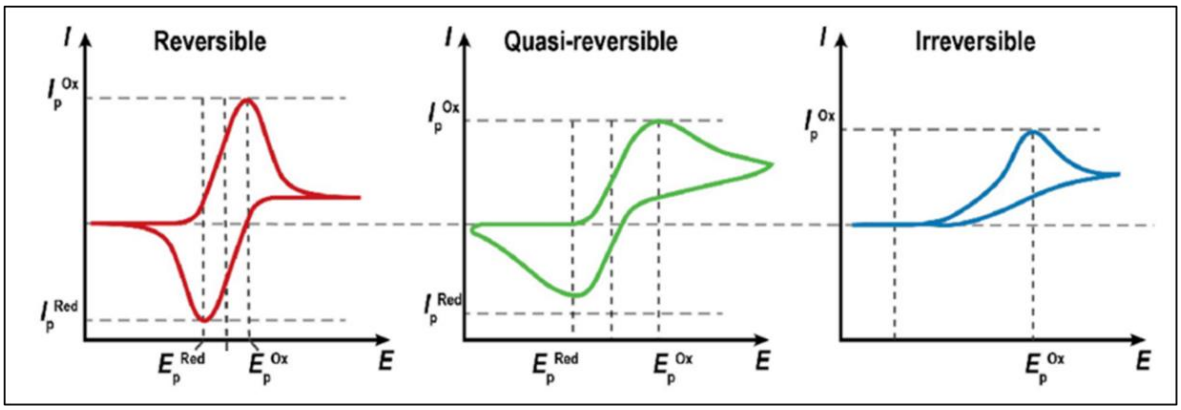

Figure 1.4. Cyclic voltammograms for reversible, quasi-reversible, and irreversible electron transfer

1.4.4.3 Pulse methods

Pulse voltammetric techniques introduced by Barker and Jenkin, were aimed at increasing the sensitivity or lowering the detection limits/limit of detection (LOD), and increasing the speed of voltammetric measurements. The key advantage of these techniques is that they permit convenient measurements even up to nanomolar concentration levels and because of this greatly improved performance, modern pulse techniques have largely replaced classical EC techniques to an extent. The idea behind all pulse-voltammetric methods is to measure the current at a time when the difference between the desired faradaic curve and the interfering charging current is large, the latter being on the lower side. The difference in the rate of the decay of the charging and the faradaic currents follows a potential step (or "pulse", typically 50 mV). A sequence of such potential steps, each with duration of about 50 milliseconds, is applied on to the WE. After the potential is stepped, the charging current, one of the major contributors of non-Faradaic current, decays exponentially, whereas the faradaic current (for a diffusion-controlled current) decays as a function of 1/(time)½; that is, the rate of decay of the charging current is considerably faster than the decay of the faradaic current (Aoki et al., 1980). Charging currents result in high background noise in voltammetric analyses. This ultimately compromises signalto-noise ratios and thus limits the detection at low analyte concentrations. To be more precise, the greater sensitivity of pulse techniques can be attributed to two factors. The first is an enhancement of the faradaic current, and the second is a decrease in the non-Faradaic charging current. To account for the enhancement, let us consider the events that must occur in the surface layer around an electrode as the potential is suddenly increased by 50 mV. If an electroactive species is present in this layer,

there will be a surge of current that lowers the reactant concentration to that demanded by the new potential. As the equilibrium concentration for that potential is approached, however, the current decays to a level just sufficient to counteract diffusion; that is, to the diffusion-controlled current. In classical voltammetry, the initial surge of current is not observed because the time scale of the measurement is long relative to the lifetime of the momentary current. On the other hand, in pulse voltammetry, the current measurement is made before the surge has completely decayed. Thus, the current measured contains both a diffusion-controlled component and a component that has to do with reducing the surface layer to the concentration demanded by the Nernst expression; the total current is typically several times larger than the diffusion current. Note that, under hydrodynamic conditions, the solution becomes homogeneous with respect to the analyte by the time the next pulse sequence occurs. Thus, at any given applied voltage, an identical current surge accompanies each voltage pulse. When the potential pulse is first applied to the electrode, a surge in the non-Faradaic current also occurs as the charge increases. This current, however, decays exponentially with time and approaches zero with time. Thus, by measuring currents at this time only, the non-Faradaic residual current is greatly reduced, and the signal-to-noise ratio is larger. Enhanced sensitivity results. Therefore, in pulse techniques, in order to maximize the signal-to-noise (S/N) ratio, linear time– potential scans have been supplemented by more complex waveforms where time and potential are manipulated to maximize the ratio of faradaic to non-Faradaic current. As discussed, this is typically done by sampling the current at a specific time interval where the faradaic response is large and the non-Faradaic charging current is small (Cazes, 2004). The discrimination against the charging current (non-Faradaic current) that is inherent in these techniques leads to lower LODs (when compared to linear sweep techniques), which makes these techniques suitable for quantitative analysis. A number of different pulse techniques have been tried over the years, which differ in their potential pulse wave forms, the number of sampling points, and whether a solid electrode (voltammetry) or a mercury drop electrode (polarography) is used. Waveforms are simply the variation in potential with time. The simplest waveform is a linear scan (voltage ramp) where potential is scanned linearly with time [Figure. 1.5(a)]. The waveform used for CV is simply a linear scan that is scanned forward, switched, and then scanned backward [Figure. 1.5(b)]. The CV waveform may be repeated over many cycles. Pulsed waveforms are more complex and can

be divided primarily into normal pulse voltammetry (NPV), differential pulse voltammetry (DPV), and square wave voltammetry (SWV).

i. Normal Pulse Voltammetry (NPV)

The NPV (Figure. 1.5(c)) consists of a series of pulses of increasing amplitude, with the potential returning to the initial value after each pulse. The current is measured at some sampling interval (*S*) near the end of each pulse maximum. The Faradaic response is maximized by the potential pulse (when compared with the linear scans) and a significant amount of charging current is avoided in the measurement since the current is sampled near the end of the pulse (Cazes, 2004).

ii. Differential Pulse Voltammetry (DPV)

The DPV (Figure. 1.5(d)) differs from NPV, that it uses a waveform that consists of small pulses (of constant amplitude) superimposed on a staircase wave form. Like NPV, the faradaic response is maximized and charging current is minimized by sampling the current (*S2*) near the end of each pulse maximum. Again, this is very advantageous over the linear-scan techniques since signal-tonoise is maximized. DPV differs from NPV in that the current is sampled at a second interval (*S1*). By subtracting *S1* from *S2*, a voltammogram is obtained that

is a measure of the change in current with potential. This will appear very different from the shape of the NPV voltammogram. If the NPV voltammogram gives a classical, sigmoidal response (i vs. E) for the oxidation or reduction of the analyte, the equivalent response using DPV will be the derivative of the NPV response (Δi vs. E) and will result in a peak instead of a wave. This can be attributed to the fact that Δi becomes small and approaches zero as the limiting current is approached. This differential output allows the observation of individual peak maxima that differ by as little as 50 mV. In comparison, NPV (as well as classical techniques) requires approximately 200 mV between the waves to resolve them (Cazes, 2004).

iii. Square Wave Voltammetry (SWV)

The SWV is similar to DPV in that current is sampled at two different times in the waveform and results in a differential output (Δi vs. E). The SWV waveform (Figure. 1.5(e))

is essentially the combination of a square wave (bold, solid line) of period τ with a staircase voltage function (dotted lines), of period τ. The "forward" current is measured at *t1* just before the "down" pulse is applied. The "reverse" current is measured at *t2*. The net current is defined as the current measured at *t1* minus the current measured at *t2*, or $\Delta i = i1 - i2$. The SWV waveform is advantageous in such a way that the detrimental effects of charging current are reduced, allowing very fast potential scans. The charging current developed on the forward scan (from the "up" pulse) is essentially subtracted out when the reverse scan (the "down" pulse) is applied. Because of the rapid analysis time, repetitive scanning can be used with SWV to increase signal-to-noise by signal-averaging. The true advantage of SWV is therefore, the speed of analysis together with excellent sensitivity and the rejection of background currents (Cazes, 2004).

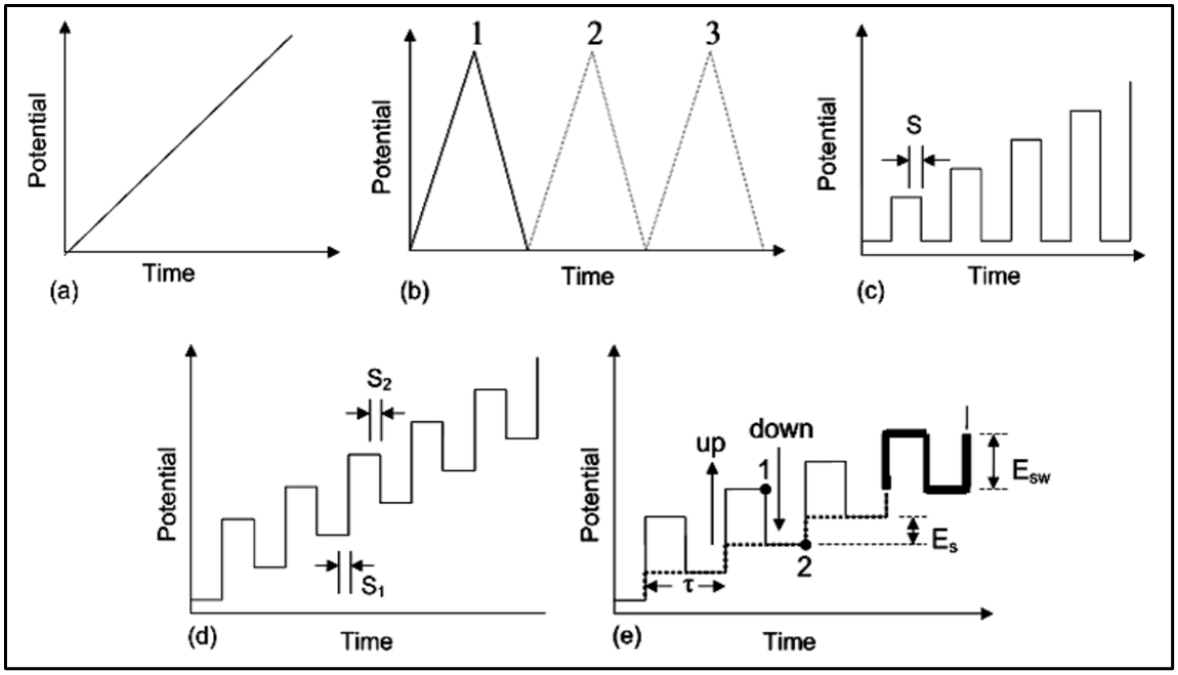

Figure 1.5. The pictorial representation of the different types of waveforms of the different voltammetric techniques; (a) LSV (b) CV (c) NPV (d) DPV and (e) SWV (Cazes, 2004)

1.4.5 Surface modification methods for the electrodes

In recent times, electrochemists have become interested in purposely modifying electrodes by adsorbing, coating, or attaching specific molecules to the surface. A surface modified electrode is the one in which, if a specific material is attached to the electrode, then that material imparts on the electrode some chemical, EC or desirable properties which are

not available at the unmodified electrode. Most frequently the layer or coating on the electrode surface is electroactive, i.e., it can exchange electrons with the underlying substrate material and be oxidized or reduced. This deliberate and controlled modification of the electrode surface can produce electrodes with new and interesting properties that may form the basis of new applications of electrochemistry and novel devices (Allen J Bard, 1983). A primary interest has been in the area of electrocatalysis. Another application is in the production of electrochromic devices that change colour on oxidation and reduction. Finally, the most important analytical use of the electrodes is as analytical sensors selectively for particular species or functional groups (Sindhu & Girish Kumar, 2011). One of the most important properties of the modified electrodes is their ability to catalyze the oxidation or reduction of solute species at comparatively lower voltages, which otherwise exhibits higher voltages or does not give a response at the unmodified surfaces. Thus, they play an important role in reducing the high overvoltage required for the voltammetric determination of such analytes. Surface modification changes the surface layers of the electrode itself or creates a layer with some form of chemical as well as physical selectivity. Modified electrodes can be prepared by several different techniques which include,

- ***Chemical modification****:* The electrode surface is activated by certain chemical reactions, for example, with silane, which is then used to react with another chemical species that becomes immobilized on the surface.
- ***Adsorption****:* Some species find the surface of the electrode much more hospitable than the bulk solution and so attach spontaneously to the surface. For example, organic species such as those containing double bonds, are often hydrophobic and strongly adsorb from aqueous solutions on carbon or Pt surfaces (Allen J Bard, 1983).

The adsorption methods involve, ***i) Drop-dry Coating/ Drop-dry casting*** (or solvent evaporation), where a few drops of the polymer, modifier or catalyst solution/dispersion are dropped onto the electrode surface and left to stand for the solvent to dry out***. ii) Dip-dry Coating***, where the electrode is immersed in a solution/dispersion of the polymer, modifier or catalyst for a period sufficient for spontaneous film formation to occur by adsorption. The electrode is then removed from the solution and the solvent is removed by drying. ***iii) Spin-Coating*** *(or spin-casting),* which involves evaporating a drop of polymer, modifier or catalyst

solution/dispersion from an electrode surface by using centrifugal force at high-speed rotations (Pillay, 2009).

- ***Electroadsorption and electrodeposition***: If adsorption is carried out under the influence of an applied potential, then thicker modifier layers usually result, but there is a probably of a greater guarantee of uniformity. Electro polymerisation of monomers is possible; such procedures are used for the formation of conducting polymers.
- ***Plasma:*** The electrode surface is cleaned by plasma leaving the surface with dangling bonds which are highly active and thus promotes the adsorption of species, such as amines or ethenes or similar (Laina & Girish Kumar, 2013).

1.5 Materials of Interest: Functional Nanomaterials

The emergence of the field of nanoscience has made huge changes in the the properties and applications of materials. Nanomaterials or matrices with dimensions (grain size, layer thickness or shapes) below 100 nm display unique physical and chemical features that lead to new properties that are generally not available in bulk. Nanotechnology was introduced by Nobel laureate Richard P. Feynman during his now famous 1959 lecture "There's Plenty of Room at the Bottom". Feynman's prescient 'on the head of a pin' greatly inspired scientists and technologists to venture into this uncharted nano-terrain to do something big with something small. Thus, the emergence of nanoscience has made huge changes in materials applications. The science and technology of nanoscience materials, devices, and their applications in functionally classified materials, molecular electronics, sensors, actuators, nanocomputers, and molecular machines outline the world of nanotechnology (Pérez López, 2009). Nanotechnology is the understanding and control of matter at dimensions between approximately 1-100 nanometers, where unique phenomena enable novel applications. Nanotechnology encompasses two main approaches: (i) the 'top-down' approach, in which larger structures are reduced in size to the nanoscale, and (ii) the 'bottom-up' approach, also called 'molecular nanotechnology' or 'molecular manufacturing' introduced by Drexler et al., in which materials are engineered from atoms or molecular components (Figure 1.6).

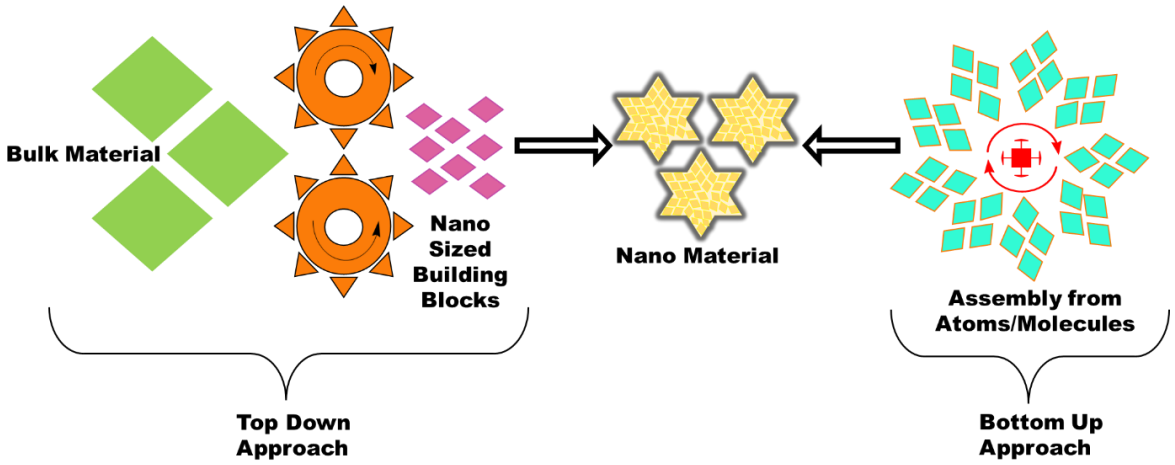

Figure 1.6. An illustration of the '*top-down*' and '*bottom-up*' approaches in nanotechnology.

One of the most intuitive effects arises in nanomaterials are the surface area to volume ratio change. When the size of the structure is decreased, the surface area to the volume ratio increases considerably, and the surface phenomena predominate over the bulk. Therefore, the decrease in the size of the transducer in a sensor to nano size can lead to new phenomena, and new sensor devices are being built taking advantage of these factors. The sensitivity of the bio/chemical sensors greatly depends on the characteristics of the transducer (shape, type of the material, size, etc.). As the high surface-to-volume ratio of the transducing element can increase the signal transfer efficiency, nanomaterials are ideal candidates to be used as components of transducers. Another major advantage of using nanostructures in sensing is that the number of receptors immobilized on the detector surface can be as low as a single molecule (Ambrosi, 2007). As a result, the amount of analyte required to generate a measurable signal could be just a few, providing for very low LODs. Therefore, in brief, the advantages of using nanomaterials in sensing include the following: nanomaterials can produce a synergic effect among catalytic activity, conductivity, and biocompatibility to accelerate the signal transduction; lower LODs, analysis of samples with lower amount/volume, cost reductions, direct detection and simpler assays (Kurkina, 2012) .

Real progress in nanotechnology has been commenced and huge activity has been generated in most areas of science since the discovery of atomically precise carbon nanomaterials and layered nanomaterials, due to the combination of exceptionally unique electrical, thermal, catalytic, optical and mechanical properties. These properties made them ideal for many applications in multifunctional fields. Particularly, graphene quantum dots

(GQDs), a carbon-based fluorescent nanomaterial, has emerged as a rapidly rising star in the field of material science. Recently metal nanoclusters (MNCs) are gaining attention amongst the researchers because of their merits such as emissive properties, prominent photostability, large Stokes shift of ≥100 nm, and lack of toxicity, which make them much suitable for applications such as sensors, biological imaging, catalysis, and light-emitting devices. Here, we wish to detail the exciting area of electrochemistry of GQDs and MNCs and the many advantages they bring forth for developing EC sensors.

1.5.1 Hetero Atom Doped Graphene Quantum Dots

Among advanced functional materials, carbon, one of the most abundant elements in the biosphere, plays a crucial role in developing high-performance and sustainable materials(Facure et al. 2020). It is well known that carbon-based materials comprise the most effective properties among all the resources on the earth, such as lightweight, high porosity high-temperature resistance, acid and alkali resistance, good structural stability, and easy conductivity(Saisree, Nair, and Sandhya 2022). The above-mentioned characteristics, together with the small background current, the wide potential window, and good electrocatalytic performance, have made carbon materials effective in many applications and devices with unlimited possibilities for development. In the carbon-based materials family, graphene remains one of the well-explored species.

Graphene is a mono-layer carbon nanostructure in which carbon atoms are assembled in a two-dimensional (2D) honeycomb crystal lattice. Graphene has had various applications due to its unique chemical, thermal, mechanical, and physical properties since its discovery in 2004 (Geim et al., 2004). These properties can be improved by manipulating redox reactions by manipulating the shape, size, and sp2- hybridized carbon domains. Photoluminescence is not observed in the case of graphene due to its zero bandgap which makes it an unsuitable material for optoelectronics and electronics applications (D. Chen et al., 2010). However, in zero-dimensional (0D) GQDs, the size is smaller (≤ 10 nm) than the exciton Bohr radius, there is a significant modification of the electron distribution that leads to size-dependent properties and quantum effects confinement and edge effects, which give rise to quantized energy states and size dependent bandgaps. Thus, by the intervening time from its discovery in 2008, the fluorescent nanomaterial, GQDs have attained great attention

in research areas due to their attractive properties such as tunable color emissions, photostability, biocompatibility, chemical inertness, higher surface area, reliable electrical properties, low toxicity, tunable properties by this pronounced quantum confinement, and edge effects(Hassan et al. 2014). An essential feature of GQDs is the presence of highly crystalline graphene sheets having dimensions below 100 nm in one-, two- and few layers (<10 layers). Generally, GQDs contain sp^2 or sp^3 carbon atoms and functional groups based on oxygen. GQDs are formed when graphene sheets are fragmented into less than the exciton Bohr radius (20 nm). The carboxylic groups located at the edges of GQDs enhance their water solubility as well as provide the potential for functionalization with many inorganic, organic, polymeric, and biomolecules. GQDs act as electron donors and acceptors due to their great surface area and many edge sites. A representative structure of GQDs is given in Figure 1.7a. These extraordinary properties of GQDs lead to the enhancement of their applications in various fields such as energy storage, biosensing, bioimaging, drug delivery, photocatalysis, and many others(Kumar et al. 2017).

In recent years, GQDs have been explored as a great candidate for sensing and detecting metal ions/biomolecules. The enhancement in sensing properties can be achieved through surface functionalization and doping with heteroatoms such as nitrogen (N), sulfur (S), boron, and phosphorous(B. X. Zhang, Gao, and Li 2014)-(Ge et al. 2019). Metal and transition metal ions can be toxic, limiting their doping application, furthermore, the radius of metal and transition metal atoms is generally larger than that of carbon atoms, so doping them into GQDs often leads to inhomogeneous and ineffective incorporation. The heteroatom doping can effectively tune the intrinsic properties of GQDs, including electronic characteristics, optical activity, and surface and chemical features. In addition, they have better biocompatibility for applications in human medicine. The N-atom has been widely used for the chemical doping of GQDs. The N possesses similarity in atomic radius (0.75 Aº) with carbon (0.77 Aº) and greater electronegativity (χ_N = 3.04) than C (χ_C = 2.55), making it easier to incorporate N into the carbon network(Mondal, Dinda, and Saha 2018). A general structural representation of N-GQD is given in Figure 1.7b. The N-GQDs mainly consists of three major types of bonding configurations: (i) graphitic N, where nitrogen heteroatoms are substituted on the inner surface of graphene in a hexagonal ring, (ii) pyrrolic, and (iii) pyridinic, where both are found at edge defects. The hybridization of pyridinic N is $sp^{2,}$

whereas pyrrolic N is sp^3 hybridized. A difference between the electronegativity of N and C in the N-GQD resulted in numerous applications in sensing, electronics, energy storage devices, and catalysis. Conductive properties have been explored for their applications in EC sensing, batteries, and supercapacitors. Optical and catalytic properties are also envisioned for their applications in sensing and catalysis.

The S atom (1.05 Aº) being much larger than the C atom. Because the two atoms have different outermost orbitals, the combination of S in GQDs results in an uneven spin density distribution. The difference in electronegativity between S (2.58) and C (2.55) is very small, suggesting that the driving force for electron transfer between the C and S is low. These characteristics all make S doping into a GQD framework difficult and doping GQDs with S atoms can lead to enhanced electronic, catalytic and emissive properties(Sohal, Maity, and Basu 2021). Despite these challenges, multiple methods for preparing S-doped GQDs (S-GQDs) and S and N co-doped GQDs (S,N-GQDs) have recently been reported, showing the potential interest by the research communal(B. Li et al. 2021). The superior photocatalytic ability and promising prospects were well explored on lithium batteries due to the high electrocatalytic activity and conductivity resulting from N to S co-doping. Optical property characterization is an important method for understanding carbon-based nanomaterials. Although doping with N could effectively tune the absorption and photoluminescent characteristics of GQDs, S co-doping can significantly alter the emission properties further(Bian et al. 2016). Thus, S,N-GQD provides a higher quantum yield than N-GQD and GQD. These results can be attributed to the higher N coverage on the C sp^2 skeleton of S,N-GQDs, and the sulfur-containing groups, which promote the electron-hole recombination. Thus, these properties make hetero atom doped GQDs, N-GQDs, and S,N-GQDs highly suitable for EC sensing platforms. Here we focus on the synthesis of heteroatom(s) (S and N) doped GQD using simple hydrothermal synthetic approaches and further exploring their diverse properties in EC sensors for sensing toxic metal ions and biomolecules.

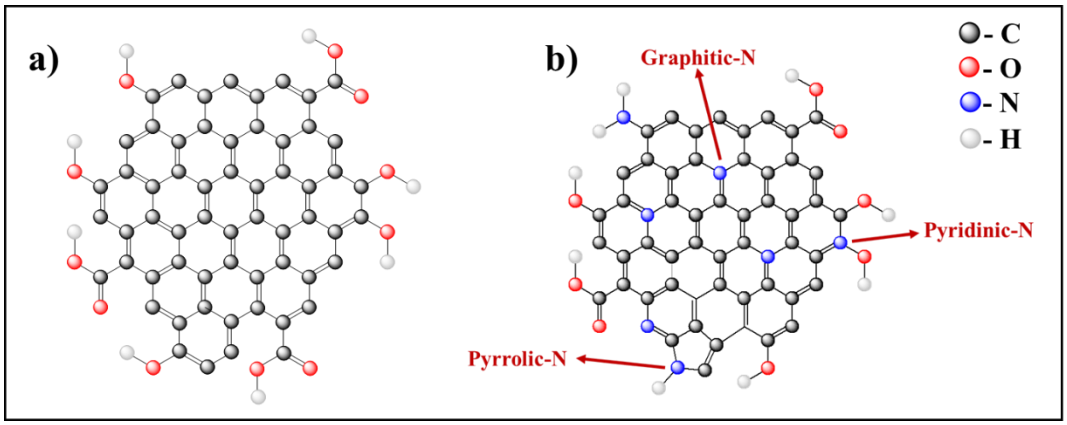

Figure1.7. A representative structure of (a) GQDs and (b) N-GQDs

1.5.2 Metal Nano Clusters (MNCs)

Noble MNCs are a class of materials that bridge the gap between nanoparticles and atoms, making this area fascinating(Publication et al. 2017). They possess a sub nanometer core size with discrete energy levels and exhibit molecule-like properties in their absorption and photoluminescence features. MNCs are made up of tens to hundreds of atoms and have intermediate composition between bulk and molecular regimes, where the electronic band structure of the bulk gets modified to discrete electronic states as a result of quantum confinement. MNCs exhibit strong photoluminescence, and their emission can be tuned from the near-infrared (NIR) region to ultraviolet (UV) by decreasing the core size and also by varying the metal used. In the past decade, gold (Au) and silver (Ag) have been extensively synthesized and studied using alkanethiols and other ligands as protecting agents by taking advantage of the strong affinity of thiol, amido, or phosphine groups to noble metal surfaces and their excellent stability in different media(Gui et al. 2014). AuNCs have been particularly well-studied because of their extraordinary chemical stability and a wide variety of optical properties. However, commensurate expansion has not happened in the area of AgNCs. Copper (Cu) is widely used in industry because of its high conductivity, similar properties to gold and silver, and much lower cost. However, compared to the extensive studies on Au and Ag, reports on CuNCs are still scarce primarily because of their susceptibility to oxidation(W. Wang et al. 2014). Hence, we detail the synthesis of stable CuNCs using various synthetic approaches which give them different properties, and the many advantages they bring forth in EC sensors for sensing toxic metal ions and biomolecules.

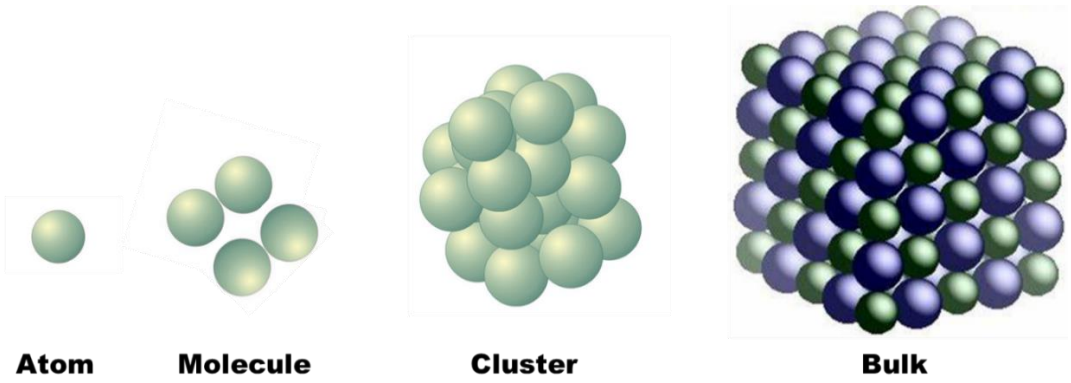

Figure 1.8. Schematic representation showing the distinction of cluster from molecule and bulk material.

MNCs have recently attracted a great deal of interest in sensing, catalysis, biology, biomedicine and energy applications due to many unique properties of MNCs, such as the well-defined structures, optical absorption, luminescence, catalytic activity, and magnetism, to name a few. Such properties are not seen in the corresponding bulk materials or nanomaterials with larger sizes. More significantly, the properties of MNCs are sensitive to the size, composition, surface charge state, and structure, therefore providing opportunities for tailoring of properties and guiding the design for specific applications of MNCs. One of the most attractive properties of MNCs is their strong photoluminescence combined with good photostability, large Stokes shift, and high emission. Each size of NCs has its feature profile of optical absorption, which is different from plasmonic nanoparticles. These unique aspects make MNCs highly promising in chemical sensing and biosensing applications. The ligand shell in the outer layer of the MNCs can be tailored by employing biomolecules, such as polymers, dendrimers, proteins, peptides, and DNAs to control the biocompatibility and to enhance the stability and luminescence intensity, thus establishing MNCs as a new class of ultrasmall biocompatible fluorophores in bioassays. MNCs have also shown great potential for catalyzing many important chemical transformation reactions owing to their good activity (higher surface-to-volume ratio than conventional nanoparticles) and high selectivity under relatively mild conditions. Niesen et al. developed a novel thin-film light-emitting device using MNCs. The electroluminescence of these light-emitting devices is tunable by choice of MNC. Apart from AuNCs, Ag, and CuNCs have also been used for organic light-emitting devices. The sensing or detection of chemical and biological agents plays a fundamental role in the environmental, biomedical, and forensic fields. Fortunately, MNCs provide excellent

scaffolds for sensing various compounds since the atomically precise NCs are better for understanding the sensing mechanism, including, for example, metallophilic interactions, electron or energy transfer, Förster resonance energy transfer, anti-galvanic reaction, etc. The atomically precise MNCs are expected to have a great leap in future research, not only in fundamental science research but also in practical applications. The development of multifunctional sensors is quite attractive for practical applications. In the wake of this, the cluster community has begun to investigate functional NCs comprising two or more metal species. Such bi- or multi-metallic NCs have quickly emerged as new and promising members of the MNC family.

In principle, integrating two or more metal species into one cluster may have the following attractive features as compared to their mono-MNC analogs:

1) The physicochemical properties of two metal species can be easily integrated into one bi-MNC.
2) Some synergistic effects such as strong luminescence could be realized in bi-MNCs.
3) Bi-MNCs' electronic structures could be further tailored by controlling their sizes, compositions, and structures (e.g., core-shell, alloy, and hetero-structure), particularly at the atomic level.

Thus, atomically precise NC research has emerged as an exciting frontier in recent years and is expected to flourish in the future.

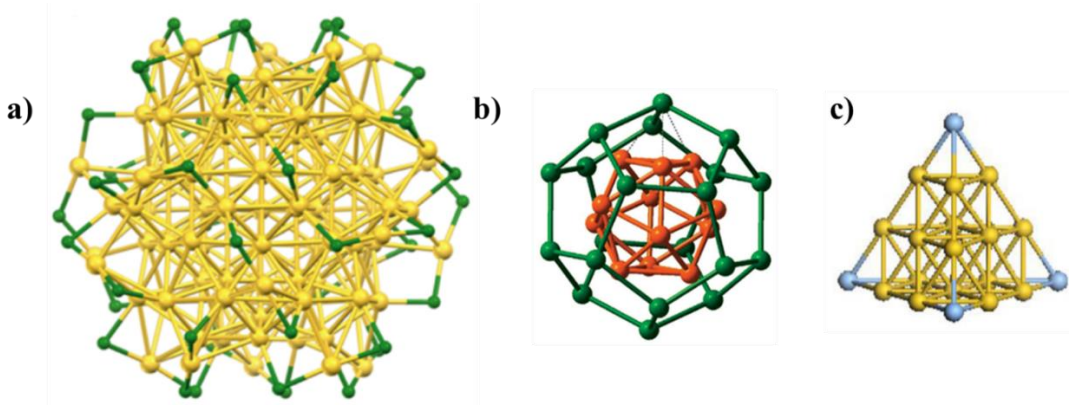

Figure 1.9. The structural representations of (a) AuNC, (b) and (c) AuCuNC

1.6 A Brief Review on GQD and MNC Based Materials in EC Sensing Applications

As mentioned earlier, the outstanding physical and chemical properties of GQDs were exploited for the EC sensing of various chemical/ biological species. The GQD-based EC sensors include modified electrodes with GQDs, functionalized GQDs, and heteroatom-doped GQDs. The EC sensing capability of GQD-based materials is the most extensively studied towards biomolecules and toxic contaminant sensing. Here we describe a few examples of GQD-based materials for the EC sensing of biomolecules and harmful contaminants, including metal ions.

In the last decade, there have been enriched studies on EC sensing capabilities of GQDs owing to their ease of synthesis and subsequent functionalization, intense surface chemistry, biocompatibility, and high electron mobility with high-speed reaction, which makes them to be recognized as an excellent sensing material. Because of more surface atoms and edge atoms that facilitate higher surface interaction/adsorption in GQDs makes them a better sensor material than 2D nanomaterials. In addition, the better solubility of GQDs in water can lead to easy processing and facilitate its functionalization through the hydrophilic groups present on their surface (e.g., hydroxyl, carboxyl, etc.), increasing their catalytic effect on various redox reactions.

The significant development of industrial and agricultural activities greatly contributes to the improper discharge of pollutants into the environment. Consequently, environmental monitoring of toxic pollutants in various environmental media has become a great healthcare concern due to their lethal, hazardous, and adverse effects on the environment and human health. Several reports appeared in the literature that discuss the selective and simultaneous EC sensing of hazardous pollutants in the environment. GQDs-based materials have been reported for the detection of toxic metal ions, including that of mercury(B. Li et al. 2021), chromium(Shellaiah et al. 2019), and copper(B. Li et al. 2021). In 2016, Xuan Jian et al. developed a GQDs modified glassy carbon electrode to detect hydroquinone and catechol in water (Jian et al., 2016). A N-GQD synthesized from citric acid

and urea, and combined with luminol, has been investigated for the detection of hydrogen peroxide in water samples (Jiang et al., 2016). Likewise, Tan et al. developed an EC sensor based on the GQDs composite electrode for the detection of bisphenol A in water by using DPV (Tan et al., 2016). A highly selective and sensitive detection of 4-nitrophenol in an aqueous solution was achieved through S-doped GQD based material(Anh and Doong 2018). Further, there are reports on the EC sensing of olanzapine; an anti-schizophrenic drug that employs the sensing capability of N and S co-doped GQD-based nanohybrid materia(Mahmoud et al. 2020). A simple and diverse approach to the synthesis of N-GQDs for the ultra-trace level EC detection of trinitrophenol and an effective differentiation strategy for the nitroaromatics were put forward by Aswathi et al. (Aswathi et al., 2019).

Selective and simultaneous EC sensing of neurotransmitters, which constitute a series of compounds, that have important physiological roles in the metabolic system of living bodies, holds another important application of GQD-based electrodes for which a number of reports have appeared in the literature. Neurotransmitters, for instance, dopamine (DA), epinephrine (EP), serotonin (SER), etc., are endogenous chemical messengers in the nervous system that influence a wide range of both psychological and physiological functions of the brain. An abnormal level of their concentration in the human body leads to various neurodegenerative diseases such as Alzheimer's, Parkinson's, Huntington's, depression, and schizophrenia(Cai et al. 2020). For this reason, the use of fast, accurate, inexpensive, and biocompatible GQD-based electrochemical sensors that allow on-site detection and the possibility of detecting two or more analytes instantaneously ensures high selectivity and sensitivity, has aroused particular interest in scientific research.

Similarly, a chitosan/N-GQDs nanocomposite has been utilized as an EP sensor by Tashkhourian et al. (Tashkhourian et al, 2018). An ultra-sensitive DA sensor was developed by Ruiyi et al., involving histidine functionalized GQDs (Ruiyi et al., 2017). In another study, a GQD-based screen-printed carbon electrode sensor responded by a redox reaction with DA, AA, and UA. One of the most interesting EC approaches for detecting DA and EP was proposed by Vinoth et al. (Vinoth et al., 2019). The large electroactive surface area, effective ring-stacking, π–π bonding and electrostatic interaction between the GQDs and DA-led to an excellent electrocatalytic activity in oxidizing DA and providing high sensitivity and selectivity. Additionally, GQD-based materials were also utilized to sense other biologically

relevant molecules. Hasanzadeh et al. synthesized a nanocomposite of Fe_3O_4 magnetic nanoparticles and GQDs, which exhibits an excellent electrocatalytic activity toward the electrooxidation and detection of many amino acids such as L-cysteine, L-aspartic acid, L-phenylalanine and L-tyrosine (Hasanzadeh et al., 2016). Further, simultaneous sensing of estradiol and progesterone was put forward based on poly (sulfosalicylic acid) doped GQDs (Arvand et al., 2017). Similarly, GQD-based electrodes have been fabricated as effective sensors for the sensitive detection of molecules such as quercetin (Li et al., 2016), norepinephrine (Fajardo 2019).

Similar to GQD, MNC-based materials are also emerging as attractive materials for EC applications recently, owing to their high electrocatalytic efficiency, which has been harnessed for developing highly sensitive EC sensors. The emergence of MNCs grab the position held by metal nanoparticles in EC sensing through its unique redox properties. The metal nanoparticles are redox inactive, and thus, they were typically immobilized into a modified electrode along with a redox mediator or a redox enzyme. Whereas the extraordinary electrochemical characteristics of MNCs comprise their redox-active nature and thus can function as an electron transfer mediator as well as an electronic conductor. Kumar et al. first demonstrated the AuNC-based amperometric sensing of biologically important analytes; AA and UA (Kumar et al., 2011). Kwak et al. reported selective determination of DA (Kwak et al., 2012). Similarly, another nonenzymatic glucose biosensor was put forward based on AgNCs(X. Gao et al. 2018). An EC sensor for nitrate ion and total N based on a CuNC-based sensor was put forward by Xia et al. (Xia et al., 2013). Parallelly, reports on sensitive EC detection of H_2O_2 by applying the sensing capabilities of CuNCs are also available(X. H. Gao et al. 2016). Another advantage of an MNC-based sensor is that the ligand shell can be engineered to improve the sensing characteristics such as sensitivity and selectivity. For instance, an excellent DA sensor was developed by utilizing an AuNC-glutathione-based sensor, where glutathione act as charge selective ligands that enable better sensing characteristics for AuNC towards DA.

As mentioned earlier, graphene is an ideal material for many electrochemistry applications because of its large surface area and excellent 2D electron conductivity. Thus, combining metal NCs with graphene and graphene-based systems is expected to endow the NC composites with enhanced electrochemical properties and improved electrochemical

sensing. An AgNC-graphene-based nanocomposite was labelled with a detection antibody for the EC sensing of carcinoembryonic antigen, a tumor marker present in several cancer types (Wang et al., 2016). The catalytic activity of these AgNC-graphene oxide nanocomposites toward the EC reduction of H_2O_2 was significantly higher than the bare AgNCs due to synergistic effects between AgNCs and graphene oxide (Chen et al., 2011). Moreover, a sensitive electrochemical acetylcholinesterase biosensor based on AgNC-graphene composites was also developed (Zhang et al., 2015)). Then again, AuNCs were incorporated into graphene to sense HIV DNA (Wang et al., 2015) electrochemically.

1.7 Objective and Scope of the Thesis

As mentioned, electrochemistry-based analytical methods such as EC sensors have impacted multiple fields, including diagnostics, environmental analysis, food sciences, enzymatic kinetics, and pharmacology (Govindhan et al.,2014). Recently, the assembly of miniaturized EC devices using various nano functional materials/ their composites have been demonstrated for the EC detection of several electroactive targets of importance in food analyses, environmental monitoring, and clinical diagnosis. The electrode materials play a critical role in the selectivity and sensitivity of EC sensing platforms for detecting target molecules through various analytical principles. Furthermore, in addition to the electrode materials property, making them nanosized can produce a synergic effect among catalytic activity, conductivity, and biocompatibility to accelerate the signal transduction and amplify recognition events by specifically designed signal tags, leading to highly sensitive sensing (C. Zhu et al., 2014). Significantly, extensive research on the construction of functional electrode materials, coupled with numerous EC methods, is advancing the wide applications of EC devices. Motivated by the excellent properties ofe GQD and MNC in this work we have tried to exploit these materials for the EC sensing applications of various analytes owing to their interactions with these materials. The Materials too we have adopted methods or strategies to exhibit better properties such as conductivity, stability and catalytic activity for acheiving better sensing results.

For the successful EC sensing applications, there may exist a number of challenges associated with both the electrode material (here GQD and MNC based), such as processability, ease of production, bulk preparation; and the analyte

(biologically/environmentally important species) under consideration, which include the need for high sensitivity, selectivity, reproducibility, etc. At this moment, we attempted to address some of the challenges and explore the use of GQD and MNC-based materials for the highly sensitive and selective detection of various analyte species, which are important either biologically/or environmentally. The specific challenges and merits of the electrodes developed has been discussed for each work in detail. We identify the specific objectives of the present research as,

- Development of GQD and MNC based nanomaterials (as electrode materials)
- Characterization, electrode modification, and EC sensing studies of the developed materials
- Identification of biologically/environmentally important analytes and detection of them using selected electrode materials based on affinity/interactions between them
- Investigation of the underlying mechanism involved in the sensing

1.8 Organization of the Thesis

This thesis describes the research work on the development of various GQD and MNC-based materials as EC sensors, characterization of the materials, electrode modification, and EC sensing studies. Our research focuses on identifying/selecting suitable electrode materials for detecting biologically/environmentally important analytes based on the affinity/interaction and between them so that better sensitivity and selectivity shall be achieved, which is investigated by the systematic EC sensing studies. The underlying mechanisms involved in the sensing are studied and discussed based on the results. The thesis is organized into eight chapters, as given below.

Chapter 1 provides a detailed introduction to the basics & fundamentals of electrochemistry, discusses the various EC methods, and explains the background and basics of EC sensing. It provides state-of-the-art literature survey on GQD and MNC-based materials in EC sensing. Further, it discusses the objectives of the current research work.

Chapter 2 is the experimental section that describes the materials and methods used to synthesize various GQD and MNC based materials, various experimental procedures adopted for the preparation/modification of EC electrodes, and other general procedures for

systematic EC sensing studies. Various characterization techniques used are also discussed in this chapter.

Chapter 3 explores the EC sensing properties of the polyaniline-derived N-GQD, towards the selective detection of Cd (II) with commendable sensitivity. The sensing mechanism is discussed in detail and is confirmed using various characterization techniques.

Chapter 4 discusses the synthesis of a white emissive sulfur co-doped nitrogen-doped graphene quantum dots, S,N-GQD, from polyaniline for the simultaneous EC sensing of hazardous heavy metal ions. The advantages of the structure and the possible reasons for better performance are also proposed.

Chapter 5 describes the synthesis of highly stable CuNC by utilizing the reduction capability of N-GQD, CuNC@N-GQD, and its EC sensing capability towards three functionally correlated neuro-active molecules. In addition to that, the structure of CuNC@N-GQD is proposed based on characterization studies, and the mechanism for simultaneous sensing is explained.

In **Chapter 6,** a simple and effective synthesis strategy to achieve a gold-copper bimetallic nanocluster, AuCuNC@N-GQD is discussed. Further, the highly selective EC sensing behavior of AuCuNC@N-GQD towards the amino acid glycine is explored, and the mechanism is discussed.

Chapter 7 exploits the EC sensing capability of AuCuNC@N-GQD towards the hazardous heavy metal ion, Pb(II). The selective sensing mechanism is discussed and confirmed using various characterization techniques.

Chapter 8 summarizes the highlights and the output of the research work and the future possibilities in this area.

CHAPTER 2

MATERIALS AND METHODS

This chapter gives a detailed description of the materials and the methods used for the synthesis of the GQD and MNC based functional materials and mention the various characterization instruments used for studying the structure and composition of the materials. Further, the methods used for the cleaning preparation/modification of the electrodes and the various electrochemical procedures adopted herein for the studies along with the general procedures for reusability, reproducibility and stability studies of the developed EC sensors.

2.1. Materials

Dopamine (DA), acetyl choline (Ach), glucose anhydrous (Glu) and ascorbic acid (AA), uric acid (UA), folic acid (FA), nicotine (NIC), serotonin (SER), 2,4,6-trinitrophenol (TNP), $FeCl_3$, $FeCl_2$, $SnCl_2$, $AuCl_3$, and $CuSO_4$ were purchased from Sigma Aldrich India Co. Ltd., hydrogen peroxide (H_2O_2), sulfuric acid (H_2SO_4), hydrochloric acid (HCl), sodium hydroxide (NaOH), di-sodium hydrogen phosphate dihydrate, sodium dihydrogen phosphate monohydrate, aniline, ammonium peroxydisulfate (APS), chloroform, glutathione (GSH), glycine (GLY), alanine (ALA), valine (VAL), leucine (LEU), isoleucine (IsLEU), lysine (LYS), phenylalanine (PhALA), serine (SRN), threonine (THR), tryptophan (TRY), tyrosine (TYR), methionine (MET), proline (PRO), cysteine (CYS), histidine (HIS), arginine (ARG), asparagine (ASP), aspartic acid (AsA), glutamic acid (GA), and glutamine (GLN) were purchased from Merck, India Ltd., $MgSO_4$, $MnCl_2$, $NiSO_4$, $LiCl_2$, $HgCl_2$, $AgNO_3$, $CdCl_2$, $NiSO_4$, $Zn(NO_3)_2$, $Co(NO_3)_2$, $PbNO_3$ and $K_2Cr_2O_7$, were obtained from Spectrochem Pvt. Ltd. Distilled water was used in all the procedures unless specified otherwise. All the solvents and reagents used in this study were of analytical grade.

2.2. Characterization Techniques

Several techniques such as spectroscopic, microscopic and thermal are performed for the characterizations of synthesized materials. Fourier transform Infra-red (FTIR) spectra were recorded in a Perkin Elmer spectrum100 FTIR spectrophotometer. The range of FTIR spectra is 4500- 400 cm^{-1} with an optical resolution of 0.5 cm^{-1}. Absorption spectra were recorded using CARY 100 Bio UV-Visible spectrophotometer. Photoluminescence (PL) spectra were recorded in Horiba FluoroMax-4 with the excitation and emission slits of 1 and 2 nm respectively. Raman spectroscopic measurements were carried out in Renishaw in Via Raman microscope with the excitation laser wavelength of 532 nm. X-ray diffraction (XRD) analyses were carried out on a Bruker D8 discover small angle X-ray diffractometer. The Cu Kα radiation (λ = 1.54 Å) was used as an excitation source. XRD pattern also allows estimating crystal size by Debye-Scherrer equation as given in equation 2.3. This equation gives the relationship between diffraction peak broadening (β) and crystallite size (D),

$$D = \frac{0.94\,\lambda}{\beta cos\theta} \qquad (2.1)$$

Scanning electron microscope (SEM) images were taken using Hitachi SU6600 variable pressure field emission (FE) SEM. High resolution transmission electron microscopy (HRTEM) analyses were done using JEOL JEM 2100 electron microscope with an accelerating voltage of 200 kV. X-ray photoelectron spectroscopy (XPS) analyses were carried out using Kratos analytical axis ultra-X-ray photoelectron spectrometer with the excitation source of Al Kα. X-Ray photoelectron spectra were peak-fitted using MultiPak Version 9.6.0.15. Mass spectra were recorded using a Bruker Q-time-of-flight (COMPACT) mass spectrometer through electron spray ionisation in negative ion mode with a quadrupole ion energy of 5 eV, collision energy of 10 eV and a transfer time of 120 μs. A methanol–water mixture (50 : 50) was used as the electrospray solvent. Electrochemical Impedance Spectroscopy (EIS) studies were carried out between 100 mHz and 100 kHz at the open circuit voltage.

2.3. Methods

2.3.1. Electrochemical measurements

For EC sensing studies, all the EC measurements were carried out with potentiostat/ galvanostat PG 302N, AUT 83909 (Metrohm, Autolab, Netherlands) with three electrode system using glassy carbon electrode (GCE) with 3 mm diameter as working electrode, Pt wire as counter electrode and Ag(s)/ AgCl(s)/ Cl^{-1}(aq., saturated) as reference electrode. The voltammetric experiments were carried out using various techniques including CV, DPV, LSV etc. The voltammetric parameters in each technique, as well as the electrolytes vary with the sensor material as well as the analytes under consideration, which are discussed in each chapter in detail. Amperometric measurements, particularly pre-concentration studies were done by using chronoamperometry at required (specified) voltages.

2.3.2. Electrode cleaning, preparations/Modification

Prior to modification of GCE with the samples, they were mechanically polished with a wetted microcloth containing alumina powder (0.05 mm), and then carefully cleaned in distilled water and in acetone by ultra-sonication (2 minutes each). The dried GCEs were modified with the material samples by drop-dry casing method, the details are given in each chapter separately. In a general procedure, the electrode modification was done by dropcasting 20 µL of 0.5 mg ml^{-1} freshly ultrasonicated dispersions of the materials (in suitable solvents), to ensure that roughly the same amount of material is deposited onto the electrode surfaces. The dropcasted GCEs were dried under air or sometimes under the stream of nitrogen depending on the material behaviour. After each analysis, GCEs were cleaned by mechanical polishing followed by ultrasonication in the solvent, distilled water and in acetone.

2.3.3. Reusability, reproducibility and stability studies

In general, the reusability and storage stability of the developed sensor electrodes were evaluated using CV or DPV experiments by comparing the oxidation/reduction peak currents obtained in respective electrolytes containing a particular concentration of the respective analyte species immediately after washing, and after a period of a few months respectively. The percentage of retention of the initial current responses were calculated and recorded. Measurement on five independently prepared electrodes were used to estimate the reproducibility, the relative standard deviations (% RSD) in the oxidation/reduction peak currents in CV/DPV for a particular analyte concentration were measured. RSDs were obtained by using the formula,

$$RSD = 100 \times {}^{s}/_{\bar{x}} \qquad (2.2)$$

Where s is the sample standard deviation and $\bar{x}$ is the sample mean.

2.3.4. Real sample analysis

2.3.4.1. Blood/Urine sample analysis

The general procedure adopted for real blood/urine sample analysis involve spiking of real human blood/urine sample via standard addition method, where known amounts of the analyte samples were added to the diluted(1000 times) blood/urine sample, analyzed electrochemically using CV/DPV methods and the recovery amounts were measured.

2.3.4.2. Water sample analysis

The real water sample analyses were carried out by extending the sensing studies to the samples such as sea, tap, ground and waste water. The details are given in each chapter. In general, the samples were spiked with the analyte under study at different concentration levels, analyzed with the proposed EC method and the recovery amounts were calculated.

The recovery calculations were done using the formula,

$$\%\ Recovery = \left(\frac{C_{found} - C_{spiked}}{C_{spiked}} \times 100\right) + 100 \qquad (2.3)$$

Where C is the concentration of the analyte species under study. The high recovery values in real sample analysis are indicative of the successful applicability of the developed sensors in real environments.

2.3.5. Sensitivity, LOD and Bandgap Calculation

2.3.5.1. Sensitivity Calculation

The sensitivity of an electrode depends on the current response, concentration of the analyte and also the area of the electrode used. They are related as,

$$Sensitivity = \frac{Current\ response}{Concentration\ of\ analyte * Area\ of\ electrode} \qquad (2.4)$$

2.3.5.2. LOD Calculation

$$\text{LOD} = \frac{3\sigma}{\text{m}} \qquad (2.5)$$

σ- The standard deviation of the current responses of blank

m- Slope of Current vs Concentration graph

2.3.5.3. Bandgap Calculation

Bandgap = Energy of conduction band (E_{CB})- Energy of valence band (E_{VB})

Energy of conduction band (E_{CB}) = -4.8-(E_{pa}-$E_{1/2}$) eV

Energy of valence band (E_{VB}) = $-4.8-(E_{pc}-E_{1/2})$ eV

E_{pa} – Oxidation potential

E_{pc} – Reduction potential

$E_{1/2}$ –Half wave potential

CHAPTER 3

Radical Sensitivity and Selectivity in the Electrochemical Sensing of Cadmium Ions in water by a Polyaniline Derived Nitrogen Doped Graphene Quantum Dots

In this work, the sensing capability of nitrogen doped graphene quantum dots (N-GQDs) was explored for the first time towards hazardous heavy metal ions and found to be selectively detecting cadmium ions (Cd (II)), one of the hazardous heavy metal ions in the World Health Organization's list of 10 chemicals of major public concern. The aromatic N-GQDs, synthesized through hydrothermal route using a single precursor polyaniline exhibited a 25 and 6-fold increase in the current response compared to that of a glassy carbon electrode (GCE) and GQD/GCE, respectively. Further, the reasons for the excellent selective sensing property of N-GQD were evaluated and discussed. The effective N doping seems to play a crucial role in the sensing performance of N-GQDs. The higher reducing capability of N-GQD attributed to the spontaneous reduction of Cd(II) on N-GQDs. Further, the sensing performance of N-GQD/GCE was extended to real environmental samples spiked with Cd(II) such as groundwater, seawater and wastewater efficiently.

3.1 Introduction

The toxic heavy metal ions are a class of contaminants which requires rigorous attention because of its inimical toxicity and widespread use(Saied, Zahir, and Siddique 2010; Sharma, Agrawal, and Marshall 2006; Shtepliuk et al. 2017). Because of this, cadmium (Cd), mercury, lead and arsenic etc. appear in the World Health Organization's (WHO) list of 10 chemicals of major public concern. The wide use of Cd (II) in industrial applications including Ni-Cd rechargeable batteries, electroplating, cigarette smoke, industrial, agricultural fields and so on (Nordic Council of Ministers 2003) and the acute and chronic effects of Cd (II) on health such as reproductive failure, damage to the central nervous system, heart diseases, emphysema, hypertension, renal damage, DNA damage and cancer and on the

environment emphasis the need for the strict monitoring of Cd (II) in water sources. The maximum permissible limit of Cd (II) in drinking water is ≤ 5 ppb as per the U.S. Environmental Protection Agency (EPA)(Zazoua et al. 2018). Therefore, it is critical to develop and implement quantitative sensing methods to monitor these components in wastewater and drinking water. Currently, the detection and monitoring of the concentrations of these heavy metals including Cd (II) in the environmental samples, are done by analytical instruments(Ene, Boşneagă, and Georgescu 2010; Heidarieh et al. 2013; Saied, Zahir, and Siddique 2010) which are bulky, expensive, and complex to operate such as atomic absorption spectrometry, inductively coupled plasma emission or mass spectrometry, X-ray fluorescence spectrometry and neutron activation analysis. The electrochemical (EC) sensing is an appealing method because of its high inbuilt sensitivity, low-cost, trouble-free operation, rapid analysis and portability(Mhammedi et al. 2009), which requires a highly selective and sensitive electrode material because of the complexity of the environmental samples and the ultra-low concentrations (≤ 5 ppb) of Cd (II) that need to be detected. The previous reports of the selective EC sensing of Cd(II) by different materials include, polyphenol natural extracted from pomegranates and acorns with limit of detection (LOD) values of 0.01 and 0.1 ppb, respectively(Zazoua et al. 2018), SnO_2 quantum dots with a detection limit of 500 ppb (Bhanjana et al. 2015), a metal-organic framework and polyaniline (PANI) based material reported by Wang et al., with a 0.3 ppb LOD in the EC sensing of Cd (II) (Y. Wang et al. 2017), a coconut shell powder modified carbon paste electrode which showed a LOD of 105 ppb (Rajawat, Kumar, and Satsangee 2014), a benzenesulfonyl hydrazide based electrode with a detection limit of 0.015 ppb(Arshad et al. 2017) and kaolin platinum electrode (K/Pt) with a LOD of 0.604 ppb(Mhammedi et al. 2009). Though a few of the materials reported have sensitivity in the applicable concentration range, an ideal electrode material must have good selectivity in addition to simple synthesis procedure, low cost of production, environmentally benign along with desirable sensitivity.

Here in this work, we have utilized a non-toxic, environmentally friendly material, N-doped graphene quantum dots (N-GQDs) for the EC sensing of Cd (II). The N-GQDs were synthesized through a simple hydrothermal route from PANI using an earlier procedure from our group(Ramachandran, Arya Nair, and Karunakaran Yesodha 2019). There has been no report of the EC sensing studies of N-GQDs towards heavy metal ions and this is a first-time

report of the same. The GQDs are one of the evolving carbon-based nanomaterials(Joshi et al. 2016)with low cytotoxicity and biocompatibility and are anticipated as potential candidates in the fields of biosensors and bio-imaging devices. Graphene-based nanomaterials, more precisely the graphene quantum dots (GQD) got much attention. That is due to its exceptional characteristics from the synergistic effects of both graphene and carbon dots. Thus, the zero-dimensional GQDs holds higher surface area, reliable electrical properties, excellent photoluminescent features, low cytotoxicity and bio-compatibility. Hence, they are anticipated as appropriate candidates for biosensors, bio-imaging devices, photovoltaic devices, fuel cells and light-emitting diodes(Faridbod and Sanati 2018). The surface functionalization and heteroatom doping can alter its attributes by generating more active sites in it which further enhances the features and facilitate the suitability for these applications. Here, the N-GQDs with an efficient Nitrogen (N) doping ~10 % and aromatic structure have better electronic characteristics than that of GQDs because of the lowering band gap which enhances the availability of electrons and the conductivity of the material. Further, the doping increases the active sites in the N-GQDs and further enhances the conductivity and electrocatalytic activity and the crystalline (graphitic) structure also intensifies the conductivity, and together expected to facilitate better performance in EC sensing. Interestingly, the N-GQDs modified GCE (N-GQD/GCE) exhibited very high sensitivity towards Cd (II) with a limit of detection (LOD) of 0.00001 ppb, i.e., ppt range without pre-reduction step and that of with the pre-reduction step exhibited a LOD which is 100 times lower ie., 0.0000001 ppb (in the ppq level). The LOD obtained from the slope of the LDR (without the pre-reduction step) was 0.0008 ppb (S/N=3), i.e. in the ppt range, which is significantly lower than the safe limit (≤ 5 ppb). Both the experimental as well as the calculated LOD values are the lowest reported till date for the Cd (II) sensing. The N-GODs exhibited higher selectivity for Cd(II), with no interference from metal ions including Hg(II), Ag(I), Pb(II), Fe(II), Co(II), Ni(II), Zn(II), Sn(II), Cu(II) and Cr(VI) in the potential range of - 1.2 to - 0.4 V. The sensing performance was extended to real samples spiked with Cd (II) such as groundwater, seawater and wastewater, effectively.

3.2 Experimental Section

3.2.1 Synthesis of N-GQD

The procedure for the synthesis of N-GQDs by our group is reported(Ramachandran, Arya Nair, and Karunakaran Yesodha 2019) elsewhere in detail. PANI was used as the precursor and using a simple hydrothermal route, N-GQDs with aromatic and crystalline nature were obtained.

The GQDs were synthesized from citric acid (1 mM) as the precursor and using a simple hydrothermal route at 180°C for 4 h.

3.2.2 Preparation of electrodes for EC sensing

The pre-treatment and modification of GCE were done according to the procedure given in the experimental chapter. The N-GQDs sample was drop cast over the cleaned GCE with care and then allowed to dry for 24 hours at the RT to achieve the modified electrodes. The coating thickness was optimized by trial and error by varying the drop casting volumes from 20-100 μM.

Further for the proof for the N-GQD-Cd interaction characterizations were carried out. The procedure for the preparation of the sample for the characterization is as described. The N-GQDs were mixed with $CdCl_2$ solution and the product formed was washed well and dried.

The real environment samples spiked with Cd(II) were prepared using one groundwater, seawater from two different regions as well as one wastewater sample. The blank readings corresponding to each of the samples were carried out and the current response, if any, was subtracted from each result to obtain the values (corrected for blank). The corresponding recovery values as well as RSD were calculated.

3.2.3 Electrochemical methods

The EC behavior of various metal ions (Hg(II), Ag(I), Cd(II), Ni(II), Zn(II), Co(II), and Pb(II)) on the surface of the N-GQD/GCE was investigated using CV, DPV and

chronoamperometry at RT. 0.1 M PBS was used as the electrolyte for the studies.

The pre-reduction studies are carried out by applying the reduction potential of -0.95 V prior to the oxidation sweep. Then the oxidation and reduction half cycles were carried out.

3.3 Results and Discussions

3.3.1 Synthesis and characterization of N-GQD

The N-GQDs were synthesized using an earlier method reported by our group. The significance of this synthesis approach is the aromatic nature of the precursor PANI and the presence of N in situ, which facilitates the formation of N-doped GQDs without the need of additional doping agents which yielded aromatic and crystalline N-GQDs. The structure benefits N-GQDs as an electrode material due to the improved conducting properties and to act as a good reducing agent. A schematic of the synthesis of N-GQDs is exemplified in Figure 3.1A. The obtained N-GQDs were characterized using various techniques.

The HRTEM images of the as-synthesized N-GQDs confirm that they have a fairly uniform and narrow size distribution (Figure 3.1B and C) ranging from 2 to 3 nm (Figure 3.1D). The formation of N-GQDs was further confirmed through its absorption and emission characteristics which are in good agreement with the previous report(Ramachandran, Arya Nair, and Karunakaran Yesodha 2019). The peak at ~ 260 nm UV-Vis spectrum of N-GQDs (Figure 3.1E) is ascribed to the π–π^* transition of the aromatic sp^2 domains. The typical absorption peaks of graphene derivatives are in 200-300 nm. The effective N doping in N-GQDs is attributed to the peak around 510 nm due to the n–π^* transition. The photoluminescence characterization revealed that the N-GQDs is exhibiting an excitation-dependent emission (Figure 3.1F). The quantum confinement effect (the size effect), is one of the most expansively accepted mechanism for the excitation-dependent emission, which is prominent in carbon-based nanomaterials of ≤ 5 nm size because the smaller size limits the formation of conjugated aromatic domains (isolated sp^2 clusters) which are responsible for the excitation independent emission. The size of the N-GQDs obtained from the HRTEM images were ≤ 4 nm, and was in the range of 1.5 to 3.5 nm which supports the observed phenomenon of excitation-dependent emission. The combination of the non-formation of the

isolated sp^2 clusters, and size lead bigger HOMO to LUMO energy gap and the size distribution causes broadened emission wavelengths in the range of 430–650 nm(Fu, Gao, and Zhi 2019) resulting in the observed excitation dependent emission. The strongest peak around 450 nm corresponds to the excitation at 340 nm with a Stokes shift of 110 nm and is responsible for the blue emission observed. The rapid decrease in the emission intensity with the increase in the excitation wavelength is a characteristic emission behavior of N-GQDs (luminescent carbon nanoparticles), which are in good agreement with the previous reports (Faridbod and Sanati 2018). The bluish emission confirms the oxygen-rich functionalities in the N-GQDs(Ramachandran, Arya Nair, and Karunakaran Yesodha 2019). The results confirm the formation and the structure of N-GQDs.

The FTIR spectra of N-GQDs and PANI (Figure 3.1G) further confirms the formation of N-GQDs. The peaks at 3466 and 2916 cm^{-1} in the spectrum of PANI correspond to N-H and C–H stretching respectively. The peak at 1532 cm^{-1} corresponds to C-C stretching of the benzenoid ring. The C=C stretching is obtained at 1451 cm^{-1} and the C-N stretching corresponds to 1080 cm^{-1}. In N-GQDs, a broad band at 3345 cm^{-1} is assigned to the combined effect of N-H stretching vibrations along with the –O-H stretching and the aromatic –C-H stretching. The peak around 2135 cm^{-1} indicates the presence of C=N functionality. The peak around 1637 cm^{-1} suggests the presence of amide functionality. The peak around 1331 cm^{-1} corresponds to the C-N stretching vibrations. The peak around 1499 cm^{-1} is indicative of sp^2 bonded C-N. Thus, the results further confirm the formation of N rich N-GQDs. The XRD pattern of N-GQDs consists of sharp peaks which correspond to the crystalline nature of N-GQDs. The $2\theta = 23.3^{\circ}$ and 43° corresponds to the (002) and (100) graphitic plane reflections (Figure 3.1H). The Raman spectra of N-GQDs consist of two peaks corresponding to 1322 and 1529 cm^{-1} which were assigned to the D and G bands known for GQDs. The peak at 1003 and 1108 cm^{-1} attributed to the C-C and C=C functional group vibrations and the peak at 1624, 1938 cm^{-1} corresponds to C-O/C=O vibrations (Figure 3.1I)(Ramachandran, Arya Nair, and Karunakaran Yesodha 2019).

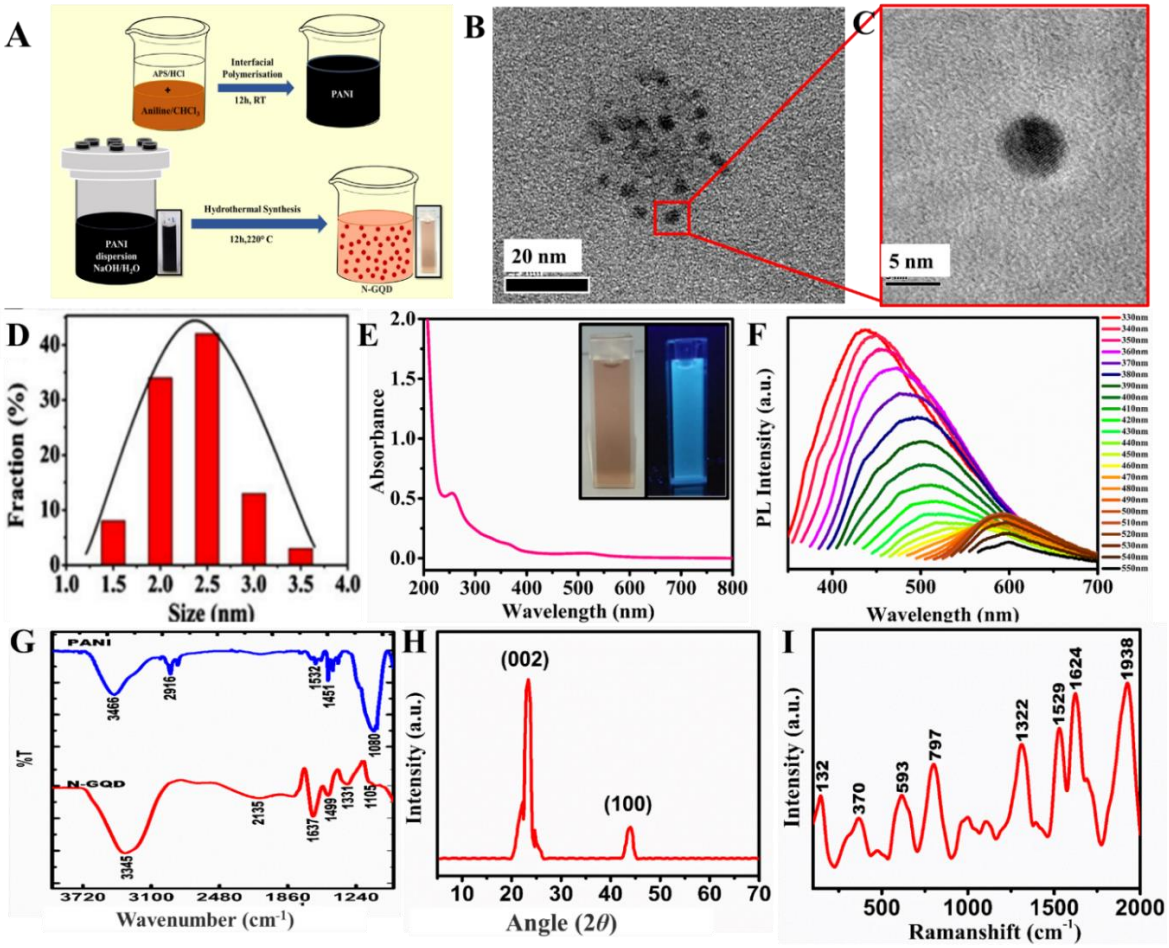

Figure 3.1. (A) Schematic of the synthesis of N-GQDs along with the digital images of the aqueous dispersion/solution of PANI and the N-GQDs; (B) and (C) The HR-TEM images of the synthesized N-GQD; (D) The size distribution of the synthesized N-GQD as obtained from HR-TEM; (E) The UV-Vis spectrum of N-GQDs (Inset: (E) digital images of PL of the N-GQDs under normal light and at UV (365 nm) irradiation); (F) Dependence of the PL spectrum of N-GQDs on the excitation wavelength from 300 to 560 nm; (G) The FTIR spectra of N-GQDs and PANI; (H) The XRD diffractogram and (I) The Raman spectrum of N-GQDs.

3.3.2 EC sensing studies of N-GQD towards heavy metal ions

The preliminary EC sensing property of N-GQD/GCE was studied using the toxic heavy metal ions Cd(II), Hg(II), Ag(I), Pb(II), Fe(II), Co(II), Ni(II), Zn(II), Sn(II), Cu(II)and Cr(VI). It was observed that the N-GQD/GCE exhibited current response for Cd(II) alone and no peak was observed for any of the other metal ions. Therefore, further the sensing of Cd(II) by N-GQDs was studied in detail. The CVs obtained by varying the concentrations of N-GQD from 20 to 100 μL is given in Figure 3.2A. It can be seen that an optimum result was obtained for the concentration of 20 μL of N-GQDs, with a better CV curve of comparatively

lower redox peak separation. Further increase in the concentration of N-GQD (40 to 100 μL), resulted in a higher separation between the redox peaks and the reduction peak shifts to a higher potential value. Hence a 20 μL concentration of N-GQD was taken for the modification of GCE, using which the further studies were carried out. The CV profile for the EC sensing of 1 mM Cd (II) on bare GCE, N-GQD/GCE, GQD/GCE, (Figure 3.2B), shows that the current response on N-GQD/GCE is ~ 25, 7 and 6 times higher than that of the bare GCE, PANI/GCE, and GQD/GCE, respectively which is apparent of the superior EC sensing of Cd (II) by the N-GQDs. The enhancement in the current response is possibly due to the synergistic effect of the increased conductivity of N-GQDs due to the graphene structure (sp^2 hexagonal skeleton) and the hetero N- atom doping which enhances the conductivity and the electrocatalytic property. The oxidation peak in the anodic sweep suggests that Cd(II) is in the reduced form Cd(0) and is attributed to the reducing capability of N-GQD to Cd(0). The synthesized N-GQDs contains aromatic basal plane enriched with N atoms, in the form of graphitic-N, pyrrolic-N, pyridinic-N and in addition has side functionalities such as -NH_2, –OH, -COOH, -$CONH_2$ etc. Most of the nitrogen functionalities scan act as reducing agents since they contain a lone pair of electrons which can be donated to Cd(II). On the other hand, the C-Cd linkages formed can be resonance stabilized by donating the lone pair on N. The positive charges created by the donation of electrons are highly resonance stabilized by the electron releasing groups in the aromatic skeleton of N-GQDs. Thus the electron-rich environment of N-GQDs can act as a good reducing agent of Cd(II), thus spontaneously reducing Cd (II) to Cd(0) on N-GQDs. Further by varying the concentration of Cd(II) to higher concentrations, (2 to 10 mM), the current response become saturated (Figure 3.2C and 3.2D). This observation backing the spontaneous reduction of Cd(II) on N-GQDs. These observations are in good agreement with the results obtained from FTIR, Raman and XPS studies. This is the reason why an oxidation peak is observed in the anodic sweep without a pre-concentration step.

The effect of solution pH on the electrochemical sensing of Cd(II) on N-GQDs were studied using both CV and DPV in the range of 2-12. The Figure 3.2E and 3.2F shows that there is a gradual increase in the peak current with decrease in acidity (pH 2-6) and become maximum at the neutral pH (7) which again gradually decreases with the increase in the basic

pH (8-12). This can be explained with respect to the protonation–deprotonation properties of Cd (II). From pH, 2-6, N in N-GQDs acquires higher Lewis base nature thus the interaction between Cd(II) and the N in N-GQDs got affected since Cd(II) is of soft acid character it interacts with soft bases more. The Cd(II) has the tendency to form cadmium hydroxy species [$(Cd(OH)^{+}$] which has a tendency to adsorb preferentially over the Cd(II) ion(Osmond et al. 1994). At higher pH values, the formation of $(Cd(OH)^{+}$ species is more feasible. Hence at higher pH, the effective concentration of Cd(II) in the electrolyte become less and thus lower current responses are obtained.

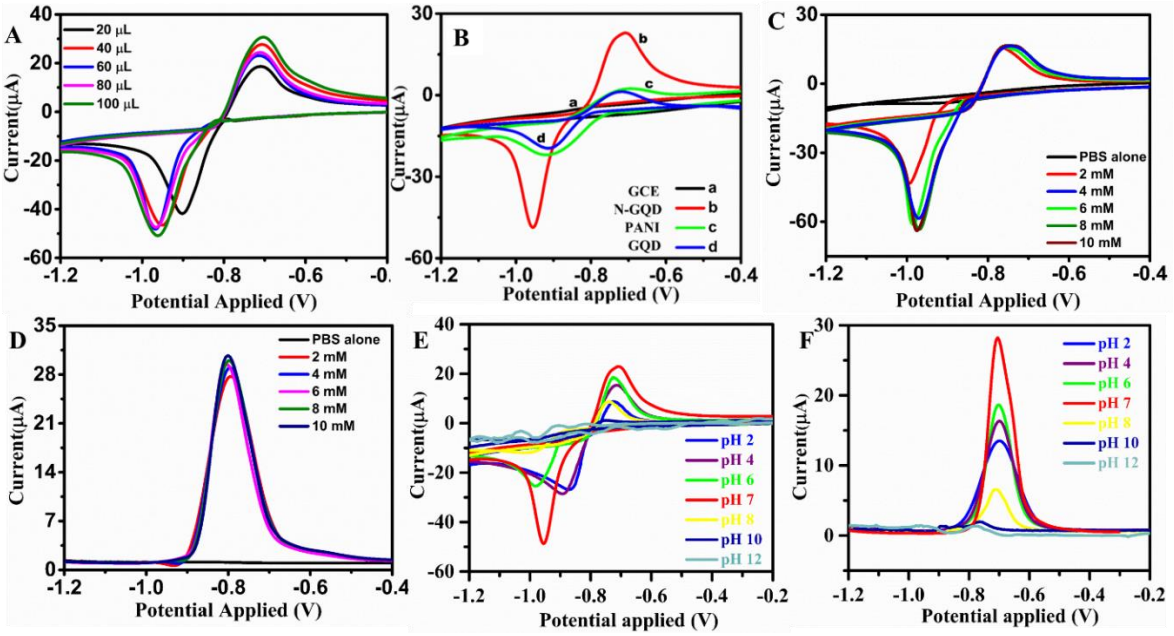

Figure 3.2. (A) The CV scans obtained by varying the drop casting volumes of N-GQDs for 1 mM Cd(II) on N-GQD/GCE; (B) The CV for 1mM Cd (II) in 0.1 M PBS on (a) Bare GCE (b)N-GQD/GCE; (c) PANI/GCE; and (d) GQD/GCE at the scan rate of 50 mV/s; (C) & (D) The CV and DPV scans obtained for higher concentrations of Cd(II) on N-GQD/GCE from 2 to 10 mM showing the current response reaching the saturation at higher concentrations; (E) & (F) The CV and DPV scans obtained for 1mM Cd(II) on N-GQD/GCE by varying the pH of the electrolytes from 2 to 12.

3.3.3 Sensitivity, LDR and LOD

In order to investigate the efficiency of N-GQDs as an electrode for the quantitative sensing of Cd (II), the current response with the increasing concentration was examined by varying the concentration of Cd (II) from 10^{-13} to 10^{-3} M. The result (Figure 3.3A) shows that

the current responses increased with the increase in the concentration of Cd (II). The LDR obtained for Cd (II) sensing is depicted in Figure 3.3B. The concentration ranges, 10^{-11} to 10^{-3} M (0.00001 to 1000μM) fits into two linear ranges. The concentration range of 10^{-11} to 10^{-4} M ((0.00001 to 100 μM) falls into the first linear range with a correlation coefficient (R^2) of 0.995 and the second linear range corresponds to the concentration ranges 2×10^{-4} to 10^{-3} M ((200 to 1000 μM) with a R^2 of 0.976. The corresponding linear regression equations can be expressed as, the oxidation peak current [I_{pa} (μA)] = 0.2524x (μM) + 0.0201 (R^2 = 0.9950) and I_{pa} (μA) = 0.0052x (μM) +24.1013 (R^2 = 0.9760) respectively. The sensitivity values corresponding to these LDR are 3.570 and 0.074 $\mu A \mu M^{-1} cm^{-2}$, respectively. The calculated LOD from the lowest concentration range of LDR is 7.12×10^{-12} M, i.e. 0.0008 ppb (S/N=3). Whereas the experimental LOD obtained for Cd (II) on N-GQDs is 10^{-13} M, i.e. 0.00001 ppb (Inset of Figure 3.3C). The values obtained are for that without the pre-reduction step and further the LOD was measured after pre-reduction and the N-GQDs exhibited a LOD of 10^{-15} M which corresponds to 0.0000001 ppb, i.e. 0.01 ppq (inset of Figure 3.3E). Further, in order to validate the LOD and the corresponding current response, the concentration was gradually increased from (10^{-13} to 10^{-9} M and 10^{-15} to 10^{-9} M for the studies without pre-reduction and with pre-reduction, respectively), and the result (Figure 3.3C and 3.3D) is evident of the reproducibility of the current response. The corresponding increase in the current response with pre-reduction is ~ 20%.

Table 3.1 compares the analytical performances of N-GQD/GCE with the various reported EC Cd (II) sensors based on the LOD values and the LDRs. The Cd(II) sensing studies were carried out with either stripping voltammetric techniques(J. Li et al. 2009; L. Li et al. 2018; Rajawat, Kumar, and Satsangee 2014) or without the pre-concentration step (Bhanjana et al. 2015; Dai et al. 2016; Y. Wang et al. 2017; Chamjangali et al. 2015). A SnO_2 QDs has been reported to have a LOD of 500 ppb with corresponding linear concentration range falls in the 10000-45000 ppb concentration range. The fabricated sensor exhibited a sensitivity of 77.5×10^2 nA ppm^{-1} cm^{-2}(Bhanjana et al. 2015). A phytic acid functionalized polypyrrole/graphene oxide-based sensor exhibited a LOD of 2.1 ppb with a linear range of 5–150 ppb(Dai et al. 2016). A metal organic framework Cd(II) sensor was reported with a linear detection in the concentration range of 0.5–600 ppb and LOD of 0.3 ppb(Y. Wang et

al. 2017), a MWCNT/poly (pyrocatechol violet) modified electrode with LOD of 0.2 ppb exhibited a linear range of 1–300 ppb (Chamjangali et al. 2015) and a glutathione functionalized magnetic nanocomposite shows a LOD of 0.17 ppb with a LDR of 0.5-100 ppb(Baghayeri et al. 2018). Thus, it is clear that the LOD value of 0.00001 ppb by N-GQDs is the lowest and is 3-4 magnitudes lower than the previously reported values. The LDR ranges obtained covers a wide range starting from nM to mM (0.00001 to 1000 μM, i.e. 0.001-112000 ppb). The fabricated sensor exhibited a good sensitivity of 3.570 $\mu A \mu M^{-1} cm^{-2}$. Table 3.1 shows that the performance of the N-GQD/GCE is better in terms of sensing property and detection limit compared to that of the previous Cd(II) sensor reports with the lowest LOD and a better LDR. The simplicity of the material and the extortionate sensing and selectivity of N-GQDs make it a potential material for practical applications.

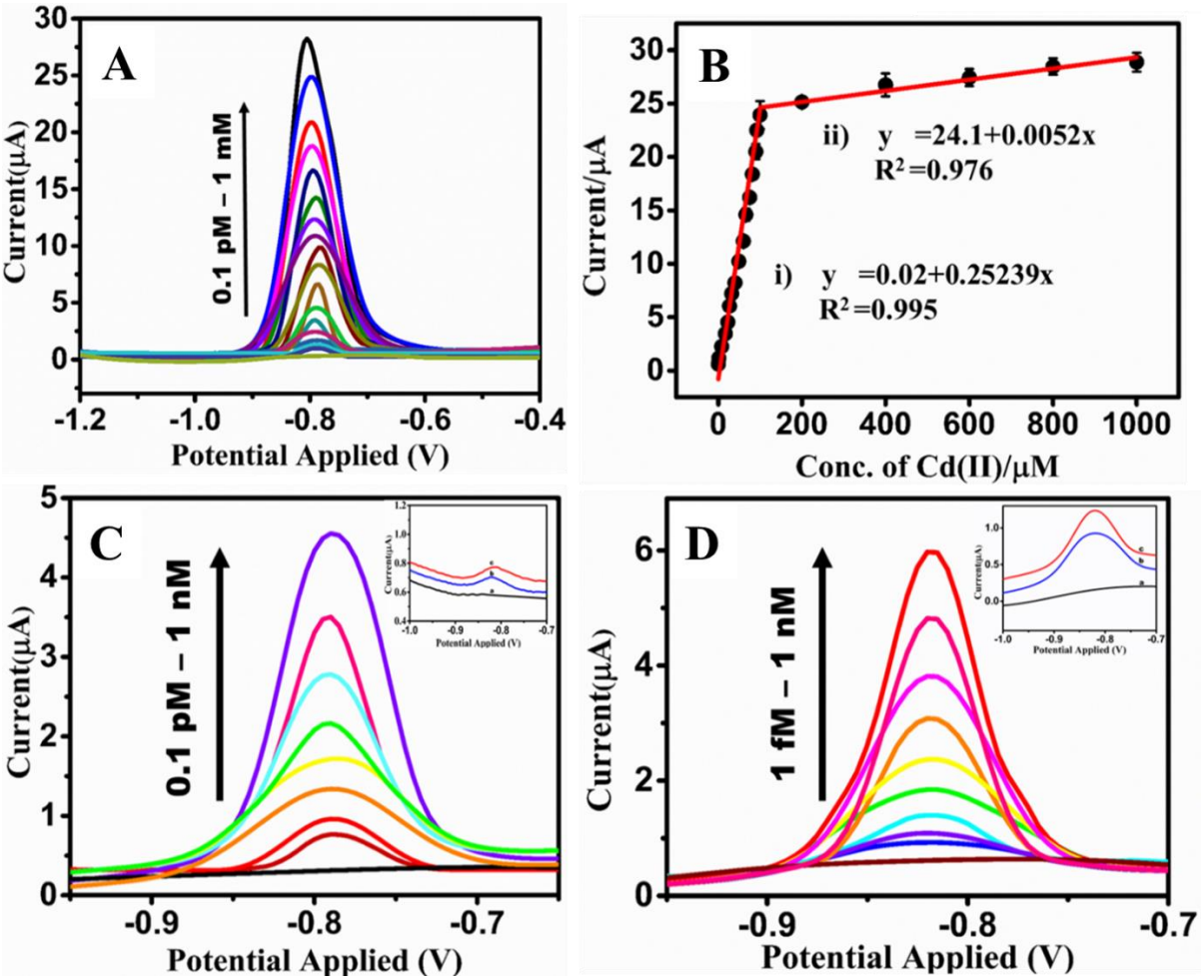

Figure 3.3. (A) The DPV responses of Cd (II) on N-GQD/GCE from 10^{-13} to 10^{-3} M; (B) The LDRs obtained for the sensing of Cd(II) on the N-GQD/GCE for the concentration range of 10^{-11} to 10^{-3} M (0.001 to 112000 ppb); (C and D) The DPV response of Cd (II) on N-GQD/GCE for the concentration range of 10^{-13} to 10^{-9} M; and that of with pre-reduction from 10^{-15} to 10^{-9} M, respectively; (Insets C and D: DPV response without pre-reduction and with pre-reduction in 0.1 M PBS (a) absence of Cd (II) and (b, c) in the presence of 0.1 and 1 pM Cd (II), respectively; and the DPV response of the N-GQD/GCE in 0.1 M PBS (a) in the absence and (b, c) in the presence of 1 and 10 fM Cd (II), respectively).

Table 3.1. Comparison of the LOD of N-GQD/GCE with that of the literature reports of EC Cd (II) sensors.

Materials/ Electrodes	**With/Without Pre reduction**	**LOD (ppb)**	**LDR (ppb)**	**Reference**
Glutathione functionalized magnetic nanocomposite ($GSH@Fe_3O_4$)	With pre reduction	0.172	0.5-100	(Baghayeri et al. 2018)
	Without pre reduction	NA	-	
N-doped carbon quantum dots-graphene oxide hybrid (NCQDs -GO)	With pre reduction	7.45	5.62-5620	(L. Li et al. 2018)
	Without pre reduction	NA	-	
SnO_2 quantum dots	With pre reduction	NA	-	(Bhanjana et al. 2015)
	Without pre reduction	500	10000-45000	
MOF	With pre reduction	0.3	0.5-600	(Y. Wang et al. 2017)
	Without pre reduction	NA		
Reduced graphene oxide (rGO) and carbon nanotube (CNT) composite	With pre reduction	0.6	20-200	(Xuan and Park 2018)
	Without pre reduction	NA	-	

MWCNT/poly (pyrocatechol violet) (PCV)	With pre reduction	0.2	1-300	(Chamjangali et al. 2015)
	Without pre reduction	NA	-	
Phytic acid functionalized polypyrrole/graphene oxide (PA/PPy/GO)	With pre reduction	NA	-	(Dai et al. 2016)
	Without pre reduction	2.1	5–150	
Chemically modified glassy carbon spheres	With pre reduction	22.48	112.4–1124	(Raghu 2012)
	Without pre reduction	N		
Thiomorpholine-functionalized nanoporous mesopore	With pre reduction	67.4	112.4 - 1124000	(Ganjali and Asgari 2010)
	Without pre reduction	NA		
Poly(4-vinylpyridine-*co*-aniline) (poly(4VP-*co*-Ani))-based solid-state ion sensor	With pre reduction	NA		(Lim, Ling, and Ghani 2013)
	Without pre reduction	89.2	112.4 - 11240000	
Amino-calixarene-derivatized graphitic carbon electrode	With pre reduction	0.0003	0.0011-0.0134	(Adarakatti and Malingappa 2016)
	Without pre reduction	NA		
N-GQD	With pre reduction	0.000000 1		Our Result
	Without pre reduction	0.000011	0.001-112000	

*NA- Not available

3.3.4 Evidence for Cd(II) and N-GQD interaction

In order to understand the interaction between N-GQDs and Cd (II), the N-GQDs were mixed with $CdCl_2$ solution and the product formed was washed and dried. The N-GQD-Cd was analyzed using FTIR, Raman spectroscopy, XRD and XPS. The FTIR spectra of the N-GQD-Cd and N-GQDs are shown in Figure 3.4A. The FTIR spectrum of N-GQD-Cd has an additional peak from that of the N-GQDs, at around 1741 cm^{-1}, which is attributed to metal-carbon stretching frequency. The Cd (II) may bond more towards the hetero atom linked C bonds due to its comparatively electron rich nature. There is also an observed shift of wavenumbers towards the lower regions(Shah et al. 2019). The peak shift towards the lower wavenumber side implies that the mass of that bond is increased. That observation supports the interaction of Cd (II) on N-GQDs and it confirms the bonding of atoms with Cd. The peak corresponding to the -C=O stretching frequency in N-GQDs at 1637 cm^{-1} shifted to 1567 cm^{-1} in N-GQD-Cd shall possibly be due to the Cd linkage to the carbonyl carbon. The C-C stretching vibrations of pyridine are assigned to the band at 1499 cm^{-1} in N-GQDs and were shifted to 1399 cm^{-1} in N-GQD-Cd due to the bonding between the pyridinic C and Cd. The reduction in the intensity of the C=N peak at 2135 cm^{-1} in the FTIR spectrum of N-GQD-Cd suggests the interaction of Cd(II) with the N-GQDs through these linkages. However, the peaks corresponding to N-GQDs functionalities are retained in the N-GQD-Cd spectrum indicating the stability of the N-GQDs. There are similar observations in the Raman spectrum of N-GQD-Cd (Figure 3.4B) as well, two additional peaks corresponding to Cd-C and N-Cd linkage at ~1820 and 900 cm^{-1} were observed compared to that of the N-GQD, in addition to the peak corresponding to the N-GQDs. The XRD pattern (Figure 3.4C) of N-GQD-Cd retains the peaks of N-GQDs at around $2\theta = 23^{\circ}$ and 43°, corresponding to the (002) and (100) graphitic planes with d-spacings of 3.85 and 2.09 A°, respectively(Ramachandran, Arya Nair, and Karunakaran Yesodha 2019). In addition, N-GQD-Cd shows peaks at around $2\theta = 10^{\circ}$ and 15°, corresponding to the d-spacings of 8.75 and 5.89 A°, respectively, which can be assigned to the (110) and (202) planes of N-GQD-Cd complex(Thukral et al. 2014). While comparing the XRD diffractograms of N-GQDs and N-GQD-Cd, it is clear that the intensity and position of graphitic peaks remains same for N-GQDs and the N-GQD-Cd, suggesting the unaltered structure and crystallinity of N-GQD after the addition of Cd(II). Thus these

results indicate the interaction between N-GQD and Cd(II) through N and also the hetero functional C in the aromatic basal plane. The XPS survey spectrum further confirms the above observations. The survey scan spectrum of the N-GQD (Figure 3.4D), which revealed the C1s peak at ~ 284.5 eV, O1s peak at ~ 530.5 eV and N1s peak at ~ 400.5 eV. Along with these peaks in the survey scan spectrum of the N-GQD-Cd, Figure 3.4E, a pronounced Cd 3d peak at ~ 411.8 eV was observed. The high resolution XPS spectra of N1s in N-GQDs indicates the presence of pyridinic (~398.7 eV), pyrrolic(~ 400.2 eV), graphitic (~400.7 eV) and oxidized pyridinic (~ 402.3 eV) N species (Figure 3.4G) and that of C1s spectrum of the N-GQDs revealed the presence of C-C/ C=C (284.7 eV), C-O (286.4 eV), C=O (287.9 eV) O-C=O (290 eV), C–N (~ 285.8 eV) and C=N (287 eV) (Figure 3.4F) functional groups. Where as in the high resolution XPS spectra of C1s as well as N1s of N-GQD-Cd (Figure 3.4I & J), the peaks correspond to the C-N, C=N, C-O, O-C=O, pyridinic-N, and Pyrrolic-N etc are not observed and there is a huge reduction in the intensity of the peaks obtained and is possibly due to the formation of new bonds between C and N with Cd. The linkage between C functionalities (C-O, C=O etc) with Cd reduces the intensity of these functionalities instead new C-Cd peaks will be formed. Similar observations are there in the case of N functionalities and the new N-Cd species is formed which is clear from the high resolution XPS spectrum of Cd. These observations agree to the FTIR and Raman observations. The variation in the peak characteristics suggests the interaction among Cd, C and N functionalities. The doped N have profound capability in the Cd binding/sensing as it is evident from the huge incongruity in its peak characteristics. From the high resolution C1s and N1s XPS spectra of N-GQDs and N-GQD-Cd, the decrease in intensity of C-hetero (N and O) based functionalities or groups are evident, whereas the peak corresponding to basic C=C skeleton remains unchanged. The result indicates the higher interaction of Cd towards the C linked with N or O-atom or directly to the hetero-atoms. Thus, the hetero atom doping has a profound effect in the selective sensing of Cd by N-GQDs, the lower response of GQDs to that of N-GQDs supports the observation. The high-resolution Cd 3d spectrum display two characteristic peaks of Cd $3d_{5/2}$ and Cd $3d_{3/2}$ centered at 404.8 and 411.9 eV respectively indicates the Cd (II) states [54] (Figure 3.4H). The obtained peak positions are having a shift towards the lower binding energies (BE) of 404.8 and 411.9 eV from that of 405.1 and 412

eV which corresponds to $3d_{5/2}$ and Cd $3d_{3/2}$ of Cd (II) state. The lowering of BE is an indication of lowering of oxidation state(Aswathi and Sandhya 2018). This is attributed to the spontaneous reduction of Cd (II) to Cd (0) on the surface of N-GQDs, which in turn confirms the spontaneous reduction of Cd (II) by N-GQD. The enhanced reducing property of N-GQDs is owing to the effective N doping. Thus, the XPS and FTIR results indicate that the N-doping has an important role in the sensing properties of N-GQDs and is supported by the fact that N-GQDs does show enhanced sensitivity towards Cd (II) to that of the undoped GQDs. The higher selectivity of N-GQDs towards Cd(II) may possibly be due to the affinity between Cd(II) and N. The softness/hardness of metal ions is seen as a useful parameter to explain the affinity between metal ions and ligands. It is generally agreed that soft metals acids have higher affinities for soft bases (ligands). Though N-functionalities are considered relatively hard bases, the N containing aromatic heterocyclic as well as N attached aromatics rings are termed as soft bases due to the resonance of electrons in the aromatic ring. Hence N based functionalities in the N-GQDs which are pyridinic, pyrrolic etc and are soft in nature(Lim, Ling, and Ghani 2013). It is shown that the N-GQDs is enriched with N based hetero atom functionalities such as pyridinic, pyrrolic etc(Ramachandran, Arya Nair, and Karunakaran Yesodha 2019). Thus, these pyridinic, pyrrolic groups can have a better interaction towards the soft acid Cd(II) through C and N linkages than that to Pb(II), Co(II), Cu(II), Zn(II), Cr(VI) etc., which are of moderate to high hard acid characteristics(Lim, Ling, and Ghani 2013). Thus this higher affinity of N containing heterocyclic aromatic systems towards Cd(II) compared to other (studied) metal ions, may be the reason for the selectivity of the N-GQD towards Cd (II). Thus, the selectivity of N-GQDs towards Cd(II) and not Pb(II) and other similar metal ions shall be assigned to the structure, the aromatic nature and the functionalities of N-GQDs.

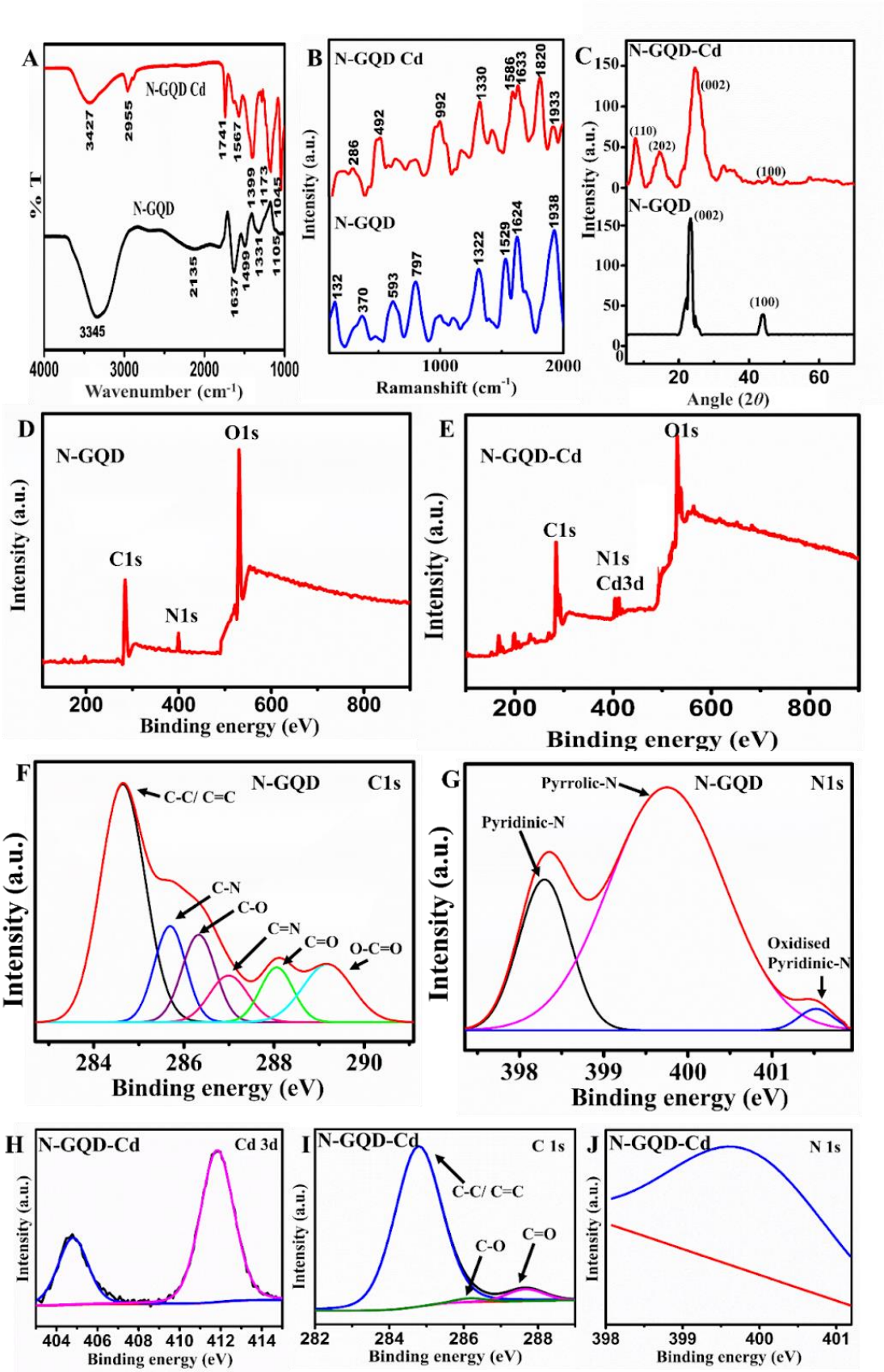
A
N-GQD Cd
N-GQD
% T
3427
2955
1741
1567
1399
1173
1045
2135
1637
1499
1331
1105
3345
4000
3000
2000
1000
Wavenumber (cm-1)
B
N-GQD Cd
N-GQD
Intensity (a.u.)
286
492
992
1330
1586
1633
1820
1933
132
370
593
797
1322
1529
1624
1938
1000
2000
Ramanshift (cm-1)
C
N-GQD-Cd
N-GQD
Intensity (a.u.)
(002)
(110)
(202)
(100)
20
40
60
Angle (2θ)
D
N-GQD
O1s
C1s
N1s
Intensity (a.u.)
200
400
600
800
Binding energy (eV)
E
N-GQD-Cd
O1s
C1s
N1s
Cd3d
Intensity (a.u.)
200
400
600
800
Binding energy (eV)
F
N-GQD
C1s
C-C/ C=C
C-N
C-O
C=N
C=O
O-C=O
Intensity (a.u.)
284
286
288
290
Binding energy (eV)
G
N-GQD
N1s
Pyrrolic-N
Pyridinic-N
Oxidised Pyridinic-N
Intensity (a.u.)
398
399
400
401
Binding energy (eV)
H
N-GQD-Cd
Cd 3d
Intensity (a.u.)
404
406
408
410
412
414
Binding energy (eV)
I
N-GQD-Cd
C 1s
C-C/ C=C
C-O
C=O
Intensity (a.u.)
282
284
286
288
Binding energy (eV)
J
N-GQD-Cd
N 1s
Intensity (a.u.)
398
399
400
401
Binding energy (eV)

Figure 3.4. (A, B and C) The FTIR, Raman and the XRD diffractograms of N-GQD and N-GQD-Cd, respectively; (D and E) The XPS (Survey) spectra of N-GQDs and N-GQD-Cd, respectively; (F and G) The high resolution XPS spectra of the C 1s and N 1s of N-GQD; (H, I and J) The Cd 3d, C 1s and N 1s high resolution XPS spectra of N-GQD-Cd.

A schematic of the sensing of Cd(II) on N-GQD/GCE and enhancement in the current response is shown in Figure 3.5. As mentioned earlier, the N-GQD/GCE did not require a separate pre-reduction step prior to achieving the oxidation peak of Cd(0) to Cd(II) in the N-GQD/GCE, as the nonbonding electrons mainly from N-atom (doped) and the aromatic π electrons can reduce Cd(II) to Cd(0) on N-GQD. Thus, on the surface of N-GQD/GCE, Cd(II) will undergo reduction to give Cd(0) which on the application of an EC potential results in the corresponding redox peaks; which is illustrated in the figure.

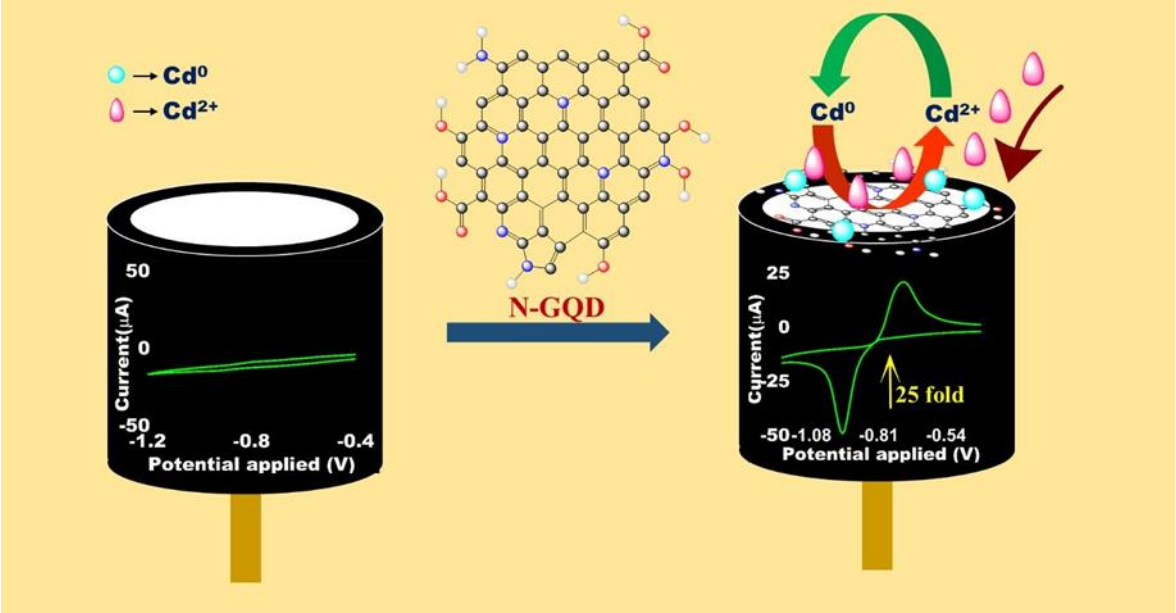

Figure 3.5. The schematic diagram showing the modification of GCE with the N-GQDs and the resultant enhanced sensing of Cd(II) in CV

3.3.5 Scan rate Study

The CV profile at different scan rates without and with pre-reduction is shown in Figure 3.6A and 3.6B, respectively. A linear fit of current response Vs. scan rate corresponds to adsorption-controlled process whereas that of current response Vs square root of scan rate corresponds to a diffusion-controlled process(Aswathi and Sandhya 2018). The studies are carried out by varying the scan rate values from 10 to 1000 mV/s for both with and without pre-reduction Figure 3.6C-3.6F. With pre-reduction, the R^2 values are 0.8668 and 0.9368 for the current responses Vs scan rate; for the anodic and cathodic peak currents, respectively, and the R^2 values are 0.9205 and 0.9665 for the current response Vs square root of scan rate; for the anodic and cathodic peak currents, respectively (Figure 3.6D and 3.6F respectively). The result suggests that the system is governed by a diffusion-controlled process as it is giving a better fit with R^2 = 0.9205 and 0.9665 for the pre-reduction studies. The shifting of CV peaks with increasing the Cd(II) concentration is the clear reflection of diffusion-controlled process, which is in agreement to the above observation. The corresponding graphs of without and with pre-reduction studies are demonstrated in Figure 3.6.

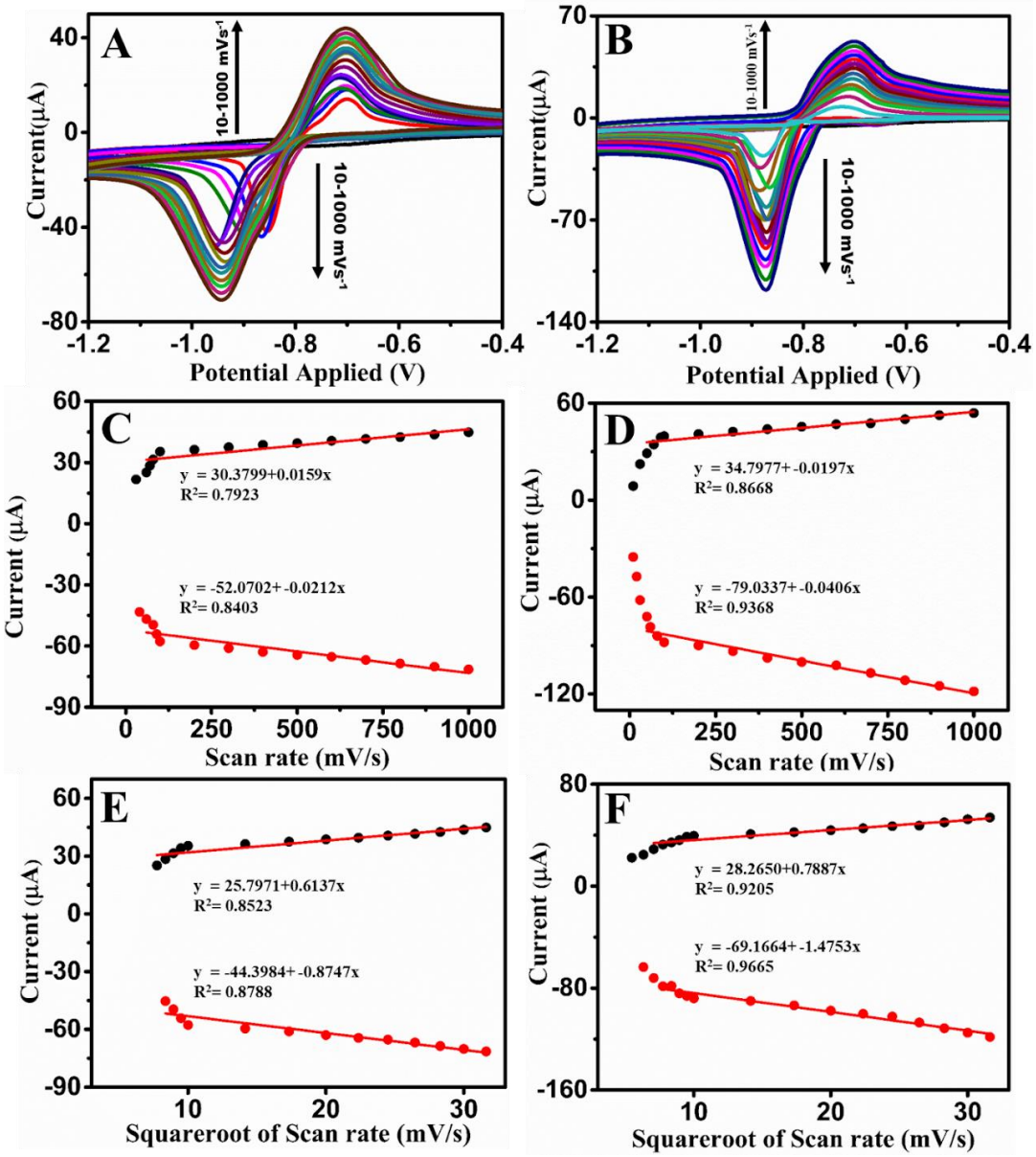

Figure 3.6.(A) and (B) CV profiles of the N-GQD/GCE in 0.1 M PBS containing 1 mM Cd (II) at various scan rates (10-1000 mV/s) without and with pre-reduction respectively; (C) and (D) Calibration plots of cathodic and anodic peak current Vs. scan rate for without and with pre-reduction respectively; (E) and (F) Calibration plots of cathodic and anodic peak current Vs. square root of scan rate for without and with pre-reduction respectively.

3.3.6 Mechanism of sensing of Cd(II) by N-GQD

The enhanced sensitivity of N-GQDs towards Cd(II) shall be assigned to the better electrocatalytic activity and electronic conductivity of N-GQD/GCE. As mentioned earlier, the hetero atom doping from the precursor incorporates N atoms

into the hexagonal sp^2 graphitic aromatic rings without disrupting the aromatic structure. The incorporation of aromatic pyridinic, pyrrolic N functionalities in the sp^2 hexagonal plane resulted in an increased reactive surface area than that of the GQDs. The pyridinic, pyrrolic N functionalities along with the edge hydrophilic group provide an efficient electron cloud which enhances the electronic properties of N-GQDs as compared to that of GQDs and PANI which is evident from the multi-fold increase in the current response by N-GQDs. The N-doping incorporates N into the aromatic lattices without disturbing its honeycomb structure gives a strong aromatic basal plane enriched with the charge carriers. The π-electrons from the graphene structure and the non-bonded electrons from the hetero atom N provide the electron rich environment for the system. Thus, due to the enrichment of electrons in the system as a whole, the HOMO-LUMO band gap in N-GQDs decreases.

As the relationship between band gap and conductivity are inversely proportional, the conductivity of N-GQDs increases. Thus, the higher sensitivity of N-GQDs is assigned to the better electron transfer ability and conductivity which in turn facilitates the electrocatalytic activity of N-GQDs. The electron transfer ability of the N-GQD/GCE, GQD/GCE and bare GCE were studied by EIS and the results are given in Figure 3.7. From the EIS plots, it can be seen that the diameter of the semicircles are in the order of bare GCE (66 kΩ) > GQD/GCE (20 kΩ) >N-GQD/GCE (3.81 kΩ) which suggest that the charge transfer resistance (R_{ct}) is lowest for N-GQD/GCE compared to GCE and GQD/GCE. The N-GQD/GCE has the lowest R_{ct} compared to that of GQD/GCE and to that of bare GCE. Thus, the result indicates the better charge-transfer property of N-GQD which is assigned to the comparatively better electron transfer ability of the N-GQD/GCE.

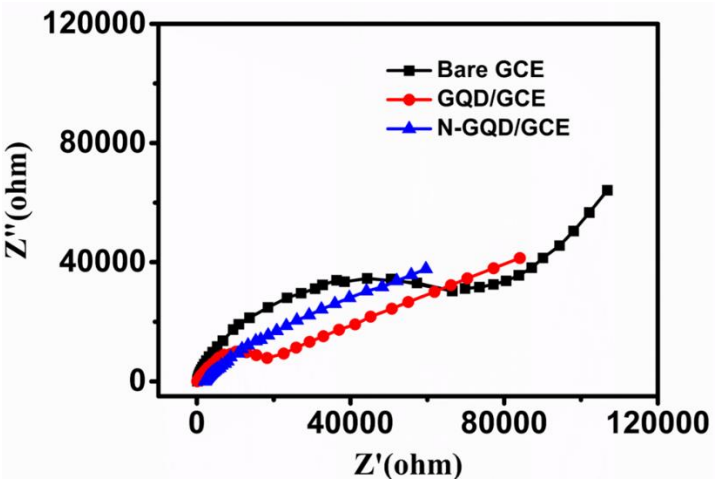

Figure 3.7. The Electrochemical impedance spectra of bare GCE, GQD/GCE and N-GQD/GCE.

The selectivity offered by N-GQDs towards Cd(II) shall possibly be due to the presence of N hetero atom functionalities such as pyridine, pyrrole etc. in the aromatic plane through doping. In most of the reported heavy metal ion sensors, a pre-deposition step is conducted to deposit the metal ion in its reduced state on the modified electrode which then undergoes oxidation while applying the oxidation potential, in the CV. But in this study the modified electrode, N-GQD/GCE, is giving both oxidation and reduction peaks for Cd(II) without any pre-deposition step (oxidation sweep being run first). This implies that Cd(II) got reduced spontaneously on N-GQDs and indicates that N-GQDs can act as a reducing agent, and donate electrons to Cd (II) to form Cd (0). The morphological characterizations of N-GQDs and N-GQD-Cd are done through SEM analysis (Figure 3.8A & 3.8B). The SEM elemental mapping results of the N-GQD-Cd and the N-GQDs are shown in Figure 3.8C-F, respectively. The SEM images clearly show the distribution of Cd on the surface of N-GQDs, which indicates the specific interaction of N-GQDs and Cd. This is possibly due to the spontaneous reduction of Cd(II) on the surface of N-GQDs through the N-functionalities. Further the elemental mapping result (Figure 3.8D) clearly shows the presence of Cd.

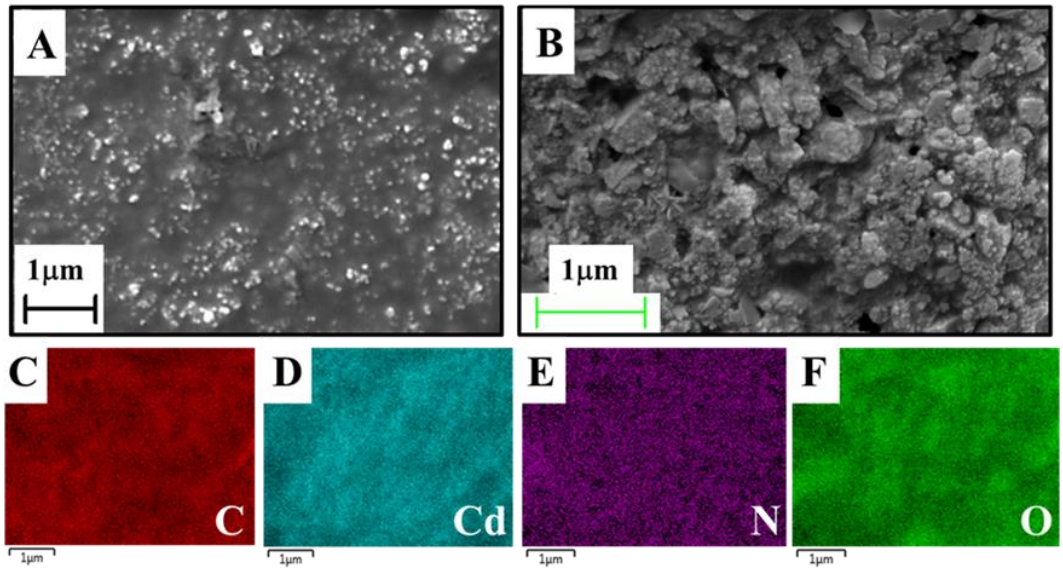

Figure 3.8.(A) and (B) The SEM images of the synthesized N-GQD and N-GQD-Cd respectively; (C)-(F) SEM elemental mapping results of N-GQD-Cd revealing the distribution of C, Cd, N and O.

3.3.7 Selectivity and Interference Studies

The selectivity and sensitivity are the two significant parameters which act as the criterion for the practical applicability of a sensor. Since N-GQD/GCE exhibited remarkable sensitivity (3.570 $\mu A \mu M^{-1} cm^{-2}$), exploring its selectivity towards Cd(II) is vital. The CV profile of Cd(II) in amixture containing other metal ions (Hg(II), Ag(I), Pb(II), Fe(II), Co(II), Ni(II), Zn(II), Sn(II), Cu(II) and Cr(VI)) of 1x concentrations of Cd(II) (Figure 3.9A) showed that N-GQD/GCE is highly selective towards 1 mM Cd(II) in the chosen potential range of -1.2 to - 0.4 V and the current response is similar to that obtained in the absence of the metal ions (~ 23 ± 0.25 μA for 1 mM Cd(II)). The result is an indication of the ultra-selectivity of N-GQDs towards Cd(II) in the potential window of -1.2 to - 0.4 V and is portrayed in the bar diagram (Figure 3.9B). Further, the result of the interference studies by chrono-amperometric technique at a fixed operational potential of - 0.85 V, (Figure 3.9C), showed nil current responses for the other metal ions and TNP (1000 x concentration to that of Cd(II)), TNP was tested, as an earlier work from our group showed sensing property for N-GQDs towards TNP in the reduction scan [23]. Inspired by this result, the interference study was repeated at the lower concentration of Cd(II) i.e., 10^{-15} M and other species at 10^{-3} M concentration (10^{12} x) to that of

Cd(II). The result (Figure 3.9D) is evident of the ability of N-GQDs to sense Cd(II) at the ultra-low-level concentration of Cd(II) without any interference from the other metal ions, which showed current response only for Cd(II).

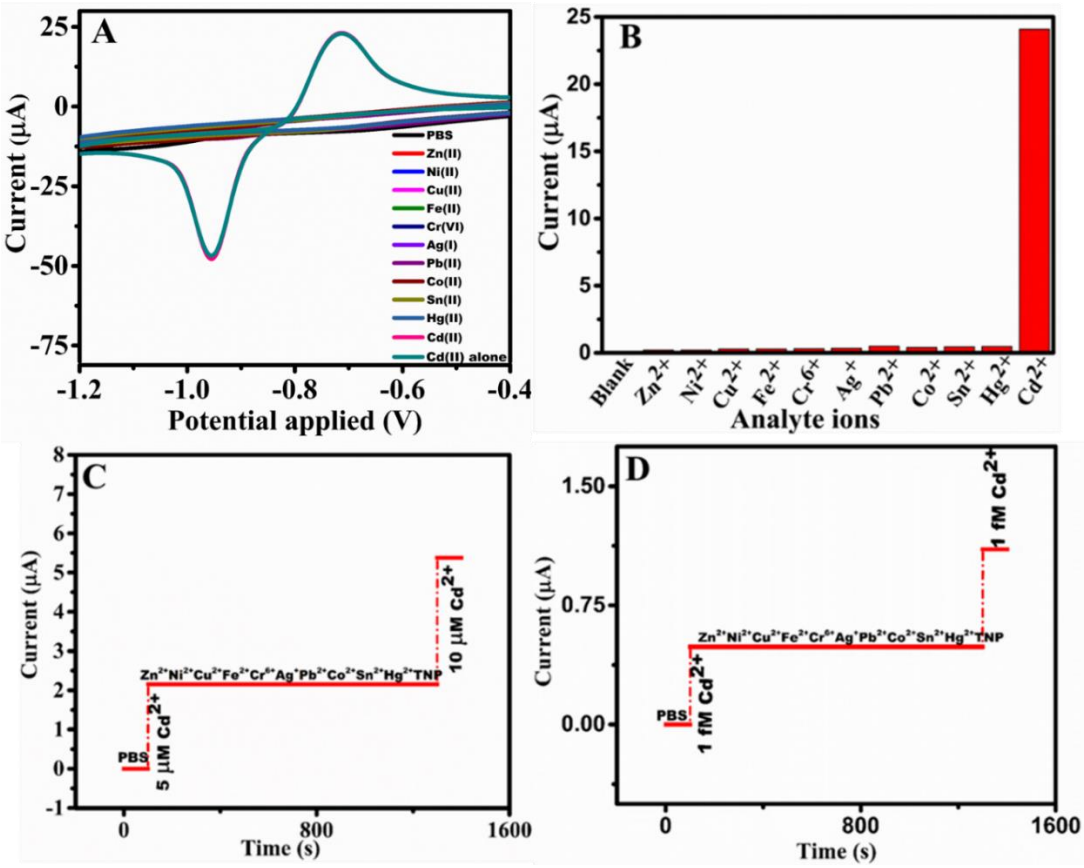

Figure 3.9. (A) and (B) Selectivity studies of N-GQD/GCE towards 1 mM Cd (II) in the presence of various analyte species with 1 mM concentration for each; (C) Interference studies of N-GQD/GCE for the detection of 5 and 10 µM Cd (II) in the presence of other metal ions in 1 mM concentration; (D) Interference studies of N-GQD/GCE for the detection of Cd(II) at 1 fM concentration in the presence of other metal ions in 1 mM concentration.

3.3.8 Reusability, Reproducibility and Stability Studies

In addition to selectivity and sensitivity, the practical applicability of an electrode depends on its reproducibility, reusability and stability. The reusability of the N-GQD/GCE electrode was scrutinized by comparing the peak currents for 1 mM Cd(II) on N-GQD/GCE (Figure 3.10A) before and after multiple washings and showed ~ 96% retention after 3 times of washing. The stability studies conducted after one- and three-months' time, retained ~ 87% and ~ 70% of the initial current response, respectively, which is depicted in Figure 3.10B. For reproducibility

studies, the current responses of five different electrodes towards 1mM Cd (II) were examined. The relative standard deviation (RSD) of the peak currents of these individually prepared electrodes was found to be 2.26 % which specifies its reproducibility (Figure 3.10C).

3.3.9 Environmental sample studies

Further, the studies were extended to real environment samples spiked with the analyte such as groundwater, seawater from two locations, and wastewater. The recovery values of all the four samples are in the range of 100.28-102.23%. The LOD (10^{-13} M) values obtained in these samples as electrolyte (Figure 3.10D-F) were the same as that obtained in PBS. The results thus show the impressive potential of N-GQD/GCE in sensing of Cd (II) in real water samples with no interference and are an indication of the selectivity of N-GQD/GCE for Cd (II). The recovery information in real samples is summarized in Table 3.2. The DPV response obtained using real water analyses is given in Figure 3.10G.

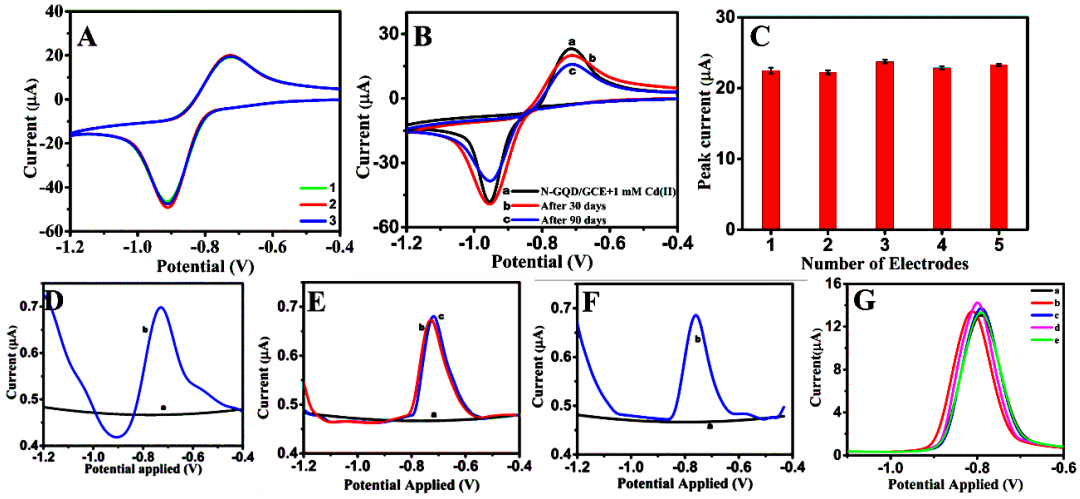

Figure 3.10. CV scans obtained for 1mM Cd(II) on N-GQD/GCE (A) after immediate washing for three times showing the reusability; (B) after 1and 3 months of storage showing the stability and (C) The peak current of five independently coated electrodes showing reproducibility of N-GQD/GCE; The DPV response of LOD of Cd(II), 10^{-13} M on N-GQD/GCE using real samples as electrolytes (D) Groundwater as electrolyte (a) in the absence and (b) in the presence of 10^{-13} M Cd(II); (E) Seawater samples 1 and 2 as electrolyte (a) in the absence and (b) and (c) in the presence of 10^{-13} M Cd(II), respectively; (F) Wastewater as electrolyte (a) in the absence and (b) in the presence of 10^{-13} M Cd(II); The DPV response of Cd(II) on N-GQD/GCE for the concentration of 10^{-6} M (a) in 0.1 M PBS, (b) spiked seawater 1, (c) spiked seawater 2, (d) spiked wastewater and (e) spiked

groundwater

Table 3.2. The recovery test results of Cd (II) in environmental samples

Sl No.	Cd(II) Spiked (μM))	Environmental Samples	Cd(II) found (μM))	Recovery (%)	RSD (%)
1	0.5	Groundwater	0.5014	100.28	0.19
		Seawater 1	0.5041	100.82	0.57
		Seawater 2	0.5040	100.80	0.56
		Wastewater	0.5067	101.34	0.94
2	1	Groundwater	1.0084	100.84	0. 59
		Seawater 1	1.0111	101.11	0.78
		Seawater 2	1.0140	101.40	0.98
		Wastewater	1.0217	102.17	1. 51
3	2	Groundwater	2.0104	100.52	0.36
		Seawater 1	2.0331	101. 65	1.16
		Seawater 2	2.0360	101.80	1.26
		Wastewater	2.0447	102.23	1. 56

3.4 Conclusion

Here in this work, we have successfully demonstrated for the first time, the ultra-high sensitivity and selective EC sensing of Cd(II) by N-GQDs. Interestingly it can detect Cd(II) up to 1×10^{-5} ppb which can be drawn-out further to 1×10^{-7} ppb (ppq) with pre-reduction. The effective N-doping, which is attributed to the synthesis procedure, seems to play a crucial role in the sensing performance of N-GQDs which spontaneously reduces Cd (II), mostly through the N-sites. Further, N-doping increases the electron availability of N-GQDs which in turn increases the ability of N-GQDs to reduce Cd (II). It was observed that the N-GQD-Cd interactions mainly happen through the hetero atom sites. Thus, this work has established a simple, as well as environmentally friendly material for the sensing of Cd (II) with remarkable selectivity and sensitivity. The N-GQDs modified electrode exhibits good reproducibility, reusability and stability. Moreover, the sensor has extended the performance to real samples such as groundwater, seawater and wastewater. The result is evident of the applicability of N-GQDs as a potential Cd (II) sensor material.

CHAPTER 4

White Emissive Sulfur Co-Doped Nitrogen-Graphene Quantum Dots as a Versatile Electrochemical Sensor for Heavy Metal Ions Cd(II), Pb(II), and Hg(II)

A white emissive sulfur co-doped nitrogen-graphene quantum dots (S,N-GQDs) was synthesized from polyaniline using sulfuric acid as an acid catalyst and S-doping agent. The S,N-GQDs, for the first time, exhibited simultaneous sensing towards three of the top ten toxic metal ions: Cd(II), Pb(II), and Hg(II) with highly sharp peaks and adequate peak-to-peak separation. The sensitivity and selectivity studies of S,N-GQD/GCE were carried out and the results were discussed. A mechanism for the enhanced and simultaneous sensing of the S,N-GQD towards Cd(II), Pb(II), and Hg(II) has been proposed based on the evidences obtained for S,N-GQD-metal ion interaction. The sensing studies were extended to real water samples such as ground water, sea water, and waste water to confirm the applicability of the sensor in real environmental samples

4.1 Introduction

Graphene quantum dots (GQDs) are highly versatile materials due to their unique combination of properties such as higher surface area, solution processability, conductivity, photoluminescence, and bio-compatibility(M. Li et al. 2019). The GQDs with tunable fluorescent emission can be an excellent alternative for the toxic fluorescent semiconductor nanocrystals and organic compounds in sensing, catalysis, imaging, etc, due to their biocompatibility(G. Wang et al. 2018)- (Zihao Wang et al. 2020). Doping of GQDs with different hetero atoms such as boron(Ge et al. 2019), nitrogen (N)(Qu et al. 2015), fluorine(C. Wang et al. 2021), and sulfur (S)(Qu et al. 2013) have been effectively pursued to tune the intrinsic properties of GQDs, including electronic characteristics, catalytic activity, optical activity, surface, and chemical features. A simple and fool-proof approach for

obtaining N-GQDs with graphene structure and effective N-doping with N-atoms in the aromatic network structure was reported by our group(Ramachandran, Arya Nair, and Karunakaran Yesodha 2019a), which yielded an N-GQD with high N-doping values of ~10%. Because of this, the N-GQD exhibited superior electronic and, in turn, superior sensing properties towards trinitro phenol(Ramachandran, Arya Nair, and Karunakaran Yesodha 2019a) and hazardous heavy metal ion, cadmium (Cd(II))(Saisree et al. 2021a)with a limit of detection (LOD) values of 1 nM and 1 fM respectively, which were the lowest than the other sensors reported so far.

Motivated by this result, we attempted to further explore and exploit the material and approach by co-doping it with sulfur (S). For this, we modified the original synthesis method of N-GQD(Ramachandran, Arya Nair, and Karunakaran Yesodha 2019a) by replacing NaOH, the base catalytic agent, with an acidic agent, H_2SO_4, which can double as an S doping agent. The product obtained was characterized to confirm the doping of both S and N and hereafter was referred to as S,N-GQD.

The excellent sensing performance of N-GQD towards Cd(II)(Saisree et al. 2021a) prompted us to explore the heavy metal ion sensing capability of S,N-GQD. It is now well-known that the monitoring of most of the toxic heavy metal ions in environmental samples is mandatory due to their widespread presence and their calamitous toxicity (T. Bin Chen et al. 2005), to both environment and human health (Cheng 2003) and their very low maximum permissible limit of ≤ 2 to 5 ppb is an indication of their toxicity(Length 2007). The high spread of contamination in groundwater and other water sources demands an urgent need for a continuous monitoring system. Presently, the detection and monitoring of the concentrations of heavy metals in the environmental samples are done by atomic absorption spectrometry(Saied, Zahir, and Siddique 2010), inductively coupled plasma emission or mass spectrometry(Rasdi, Abu Bakar, and Mohamad 2013), X-ray fluorescence spectrometry(Hutton et al. 2014), and neutron activation analysis(Abdel-Haleem et al. 2001) which requires bulkier and expensive instrumentation, expert personnel for their operation, frequent sample collection and is mostly time-consuming as well(Karimi-maleh, Karimi, and Alizadeh 2020). On the other hand, EC sensing(Ramachandran, Panda, and Karunakaran Yesodha 2018),

because of its high inbuilt sensitivity, low cost, trouble-free and simple operation, rapid analysis, and portability(Brett and Oliveira-brett 2011), is an appealing method for monitoring environmental samples as it is fast and simpler. Thus, the search for electrode materials for EC sensors for toxic metal ions is significant.

Therefore, herein, the EC sensing capabilities of S,N-GQD towards toxic metal ions were explored. Prompted by the sensing result of Cd(II) by N-GQD. Interestingly, the results of the sensing studies revealed that S,N-GQD modified glassy carbon electrode (S,N-GQD/GCE) can simultaneously sense Cd(II), Pb(II), and Hg(II) with an enhanced current response of ~ 7-fold for Cd(II), compared to that of on N-GQD. The S,N-GQD displayed high sensitivity values of 12, 13, and 5 $\mu A \mu M^{-1} cm^{-2}$ and very low LOD values of 10^{-12}, $10^{-11,}$ and 10^{-12} M for Cd(II), Pb(II), and Hg(II). The enhanced sensing performances of S, N-GQD compared to that of N-GQD can be attributed to the co-doping of S which enhanced the conductivity and electrocatalytic properties by narrowing the bandgap due to the insertion of the bonding and antibonding orbital of S between the antibonding orbital of N and the bonding orbital of C due to the lower electronegativity of S to that of N, increasing the availability of electrons in the GQD. Finally, real sample studies with spiked environmental samples were performed. All the tested samples exhibited ~ 100% recovery, which proves the first-rate proficiency of the developed sensor in real-time monitoring.

4.2 Experimental Section

4.2.1 Synthesis of S,N-GQD

The S-N-GQD was prepared by a slightly modified hydrothermal route from that used for N-GQD(Saisree et al. 2021a) and using polyaniline (PANI) as the source material. The synthesis procedure for PANI(Ramachandran, Arya Nair, and Karunakaran Yesodha 2019a) and N-GQD(Saisree et al. 2021b) by our group is reported elsewhere in detail. In a typical synthesis, 100 mg of the above-prepared PANI was dispersed in 20 ml of 0.05 M H_2SO_4 by ultrasonication for 1 hr. The dispersion was transferred into a 20 ml teflon-lined autoclave and was kept at 220 ^oC for 12 h. The reaction mixture was naturally brought down to RT, and subsequently, the supernatant liquid containing S-N-GQD was collected. The

solution was diluted 2 times, unless otherwise mentioned, for characterizations and EC sensing studies.

4.2.2 Preparation of electrodes for EC sensing

The samples (S,N-GQD, N-GQD, and PANI) were drop cast over separate cleaned GCE with care and then allowed to dry for 24 hours at RT to achieve the modified electrodes.

4.2.3 Electrochemical methods

The EC behavior of various metal ions (Pb(II), Hg(II), Ag(I), Cd(II), Fe(II), Co(II), Ni(II), Zn(II), Sn(II), Mn(II), Mg(II), Cu(II), and Cr(VI)) on the surface of the S,N-GQD/GCE was investigated using CV and DPV at RT. 20 µL of S,N-GQD solution, after 2 times dilution, was dropped and cast onto a GCE for making the working electrodes. 0.1 M PBS was used as the electrolyte for the studies unless otherwise specified.

4.3 Results and Discussions

4.3.1 Synthesis, structure, size, and the properties of S,N-GQD

The S,N-GQD was synthesized as described in the experimental section, using PANI as the precursor and H_2SO_4 as an acid catalyst and S doping agent. The aromatic nature of the precursor PANI and the presence of in situ N facilitates the formation of graphene structure and effective N-doping on GQDs, respectively, without the use of any external doping agents(Ramachandran, Arya Nair, and Karunakaran Yesodha 2019a). Herein, the NaOH was replaced with H_2SO_4 as the catalyst to promote S-doping and to deliver N and S co-doped GQD or S,N-GQD instead of N-GQD. A schematic of the synthesis is represented in Figure 4.1.

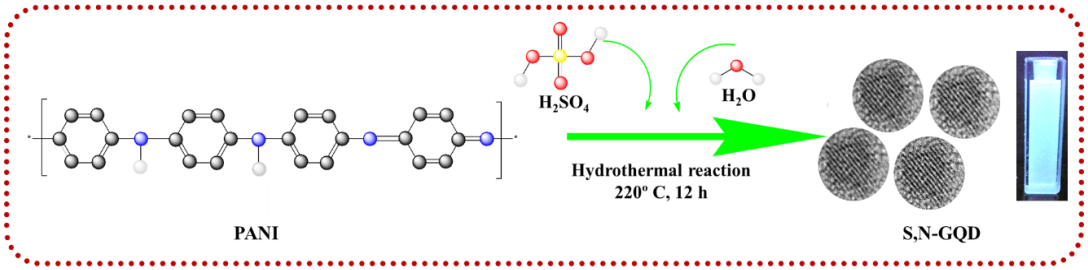

Figure 4.1 Schematic of the synthesis and a representative structure of S,N-GQD

The high-resolution transmission electron micrographs of the as-synthesized S, N-GQDs are shown in Figure 4.2A, giving an overall idea of the S,N-GQDs, such as uniformity in the structure and size. The higher magnification images (Figure 4.2B) show lattice fringes with a d-spacing of 0.21 nm, which corresponds to the (102) diffraction planes of sp^2 graphitic carbon(Ramachandran, Arya Nair, and Karunakaran Yesodha 2019a), indicating the crystallinity and the presence of graphene structure in the S,N-GQD. The histogram (Figure 4.2C) obtained from Figure 4.2A, shows a narrow size distribution for S, N-GQD, from 3.5 to 4.5 nm.

Interestingly, unlike N-GQD, which has a PL of light greenish blue (Figure 4.2E) under the UV light (365 nm), the S,N-GQD exhibited intense white light photoluminescence (Figure 4.2E). Similarly, the absorption characteristics of S,N-GQD differed from that of the N-GQD (Figure 4.2F), which exhibited a shoulder peak at ~260 nm and another broad peak at ~620 nm corresponding to the π–π* transition of the aromatic sp^2 domains(Saisree et al. 2021b) and the n–π* transition, respectively, whereas in N-GQD the corresponding peak positions are at ~260 and ~510 nm, respectively. The broadness of the peak corresponding to n–π* at ~620 nm of S,N-GQD, as compared to that of the N-GQD (~510 nm), is assigned to the effective S doping(Ouyang et al. 2019). The red-shift of ~100 nm in the n–π* absorption peak of S,N-GQD is an indication of the inclusion of the S functional groups(Ouyang et al. 2019), such as S=O bonds through the S-doping, because of the insertion of the S 'π*' orbital between the N 'π*' and the C 'n' orbital due to the lower electronegativity of S (2.58) to that of N (3.04)(Luo et al. 2017). The emission spectrum of S,N-GQD (Figure 4.2G) has three peaks at λmax= ~ 345, ~ 450, and ~ 600 nm, whereas N-GQD has two:~ 450 and ~ 600 nm (Chapter 3, Figure 3.1F). These emission peaks in a broad-band region are assigned to the white light emission of S,N-GQD(Joseph and Anappara 2016). The chromaticity index of the white light emission was analyzed by calculating the Commission Internationale de l'Elcairage (CIE) 1931 chromaticity parameters (x, y) using the software "Color Calculator" from the emission data. The CIE 1931 parameters obtained (Figure 4.2H) for white emissive S,N-GQD on photoexcitation at 350 nm, are (x = 0.31, y = 0.27); which are very close to the pure white CIE coordinates (0.33, 0.33)(Arcudi, Đorđević, and

Prato 2017) whereas that of the N-GQD are (x = 0.24, y = 0.32) (Figure 4.2I), which corresponds to the greenish-white colour.

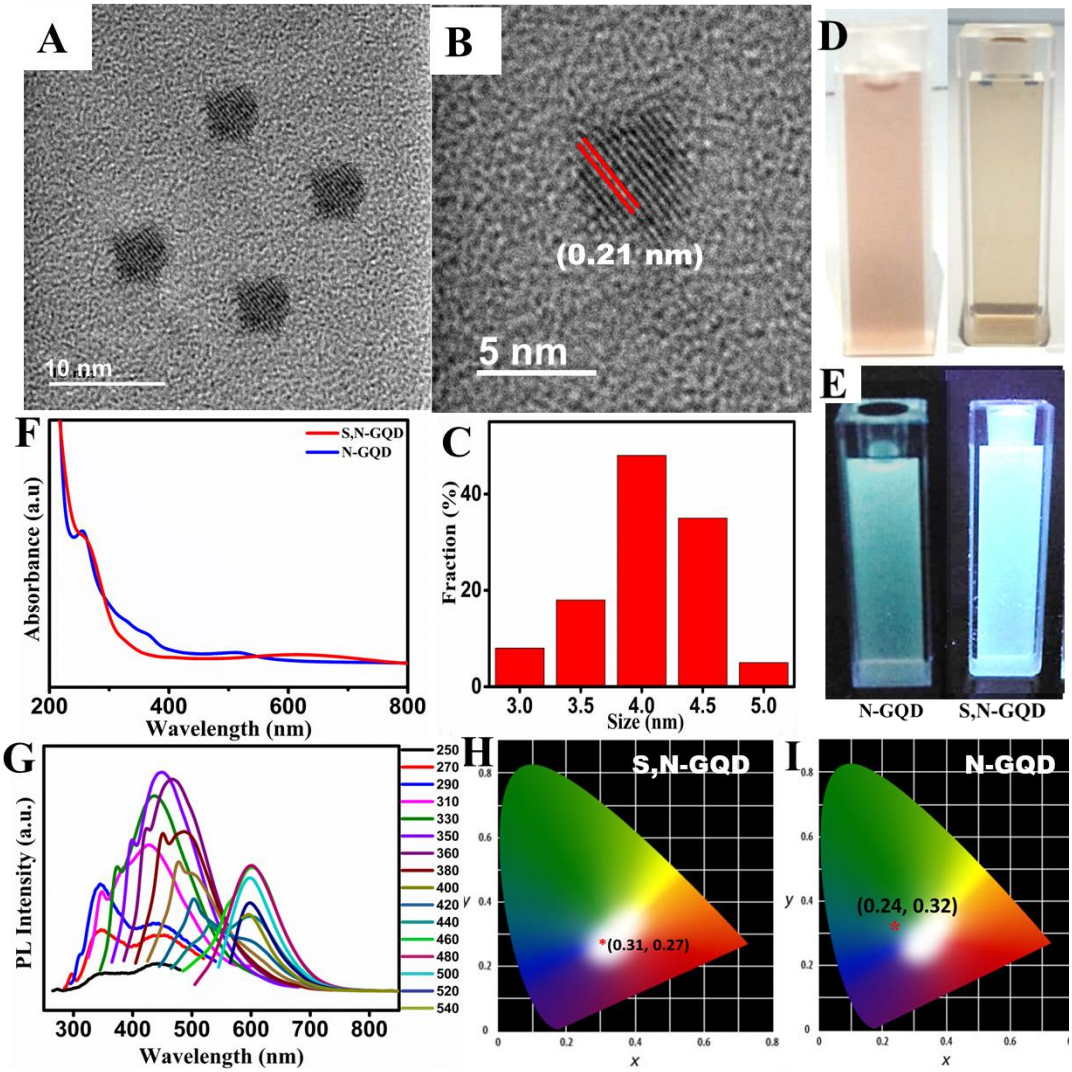

Figure 4.2. (A) The high-resolution transmission electron micrograph of the synthesized S,N-GQD; (B) The transmission electron micrograph reveals the d-spacings; (C) The size distribution of the S,N-GQD as obtained from the transmission electron micrograph images; (D) and (E) The digital images of the photoluminescence of N-GQDs and S,N-GQDs under normal light and UV (365 nm) irradiation, respectively. (F) The UV-Vis spectrum of S,N-GQD; (G The emission spectra of S,N-GQD excited using wavelengths from 250 to 540 nm ; (H) and (I) The chromaticity index diagram of S,N-GQD, and N-GQD which shows white and green color emissions, respectively.

Further, the S,N-GQD was characterized by FTIR, Raman, XPS, and XRD to confirm the formation of S,N-GQD. The FTIR spectra (Figure 4.3A) of PANI, N-GQD, and S,N-GQD, show differences in the characteristic peaks. The FTIR spectrum of PANI, the peak at ~ 3432 cm^{-1} corresponding to the N-H stretching, is

narrow compared to that of the broad peaks of N-GQD (~ 3325 cm^{-1}), and S,N-GQD (~ 3311 cm^{-1}) and is possibly due to the presence of the N–H, O–H and the aromatic C–H in the edges of the GQDs. The other peaks in the spectrum of PANI correspond to the stretching vibrations of C–H (~ 2928 cm^{-1}), C-C of the benzenoid ring (1603 cm^{-1}), C-C of the quinonoid ring (1496 cm^{-1}), and the C-N (1071 cm^{-1})(Saisree, Nair, and Sandhya 2022). The additional peaks observed at ~2115 cm^{-1}, ~ 1640 $cm^{-1,}$ and ~ 1350 cm^{-1} in the spectra of both N-GQD and S,N-GQD correspond to the C=N, amide, and the C–N functionalities showing the effective N-doping(Saisree et al. 2021a). The additional peak in that of the S,N-GQD at 1111 cm^{-1} is assigned to the of C-S(B. X. Zhang, Gao, and Li 2014), confirming the successful co-doping of S in S, N-GQD. The Raman spectrum of S,N-GQD (Figure 4.3B), reveals the presence of D and G bands(Roy et al. 2014) at ~ 1328 and ~ 1602 $cm^{-1,}$ respectively, and the I_D/I_G value was 0.81 indicating the presence of aromatic graphitic structure(Chhabra et al. 2018) in S,N-GQD. The XRD pattern (Figure 4.3C) revealed rather sharp peaks indicative of the crystalline nature of the S,N-GQD, at around $2\theta = 23.4^{\circ}$ (d = 0.355 nm), 42.9° (d = 0.221 nm) and 44.2° (d = 0.208 nm) corresponding to the (002), (100) and (101), planes of graphene, respectively(Saisree et al. 2021a). Thus, the effective S and N doping along with the aromatic graphitic structure of S,N-GQD was confirmed.

Additionally, to confirm the doping of S and N and to understand the nature of N and S in the GQD, an XPS analysis was carried out. The survey scan spectrum of the S,N-GQD (Figure 4.3D) revealed the C 1s, O 1s, N 1s, and S 2p peaks at 284.9, 532.6, 399.8, and 169.5 eV, respectively, which indicated the effective doping of GQD with N and S. The high-resolution C 1s spectrum (Figure 4.3E) revealed the presence of C-C/ C=C (284.6 eV), C=O (288.6 eV) and O-C=O (289.9 eV) groups(S., Arya, and K. Y. 2022a)(Arya Nair et al. 2022). The peak at ~285.9 eV was identified as the C–N and C-S peak. The deconvolution of the N 1s peak (Figure 4.3F) indicates the presence of pyridinic (~398.3 eV), pyrrolic (~399.7 eV), and oxidized pyridinic (~401.5 eV) N species. Whereas the deconvolution of the S 2p (Figure 4.3G) peak indicates the presence of S=O and $–SO_n–$, n = 2, 3(~169.2 and 170.7 eV) functionalities(B. X. Zhang, Gao, and Li 2014) and the absence of the peak at ~163 eV corresponding to the thiophene functionality indicates that the S-doping is mainly as the side functionalities as$–SO_n–$. The difference in the doping

sites is possibly due to the differences in the size of N and S to that of C: N has a similar radius (0.75 Å) as that of C (0.77 Å), the aromatic C-skeleton can include N with not much distortion in the aromatic structure(Gu et al. 2019). Thus, it can form a stable aromatic skeleton containing N(Saisree et al. 2021a), whereas the S (1.05 Å) atom which is larger than the C atom with two different outermost orbitals and that will result in a longer C–S bond length (1.78 Å) is ~25 % longer than those of the C–C and C–N bonds(Gu et al. 2019). Therefore, S atoms, if incorporated in aromatic, will distort the ring structure or make it unstable. Hence may preferably get incorporated on the surface or at the edges as functionalities than in the aromatic skeleton. Thus, the XPS results confirmed the successful formation and the structure of S,N-GQD, and the doping percentages were ~10.5 and ~4.8 % for N and S with N-atoms mainly incorporated in the aromatic structure and the S-atoms as the side functional groups. The N-doping percentage of the N-GQD is the same as that of the S,N-GQD, which supports the results that the S-doping is on the surface/edges as functional groups. Based on the results, a possible representative structure of S,N-GQD is exemplified in (Figure 4.4).

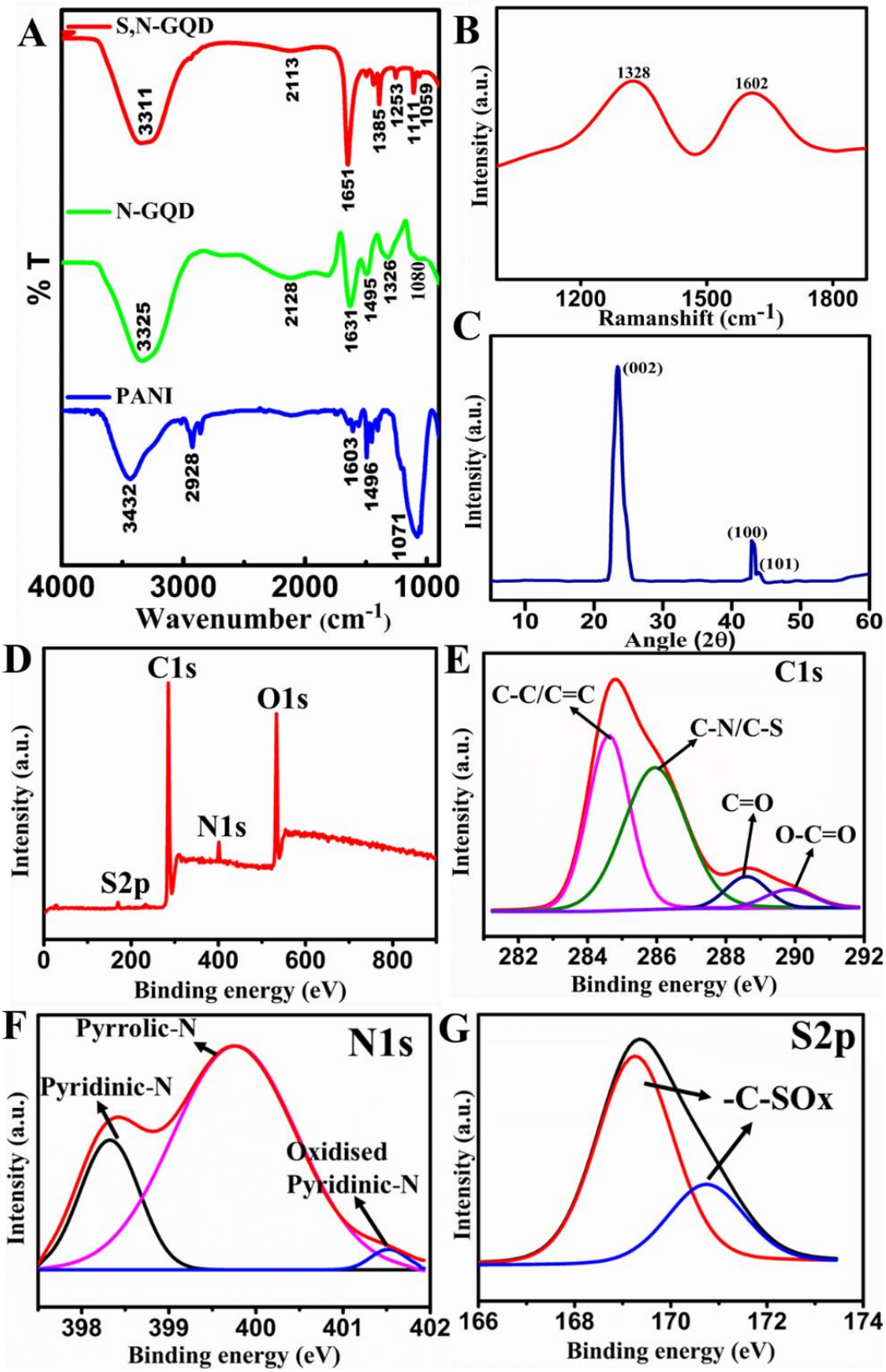

Figure 4.3. (A) The FTIR spectra of S,N-GQD, N-GQD, and PANI; (B) and (C) The Raman and XRD diffractograms of S,N-GQD; (D) The XPS (survey) Spectra of S,N-GQD; (E), (F) and (G) The high-resolution XPS spectra of the C 1s and N 1s and S 2p of S,N-GQD.

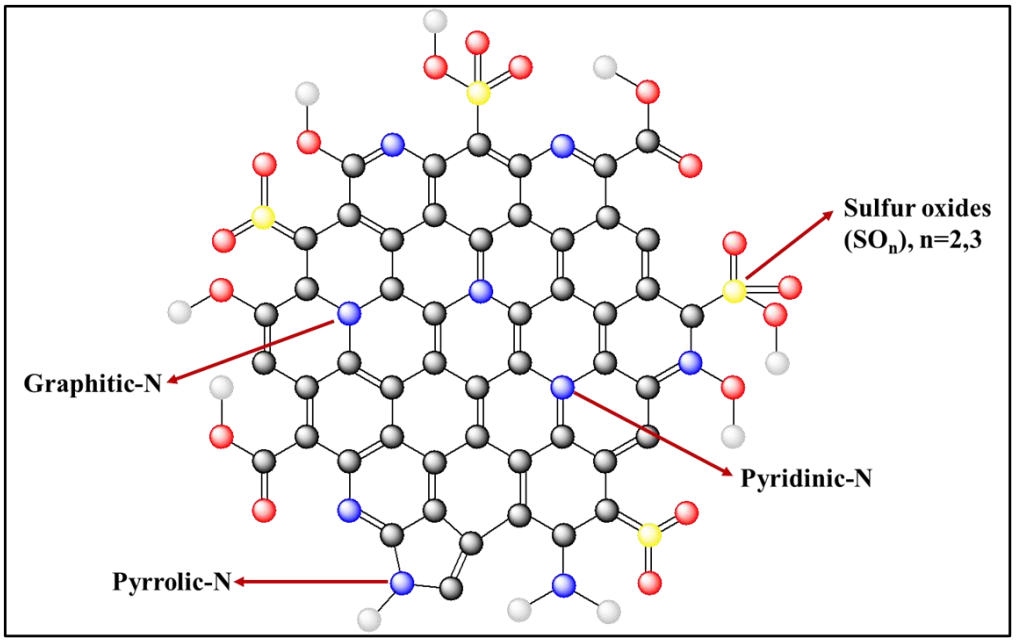

Figure 4.4. Schematic showing the representative structure of S,N-GQD

4.3.2 EC sensing studies of S,N-GQD towards heavy metal ions

Inspired by our earlier sensing studies of N-GQD(Ramachandran, Arya Nair, and Karunakaran Yesodha 2019a)-(Saisree et al. 2021a) which exhibited selective sensing towards Cd(II)(Saisree et al. 2021a), the EC sensing property of S,N-GQD/GCE towards toxic heavy metal ions was explored, and the following ions: Cd(II), Hg(II), Ag(I), Pb(II), Fe(II), Co(II), Ni(II), Zn(II), Sn(II), Cu(II), and Cr(VI) were tested initially. Curiously, the result showed that the S,N-GQD/GCE exhibited current responses towards three of the top ten toxic metal ions: Cd(II), Pb(II), and Hg(II). The comparison of the results of controls and S,N-GQD/GCE (Figure 4.5A) showed no current response for any of these ions on the bare GCE, PANI/GCE, and GQD/GCE, and current response for Cd(II) at -0.78 V on the N-GQD/GCE(Saisree et al. 2021a), whereas the S,N-GQD/GCE exhibited three distinct and very sharp oxidation peaks at -0.80, -0.57, and 0.16 V for Cd(II), Pb(II), and Hg(II), respectively. In addition, the current response for Cd(II) on S,N-GQD (Figure 4.5A) was ~ 7-fold higher than that of on the N-GQD. The results indicate that the co-doping of S has not only enabled the simultaneous sensing of multiple metal ions, it has tremendously enhanced the current response. As reported earlier by our

group(Saisree et al. 2021a), the Cd(II) sensing can be attributed to the N-groups; the additional ability of sensing of Pb(II) and Hg(II) is assigned to the presence of S, which had an affinity towards Pb(II) and Hg(II). Thus the Pb(II)-S and Hg(II)-S interaction facilitated the simultaneous sensing of Pb(II) and Hg(II) along with Cd(II) and the enhancement in the current response to the enhanced electrocatalytic and conducting property due to effective S doping in S,N-GQD. Bandgap measurement (details in the supporting file) results revealed that the S-doping has narrowed the band gap of S,N-GQD to 0.98 eV (Figure 4.5B), from that of 1.3 eV (Figure 4.5B), in N-GQD. This shall be due to the insertion of the bonding and antibonding orbital of S between the antibonding orbital of N (previous LUMO) and the bonding orbital of C (HOMO)(Luo et al. 2017) (explained in detail in section 3.1), which can further facilitate an improved electron transfer ability to the analytes (Figure 4.5B). The lower electronegativity of S to that of N, which increases the availability of electrons in the aromatic structure combined with the narrowed band gap, shall be attributed to the improved electronic characteristics and enhanced conductivity, thereby enhancing the sensing performance.

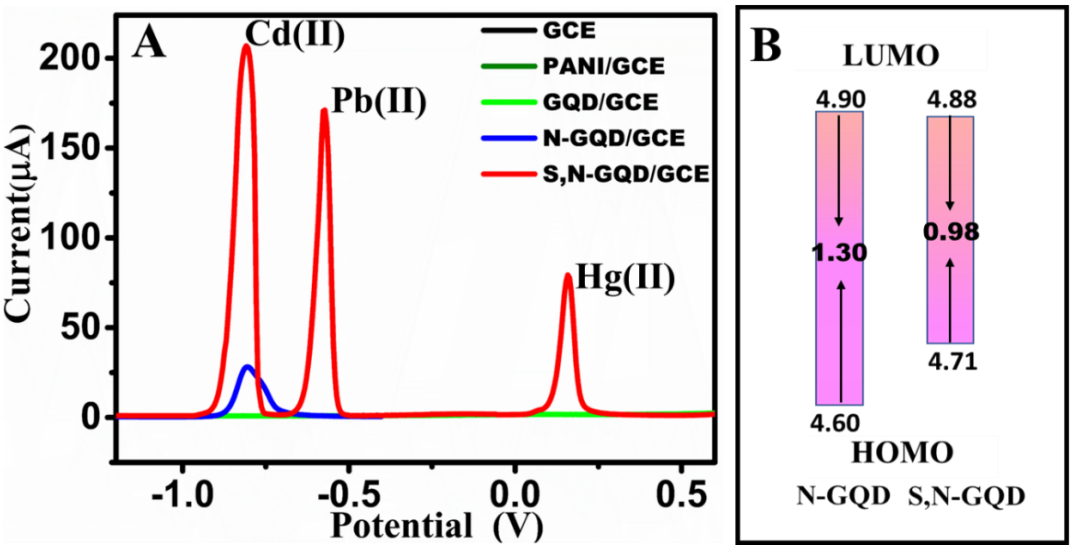

Figure 4.5. (A) The DPV responses of 1 mM each of Cd(II), Pb(II), and Hg(II) in 0.1 M PBS on Bare GCE, PANI/GCE, GQD/GCE, N-GQD/GCE and S,N-GQD/GCE respectively; (B) The HOMO and LUMO levels and bandgaps of N-GQD and S,N-GQD obtained experimentally.

4.3.3 Individual sensing studies - Sensitivity, LDR and LOD

The sensing performance of S,N-GQD towards Cd(II), Pb(II) and Hg(II) individually was explored in detail using DPV. The current responses of each analyte (Figure 4.6A-C) increased with the increase in the concentration. The corresponding linear dynamic ranges (LDR) for Cd(II), Pb(II), and Hg(II) (Figure 4.6D-F) showed a linear fit corresponding to the concentrations from 10^{-10} to 10^{-4} M with correlation coefficients of $R^2 \geq 0.97$ for each. A single LDR covering from 10^{-10} to 10^{-4} M, without the saturation of current response, shows the superior sensing capability of the S, N-GQD for a wider concentration range. The sensitivity values obtained for Cd(II), Pb(II), and Hg(II) from the respective LDRs are 12, 13, and 5 $\mu A \mu M^{-1} cm^{-2}$, and the LOD values (Figure 4.6G-I), obtained for Cd(II), Pb(II), and Hg(II) were 10^{-12}, 10^{-11}, and 10^{-12} M, respectively. The LOD values calculated theoretically from the respective LDRs, were 3.3×10^{-12}, 1.4×10^{-11}, and 1.1×10^{-12} M and are in good agreement with the experimental LOD values, which shows the correctness of the experimentally obtained value with that of the theoretically calculated one.

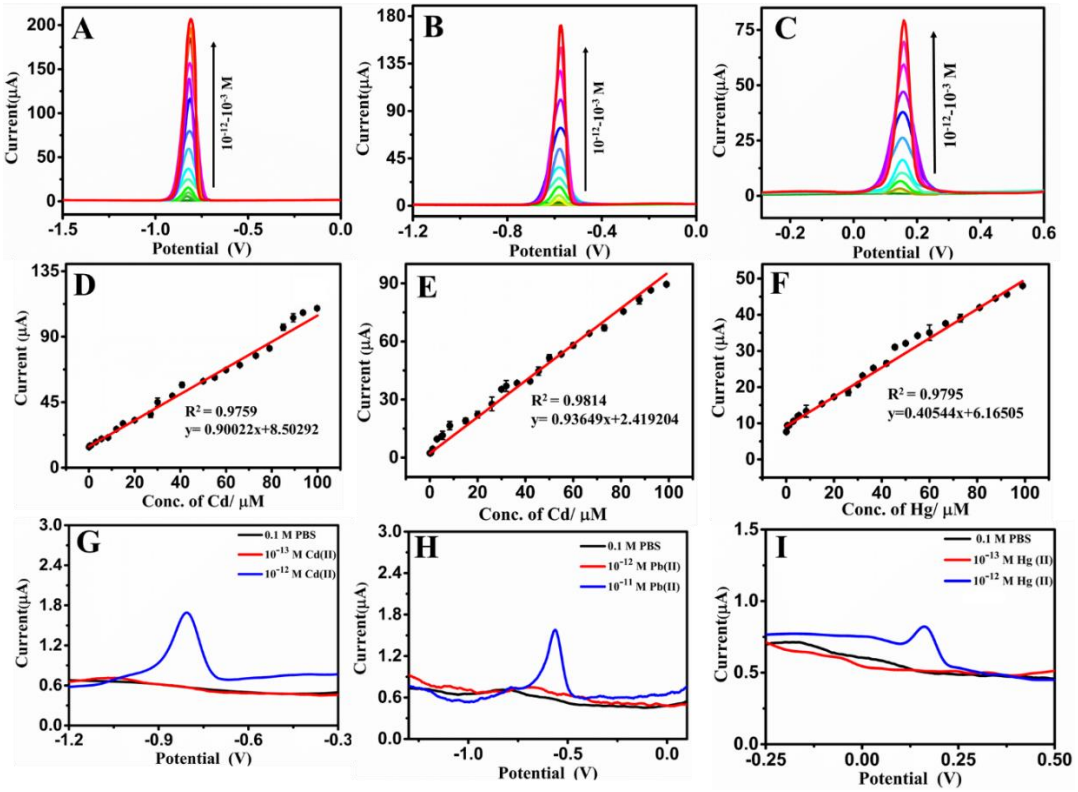

Figure 4.6 (A) , (B), and (C) The DPV responses of Cd(II), Pb(II, and Hg(II) in 0.1 M PBS on S,N-GQD/GCE from 10^{-12} to 10^{-3} M each respectively; (D), (E) and (F): The LDRs obtained for the sensing of Cd(II), Pb(II and Hg(II) on the S,N-GQD/GCE for the concentration range of 10^{-10} to 10^{-4} M, each; (G), (H) and (I) The DPV responses showing of LOD Cd(II), Pb(II and Hg(II), as 10^{-12}, 10^{-11}, and 10^{-12} M.

4.3.4 Simultaneous sensing studies - Sensitivity, LDR and LOD

The simultaneous sensing efficiency of S,N-GQD was investigated further by recording the variation of current responses of each analyte by varying its concentration from 10^{-12} to 10^{-3} M in the presence of the other two analytes maintained at a fixed concentration of 10^{-3} M. The DPV profiles (Figure 4.7A-C) indicate that the peak current values of the analytes were the same as that observed in the individual sensing studies for all three metal ions, and the corresponding LDR graphs (Figure 4.7D-F) exhibited two ranges with excellent correlation coefficients of $R^2 \geq 0.98$: from 10^{-12} to 10^{-4} M and 2×10^{-4} to 10^{-3} M; 10^{-11} to 10^{-4} M and 2×10^{-4} to 10^{-3} M; and 10^{-12} to 10^{-4} M and 2×10^{-4} to 10^{-3} M for Cd(II), Pb(II) and Hg(II), respectively. The LOD values were the same as that for the individual studies and were 10^{-12}, $10^{-11,}$ and 10^{-12} M for Cd(II), Pb(II), and Hg(II), respectively (Figure 4.6G, H, and I). The result indicates that there is more or less no interference of analytes on each other and is the indication of the effective simultaneous sensing of the metal ions by S,N-GQD.

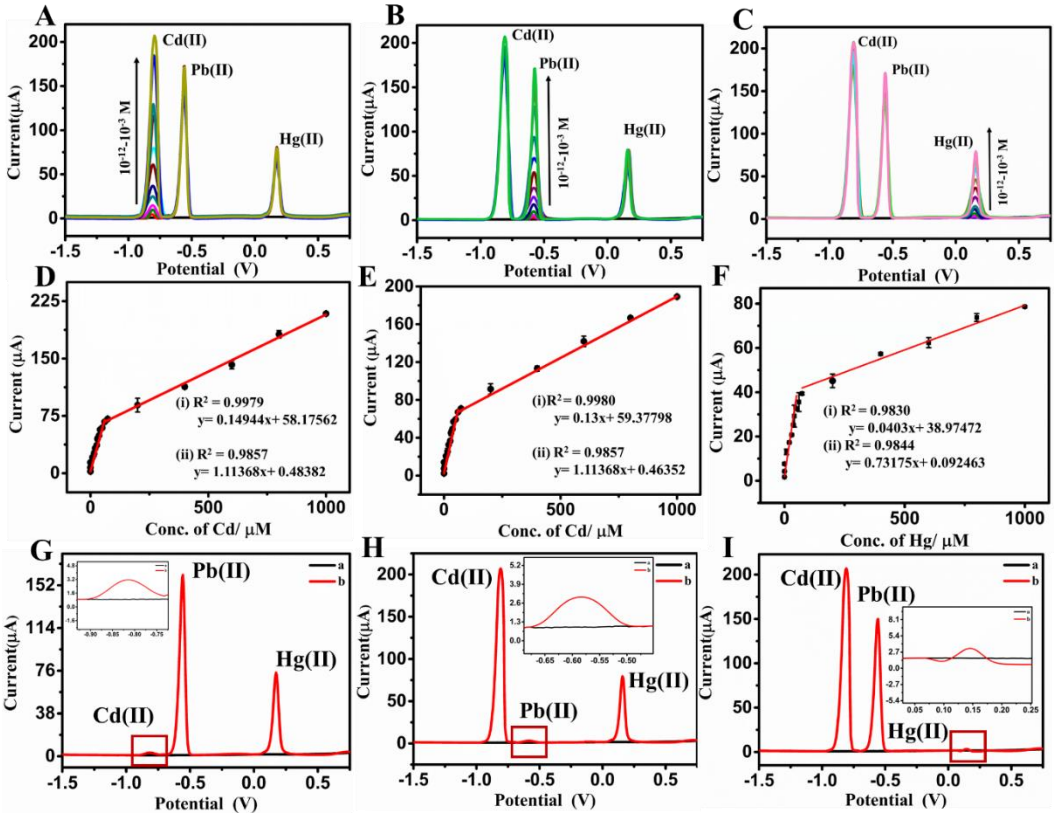

Figure 4.7. (A), (B), and (C) The simultaneous DPV responses of Cd(II), Pb(II), and Hg(II) by varying the concentrations from 10^{-12} to 10^{-3} M in the presence of 1 mM concentration of the other two analytes; (D), (E), and (F) The corresponding LDR graphs of the simultaneous sensing of Cd(II), Pb(II) and Hg(II); (G), (H) and (I) The DPV responses of (a) 0.1 M PBS and (b) the LODs of Cd(II) (1 pM), Pb(II) (10 pM) and Hg(II) (1 pM) in the presence of 1 mM concentrations of the other two analytes; (Inset of G, H and I) The enlarged images of LODs of Cd(II), Pb(II) and Hg(II) respectively.

Further, simultaneous quantitative sensing was conducted by increasing the concentration of all three ions simultaneously. The resultant DPV profiles (Figure 4.8) showed an increase in current responses with an increase in the concentrations for all the three with well-defined oxidation peaks with significant peak potential difference (ΔE_{pa}) of ~0.23, 0.72, and 0.95 V between Cd(II) & Pb(II), Pb(II) & Hg(II), Cd(II) & Hg(II), respectively, which is indicative of the non-interference and the effective simultaneous sensing capability. The LOD values obtained for Cd(II), Pb(II), and Hg(II) were 10^{-12}, 10^{-11}, and 10^{-12} M (inset of Figure 4.8), which were the same as that obtained for the individual sensing studies. This shows the simultaneous sensing capability of the material S,N-GQD.

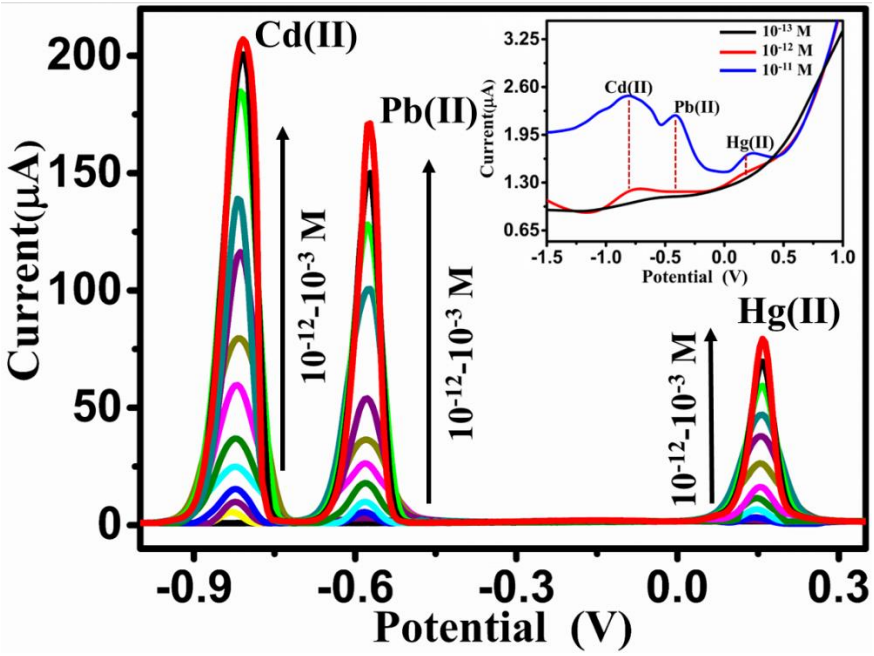

Figure 4.8. The DPV responses of Cd(II), Pb(II and Hg(II) on S,N-GQD/GCE from 10^{-12} to 10^{-3} M; Inset of (4.8.) The DPV responses showing LOD values 10^{-12} M , 10^{-11} M and 10^{-12} M for Cd(II), Pb(II) and Hg(II).

The simultaneous sensing reports of Cd(II), Pb(II), and Hg(II) by various electrode materials are very few compared to the individual sensing studies, and the

comparison of LOD values in the reports with that of the S,N-GQD electrode is given in Table 1. Amongst the reports SnO_2/reduced graphene oxide nanocomposite (SnO_2/rGO)(Y. Wei et al. 2012), $MnFe_2O_4$@Cys(Yao et al. 2014), and alkaline-Ti_3C_2 MXene(Zhu et al. 2017) utilized square-wave anodic stripping voltammetry (SWASV) for the simultaneous sensing. Similarly, there are reports on differential pulse stripping voltammetry (DPSV) and DPV, which were also utilized for sensing. The stripping voltammetric techniques are used because of the oxidized nature of metal ions or to improve the sensitivity and LOD values of the sensor. However, they are time-consuming as it requires an additional pre-reduction step which is done for a certain period of time compared to the normal DPV. Here in this work, we followed the normal DPV analysis, without a pre-reduction, for the detection of Cd(II), Pb(II), and Hg(II), as the S,N-GQD was able to spontaneously reduce the metal ions, and the sensitivity and LOD values obtained were 12, 13 & 5 $\mu A \mu M^{-1} cm^{-2}$ and 10^{-12}, 10^{-11} &10^{-12} M. It can be observed that the reports had LODs in nM range for the three metal ions, whereas S,N-GQD exhibited LOD values in pM range by DPV, which is roughly 100 times lower than all the reports. Thus, from the Table, it is clear that the achieved LOD by S,N-GQD is the lowest for the simultaneous sensing of the three metal ions reported hitherto to the best of our knowledge, with a commendable LDR corresponding to a wide range from 0.1 to 100000 nM. These excellent sensing characteristics of S,N-GQD towards heavy metal ions are due to its higher reducing capability, which is explained in detail in the next section, 3.5.

Table 4.1. Comparison of the limit of detection of S,N-GQD/GCE with that of the literature reports of electrochemical sensors of Cd(II), Pb(II) and Hg(II).

Material	**Measurement technique**	**Pre-reduction**	**LOD (nM)**			**LDR (nM)**			**Ref.**
			Cd (II)	**Pb (II)**	**Hg (II)**	**Cd (II)**	**Pb (II)**	**Hg (II)**	
SnO_2/rGO	SWASV	Yes	0.1	0.1	0.2	300 – 1200	300 – 1200	400 – 1200	(Y. Wei et al. 2012)
NG	DPSV	Yes	50	5	5	50 – 9000	50 - 9000	50 - 9000	(Xing et al. 2015)

$MnFe_2O_4$ @Cys	SWASV	Yes	63.2	84.3	208	0.4–1.5	0.1–1.0	1.4–3.0	(Yao et al. 2014)
alk-Ti_3C_2 MXene	SWASV	Yes	98	41	130	100−1000	100−550	1000−1900	(Zhu et al. 2017)
$MnWO_4$	DPASV	Yes	3.5	3.3	3.1	10–500	10–500	10–500	(Eranjaneya et al. 2018)
Ruthenium-GO	DPV	No	13	350	340	50-300	50-250	100-1200	(Gumpu et al. 2017)
SNAC	DPV	No	24.4	5.7	24	90–4800	90–5700	90–990	(Madhu et al. 2014)
S,N-GQD	DPV	No	0.001	0.01	0.001	0.1-100000	0.1-100000	0.1-100000	This work

4.3.5 Mechanism of sensing of Cd(II), Pb(II), and Hg(II) by S,N-GQD with evidence

In the stripping voltammetric techniques,(Intarakamhang, Schuhmann, and Schulte 2018)-(Lu et al. 2018) the pre-reduction step is utilized to reduce the target metal ion/ions adsorbed on the modified electrodes, which subsequently undergoes oxidation during the oxidation potential sweep, which increases the sensitivity and reduces the LOD values. This is done because of the non-capability of the sensor material to spontaneously reduce the metal ions or to improve the current response of the sensor material, which is a time-consuming process. The sensing studies using S,N-GQD as the electrode did not need any pre-reduction procedure due to its ability to spontaneously reduce the Cd(II), Pb(II), and Hg(II) to Cd(0), Pb(0) and Hg(0) as evidenced from the presence of oxidation peaks in the oxidation sweep without any pre-reduction step. Prior reports of N-GQD towards Cd(II)(Saisree et al. 2021a), in MoS_2 towards Hg(II)(Aswathi and Sandhya 2018), SnO_2 QDs towards Cd(II)(Bhanjana et al. 2015), MWCNT/PCV towards Cd(II)(Chamjangali et al. 2015) displayed a similar spontaneous reduction of the metal ions by the electrode

materials, and the mechanism was based on the presence of an electron-rich material which can reduce the metal ions by supplying electrons spontaneously. The structure of the S,N-GQD was similar to that of the N-GQD, considering the graphene lattice, which had N-doping, and the difference was in the presence of additional S containing side functionalities ($–SO_n$) (explained in detail in section 4.3.1) in the S,N-GQD. The significant increase in the current response for Cd(II) on S,N-GQD to that of on the N-GQD (~ 7-fold) suggests that having S functionalities as side groups makes a remarkable difference in the electron-rich environment and the reducing capability of the S, N-GQD. The earlier report of Cd(II) sensing by N-GQD was attributed to the affinity between Cd(II) and N(Saisree et al. 2021) and can also be applied here due to the presence of N in S,N-GQD. The Pb(II) and Hg(II) sensing properties exhibited by S,N-GQD, which was not present on N-GQD were attributed to the high affinity of the S-functionalities towards the ions(Aswathi and Sandhya 2018)·(Jayadharan Salini et al. 2020)⁻(Arya Nair, Saisree, and Sandhya 2022). Thus, it is evident that the presence of S and N is the reason for the simultaneous sensing of Cd(II), Pb(II), and Hg(II) on S,N-GQD with enhanced sensitivity.

In an attempt to prove the mechanism proposed, XPS analysis was carried out for the S,N-GQD-Cd, S,N-GQD-Pb and S,N-GQD-Hg obtained by physical mixing of S,N-GQD with $CdCl_2$, $PbCl_2$ and $HgCl_2$ solutions separately. The XPS survey spectra of the S,N-GQD-Cd, S,N-GQD-Pb, and S,N-GQD-Hg (Figure 4.9A-C) display the peaks of the respective metals (ions).

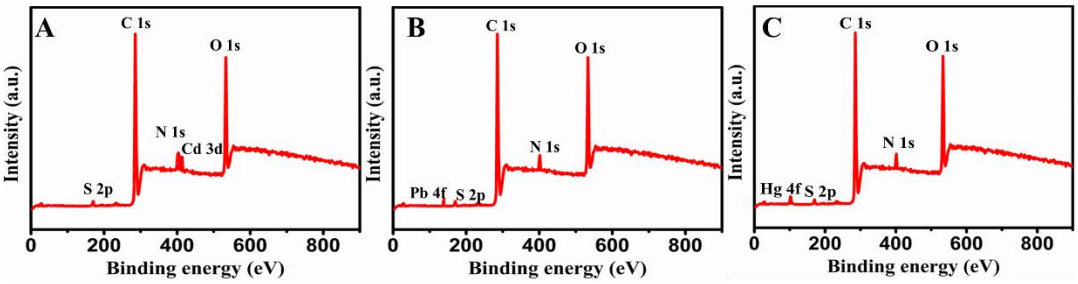

Figure 4.9. (A), (B) and (C) The XPS (survey) spectra of S,N-GQD-Cd, S,N-GQD-Pb, and S,N-GQD-Hg, respectively

The decrease in the peak intensities of C1s (Figure 4.10A-C), S2p (Figure 4.10D-F), and N1s (Figure 4.10G-I) in the high resolution spectra of S,N-GQD-Cd, S,N-GQD-Pb and S,N-GQD-Hg, with respect to that of S,N-GQD (section 3.1)

backing the interaction between S,N-GQD and the metal ions Cd(II), Pb(II) and Hg(II). The high-resolution spectrum of Cd 3d (Figure 4.10J) in S,N-GQD-Cd reveals the characteristic $3d_{5/2}$ and $3d_{3/2}$ peaks at 405.09 and 412.10 eV, respectively corresponds to Cd(0) and that of Pb 4f in S,N-GQD-Pb reveals the characteristic $4f_{7/2}$ and $4f_{5/2}$ peaks at 138.56 and 143.30 eV (Figure 4.10K), respectively commensurate to Pb(0). Similarly, the high-resolution spectrum of Hg 4f in S,N-GQD-Hg, reveals the characteristic Hg 4f peaks at 101.43 and 104.65 eV (Figure 4.10L) corresponding to the Hg $4f_{7/2}$ and $4f_{5/2}$, respectively with Hg(0) state. These peaks confirms the existence of Cd(0)(Saisree et al. 2021a), Pb(0)(Knight, Nigam, and Jones 2019) and Hg(0)(Aswathi and Sandhya 2018) in the system. Thus these results clearly confirm the reduction of Cd(II), Pb(II), and Hg(II) to Cd(0), Pb(0), and Hg(0) by S,N-GQD. An illustration of the enhanced and simultaneous sensing of Cd(II), Pb(II), and Hg(II) on S,N-GQD/GCE is depicted in Figure 4.11.

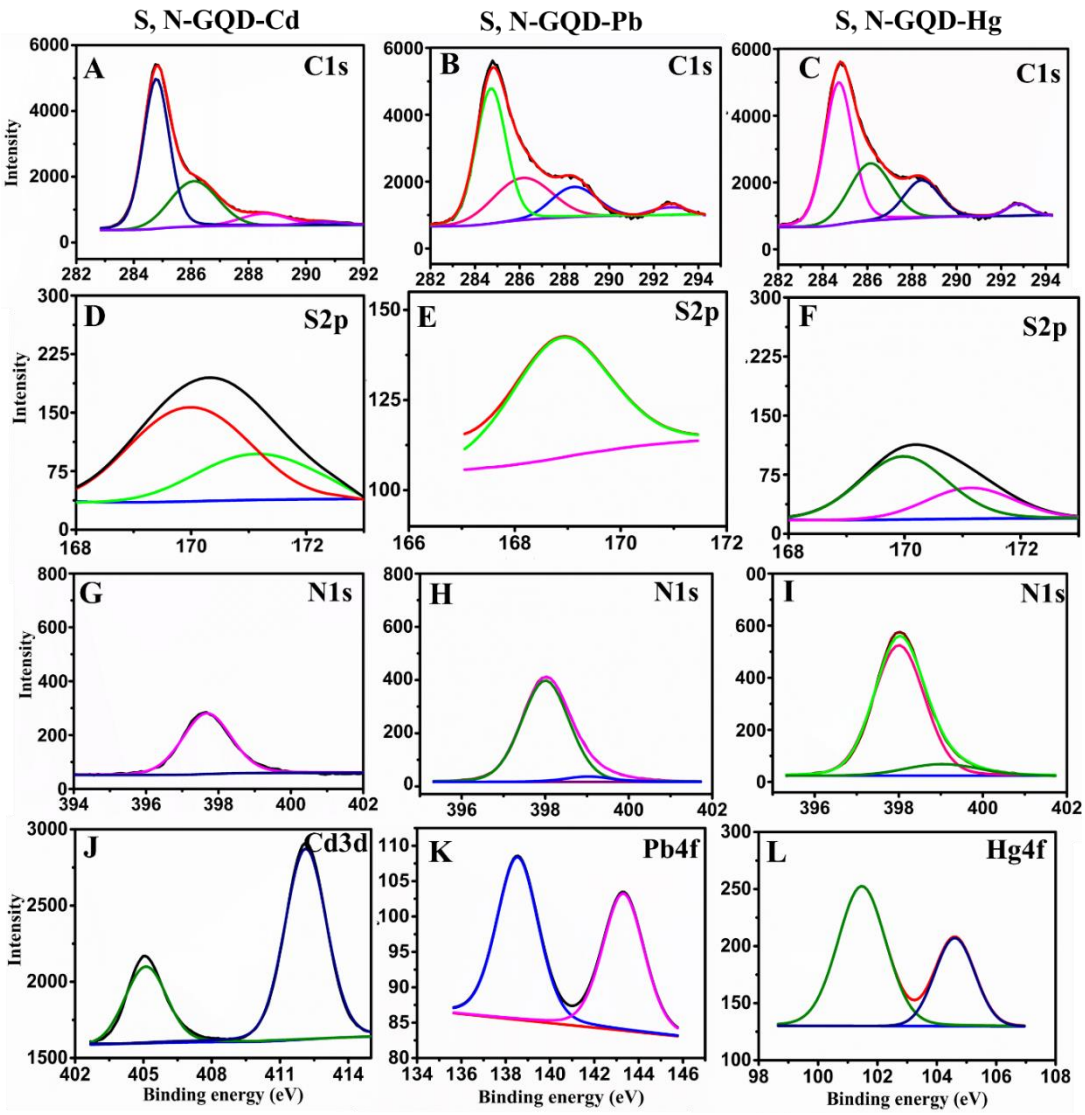

Figure 4.10 (A), (B) and (C) The high-resolution C 1s XPS spectra of S,N-GQD–Cd, S,N-GQD–Pb and S,N-GQD–Hg respectively; (D), (E) and (F) The high-resolution S 2p XPS spectra of S,N-GQD–Cd, S,N-GQD– Pb and S,N-GQD–Hg respectively; (G), (H) and (I) The high–resolution S 2p XPS spectra of S,N-GQD–Cd, S,N-GQD– Pb and S,N-GQD–Hg respectively; (J), (K) and (L) The high–resolution Cd 3d, Pb 4f and Hg 4f XPS spectra of S,N-GQD–Cd, S,N-GQD– Pb and S,N-GQD–Hg respectively.

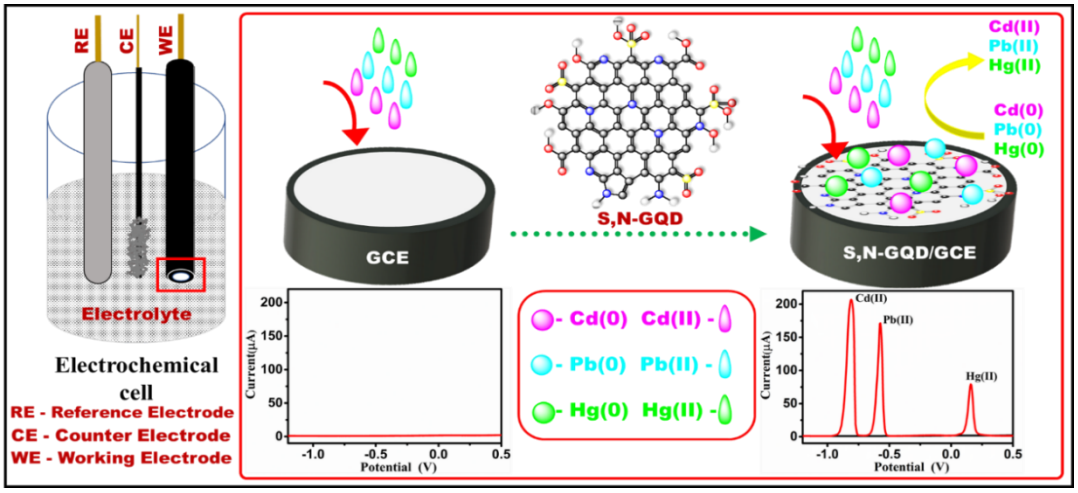

Figure 4.11. Schematic diagram showing the modification of the GCE in the three-electrode system with the S,N-GQD, and the resulting enhanced simultaneous sensing of Cd(II), Pb(II), and Hg(II) by DPV

4.3.6 Selectivity and Interference Studies

Selectivity is one of the most significant parameters considered as the criteria for ensuring the practical applicability of a sensor. The DPV profiles of the simultaneous sensing of 1nM each of Cd(II), Pb(II), and Hg(II) in a mixture of 1000000x concentrations of other metal ions, Ag(I), Fe(III), Fe(II), Co(II), Ni(II), Zn(II), Mg(II), Li(II), Mn(II), Sn(II), Cu(II), and Cr(VI)) (1 mM each) (Figure 4.12A) and the corresponding bar diagram (Figure 4.12B) show no significant current response from any of the other metal ions, indicating the high-rate selectivity of the material towards the simultaneous as well as individual sensing of Cd(II), Pb(II) and Hg(II).

4.3.7 Reusability, Reproducibility, and Stability Studies

The reusability, stability, and reproducibility studies are essential when it comes to the practical applicability of a sensor. For the reproducibility studies, the current responses of five different electrodes toward 1 mM each of Cd(II), Pb(II) and Hg(II) were examined. The relative standard deviation (RSD) of the peak currents of these individually prepared electrodes was found to be ~1.1 % for Cd(II), ~0.5 % for Pb(II), and ~2.0 % for Hg(II), which showed its good reproducibility (Figure 4.12C). The stability studies were conducted after 30 and 60 days, and the result showed that it retained ~ 97% and ~ 93% for Cd(II), ~ 90% and 80% for Pb(II), and ~ 90% and 80% for Hg(II) (Figure 4.12D) of its initial current responses,

respectively. The reusability of the S,N-GQD/GCE electrode was scrutinized by comparing the peak currents for 1 mM each of Cd(II), Pb(II) and Hg(II) on S,N-GQD/GCE (Figure 4.12E) before and after multiple washings and the results showed it had ≥ 98% retention after 30 cycles of washing.

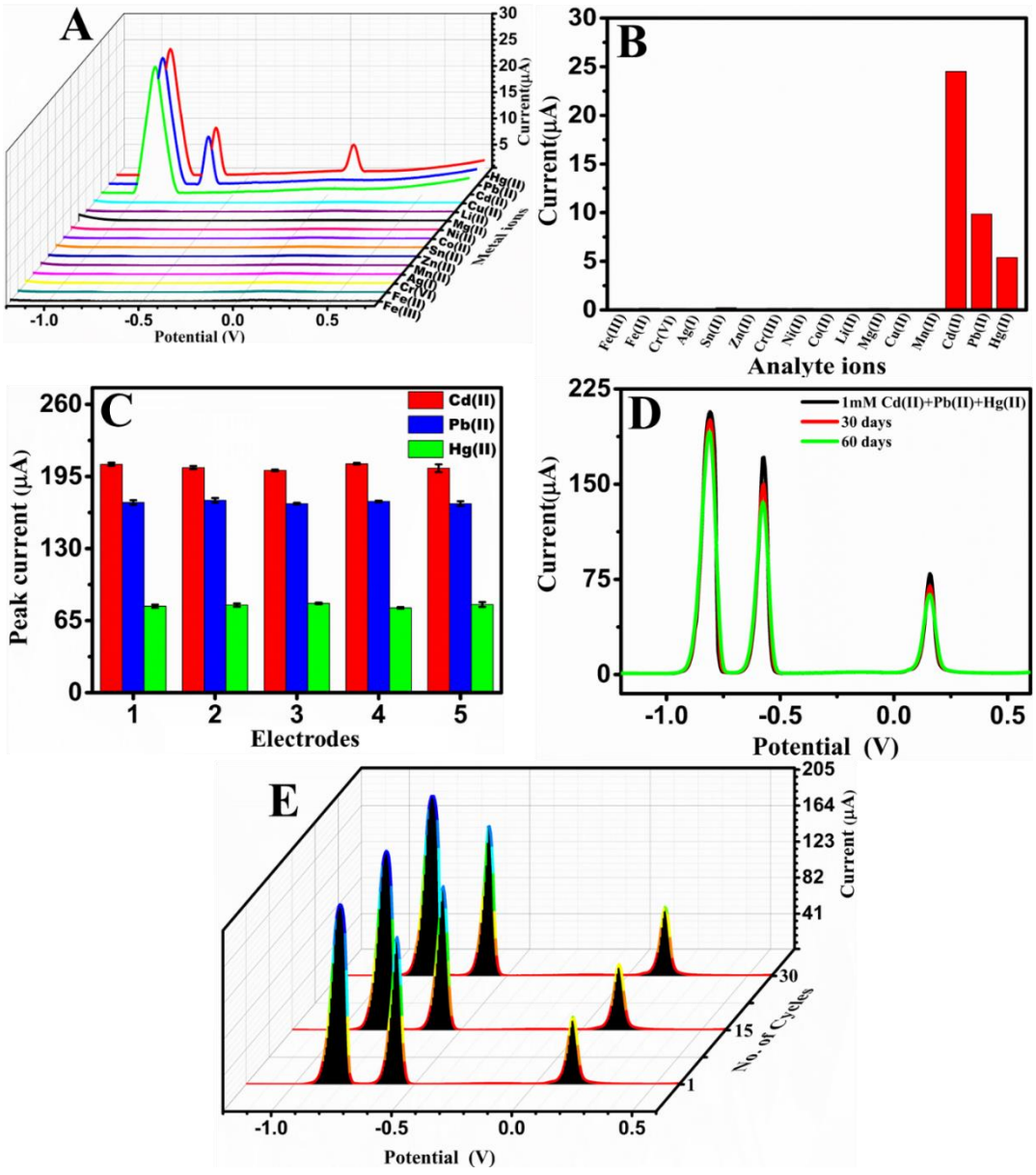

Figure 4.12. (A) and (B) Selectivity studies of S,N-GQD/GCE towards 1 nM Cd(II), Pb(II) and Hg(II) in the presence of various analyte species (1 mM each); (C) The peak currents of five independently coated electrodes showing the reproducibility of S,N-GQD/GCE; (D) DPV profiles obtained for Cd(II), Pb(II) and Hg(II) (1 mM each) on S,N-GQD/GCE showing the stability of the sensor for 30 and 60 days; (E) The DPV curves after immediate washing for thirty times showing the reusability of the sensor.

4.3.8 Environmental sample studies

Further, the studies were extended to real environmental samples such as groundwater, seawater, and wastewater spiked with the analytes. The high recovery values of ~ 100 % (Tabel 4.2 & Figure 4.13.A-B) indicate the possibility of the electrode for the determination of Cd(II), Pb(II), and Hg(II) in real water samples. In addition to the spiking and recovery analysis, seawater (SW) (collected from the Arabian Sea near Thiruvananthapuram) was taken as the electrolyte, and the sensing studies were carried out by adding Cd(II), Pb(II), and Hg(II). Interestingly, the same LOD values were obtained for Cd(II) (1 pM), Pb(II) (10 pM) and Hg(II) (1 pM) (Figure 4.13.C-E) in SW. The result is indicative of the sensitivity and selectivity of the electrode towards the simultaneous sensing of Cd(II), Pb(II), and Hg(II) in complex real water samples where the presence of different organic compounds or species will make the sensing usually difficult.

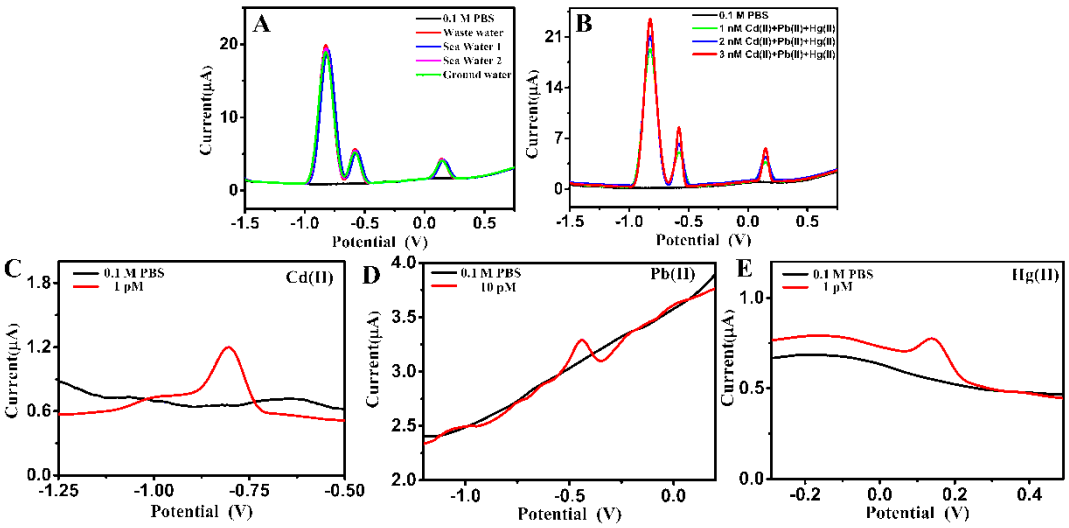

Figure 4.13. (A) The DPV response of 1 nM each of Cd(II), Pb(II), and Hg(II) in wastewater, two different seawater samples, and groundwater sample, respectively; (B) The DPV responses of 1, 2, and 3 nM each of Cd(II), Pb(II), and Hg(II) in seawater samples; (C), (D) and (E) The DPV responses showing the LOD values of 10^{-12}, 10^{-11}, and 10^{-12} M for Cd(II), Pb(II), and Hg(II) in the seawater samples.

Table 4.2. The recovery test results of Cd(II), Pb(II) and Hg(II) in environmental samples.

Sample No.	Metal ions	Environmental samples	Spiked Quantity (ppb)	Found Quantity (ppb)	ICP-MS (ppb)	Recovery (%)
1	Cd(II)	Groundwater	0.2	0.199	0.199±0.11	99.5
		Seawater	0.2	0.201	0.200±0.16	100.5
		Wastewater	0.2	0.201	0.201±0.13	100.5
2	Pb(II)	Groundwater	0.2	0.199	0.198±0.15	99.5
		Seawater	0.2	0.200	0.199±0.19	100
		Wastewater	0.2	0.201	0.200±0.12	100.5
3	Hg(II)	Groundwater	0.2	0.199	0.198±0.18	99.5
		Seawater	0.2	0.198	0.199±0.10	99
		Wastewater	0.2	0.200	0.199±0.17	100

* All the recovery values fall within the RSD of 0.5%

4.4 Conclusion

Herein, a white emissive S,N-GQD was synthesized for the first time from polyaniline using H_2SO_4 which doubles as an acid catalyst and S doping agent. The S doping induced an additional emission peak at ~ 345 nm, resulting in a white light emitting S,N-GQD. The S,N-GQDs displayed simultaneous EC sensing towards three of the top ten toxic heavy metal ions: Cd(II), Pb(II), and Hg(II), with highly sharp peaks and enhanced current response. The interaction of the heteroatoms N and S with the metal ions Cd(II), Pb(II), and Hg(II) were assigned to the simultaneous sensing capability of S,N-GQD and exhibited the lowest LODs so far reported for the simultaneous sensing. Thus, herein, we have demonstrated how minute difference, or a co-doping, leads to a miraculous augmentation in the characteristics/sensing properties of a GQD. The results are assigned to the enrichment in the active sites, improved electron cloud, and better electrocatalytic

activity gained by the S co-doping. The excellent reusability (~98%), the reproducibility with an RSD of ≤ 2%, and the admirable stability of ≥ 80% even after 60 days further prove the efficiency of the developed sensor. The potential applicability of the sensor in real-time monitoring was put forward in the excellent recovery percentages (~ 100%) with a relative standard deviation of ≤0.5% in the tested environmental samples.

CHAPTER 5

Highly Stable Copper Nano Cluster on Nitrogen-Doped Graphene Quantum Dots for the Simultaneous Electrochemical Sensing of Dopamine, Serotonin, and Nicotine; a Possible Addiction Scrutinizing Strategy

A highly stable copper (Cu) nanocluster (NC), which exhibited stability for more than one year, was synthesized. The synthesis utilizes nitrogen-doped graphene quantum dots (N-GQDs) as reducing and capping agents and smaller glutathione molecules as additional capping agents. The synthesized NC, CuNC@N-GQD successfully sensed dopamine (DA), serotonin (SER), and nicotine (NIC) simultaneously with well-defined peaks and good peak-to-peak separation. The higher sensitivity and the simultaneous sensing are indicative of the synergistic effect of CuNC and N-GQD in the CuNC@N-GQD. Thus, a mechanism for the enhanced simultaneous sensing of DA, SER and NIC were explored further. The interactions between the sensor and the analytes through ring stacking or heteroatom sites or the π–π interaction between the aromatic basal planes or the combination of all is assigned to the enhanced sensitivity. The sensing performance was successfully extended to real blood and urine samples spiked with DA, SER, and NIC.

5.1 Introduction

Recently metal nanoclusters[1-5] (MNCs) are gaining attention amongst researchers because of their merits such as emissive properties(Zhenguang Wang, Chen, and Rogach 2017), prominent photostability, large Stokes shift of ≥100 nm(Koninti, Satpathi, and Hazra 2018), and lack of toxicity(Tao et al. 2015) for applications such as sensors[1,2,6,](Hu et al. 2016), biological imaging(Publication et al. 2017), catalysis, and light-emitting devices(Zhenguang Wang, Chen, and Rogach

2017). Amongst the MNCs, that of gold (Au) and silver (Ag) have been extensively explored due to their higher stability, ease of synthesis, and biocompatibility(Lin et al. 2021). Recently, NCs of copper (Cu) has begun to attract the attention of researchers because of their abundance, cost-effectiveness, and easy availability. Despite their advantages, Cu NCs often exhibit low oxidation stability[2] and the synthesis of small, brightly emissive Cu NCs (1-5 nm) is particularly challenging[12]. In this respect, capping / stabilising agents are often used to stabilise the clusters, while being synthesized. Earlier approaches have utilized larger molecules such as polymers(Zhenguang Wang,a Andrei S. Susha,a Bingkun Chen,a, b Claas Reckmeier,a Ondrej Tomanec,c Radek Zboril,c Haizheng Zhong 2016)-(H. Zhang et al. 2012), DNA(Borghei et al. 2017)-(C. A. Chen et al. 2015), proteins(Su and Liu 2017)-(Qiao et al. 2015), and peptides(Singh et al. 2020) as steric capping agents to overcome the problem of aggregation and oxidation of CuNCs. Even though a few CuNCs(Maity, Bain, and Patra 2019)-(Zhenguang Wang et al. 2016) synthesized using smaller thiolated ligands as capping agents have been reported, the stability of the nanoclusters is lower (~1 month) than that of the NCs prepared using large ligands (~6 months). However, the advantage of using smaller capping agents is that it can simplify the characterization of NCs. In the present work, we report an aqueous medium synthesis of a stable CuNCs using nitrogen-doped graphene quantum dots (N-GQDs) as reducing agents and glutathione as capping agents instead of the larger ligands such as proteins and DNAs. The presence of N-GQD in the formed NCs was confirmed by the emission and mass spectroscopic analyses, and they are hereafter referred to as CuNC@N-GQD.

Our group has previous reported[54] the selective and superior sensing of dopamine (DA) by materials with graphene structure due to their favorable interactions with each other that arose from their structural similarity. This preliminary information prompted us to choose DA and similar neurotransmitters such as serotonin (SER), epinephrine (EP), nor-epinephrine (NEP) as analytes due to the presence of N-GQD with a graphene structure. In our preliminary sensing studies, overlapped peaks for DA and SER were obtained at an N-GQD-modified electrode. CuNCs have been reportedly utilized for the EC sensing of nitrite[69] zinc ions[70]. To utilize the sensing property of the CuNCs in CuNC@N-GQD, nicotine (NIC) was selected as one of the analyte because of (i) the neurofunctional

correlation among DA, SER and NIC (ii) and the knowledge that Cu can interact with N-containing molecules[41,50], which will complement the study because of the well-known addictional[30-31] property of NIC affecting the emotions and behavior due to its ability to prompt the release of several neurotransmitters(Jiloha 2010). Thus, in addition to the neurotransmitters, NIC was chosen as one of the analytes for the study. The sensing results revealed that the CuNC@N-GQD displayed synergistic effect by exhibiting both simultaneous sensing (non-overlapping peaks) and enhanced current response for DA, SER, and NIC, compared to that of the individual CuNC and N-GQD, which is attributed to the improved structure of CuNC@N-GQD. The exfoliated graphene structure of N-GQD due to the attachment of CuNC in CuNC@N-GQD is assigned to the simultaneous sensing of DA and SER with separate peaks for each. The augmentation of electrons through N-GQD enabled the CuNC to sense NIC with enhanced current response compared to that of the CuNC@AA. Thus, the results show the merits of CuNC@N-GQD compared to the individual materials and the other reports of CuNC[42-57] in terms of stability and enhanced and simultaneous sensing properties. Moreover, as mentioned previously, the lower stability of CuNCs than other metal clusters such as AuNCs and AgNCs is a problem encountered during the synthesis of CuNCs using smaller capping agents than larger capping agents (e.g., DNA, proteins). It is understandable that stability is an important parameter for a sensor material that affects its properties such as reproducibility and reusability. Interestingly, in this work, the CuNC exhibited a stability of $\geq$ 1 year, which was assigned to the presence of the electron rich N-GQD. A detailed explanation for the enhancement in the stability and the simultaneous and enhanced EC sensing of DA, SER, and NIC by CuNC@N-GQD is given in Sections 3.1 and 3.5. Further, the possible miniaturization properties of EC sensors and the observed simultaneous and enhanced sensing make the developed sensor, CuNC@N-GQD significant for in vivo medical research and diagnosis purposes.

5.2 Experimental Section

5.2.1 Synthesis of N-GQDs, CuNC@N-GQDs, and CuNC@AA

Detailed synthesis procedure for N-GQDs was reported elsewhere(Ramachandran, Arya Nair, and Karunakaran Yesodha 2019b) by us. Briefly, polyaniline was used as a precursor, and a simple hydrothermal route was followed, resulting in crystalline N-GQDs forming aromatic graphitic basal planes.

In a typical synthesis of CuNC@N-GQDs, 1 mL of $CuSO_4$ solution (~ 0.17 M) was added to 3 mL of GSH (25 mg/mL) and stirred well for 10 min. The solution gradually turned turbid due to the formation of a copper thiolate complex, and then 6 mL of the synthesized N-GQDs was added to this solution with constant stirring, and the reaction mixture was kept at 65 °C with stirring for 3 h. The turbid solution became clear, indicating the formation of CuNC@N-GQDs. Then the solution was allowed to cool down to room temperature. The clear solution obtained was centrifuged at 14000 rpm for 20 minutes, and the obtained supernatant solution was stored at 4 °C for further studies.

The control CuNC, CuNC@AA was synthesized using a reported procedure[1]. In this synthesis procedure, AA was utilized as a reducing agent.

5.2.2 Preparation of electrodes for electrochemical sensing

The pre-treatment and modification of GCE were done according to the procedure given in the Chapter 2. The samples (CuNC@N-GQD, N-GQDs and CuNC@AA were applied dropwise on a separate, cleaned GCE with care and then allowed to dry for 24 h at room temperature to achieve the modified electrodes.

5.2.3 Preparation of samples for mass spectrometric analysis

The CuNC@N-GQD and N-GQD sample solution was diluted 10 times using the solvent system of water/methanol at a 1:1 (v/v) ratio. The experiments were conducted in a negative ion mode.

5.2.4 Electrochemical methods

The EC behavior of the analytes (DA, SER, NIC, FA, UA, AA, acetylcholine, glucose, hydrogen peroxide, and metal ions (Hg(II), Ag(I), Cd(II), Ni(II), Zn(II), Co(II), Cr(VI), Fe(II), Mg(II), Mn(II), Pb(II))) at the surface of the CuNC@N-GQD/GCE was investigated using CV, DPV and chronoamperometry at RT. In our work, a 20 µL of CuNC@N-GQD solution was applied to the GCE placed in a 0.1 M phosphate-buffered saline as the supporting electrolyte, unless specified otherwise.

5.3 Results and Discussions

5.3.1 Synthesis and Stability of CuNC@N-GQD

The synthesis of CuNC@N-GQDs were synthesised as described in Experimental using $CuSO_4$, GSH, and N-GQDs, where N-GQDs were used as a reducing agent and GSH as a capping agent. Owing to the graphene structure (π electron cloud), N-GQDs have been used to reduce Cu(II) to Cu(0) in our work. The reduction of (noble) metal ions by graphene has been well reported by Aswathi et al(Ramachandran, Arya Nair, and Karunakaran Yesodha 2019). In addition, we have previously(Saisree et al. 2021) demonstrated that N-doping and N-functionalities in N-GQDs would enhance the electron-donating capability. Further, the structure and stability of the CuNC@N-GQDs were analyzed using absorption and emission studies. The absorption spectrum of CuNC@N-GQDs (Figure 5.1A) shows a peak at ~230 nm, and GSH shows a peak at ~210 nm, both corresponding to π–π^* transitions and the N-GQDs shows peaks at ~260 and ~512 nm corresponding to π –π^* and n–π^* transitions(Ramachandran, Arya Nair, and Karunakaran Yesodha 2019). After adding N-GQDs alone (without GSH), the corresponding spectrum in Figure 5.1B shows a peak at ~320 nm with a much higher intensity than that of the 230 nm peak of CuNCs. In Figure 5.1B, an intense surface plasmonic resonance peak is also observed at ~640 nm, characteristic of CuNPs (CuNP@N-GQDs). The CuNC@N-GQD (Figure 5.1A) did not show any surface plasmonic resonance peak characteristic of the nanoparticle, suggesting the formation of CuNC@N-GQD. Thus, the formation of a CuNC@N-GQD using comparatively smaller molecules:

GSH and N-GQDs, instead of bigger molecules such as DNA, protein as stabilizing agents(Lin et al. 2021; Z. Zhou, Du, and Dong 2011), indicates the merit of the synthesis strategy. This can further simplify the characterization difficulties of NCs. The emission spectrum of CuNC@N-GQD (Figure 5.1C) shows two peaks at λmax= ~ 330 and ~ 450, which are attributed to the CuNCs and N-GQDs, respectively, and is green emissive (Figure 5.1E) whereas the individual spectrum of N-GQD exhibits λmax of ~ 450 nm to 600 nm, depending on the excitation wavelength (Figure 5.1D) and has a greenish-blue emission (Figure 5.1E) and that of CuNC@AA has a λmax of ~ 365 nm and is blue emissive(X. H. Gao et al. 2016)**,** due to the absence of N-GQD. Thus, it can be assumed that the red-shifted (blue to green fluorescence) of CuNC@N-GQD compared to that of CuNC@AA is due to the presence of N-GQD. A scheme describing the step-wise synthesis procedure of CuNC@N-GQDs in two steps (i) first step comprising the formation of a copper thiolate complex from the precursor, $CuSO_4$ followed by (ii) a second step which consists of addition of N-GQDs to the copper thiolate complex resulting in CuNC@N-GQDs is depicted in Figure 5.2.

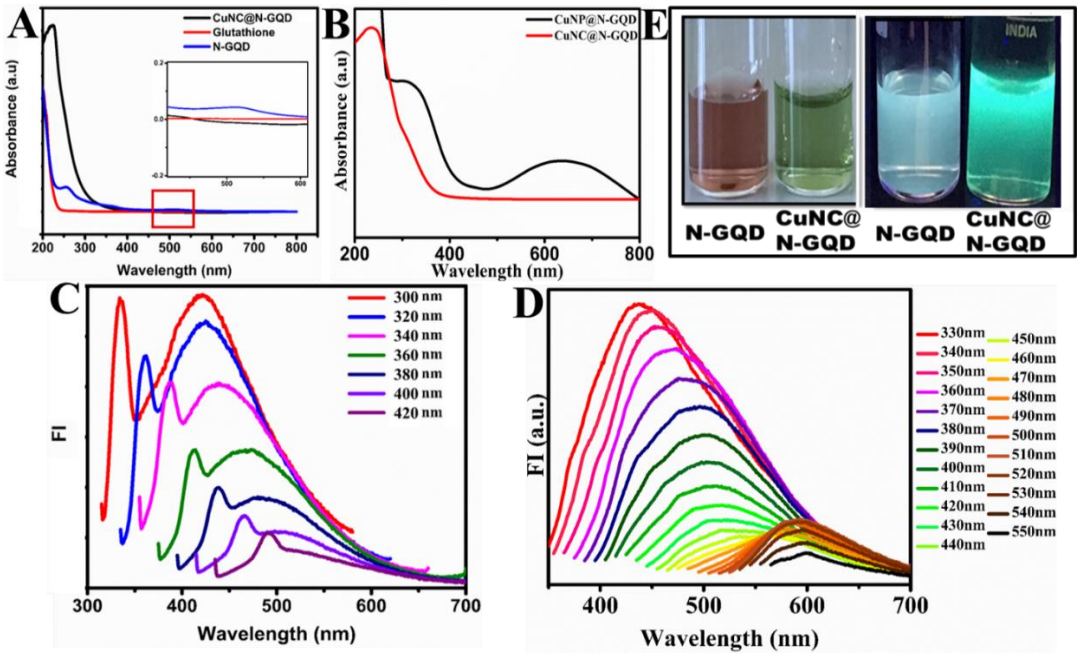

Figure 5.1. (A) The UV-Vis spectra of CuNC@N-GQD, N-GQDs, and GSH; (Inset of A) The enlarged image of UV-Vis spectra in the visible region; (B) The UV-Vis spectra of CuNC@N-GQD and CuNP@N-GQD; (C and D) The emission spectra of CuNC@N-GQD and N-GQD excited using wavelengths from 300 to 420 nm (the excitation wavelengths of each are given in the right-hand side of the emission spectrum); (E) The digital images of

the photoluminescence of N-GQDs and CuNC@N-GQDs under normal light and UV (365 nm) irradiation.

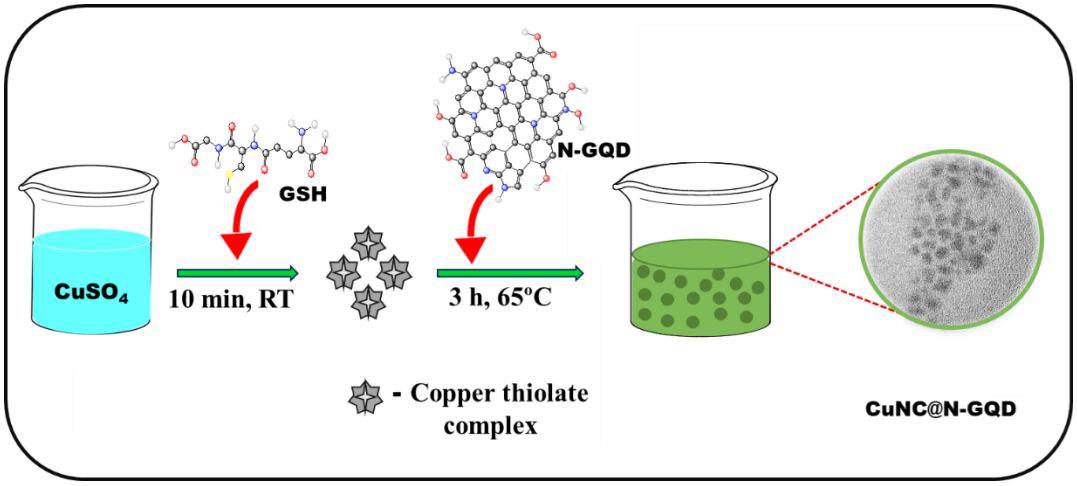

Figure 5.2. Schematic of the synthesis and a representative structure of CuNC@N-GQD: the first step shows the formation of copper thiolate complex from $CuSO_4$. In the second step, the copper thiolate complex, N-GQD is added, resulting in the formation of CuNC@N-GQD.

The lack of good temporal stability and stable photoluminescent characteristics of CuNCs remains a limiting factor for their practical applications. Hence, there is an urge to develop CuNCs with enhanced stability and luminescent features(Singh et al. 2020). The digital images of CuNC@N-GQD at the beginning (a and c) and at the end (b and d) of a one-year period in given in Figure 5.3A. The temporal stability of the CuNC@N-GQD was ≥ 365 days, which was demonstrated by the absorption and emission characteristics (Figure 5.3B-D) before and after ~365 days, which show no apparent change in the emission profile over a one-year period. The retention of the absorption and emission intensity after one year with respect to the initial intensities were ~ 98 and ~ 91%, indicates a stable CuNC@N-GQD. The temporal stability reported(Koninti, Satpathi, and Hazra 2018; Shi et al. 2017; Singh et al. 2020) for CuNCs are 21, 30 and 180 days and the highest hitherto is ~180 days(Koninti, Satpathi, and Hazra 2018). The comparatively higher stability of CuNC@N-GQD is therefore attributed to the presence of N-GQDs. Even though the N-GQD was added as a reducing agent, its presence in the product NC indicates that it acts as a capping agent/ligand similar to that of GSH. The CuNC is assumed to be interacting with the N-GQDs through the N-doped sites(Govindhan and Karthikeyan 2017). The presence of N-GQD can make the CuNC more stable through (i) sterically protecting as a capping agent and (ii) by supplying electrons because of its

electron-rich aromatic basal planes containing conjugated π electrons and the non-bonded electrons due to the effective N doping, which is explained in detail elsewhere(Saisree et al. 2021) which stabilizes the CuNCs from being oxidized, which is one of the main reasons for the CuNC being unstable.

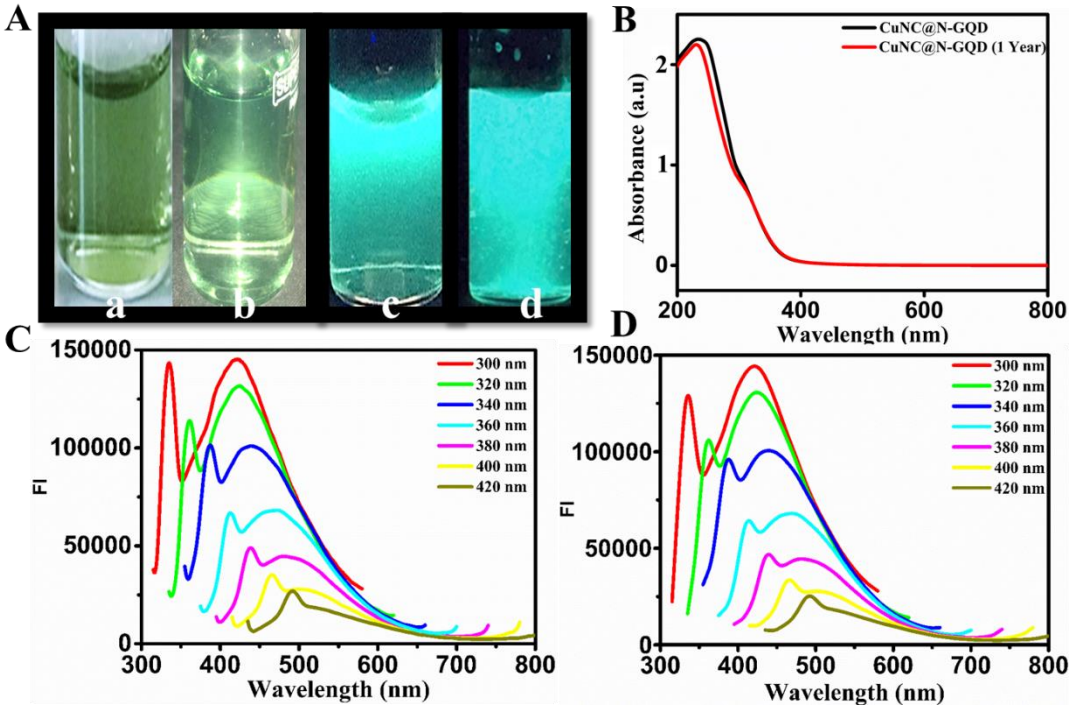

Figure 5.3. (A) The digital images of the emissions of the CuNC@N-GQDs before (a and c) and after ~ 1 year of storage (b and d) under normal light (a and b) and at UV (365 nm) irradiation (c and d); (B) The UV-Vis spectra of CuNC@N-GQD; (C) and (D) The emission spectra of CuNC@N-GQD from 300 nm to 420 nm excitations; before and the after ~ 1 year of storage, respectively.

5.3.2 Structure, size, and properties of CuNC@N-GQD

The high-resolution transmission electron micrographs of the as-synthesized CuNC@N-GQDs are shown in Figure 5.4A, which is of relatively lower magnification and gives an overall idea of the NCs as its size distribution or uniformity in the size. The crystalline lattice fringes (Figure 5.4B) with an interlayer spacing of 0.21 nm are assigned to the (102) diffraction planes of sp^2 graphitic carbon corresponding to the spacing between successive (102) C-C planes and that of 0.18 and 0.20 nm to the (200) and (111) planes(Hu, Wang, and Huang 2016) of Cu^0 corresponding to the inter-atomic spacing between successive (200) and (111) Cu-Cu planes. The data for plotting the histogram in Figure 5.4C is obtained from Figure

5.4A, which shows the average size distribution of CuNC@N-GQDs is from ~4 to 5 nm.

In an attempt to understand the number of Cu atoms in the NC, the CuNC@N-GQD were studied using electrospray ionization mass spectrometry time-flight mass spectrometry. The mass spectrum of N-GQDs (Figure 5.4D) shows a base peak at the m/z value of 485 and that of the CuNC@N-GQD at 1675 (Figure 5.4E). The calculated mass spectra (black traces) of N-GQDs and CuNC@N-GQDs match the experimentally observed (red traces) results, as shown in Figures 3F and 3G, respectively. The dominant m/z peaks at 672 (Figure 5.4H) and 1675 indicate a possible Cu_{1-13}(N-GQD)GSH cluster fragments, and the molecular ion peak corresponding to m/z 1675 can be denoted as Cu_{13}(N-GQD)GSH$(CH_3O^-)_3$. The results indicate that the CuNC formed contains one N-GQD, and one GSH molecule; a possible structure of the CuNC@N-GQD is proposed, given in Figure 5.4I.

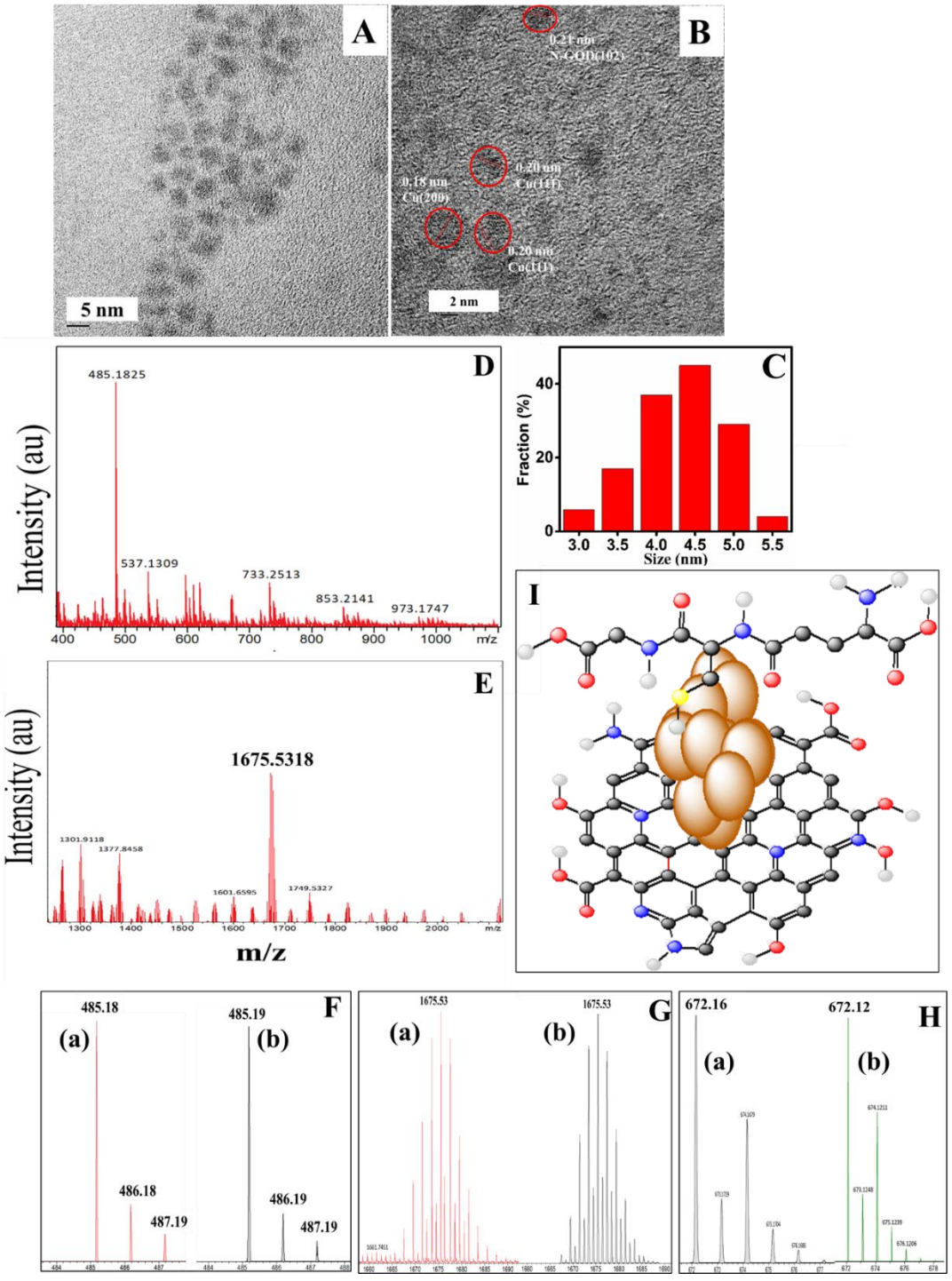

Figure 5.4. (A) The The high-resolution transmission electron micrograph of the synthesized CuNC@N-GQD; (B) The transmission electron micrograph reveals the d-spacings; (C) The size distribution of the CuNC@N-GQD as obtained from the transmission electron micrograph images; (D) The electrospray ionization mass spectrometry time-flight mass spectra of N-GQDs; (E) The electrospray ionization mass spectrometry time-flight mass spectra of CuNC@N-GQD; (F) and (G) Expanded negative mode electrospray ionization mass spectrometry time-flight mass spectra of N-GQDs and CuNC@N-GQD in m/z 485 and 1675, respectively showing (a) experimental spectrum (red trace) is in good agreement

with (b) the calculated mass spectrum (black trace); (H) Expanded negative mode electrospray ionization mass spectrometry time-flight mass spectra of CuNC@N-GQD in m/z 672, showing (a) the calculated mass spectrum (black trace) is in good agreement with (b) experimental spectrum (green trace); (I) The possible structure of CuNC@N-GQD.

XPS analysis was carried out to confirm the presence of Cu and to determine the oxidation state of Cu in the samples along with the other elements. The survey scan spectrum of the CuNC@N-GQD (Figure 5.5A) revealed the peaks of C 1s (284.1 eV), O 1s (530.9 eV), N 1s (400.7 eV), and Cu 2p (934.4 eV). The high-resolution C 1s X-ray photoelectron spectrum (Figure 5.5B) revealed the presence of C-C/C=C (284.7 eV), C-O (285.9 eV), C=O (287.9 eV), C–N (284.9 eV), and C=N (288 eV), and that of the N 1s (Figure 5.5C) indicates the presence of pyridinic (399.7 eV), pyrrolic (400.1 eV) and oxidized pyridinic (401.3 eV) N species[39], which provide further evidence of the inclusion of N-GQDs with CuNCs. The two intense peaks at 932.7 and 951.9 eV (Figure 5.5D) are assigned to the $2p_{3/2}$ and $2p_{1/2}$ of Cu(0)(Han et al. 2018). A small peak at 954.7 eV suggests a very minimal presence of Cu(II) in the system, which may be the surface atoms. It can be noted that while comparing the high-resolution X-ray photoelectron spectroscopy spectrum of C 1s (Figure 5.5B), N 1s (Figure 5.5C), and O 1s (Figure 5.5E) of CuNC@N-GQD with that of the N-GQDs (Chapter 3, Figure 3.4 D, 3.4F-G), an observable difference exists in the peak characteristics such as a ~ 20% decrease in the peak intensities of C 1s, ~ 40% for N 1s and ~ 45% for O 1s with a corresponding shift in the peak positions of about ±1 eV for all the functionalities. The shift in the peak positions and the decrease in the peak intensity can be assigned to the formation of CuNC on N-GQDs facilitated mainly through the O and N functionalities of N-GQDs as the comparatively greater decrease in the intensity suggests.

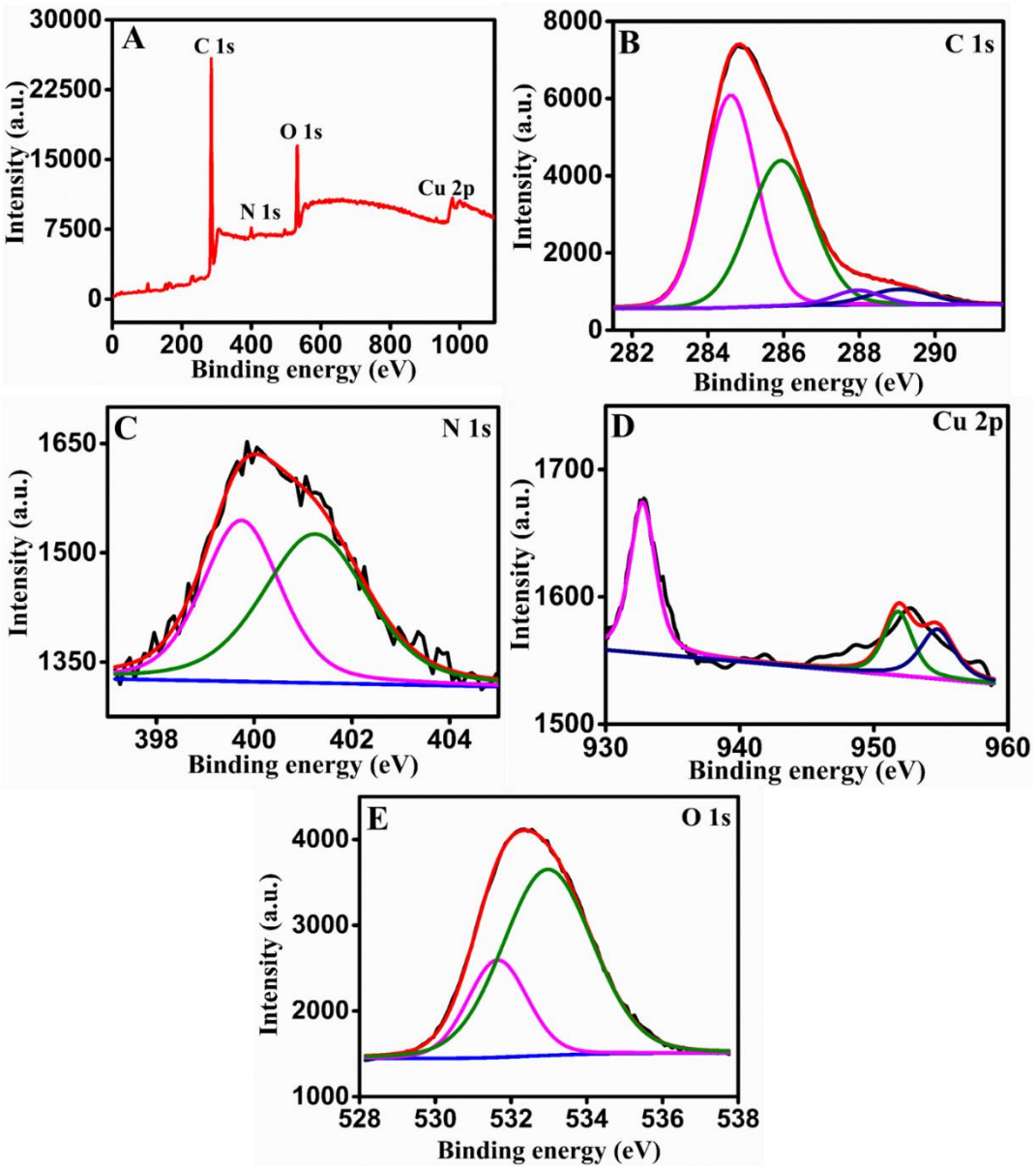

Figure 5.5. (A) Survey X-ray photoelectron spectrum of CuNC@N-GQD; (B, C, D, and E) high-resolution X-ray photoelectron spectra of the C 1s, N 1s, Cu 2p, and O 1s, with the experimental results (black traces) and their related curve-fitted components (other coloured traces), of CuNC@N-GQD

5.3.3 Electrochemical sensing studies of CuNC@N-GQDs

Initially, the sensing properties of CuNC@N-GQD/GCEs were investigated using the following biomolecules: DA, SER, NIC, FA, UA, AA, glucose, acetylcholine, EP, and NEP. The preliminary sensing studies showed that CuNC@N-GQD displays sensing ability towards only three biomolecules: DA, SER, and NIC. The comparative DPV profiles for the EC sensing of DA, SER, and

NIC (1 mM each) at a bare GCE, a CuNC@N-GQD/GCE, an N-GQD/GCE, and a CuNC@AA/GCE (Figure 5.6A) showed that CuNC@N-GQD/GCE exhibited three corresponding distinct oxidation peaks at 0.22, 0.38, and 0.95 V for DA, SER, and NIC, while NGQDs/GCE show only one broad peak arising from DA and SER. Meanwhile, the CuNC control displayed peaks only for NIC and none for DA and SER, indicating that the sensing of DA and SER on CuNC@GQD is due to the N-GQDs and that of the NIC is due to the CuNC. A corresponding ~ 23-fold, ~ 12-fold, and ~ 9-fold enhanced peak intensity was observed for DA, SER, and NIC at CuNC@N-GQDs than GCE, and this is attributed to the synergistic effects of CuNC and N-GQDs due to the structural changes that happened during the formation of the CuNC@N-GQD and the consequent improvement in the catalytic and conducting property of CuNC@N-GQD. We assume that the exfoliated nature of N-GQDs happened due to the attachment of CuNC during the formation of CuNC@N-GQD, which increased the conductivity of the N-GQD and the exposed active sites, in addition to the possible CuNC catalytic sites increased the catalytic activity. It is well known that doping graphene quantum dots with elements containing unpaired electrons such as N can improve their electron-donating ability, and our previous works[34,39] have demonstrated that N-GQDs are better than the GQDs. Further, this structure enhanced the effective interactions between the CuNC@N-GQD and the analytes by enhancing the ring stacking or π–π interaction between the aromatic basal plane of N-GQDs with the aromatic ring or the π electrons of DA, SER, and NIC. The DPV profiles of the simultaneous quantitative sensing of DA, SER, and NIC on CuNC@N-GQD/GCE (Figure 5.6B) with the increasing concentrations shows an increase in the current responses of the three well-defined oxidation peaks with significant differences in the corresponding anodic peak potential (ΔEpa) of about 0.16, 0.57, and 0.73 V between DA and SER, SER and NIC, DA and NIC, which is indicative of the non-interference and the simultaneous sensing capability. The limit of detection values obtained for DA, SER, and NIC are correspondingly 10^{-12}, 10^{-9}, and 10^{-11} M, and they are the lowest limit of detection reported so far for each of the analytes.

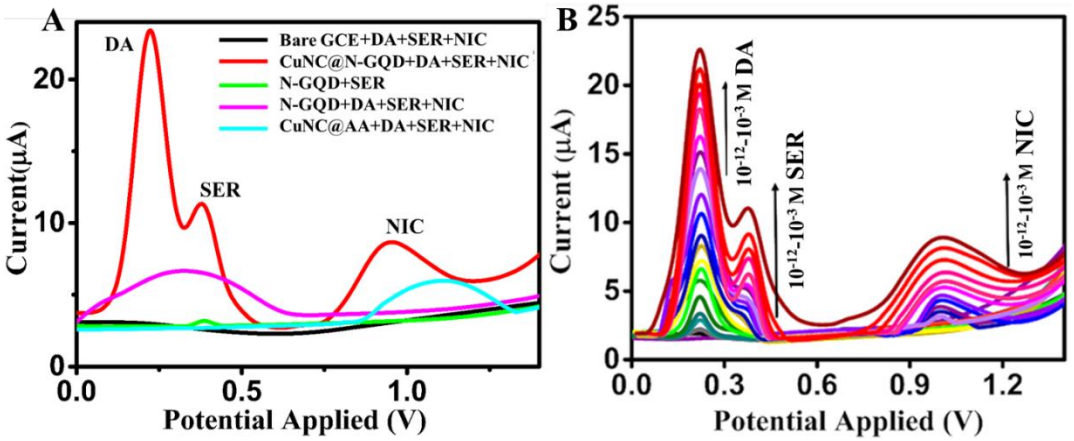

Figure 5.6. (A) The DPV responses of 1 mM each of DA, SER and NIC in 0.1 M PBS on Bare GCE, CuNC@N-GQD/GCE, N-GQDs/GCE and CuNC@AA respectively; (B) The DPV responses of DA, SER and NIC on CuNC@N-GQD/GCE from 10^{-12} to 10^{-3} M.

5.3.4 Individual sensing studies

The sensitivity and concentration dependency of CuNC@N-GQD/GCE towards the EC detection of DA, SER, and NIC were evaluated by recording the DPV response from 10^{-12} M to 10^{-5} M for DA (Figure 5.7A), 10^{-9} to 10^{-5} M for SER (Figure 5.7B), and 10^{-11} to 10^{-5} M for NIC (Figure 5.7C). The differential pulse voltammograms show that the current response of each analyte increases with concentration. The corresponding linear response towards DA, SER, and NIC falls in the corresponding concentration range of 10^{-12} to 10^{-6} M for DA (Figure 5.7D), 10^{-9} to 10^{-6} M for SER (Figure 5.7E), and 10^{-11} to 10^{-6} M for NIC (Figure 5.7F). Two separate linear dynamic ranges (linear dynamic ranges) were obtained for each analyte: from 10^{-12} to 10^{-7} M (R^2 = 0.982; N= 11) and 2×10^{-7} to 10^{-6} M (R^2 =0.998; N= 6) for DA, whereas 10^{-9} to 10^{-7}M (R^2 =0.978; N= 11) and 2×10^{-7} to 10^{-6} M (R^2 =0.988; N= 6) for SER and from 10^{-11} to 10^{-7} M (R^2 =0.977; N= 12) and 2×10^{-7} to 10^{-6} M (R^2 = 0.999; N= 6) for NIC. The corresponding sensitivity values obtained for DA, SER, and NIC from the linear dynamic ranges are 58, 24, and 20 nA nM^{-1} cm^{-2}, and the corresponding limit of detection values obtained for DA, SER, and NIC are 10^{-12} (Figure 5.7G, Curve c), 10^{-9} (Figure 5.7H, Curve c), and 10^{-11} M (Figure 5.7I, Curve c).

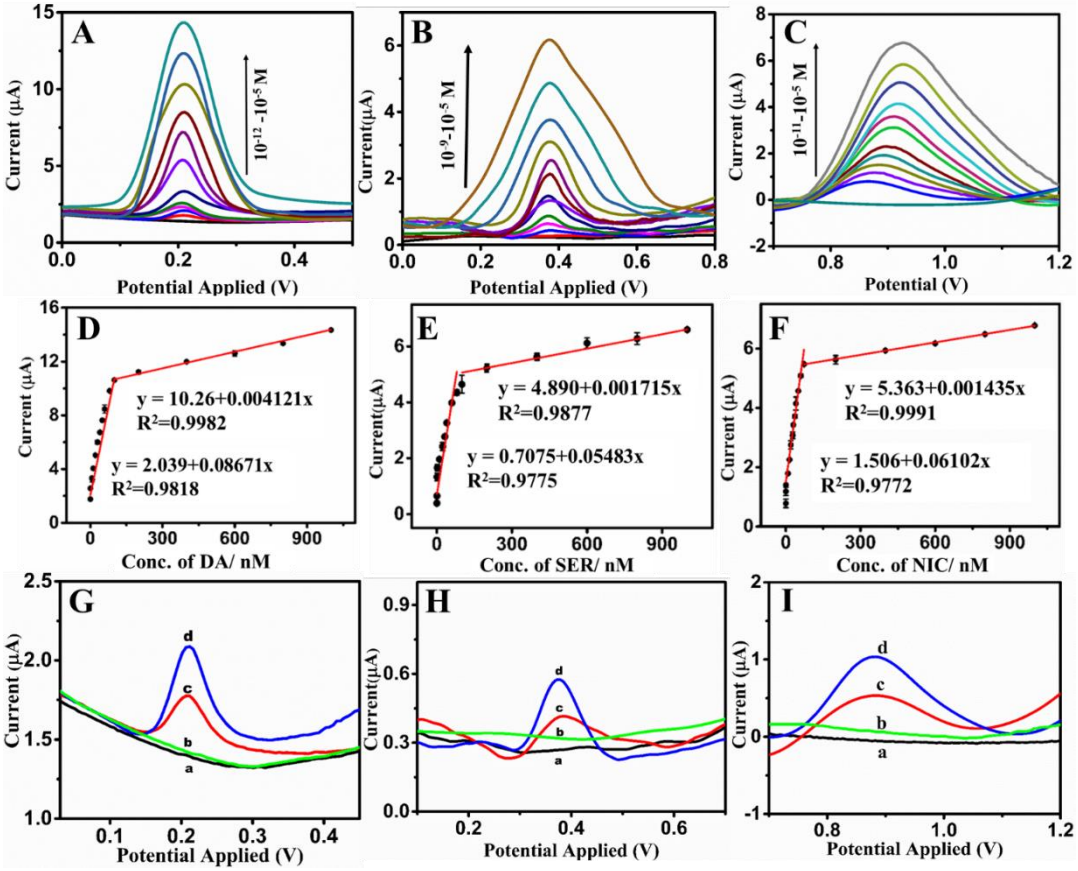

Figure 5.7. (A, B, and C) The DPV responses of DA, SER and NIC in 0.1 M PBS on CuNC@N-GQD/GCE from 10^{-12} to 10^{-5} M, 10^{-9} to 10^{-5} M and 10^{-11} to 10^{-5} M respectively; (D, E, and F) The linear dynamic ranges obtained for the sensing of DA, SER and NIC on the CuNC@N-GQD/GCE for the concentration range of 10^{-12} to 10^{-6} M, 10^{-9} to 10^{-6} M and 10^{-11} to 10^{-6} M respectively; (G) The DPV response in 0.1 M PBS on CuNC@N-GQD/GCE (a) absence of DA and (b, c and d) in the presence of 0.1, 1 and 10 pM DA, respectively; (H) The DPV response in 0.1 M PBS on CuNC@N-GQD/GCE (a) absence of SER and (b, c and d) in the presence of 0.1, 1 and 10 nM SER, respectively; (I) The DPV response in 0.1 M PBS on CuNC@N-GQD/GCE (a) absence of NIC and (b, c and d) in the presence of 1, 10 and 100 pM NIC, respectively.

In addition, the studies were carried out by varying the concentrations of each analyte by keeping the other two analytes at a constant concentration of 1 mM each: the concentration of DA was varied from 10^{-12} to 10^{-3} M, SER from 10^{-9} to 10^{-3} and that of NIC from 10^{-11} to 10^{-3} M. The results show that there was no interference for the analytes from the other even at the limit of the detection range (are 10^{-12}, 10^{-9}, and 10^{-11} M for DA, SER, and NIC). The value of the current responses of each analyte in the individual sensing (Figure 5.8A-7C) was in good agreement with that of in the simultaneous sensing studies (Fig. 5.6B), suggesting no interference of any of the analyte in the sensing of the other. The corresponding linear dynamic range

graphs (Figure 5.8D-F) exhibited two ranges with a coefficient of determination of $R^2 \geq 0.96$; N=16: from 10^{-12} to 9×10^{-5} M and 10^{-4} to 10^{-3} M; 10^{-8} to 8×10^{-5} M and 9×10^{-5} to 10^{-3} M; and 10^{-11} to 5×10^{-5} M and 6×10^{-5} to 10^{-3} M for DA, SER, and NIC. The limit of detection values was the same for individual studies and are 10^{-12}, $10^{-9,}$ and 10^{-11} M for DA, SER, and NIC (Figure 5.8G, H, and I and insets). The unaltered peak positions, current responses with similar values in the presence (Figure 5.8A-C) and the absence of the interferents (Figure 5.7A-C), and the same value for the limit of detection for analytes in the absence (Figure 5.7G-I) and in the presence (Figure 5.8G-I) of the analytes DA, SER and NIC indicate that there is no interference of analytes on each other and are evidence of the effective simultaneous sensing capability of CuNC@N-GQD.

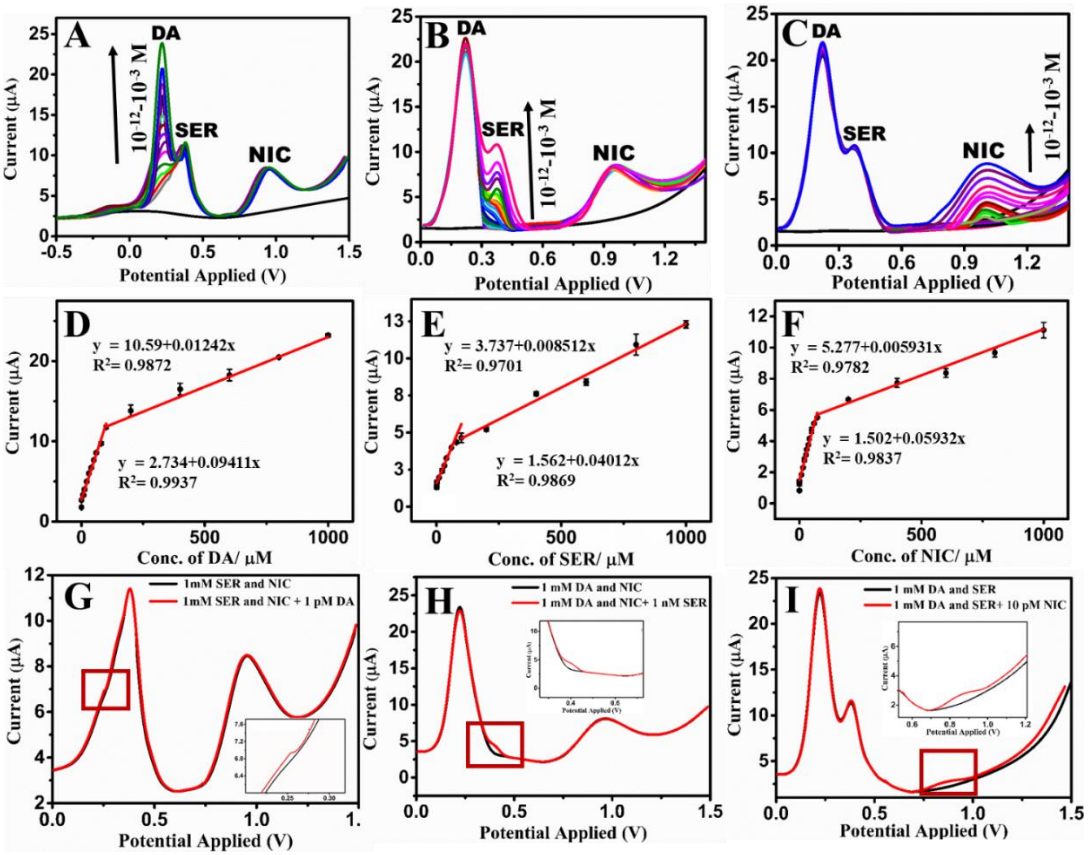

Figure 5.8. (A, B, and C) The simultaneous DPV responses of DA, SER, and NIC respectively by varying the concentrations from 10^{-12} to 10^{-3} M in the presence of 1 mM concentration of the other two analytes; (D, E, and F) The corresponding linear dynamic range graphs of the simultaneous sensing of DA, SER, and NIC; (G, H and I) The DPV responses of the limit of detection values of DA (1 pM), SER (I nM) and NIC (10 pM) in the presence of 1 mM concentrations of the other two analytes; (Inset of G, H and I) The enlarged images of the limit of detections of DA, SER, and NIC.

As there are no literature reports of the simultaneous sensing of the three biomolecules: DA, SER, and NIC, the comparison of the analytical performance of CuNC@N-GQD/GCE were made with the reported EC sensor materials for DA(Arya Nair et al. 2022; Shellaiah et al. 2019), SER(Ashraf et al. 2021; Panneer Selvam and Yun 2020), or NIC(X. Li et al. 2017; Veeralingam and Badhulika 2020) or a combination of these (Table 5.1), if any. Fluorescence-based sensors such as carbon dots-gold nanoclusters(He et al. 2018) for DA, single-walled carbon nanotubes(Manuscript 2021) for SER, and o-carborane derivatives (K. Liu et al. 2019) for NIC exhibited a limit of detection values of 2.9, 301, and 6.1 nM. The colorimetric based sensor such as 1-H-3-methylimidazolium acetate ionic liquid-coated silver nanoparticles(Nishan et al. 2020) for DA, gold nanoparticle-dithio bis(succinimidylpropionate)-N-acetyl-L-cysteine for SER(Yilmaz 2018), and potassium permanganate and sodium hydroxide for NIC(Al-Tamrah 1999) exhibited lower detection limits of 11.8, 0.1, and 0.43 μM. In all the above-mentioned sensors including those given in Table 5.1, CuNC@N-GQD exhibited the lowest reported detection limit for all the three analytes, which indicates the merit of the sensor material. The simultaneous sensing is attributed to the combination of CuNC and N-GQD and is understood from the observations that the aromatic basal plane of N-GQDs is responsible for DA and SER sensing and the effective π–π interaction between the aromatic basal plane of N-GQDs in CuNC@N-GQD with the aromatic rings of DA facilitated the comparatively enhanced sensitivity towards DA. In contrast, the CuNC facilitated the NIC sensing through the pyrrolic-N interaction. Hence the synergic effect of CuNC and N-GQD is responsible for the excellent simultaneous sensing applicability. The enhancement in the current response of all the three analytes in the CuNC@N-GQD compared to the controls is attributed to the electron-rich N-GQDs. The N-doping in N-GQD provides an electron-rich environment that facilitates the uphold sensitivity along with the CuNC and is also responsible for the stability of CuNC@N-GQD. Hence, the N-GQDs play a significant role in the synthesis and application in the present study

Table 5.1. Comparison of the limit of detection of CuNC@N-GQD/GCE with that of the literature reports of EC sensors of DA, SER, and (or) NIC.

Materials/ Electrodes	Detection Strategy	Analytes	LOD (μM)	LDR (μM)	Reference
Graphene oxide and electropolymerized p-aminobenzenesulfonic acid mixed film	Simultaneous	DA	0.09	0.3–20	(Ran, Li, and Xia 2020)
		SER	0.2	0.6–20	
Reduced graphene oxide/ Fe_3O_4 nanoparticles/ hydroxypropyl-β-cyclodextrin nanocomposite	Simultaneous	DA	0.0067	0.02 – 25	(Liang et al. 2019)
		SER	0.0033	0.01 – 25	
NiO/carbon nanotube (CNT)/poly(3, 4-ethylenedioxythiophene) composite	Simultaneous	DA	0.026	0.03–20	(Sun et al. 2018)
		SER	0.063	0.3–35	
Fe-doped $MgNi_2O_3$ nanoparticles	Simultaneous	DA	0.017	0.1–1000	(Reddy et al. 2020)
		NIC	0.098	50–6000	
CuNC@N-GQD	Simultaneous	DA	0.000001	0.000001-1	Our Result
		SER	0.001	0.001-1	
		NIC	0.00001	0.00001-1	

5.3.5 Mechanism of sensing of DA, SER, and NIC by CuNC@N-GQD

In the sensing property of CuNC@N-GQD, comparing the results for DA and SER, it can be observed that DA has a ~ 2-fold higher current response than that of SER, which indicates that CuNC@N-GQD is better electrode material for DA than that of for SER. The simultaneous sensing capability can be explained by the different interactions between the aromatic benzene ring of DA, compared to the indole ring of SER, with the benzene rings of the graphene structure of N-GQDs. More specifically, the benzene ring is more planar and aromatic than the indole ring,

making the former more effectively interact with graphene through ring-stacking and $\pi - \pi$ bonds. The effective interaction between the graphitic basal plane and benzene ring of DA has previously been reported by us(Ramachandran, Panda, and Karunakaran Yesodha 2018) to lead to superior sensing of DA. Though NIC is aromatic, the non-planar nature of the ring structure makes the effective interaction between the NIC and N-GQDs difficult. The interaction between the pyrrolic-N of NIC with the Cu moieties of the CuNC is thought to be the reason for the sensing of NIC by CuNC(Inoue et al. 1990). It is known that N-atoms can preferentially interact with Cu, and the pyrrolic N-atom in the NIC can interact with the Cu through oxidative addition or by the charge transfer from the Cu to the N atoms which may be the reason for the sensing of NIC by CuNC@N-GQD(Karthika et al. 2019). However, an enhancement in the current response was observed with CuNC@N-GQD for NIC compared to that of the control CuNC. It can be assumed that since during the interaction with CuNC, the NIC comes in close proximity with N-GQDs which may lead to $\pi-\pi$ stacking interaction between the pyridine moiety in NIC and the graphene of N-GQDs, which may enhance the current response in addition to the better conductivity and catalytic activity of CuNC@N-GQD compared to that of the CuNC. Thus, the N-GQDs in the CuNC@NGQD are responsible for the sensing of DA and SER and CuNC for NIC and the exfoliated nature of N-GQDs and the presence of CuNC which enhances the active sites and the electrocatalytic activity and the conductivity responsible for the enhanced current response and the better peak-to-peak separation The schematic representation of comparative sensing capabilities of GCE and CuNC@N-GQD/GCE is shown in Figure 5.9(i). The corresponding oxidation mechanisms of DA, SER, and NIC involved on CuNC@N-GQD/GCE (Figure 5.9(ii)), a graphic representation of the enhanced release of DA and SER in the brain during NIC intake (Figure 5.9(iii)), and a flowchart diagram showing the functional correlation between DA, SER and NIC (Figure 5.9(iv)) were depicted below. Further, even though DA, EP, and NEP have almost identical basal structures, only DA was sensed by CuNC@N-GQD. An illustration of the effective $\pi-\pi$ stacking interaction among the analytes DA, SER, NIC, EP, and NEP, and CuNC@N-GQD is depicted in Figure 5.9(v). This can be explained based on the steric hindrance from the bulkier side functionalities such as OH and NH_2 for EP and NEP, which can impede the effective $\pi-\pi$ stacking interaction and the sensing

by CuNC@N-GQD. Thus, the comparatively less hindered, aromatic, and planar structural features of DA, SER, and NIC play a role in its effective simultaneous sensing on CuNC@N-GQD.

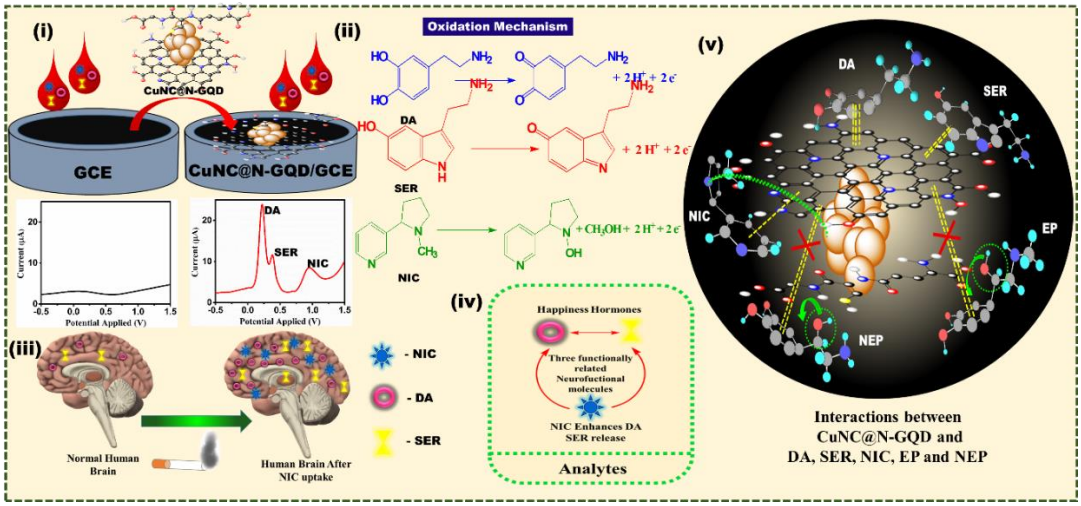

Figure 5.9 (i) The schematic diagram showing the modification of GCE with the CuNC@N-GQD and the resultant enhanced sensing of DA, SER and NIC; (ii) The oxidation mechanisms of DA, SER and NIC on CuNC@N-GQD/GCE; (iii) A diagrammatic representation of the enhanced release of DA and SER in brain during NIC intake; (iv) A flowchart diagram showing the fuctional correlation between DA,SER and NIC; (v) The interactions among CuNC@N-GQD and the analytes DA, SER, NIC, EP and NEP based on the structural and functional features.

5.3.6 Selectivity and Interference Studies

The practical applicability of a sensor is entirely hinged on its sensitivity and selectivity. The developed material CuNC@N-GQD exhibits corresponding commendable sensitivity of 58, 24, and 20 $nAnM^{-1}cm^{-2}$ towards DA, SER, and NIC. Thus, the interference studies of the developed material are necessary to validate its practical applicability. The DPV profiles of the simultaneous sensing of DA, SER, and NIC in a mixture of other analytes of biological relevance (Figure 5.10A) and the corresponding histogram (Figure 5.10B) show no significant current response from any of the other biomolecules, indicating the selectivity of the material towards DA, SER and NIC.

5.3.7 Reusability, Reproducibility and Stability Studies

Stability studies of CuNC@N-GQD were conducted for a period of three and six months. The results (Figure 5.10C) show that the percentage retention of the current response with respect to the initial current responses is ~ 96% and ~ 91% for DA, ~ 96% and ~ 89% for SER, and ~ 94% and ~ 88% for NIC in the third and sixth month, respectively. For reproducibility studies, the current responses of five different electrodes towards 1 mM each of DA, SER, and NIC (Figure 5.10D) shows a relative standard deviation of the peak currents of these individually prepared electrodes was found to be 1.32 % for DA, 0.77 % for SER, and 0.98 % for NIC, which specifies its good reproducibility. The reusability of the CuNC@N-GQD/GCE electrode was scrutinized by comparing the peak currents for 1 mM DA, SER, and NIC on CuNC@N-GQD/GCE (Figure 5.10E) before and after multiple times of washing and showed ≥ 90% retention after 20 times of washing.

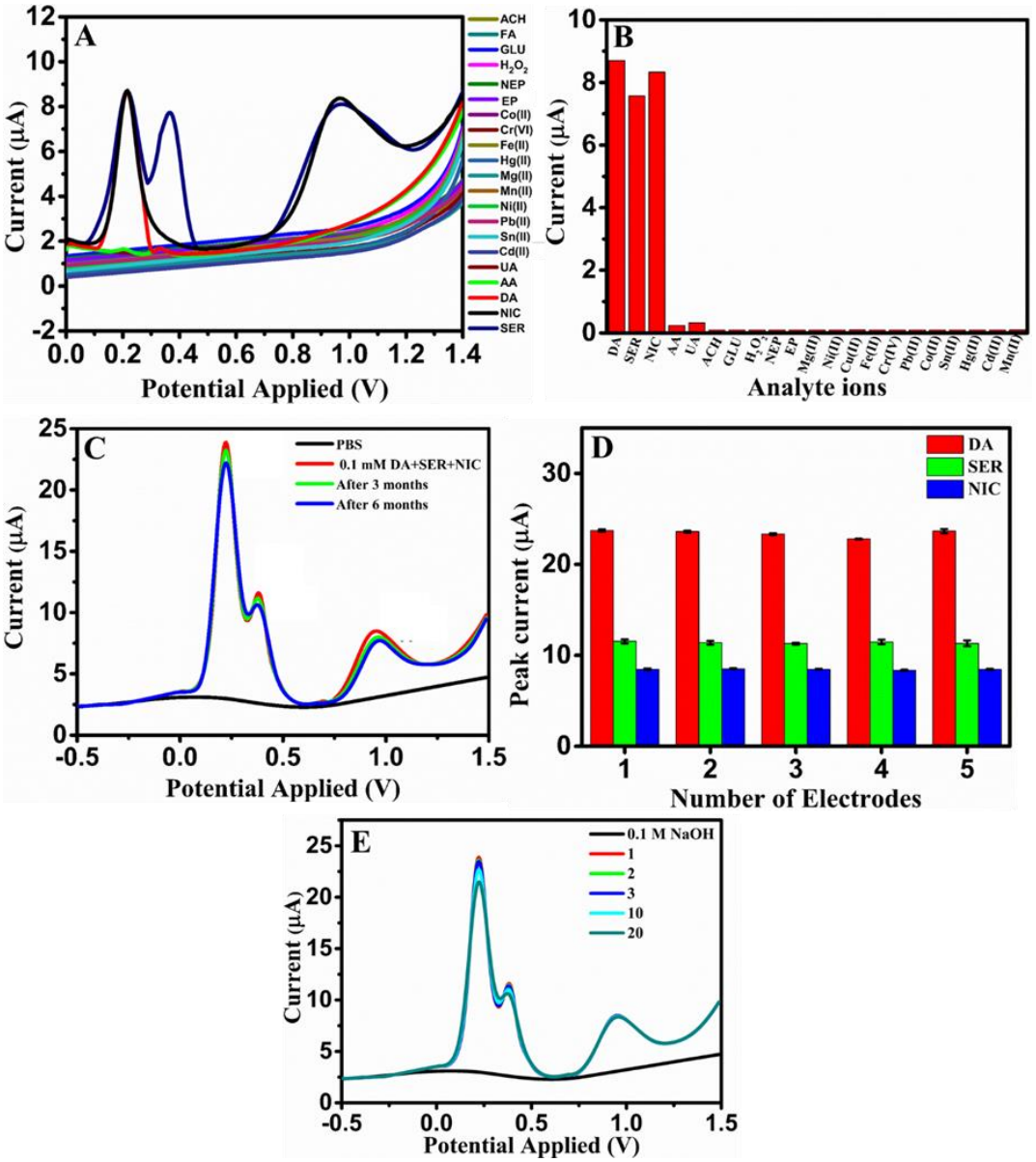

Figure 5.10. (A) and (B) Selectivity studies of CuNC@N-GQD/GCE towards DA (100 nM), SER (10 μM), and NIC (10 μM) in the presence of various analyte species (1 mM each); (C) Differential pulse voltammetry profiles obtained for DA, SER and NIC (1 mM each) on CuNC@N-GQD/GCE showing the stability of the sensor for 3 months and 6 months; (D) The peak currents of five independently coated electrodes showing the reproducibility of CuNC@N-GQD/GCE; (E) The DPV curves after immediate washing for twenty times showing the reusability of the sensor.

5.3.8 Real-life sample studies

The CuNC@N-GQD/GCE was further utilized for the detection of DA, SER, and NIC in real-life human blood and urine samples via the standard addition

method, where known amounts of DA, SER, and NIC were added to the diluted (1000x) blood and urine samples and the recovery amounts were measured. The DPV profiles are given in Figure 5.11A-H, and the corresponding measurements are summarized in Table 5.2. The recovery calculated was found to be in the range of 100.2-101.3 %. The high recovery values indicate the successful applicability of the proposed electrode for the determination of DA, SER, and NIC in real biological samples.

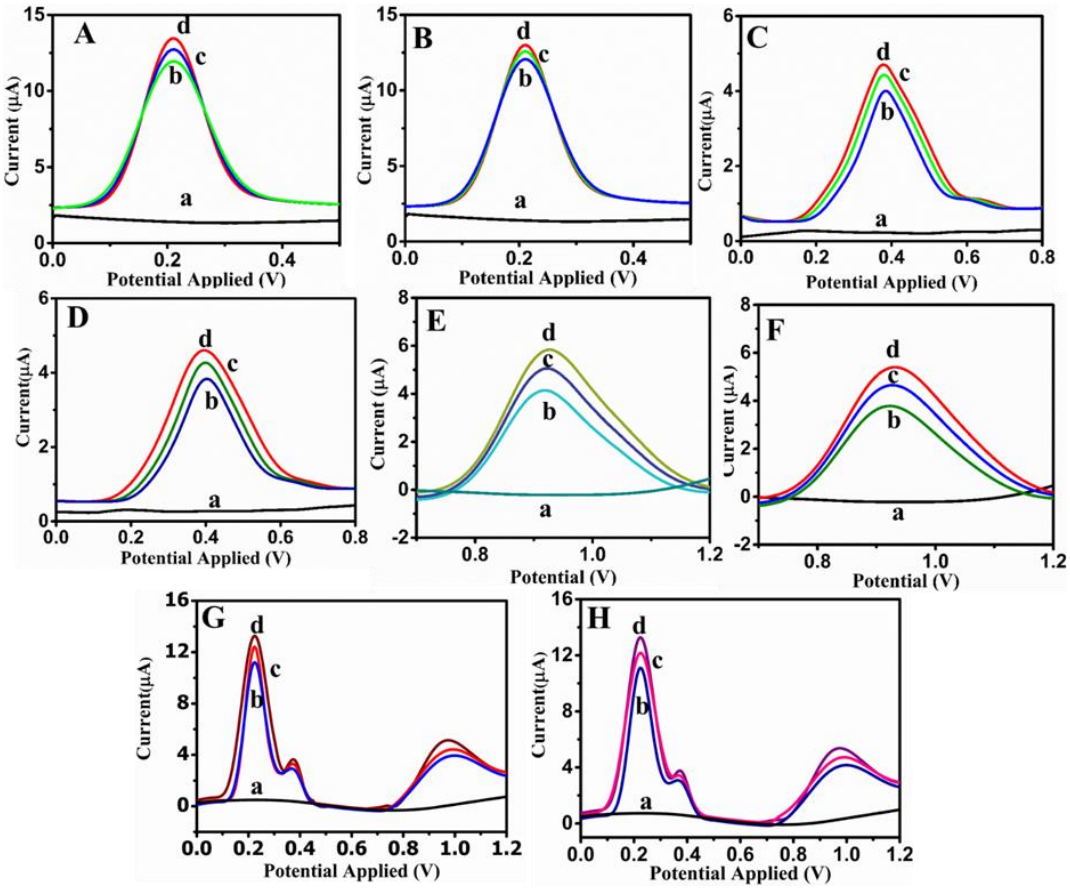

Figure 5.11. The DPV responses of (a) 0.1 M PBS, (b) 0.5 μM, (c) 1 μM and (d) 2 μM each of DA, SER and NIC (A, C and E) in blood, and (B, D and F) in urine respectively; The DPV responses of (a) 0.1 M PBS, (b) 0.5 μM, (c) 1 μM and (d) 2 μM of DA, SER and NIC simultaneously in (G) blood and (H) urine respectively

Table 5.2. The recovery test results of DA, SER, and NIC in human blood and urine samples.

Sample No.	Analyte Spiked(μM)			Found* (μM)	Recovery (%)
1	0.500	Dopamine	Blood	0.504	100.80
			Urine	0.503	100. 60
		Serotonin	Blood	0.506	101.20
			Urine	0.505	101.00
		Nicotine	Blood	0.501	100.20
			Urine	0.502	100.40
2	1.000	Dopamine	Blood	1.011	101.10
			Urine	1.009	100.90
		Serotonin	Blood	1.012	101.20
			Urine	1.013	101.30
		Nicotine	Blood	1.007	100.70
			Urine	1.008	100.80
3	2.000	Dopamine	Blood	2.008	100.40
			Urine	2.006	100.30
		Serotonin	Blood	2.015	100.75
			Urine	2.017	100.85
		Nicotine	Blood	2.021	101.05
			Urine	2.020	101.00

* All the recovery values fall within the relative standard deviation of 1%

5.4 Conclusion

In this work, a stable CuNC on N-GQDs was developed using N-GQDs as the reducing agent and N-GQDs and GSH as the stabilizing agent. The CuNC@N-GQD shows inimitable simultaneous and enhanced sensing characteristics towards the three functionally correlated neurofunctional molecules DA, SER, and NIC and exhibits exquisite sensitivity with good peak-to-peak separation. The corresponding ~4, ~4, and ~2-fold higher sensitivity of CuNC@N-GQD compared to the controls is attributed to the synergistic effect of the N-GQDs and the CuNC. During CuNC@N-GQD formation, the exfoliation of the N-GQDs due to the formation of CuNC on the N-GQDs and thus a consequent increase in the electroactive surface area, active sites, amplified electron cloud, exposed hetero atom functionalities, and the better electrocatalytic activity arises. The corresponding limit of detection obtained was 1 x 10^{-3}, 1, and 1 x 10^{-2} nM for DA, SER, and NIC, which are hitherto the lowest reported values. The interactions between the sensor and the analytes through ring stacking or heteroatom sites or the π–π interaction between the

aromatic basal planes or the combination of all is assigned to the enhanced sensitivity and the presence of different sites which promote interactions to the simultaneous sensing capability. The CuNC@N-GQD modified electrode exhibited good reproducibility, reusability, and stability. The excellent recovery percentages in the real sample study, ~ 100 %, with the recovery values falling within the relative standard deviation of 1%, in all the tested blood and urine samples, show the potential applicability of the developed sensor in real-time monitoring.

CHAPTER 6

Selective Electrochemical Sensing of Glycine by an Ultra-stable Gold-Copper Nano Cluster on Nitrogen-Doped Graphene Quantum Dot

This chapter discusses the preparation and characterization of an ultra-stable gold copper nanocluster on nitrogen-doped graphene quantum dot (AuCuNC@N-GQD), with the stability of ≥1 year, achieved through a galvanic exchange process. The AuCuNC@N-GQD was characterized by various techniques such as TEM, XPS, Mass, UV-Vis and Fluorescence spectroscopic techniques. The AuCuNC@N-GQD displayed intense solid- and solution-state near-infrared (NIR) emission. Further, the NC exhibited selective and enhanced sensing of glycine (GLY) through (non-enzymatic) electrochemical strategy. The enhanced and selective sensing of AuCuNC@N-GQD towards GLY is assigned to the preferential Au-GLY interaction and the improvement in the electronic and conductivity characteristics of the NC. Further, the sensing capabilities of AuCuNC@N-GQD were evaluated and discussed in detail and which were successfully extended to real blood and urine samples spiked with GLY to validate its practical applicability

6.1 Introduction

Benefiting from their exceptional electronic properties, quantum size effect, and high catalytic activity, metal nanoclusters (MNCs), have recently emerged as highly attractive materials for biological imaging, sensing, catalysis, and light-emitting devices(Bai et al. 2020; Y. Chen et al. 2018; Das et al. 2015; Hu et al. 2016; Lai, Wong, and Rogach 2020; Toshima et al. 2001). Fluorescent NCs of noble metals: gold (Au), silver (Ag), and copper (Cu) using various capping agents such as thiolate ligands(Nasaruddin et al. 2018), protein(Goswami et al. 2011), polymers(Gui et al. 2014), and DNA(Jia et al. 2012) has been reported and explored for various applications. Though Cu is relatively more earth-abundant and cost-efficient, reports on Cu-containing NCs, either monometallic or bimetallic, compared to Au and Ag NCs, are less in number(Lin et al. 2021) due to its

susceptibility to oxidation and the resultant lower temporal stability(Ghosh et al. 2014). Even with thiolate as a capping agent, a most functional of smaller ligand category, which has the ability to form stable metal-sulfur covalent bonds(Pei and Zeng 2012) with the metals such as Au, Ag, and Cu, the CuNCs were prone to oxidation(W. Wang et al. 2014) which led to lower temporal stability of the NCs. Therefore, usually, larger molecules such as polymers(Díez and Ras 2011), DNA(Rotaru et al. 2010), proteins(Mathew, Sukumaran, and Joseph 2018), and peptides (Zhenguang Wang, Chen, and Rogach 2017) as steric capping agents for stabilising NCs. Even though these larger molecules can comparably stabilize the NC, using larger molecules in the synthesis causes characterization difficulties(S., Arya, and K. Y. 2022a) and lower accessibility of NCs leading to lower performance. Recently, a CuNC containing nitrogen-doped graphene quantum dots (CuNC@N-GQD), with stability ≥ 1 year was reported by our group(S., Arya, and K. Y. 2022a). The improved stability of the CuNC compared to the reported ones(Koninti, Satpathi, and Hazra 2018) was attributed to the presence of N-GQD, which acted as a capping/stabilizing agent by supplying electrons and thus stabilized the CuNCs from being oxidized and the CuNC@N-GQD exhibited simultaneous and enhanced sensing characteristics towards the three functionally correlated neurofunctional molecules dopamine (DA), serotonin (SER), and nicotine (NIC).

Impressed with the sensing property and a conspicuously high stability of ~365 days(S., Arya, and K. Y. 2022a) of the CuNC@N-GQD, we attempted to synthesis a bi-MNCs version consisting of Au. The attempt was motivated by the knowledge that bimetallic NCs (bi-MNCs) have improved catalytic properties(Yuan et al. 2015) and versatility in applications compared to the monometallic NCs (mono-MNCs). Of the different strategies for the synthesis of bi-MNCs such as co-reduction which is a one-pot synthesis involving the reduction of two metal ions simultaneously in a reaction solution in the presence of a protecting ligand; and the post-treatment method which involves two steps: (i) the preparation of the precursors/intermediates and (ii) the post-treatment of the precursors/intermediates, via galvanic exchange (GE)(J. Zhou et al. 2018), anti-galvanic replacement (Shellaiah et al. 2019), under-potential deposition, thiol-etching, or re-organization(Shellaiah and Sun 2017). We adopted the latter method via GE which can generate MNCs with controlled compositions and architectures. Thus, here in

this work, we have synthesized an Au-Cu bi-MNC, from the CuNC@N-GQD(S., Arya, and K. Y. 2022a), hereafter referred to as AuCuNC@N-GQD. As expected, the synthesised AuCuNC@N-GQD exhibited impressive temporal stability of one-year, which remains the highest stability attained so far for AuCuNCs. The maximum temporal stability reported hitherto for AuCuNCs was of six-months where albumin bovine serum acts as the protecting ligand(Cai et al. 2020). As the stability is an important parameter for a sensor material, the highest temporal stability possessed by the synthesised material with a smaller protecting ligand, is one of the merits of the present study.

Further, the AuCuNC@N-GQD exhibited a red-shifted emission in the yellow region compared to the green emissive CuNC@N-GQD(S., Arya, and K. Y. 2022a), and possessed an additional property of highly intense solid-state (orange) emission in the near-infrared (NIR) region. Most of the materials which exhibits emission in their solution state, tend to lose the intensity or become non-emissive in the solid-state because of aggregation/agglomeration induced quenching(Shellaiah et al. 2019). Strategies such as utilization of macrocycles like pillarenes are employed to boost the emissive properties of compounds to obtain persistent and enhanced emission in both solution and the solid-state(Lou, Song, and Yang 2019) as they are highly applicable in optoelectronic devices, biological imaging, pollutant sensors, display media, and so forth(Lou, Song, and Yang 2019) and further solid-state emissive nanomaterials has potential in phosphor-based light-emitting diodes (LEDs), security ink, and fingerprint detection(X. F. Wang et al. 2019), which makes , the solution and solid-state emissive properties of AuCuNC@N-GQD significant.

The preferential interaction between Au-glycine (GLY) and the ability of Au to form a stable complex with GLY than other amino acids was reported elsewhere in detail(Xie, Lei, and Fang 2012). Inspired by these, we attempted the sensing of GLY using AuCuNC@N-GQD, as GLY, is an important amino acid of the proteins in the human body(Razak et al. 2017), and the deficiency of which can lead to failure of the immune response, low growth, abnormal nutrient metabolism, obesity, diabetes, gout, schizophrenia, and hyperglycinaemia (glycine encephalopathy)(Q. Wang et al. 2022), making it an additive in food products and an active pharmaceutical ingredient(Razak et al. 2017). Thus, the quantitative sensing of GLY

holds a high significance in the commercial and scientific fields of biology, medicine, and food science. Present methods of detection of GLY involves enzymes whether it is a complex method such as liquid chromatography(Marrubini, Caccialanza, and Massolini 2008), spectrophotometry(Keskin and Keskin 2014), fluorescence assay kits(Rosini et al. 2014) and it possess de-merits such as pre-sample preparation, experimental complexity, difficulty in attaining higher sensitivity and lower LOD, time-consuming and not at all cost-effective(Keskin and Keskin 2014), whereas electrochemical (EC) methods are relatively simpler, has higher sensitivity, low operating cost, easily portable nature and fast response(Saisree et al. 2021b). In this work, we demonstrate the sensing property of AuCuNC@N-GQD towards GLY via EC method. This is the first-time report of an EC non-enzymatic sensor material for GLY. The only one another report on EC GLY sensor, is an enzymatic sensor, and the method used is chronoamperometry(Q. Wang et al. 2021). The AuCuNC@N-GQD exhibited an ultra-selectivity with a sensitivity and LOD values of 0.377 $\mu A \mu M^{-1} cm^{-2}$ and 10 nM, which is the lowest reported, and an LDR ranging from 0.01 to 1000 μM. In general, enzymatic detection is high maintenance, due to high cost, one-time use, experimental complexity, and lower stability. The obtained LOD value in EC sensing platform is the lowest reported hitherto, which is significantly lower than the physiological level concentration of GLY (170-330 μM)(Q. Wang et al. 2021). The selective sensing of AuCuNC@N-GQD towards GLY was attributed to the stable and selective Au-GLY interaction and the enhancement in the current response to that of the controls to the structural characteristics of the AuCuNC@N-GQD, such as the presence of N-GQD as compared to the control AuCuNC. The selective enhanced sensing of GLY by AuCuNC@N-GQD, which is attributed to the enhanced conducting properties along with the unique interaction that is available between the sensor material and the analyte, due to the presence of both the N-GQD and AuCuNC. Furthermore, augmenting the observed selective and sensitive sensing of GLY together with the possible miniaturization properties of EC sensors, the sensing studies were extended to real sample studies to validate the potentiality of the present work in real-time sensing applications.

6.2 Experimental Section

6.2.1 Synthesis of AuCuNC@N-GQD

The synthesis of AuCuNC@N-GQD was done through the GE method as follows: in a typical synthesis, 0.5 mL of $AuCl_3$(~ 0.17 M) was added to 6 mL of CuNC@N-GQD, the synthesis procedure of N-GQD and CuNC@N-GQD are reported elsewhere(Ramachandran, Arya Nair, and Karunakaran Yesodha 2019a)- (Saisree, Arya Nair, and Sandhya 2022) by our group. The reaction mixture was stirred for 4 h at 65 °C until the turbid solution became clear. Then the solution was allowed to cool down to RT. The clear solution was centrifuged at 14000 rpm for 20 minutes, and the supernatant solution was stored at 4 ºC for further studies. An AuCuNC was made using ascorbic acid as a reducing agent using a reported procedure(S., Arya, and K. Y. 2022b)-(Huang et al. 2016) as a control.

6.2.2 Preparation of Electrodes for EC Sensing

The samples (AuCuNC@N-GQD, CuNC@N-GQD, AuCuNC and N-GQD) were drop cast over separate cleaned GCE, (pre-treatment and modification of GCE given in the experimental chapter), with care and then allowed to dry for 24 hours at the RT to achieve the modified electrodes.

6.2.3 EC Methods

The EC behaviour of the analytes: DA, NIC, SER, Glu, AA, FA, H_2O_2, ACH, GLY, ALA, VAL, LEU, IsLEU, LYS, TYR, MET, PRO, CYS, HIS, ARG, ASP, ASA, GA, GLN, on the surface of the AuCuNC@N-GQD/GCE was investigated using CV, and DPV at RT. A 20 µL of AuCuNC@N-GQD solution was drop cast onto a GCE for making the working electrodes. Since the current response corresponding to GLY in 0.1 M PBS was ~25 times lower than that of in 0.1M NaOH on AuCuNC@N-GQD/GCE, 0.1M NaOH was used as the electrolyte for the studies unless otherwise specified.

6.3 Results and Discussions

6.3.1 Synthesis and Formation of AuCuNC@N-GQD

The synthesis of AuCuNC@N-GQD was carried out as described in the experimental using the GE reaction process, where the metal (Cu) atoms in clusters/nanoparticles which have lower oxidation potential are in contact with the Au(III) ions with higher oxidation potential, oxidizes the lower oxidation potential metal atoms on the surface of cluster/nanoparticles to ions and the metal ions with higher oxidation potentials undergoes reduction and replace them on the surface of the metal cluster/nanoparticles. Thus, here when $AuCl_3$ is added to CuNC@N-GQD, some of the Cu atoms on the surface are replaced by Au atoms. As the molar concentration of $AuCl_3$ added is half that of the $CuSO_4$ initially taken in the first step for making CuNC@N-GQD, possibly only the surface Cu atoms are oxidized by Au(III) to form Au(0) and Au(I) atoms, which resulted in the formation of AuCuNC@N-GQD.

6.3.2 Structure, Size, Stability and Properties of AuCuNC@N-GQD

The HR-TEM micrographs given in Figure 6.1A, shows that the of the AuCuNC@N-GQD are of uniform in size (~4.5 nm). The crystalline lattice fringes (Figure 6.1B) with an interlayer spacing of 0.21 nm is assigned to the (102) diffraction planes of sp^2 graphitic carbon (Saisree, Nair, and Sandhya 2022) and that of 0.23 nm corresponds to (111) plane of Au-Cu alloy(M. Liu et al. 2016). The histogram shows a narrow size distribution of AuCuNC@N-GQD from 4 to 5 nm (Figure 6.1C).

While the UV-Vis spectrum of CuNC@N-GQD (Figure 6.1D) has only one peak at ~ 230 nm, AuCuNC@N-GQD has two, at ~ 230 and 360 nm, the latter is attributed to the AuNC moiety in the system, which is in good agreement with the reported values(Yang et al. 2016). The absence of the characteristic plasmonic band(S., Arya, and K. Y. 2022a) (500-600 nm) (Inset of Figure 6.1D) of larger nanoparticles (NP) in the visible region is an indicative of the absence of NP (Au/Cu) formation. The emission spectrum of AuCuNC@N-GQD (Figure 6.1E) consists of two well-defined peaks at ~ 380 and 490 nm, and that of CuNC@N-GQD consists

of two well-defined peaks at ~ 330 and 450 nm. The enhanced and red shifted (green to yellow) emission (Figure 6.1Fa-d) of AuCuNC@N-GQD compared to that of CuNC@N-GQD is assigned to the incorporation of Au atoms in the NC. The digital images (Figure 6.1Fa&b and c&d) show the comparative emission characteristics of CuNC@N-GQD and AuCuNC@N-GQD under normal light and UV (365 nm) irradiation. The CuNC@N-GQD (Figure 6.1Fc) is green emissive, whereas the AuCuNC@N-GQD (Figure 6.1Fd) is yellow emissive with the corresponding quantum yields of ~19 and 24 % respectively. In addition, unlike the CuNC@N-GQD, the AuCuNC@N-GQD possesses an intense solid-state orange emission, (Figure 6.1Fe-h).

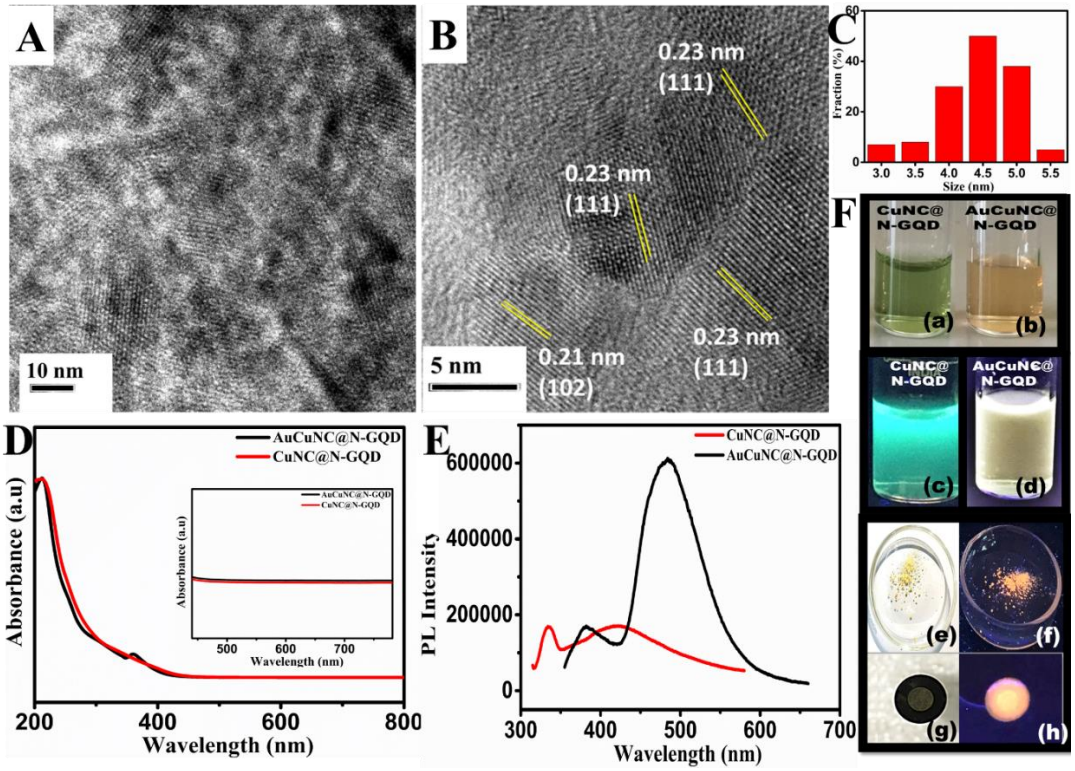

Figure 6.1. (A and B) The HR-TEM images of the AuCuNC@N-GQD and the corresponding d-spacings; (C) Histogram of the AuCuNC@N-GQD from the TEM images; (D) The UV-Vis spectra of AuCuNC@N-GQD, and CuNC@N-GQD; (Inset of D) The enlarged image of UV-Vis spectra in the visible region; (E) The emission spectra of AuCuNC@N-GQD, and CuNC@N-GQD; (F) The digital images of the photoluminescence of the CuNC@N-GQD and AuCuNC@N-GQD under normal (a and b) and short-UV (365 nm) (c and d) irradiation , the solid-state emissions of AuCuNC@N-GQD under normal light (e) and short-UV (365 nm) (f), and the emission characteristics of AuCuNC@N-GQD on GCE under normal light (g) and short-UV (365 nm) (h) respectively.

The higher susceptibility of Cu towards oxidation makes the synthesis of stable Cu containing NCs, challenging, either mono- and bi-MNCs. The lower temporal stability remains a limiting factor for their practical applications such as sensing, bioimaging and so on. Hence, it is pertinent to synthesis Cu containing NCs, with enhanced stability. The absorption (Figure 6.2A) and emission characteristics (Figure 6.2B) and the digital images of AuCuNC@N-GQD under visible and short UV (365 nm) after a one-year of storage (inset of Figure 6.2A and 6.2B), respectively, shows the invariable emission characteristics of AuCuNC@N-GQD indicating its temporal stability. It can be noted that the retention of the absorption and emission intensity after one year with respect to the initial intensities were ~ 92 and ~ 96%, indicating a temporal stability up to one year. The highest stability reported hitherto for AuCuNC was six months(Cai et al. 2020) and hence our material AuCuNC@N-GQD possess the highest stability so far. In our previous work a similar temporal stability of CuNC@N-GQD for about one year was explained based on the presence of N-GQDs(S., Arya, and K. Y. 2022a). Thus, the stability of AuCuNC@N-GQD is attributed to the presence of N-GQDs, which can (i) sterically protect the NC by acting as a capping agent and (ii) by supplying electrons from its electron-rich aromatic basal planes, thus preventing/minimizing the oxidation susceptibility of Cu atoms in the NC(S., Arya, and K. Y. 2022a).

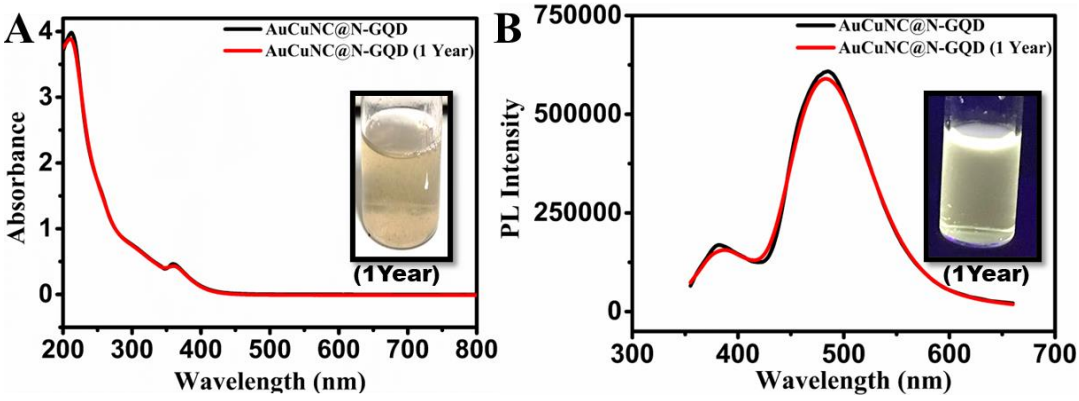

Figure 6.2. (A) The UV-Vis spectra of AuCuNC@N-GQD before and after ~1 year of storage; (B) The emission spectra of AuCuNC@N-GQD before and after ~1 year of storage; inset of (2A and 2B) The digital images of AuCuNC@N-GQD under visible and short UV (365 nm) after ~1 year of storage respectively.

In an attempt to confirm the formation and understand the number of Au and Cu atoms in the NC, the AuCuNC@N-GQD was studied using ESI-MS-TOF mass spectrometry. The mass spectra of AuCuNC@N-GQD (Figure 6.3A) showed a base

peak at the m/z value of 2199. The base peak(S., Arya, and K. Y. 2022a) obtained for N-GQD (Chapter 5, Figure 5.4D) was at 485 and for CuNC@N-GQD was at 1675 (Chapter 5, Figure 5.4E). The experimentally observed mass spectrum (Figure 6.3B) of AuCuNC@N-GQD match well with its calculated mass spectrum (Figure 6.3C). From the above spectral data, it can be suggested that the AuCuNC formed is associated with four Au atoms replacing four Cu atoms of CuNC@N-GQD by GE and thus the molecular ion peak corresponding to m/z 2199 can be denoted possibly as Au_4Cu_9(N-GQD)GSH. A schematic of the formation and the possible structure of AuCuNC@N-GQD based on the mass spectroscopic analysis is shown in Figure 6.4.

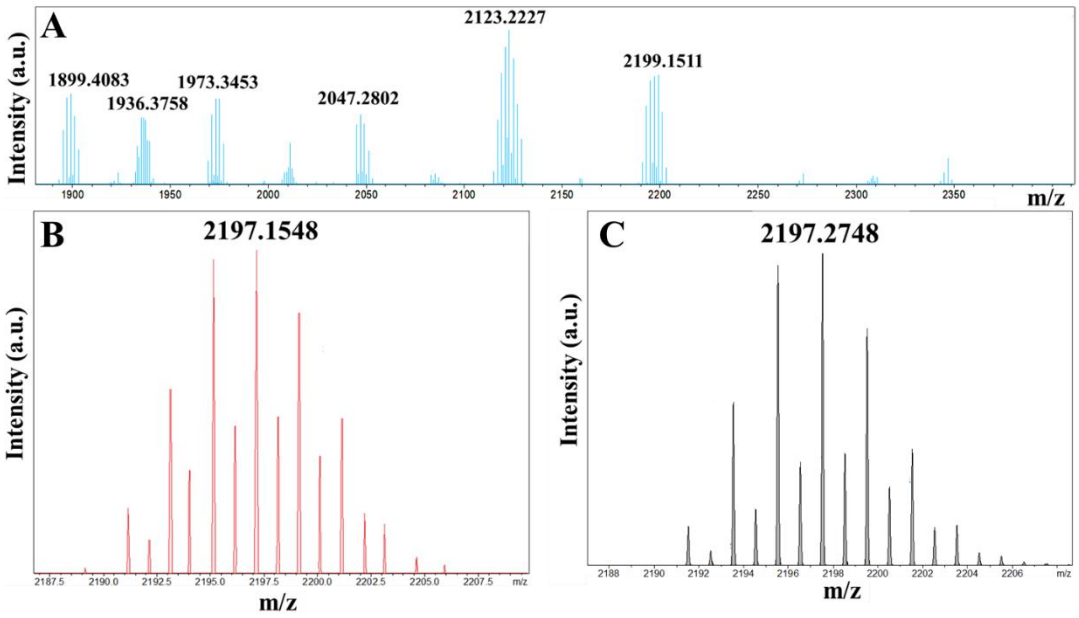

Figure 6.3. (A) MS-ESI-TOF mass spectra of AuCuNC@N-GQD; Expanded negative mode MS-ESI-TOF of AuCuNC@N-GQD in m/z 2199 showing (B) experimental spectrum (red trace) is in good agreement with (C) the calculated mass spectrum (black trace)

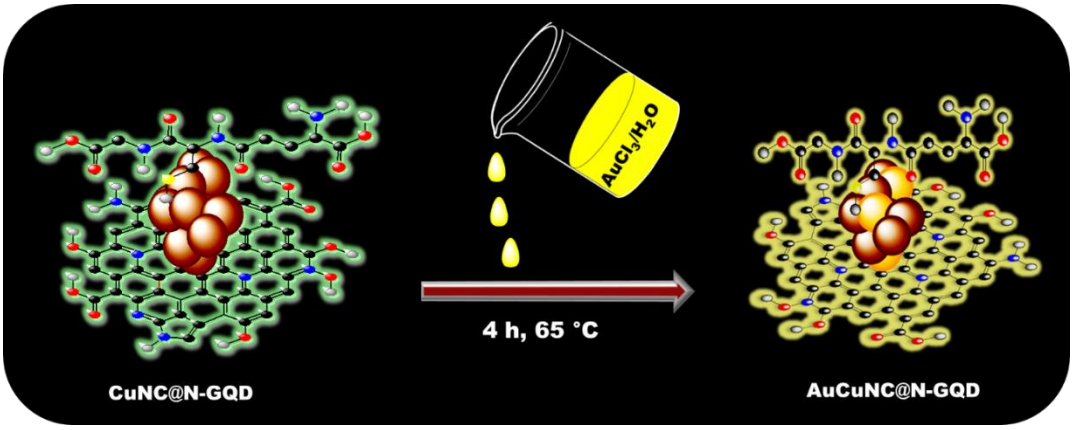

Figure 6.4. Schematic of the synthesis of AuCuNC@N-GQD from CuNC@N-GQD by the addition of $AuCl_3/H_2O$ and the illustration of the formation of yellow emissive AuCuNC@N-GQD from the green emissive CuNC@N-GQD

The XPS analysis was carried out to confirm the presence of Au and Cu and the other elements and their oxidation states. The survey scan spectrum of the CuNC@N-GQD (Figure 6.5A) exhibited the peaks of C 1s, O 1s, N 1s, and Cu 2p, whereas that of AuCuNC@N-GQD exhibited Au4f peaks in addition to C 1s, O 1s, N 1s, and Cu 2p thus confirming the inclusion of Au. The high-resolution C 1s XPS spectrum of AuCuNC@N-GQD (Figure 6.5B) revealed the presence of C-C/C=C (284.7 eV)(Mukthar Ali and Sandhya 2016), C=O (287.9 eV)(Nair J.S, Saisree, and Sandhya 2022), and C=N (288 eV)(Saisree, Nair, and Sandhya 2022) and that of the N1s (Figure 6.5C) indicating the presence of pyridinic (398.8 eV) and pyrrolic (401.1 eV) groups(Saisree et al. 2021b) which further confirms the inclusion of N-GQD in the formed NC. The binding energy of Au $4f_{7/2}$ (Figure 6.5D) was located between 84.9 eV and 88.2 eV indicating the coexistence of Au(0) and Au(I) in the AuCuNC@N-GQD(Shellaiah et al. 2019). The two intense peaks at 932.70 and 951.9 eV (Figure 6.5E) are assigned to the $2p_{3/2}$ and $2p_{1/2}$ of Cu(0). Thus, the results suggest the formation of AuCuNC@N-GQD.

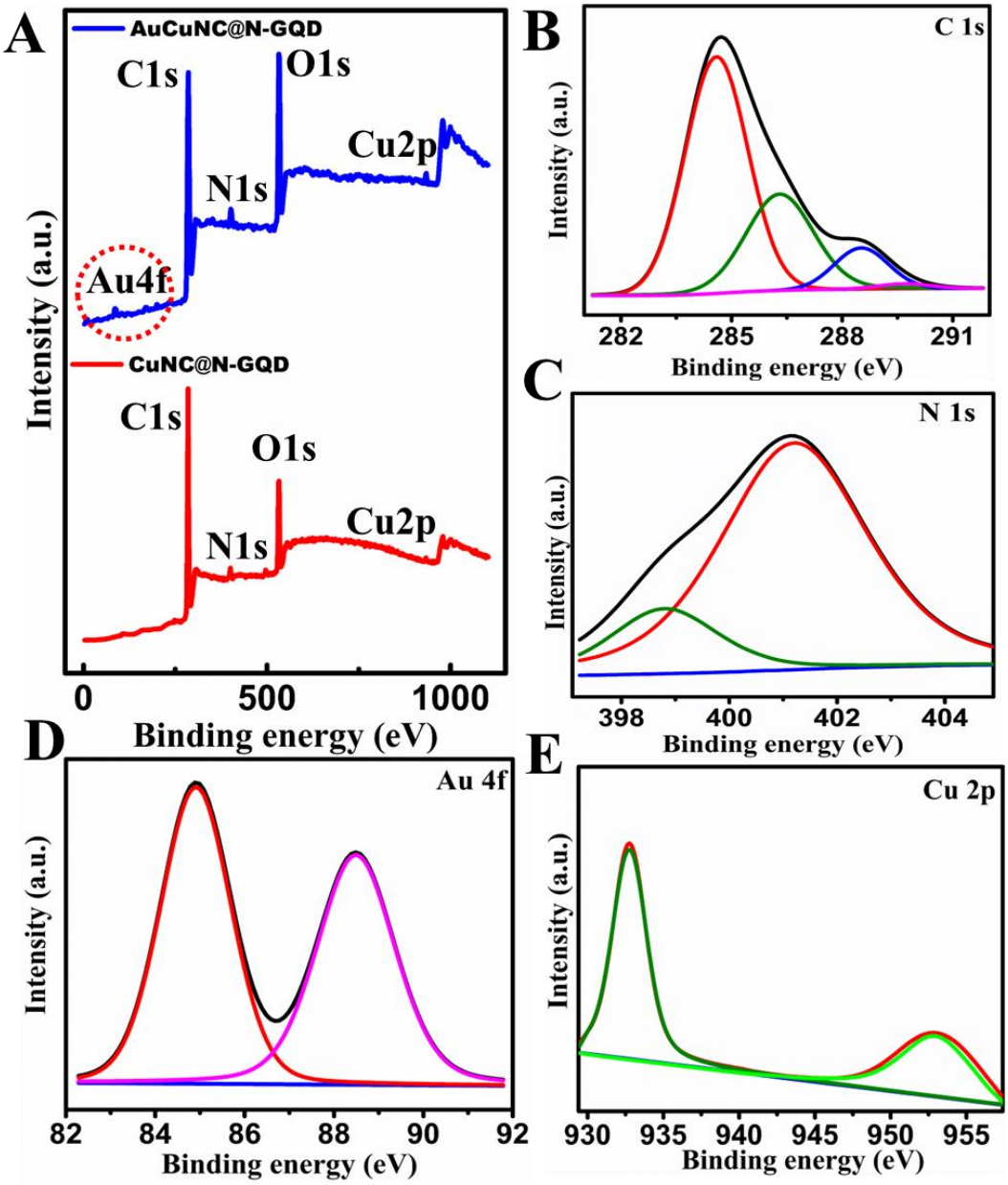

Figure 6.5. (A) The XPS survey spectra of AuCuNC@N-GQD and CuNC@N-GQD; (B, C, and D) The high-resolution XPS C 1s, Au 4f, and Cu 2p spectra of the AuCuNC@N-GQD

6.3.3 EC Sensing Studies of AuCuNC@N-GQD

There have been reports of Au-aminoacid (AA) interactions where Au-GLY interaction is well known. Further, our group has previously reported(S., Arya, and K. Y. 2022a) the simultaneous and superior sensing of DA, SER, and NIC by CuNC@N-GQD, which acts as a precursor of this NC. Because of these reasons, we attempted to investigate the sensing capability of AuCuNC@N-GQD/GCE towards various biomolecules, including DA, SER, NIC, FA, UA, AA, GLU, GLY, THR,

TRY, MET, HIS, ACH and other amino acids. The preliminary study result (Figure 6.6A) showed three distinct oxidation peaks at 0.20, 0.73, and 1.2 V for DA, GLY, and HIS, respectively, on AuCuNC@N-GQD/GCE. Because there are many reports on the EC sensing of DA(Arya Nair et al. 2022)-(Ramachandran, Panda, and Karunakaran Yesodha 2018) whereas there are no reports on the sensing of GLY by a non-enzymatic electrode and the peak current value obtained for HIS (1 mM) is so of low value (3.7 μA) and was at a higher potential value (1.2V), further studies were focused on the sensing of GLY. The DPV profiles (Figure 6.6B) for the EC sensing of GLY reveals that the modification by AuCuNC@N-GQD/GCE resulted in a ~ 27-fold increase in the current response for GLY to that of the unmodified GCE, and N-GQD/GCE, and ~23 fold than that of the CuNC@N-GQD/GCE and AuCuNC/GCE. The observed enhancement in the current response for GLY on AuCuNC@N-GQD compared to the control AuCuNC shall be attributed to the improved conductivity due to the presence of N-GQD. This observation was further validated by the EIS plots (Figure 6.6C), it can be seen that the diameter of the semicircles was in the order of: bare GCE (5 kΩ) > AuCuNC/GCE (4 kΩ) > AuCuNC@N-GQD/GCE (0.5 kΩ), which suggest that the charge-transfer resistance (R_{ct}) was lowest for AuCuNC@N-GQD/GCE. The better charge-transfer property of AuCuNC@N-GQD/GCE to that of AuCuNC, is assigned to the comparatively better conductivity properties of AuCuNC@N-GQD due to the presence of N-GQD in the latter. Thus, the higher current response of AuCuNC@N-GQD towards GLY can be assigned to the exfoliated nature N-GQD happened due to the attachment of CuNC during the formation of CuNC@N-GQD, which resulted in an enhanced conductivity and catalytic activity due to the exposed active sites(S., Arya, and K. Y. 2022a). Further, the enhancement compared to that of CuNC@N-GQD can inevitably be explained based on the Au-GLY interaction and is explained in detail in section 3.4.a. The reports of the ability of complex formation of Au with various amino acids(Pakiari and Jamshidi 2007) indicates the transfer of lone pair of electrons in the N, O, and S atoms to the antibonding orbitals of Au and reveals that of the amino acids, GLY can preferentially interact with Au because of its smaller size and hence the less steric hindrance(Xie, Lei, and Fang 2012) which leads to stable complexes with Au. Thus, the selective and enhanced sensing of GLY by AuCuNC@N-GQD is attributed to the combined effect of the combination of

AuCuNC and N-GQD and the structural changes that happened during the formation of the NCs on the N-GQD.

The DPV profiles of GLY (Figure 6.6D) with the increasing concentrations showed an increase in the current response indicating the capability of quantitative sensing by AuCuNC@N-GQD/GCE. The corresponding linear dynamic range graphs of GLY falls in the concentration range of 10^{-8} to 10^{-3} M (Figure 6.6E) with a correlation coefficient (R^2) of 0.9875 and the corresponding linear regression equation for the oxidation peak current can be expressed as I_{pa} (μA) = 0.0267x (μM) + 2.0543 (R^2 = 0.9875). The LOD (S/N=3), and sensitivity value obtained for GLY from the LDR are 0.011 μM which is the lowest LOD reported so far and 0.377 $\mu A \mu M^{-1} cm^{-2}$, respectively. The experimental LOD value was 10 nM (Figure 6.6F), and is in good agreement with the theoretically calculated LOD value of 0.011 μM.

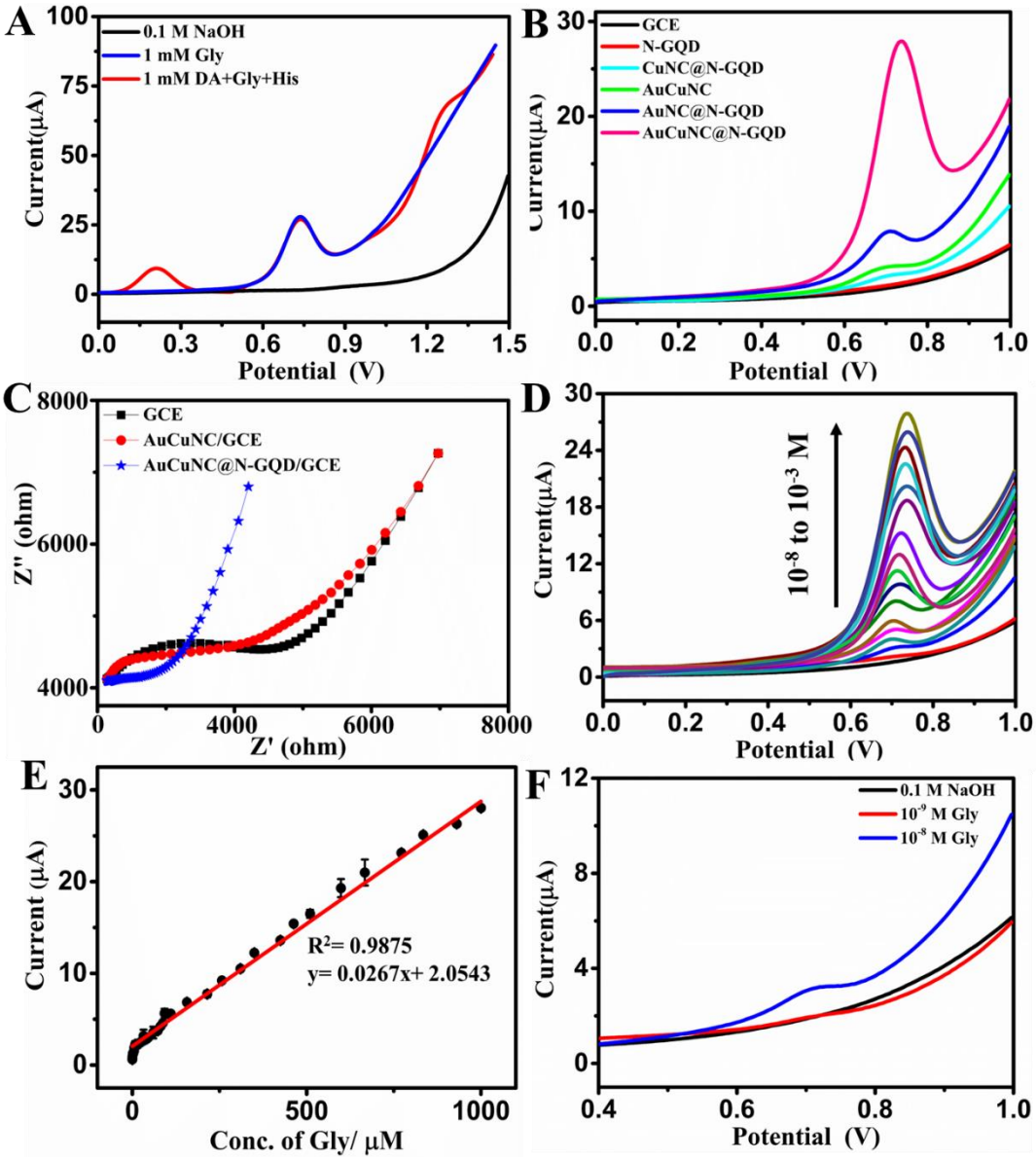

Figure 6.6. (A) The DPV responses of 1 mM GLY alone as well as 1 mM each of DA, GLY and HIS simultaneously in 0.1 M NaOH; (B) The DPV responses of of GLY (1 mM in 0.1 M NaOH) on unmodified GCE, N-GQD/GCE, CuNC@N-GQD/GCE, AuCuNC/GCE and AuCuNC@N-GQD/GCE, respectively; (C) EIS plots of bare GCE, AuCuNC/GCE and AuCuNC@N-GQD/GCE (D) The DPV responses of GLY on AuCuNC@N-GQD/GCE from 10^{-8} to 10^{-3} M; (E) The corresponding LDR graph obtained; (F) The DPV response in 0.1 M NaOH on AuCuNC@N-GQD/GCE in the absence of GLY and in the presence of 1 and 10 nM GLY respectively.

6.3.4 Selectivity and Interference Studies of GLY on AuCuNC@N-GQD and the Mechanism

The selectivity is a significant parameter which is a criterion for the practical applicability of a sensor, was carried out in a mixture of other analytes of biological relevance and are possible interferents such as various neurotransmitters, amino acids, vitamins and other biologically relevant molecules. The DPV profile (Figure 6.7A) reveals no current response for any of the biomolecules even at 1000x concentration other than that of GLY (1 μM) and the corresponding bar diagram (Figure 6.7A-B) clearly depicts the result indicating the selectivity of AuCuNC@N-GQD towards GLY.

The selective sensing capability of AuCuNC@N-GQD towards GLY is assigned to the size of GLY compared to the other amino acids. Due to the relatively smaller size of GLY the interaction between the Au and N in the amino group of GLY become stronger by the close proximity(Xie, Lei, and Fang 2012). Thus, the Au-GLY complexes become stable than the complexes of Au with other amino acids. The Au-GLY binding facilitate the oxidation of GLY to formaldehyde in the basic electrolyte solution during the positive potential sweep, which gives rise to a strong oxidation peak at 0.73 V. No current response was observed for the other amino acids studied and shall be attributed to the comparatively less effective or non-interaction with Au, due to the bigger size and the resultant steric hindrance. Even though the size of HIS is bigger, the sensing by AuCuNC@N-GQD says there is interaction, between the pyrrolic-N with the Cu moieties(Y. Zhou et al. 2014) and is attributed to the greater number of Cu compared to the Au atoms which makes the interaction possible. The lower current response and the higher peak potential is evident of the difficultness in the interaction between the HIS and the Cu atoms in the NC.

The enhancement in the current response of GLY by AuCuNC@N-GQD than that of the controls is attributed to the enhanced conductivity and electronic properties AuCuNC@N-GQD. Thus, in an attempt to understand the conductivity properties, bandgap analysis (Figure 6.7C) was done. The bandgap obtained for AuCuNC@N-GQD, CuNC@N-GQD and for AuNC@N-GQD were 1.32, 1.35 and 1.41 eV, respectively. The current responses of all three towards GLY, was in the

order AuCuNC@N-GQD >AuNC@N-GQD > CuNC@N-GQD, which is in the reverse order of the band gap values. Thus, it is clear that AuCuNC@N-GQD has the lowest bandgap, which can translate to higher conductivity than CuNC@N-GQD and AuNC@N-GQD. The observed order of band gap values can be ascribed to the higher oxidation potential of Au compared to that of Cu which in turn resulted more electronic cloud towards Au atoms. This further affects the sensing characteristics of the cluster. This electronic polarisation can be higher in AuNC@N-GQD than AuCuNC@N-GQD since the percentage Au substitution in AuCuNC@N-GQD was lesser. Hence, the AuCuNC@N-GQD shows an enhanced sensing towards GLY than AuNC@N-GQD. The absence of Au-GLY interaction in CuNC@N-GQD-GLY sensing made its current response lowest (details in section 6.3.3). The mechanism of sensing is validated further through scan rate studies (Figure 6.7D). A linear fit of the current response vs. the scan rate corresponded to an adsorption-controlled process, whereas that for the current response vs. the square root of the scan rate corresponded to a diffusion-controlled process(Aswathi et al. 2015). The linear fits of current response vs. scan rate/square root of scan rate (Figure 6.7E-F) suggest that the adsorption process majorly governs the sensing of GLY with an $R^2 \geq 0.99$, and the result agrees to the above-proposed mechanism. An illustration of the EC sensing strategy and the enhanced sensing capability of AuCuNC@N-GQD towards GLY is depicted in Figure 6.8.

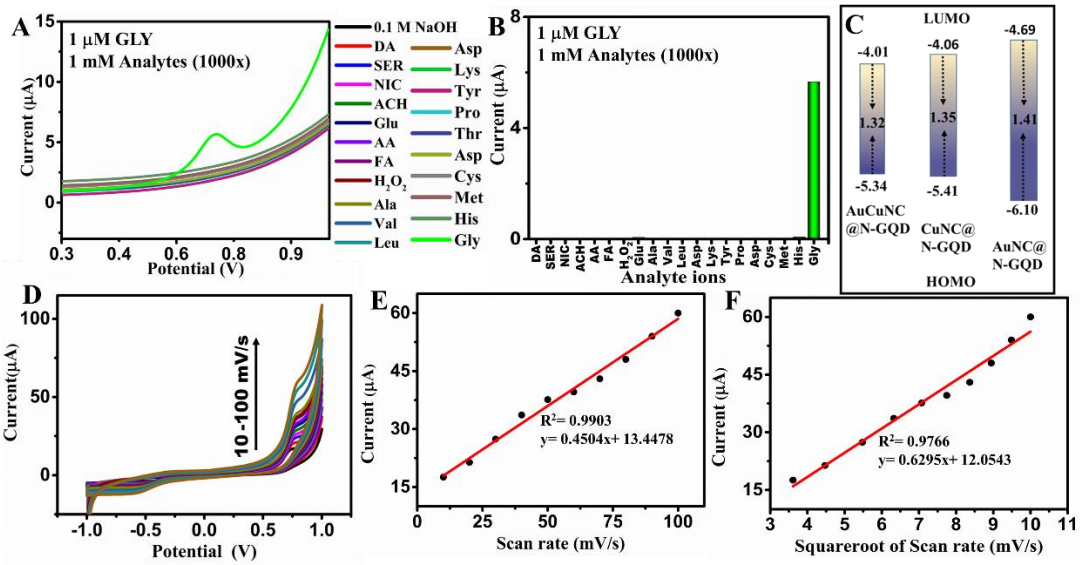

Figure 6.7. (A) and (B) Selectivity studies of AuCuNC@N-GQD/GCE towards GLY (1µM) in the presence of various analyte species (1 mM each); (C) The HOMO and LUMO levels

and bandgaps of AuCuNC@N-GQD, CuNC@N-GQD and AuNC@N-GQD obtained experimentally; (D) The CV profiles of the AuCuNC@N-GQD/GCE in 0.1 M NaOH containing 1 mM Gly at various scan rates (10–100 mV s-1); (E) and (F) The Calibration plots of the anodic peak current vs. the scan rate and the anodic peak current vs. the square-root of the scan rate, respectively.

Hitherto no literature reports of the voltammetric sensing of GLY is available, so the comparison of the sensing performance of AuCuNC@N-GQD/GCE was done with methods such as, the enzyme-based chronoamperometry(Q. Wang et al. 2021), liquid chromatography(Marrubini, Caccialanza, and Massolini 2008), spectrophotometry(Keskin and Keskin 2014), and fluorescence assay kits(Rosini et al. 2014), isotopic dilution mass spectrometry(Culea et al. 2011), electrophoretic determination(Pakhomova et al. 2010), molecularly imprinted polymer-modified piezo sensor(Zyablov et al. 2010), and capillary zone electrophoresis with contactless conductivity detection(Tůma et al. 2013), in terms of LOD, LDR and sensitivity as provided in Table 6.1. All the techniques mentioned above utilize indirect GLY sensing methods, such as enzymatic conversions, incorporation into molecularly imprinted polymers, etc. These indirect methods involve inter-reactions, making the sensing procedure more complex and hence becoming time-consuming. For instance, the enzymatic sensing procedure uses the enzyme glutamate dehydrogenase (GDH)(Keskin and Keskin 2014), to determine GLY. Here ammonia is produced from the enzymatic reactions between GLY and GDH. Hence, these methods have limitations such as lower sensitivity and accuracy, the requirement of ambient reaction conditions, and are costly. In comparison with the above-mentioned sensors, AuCuNC@N-GQD exhibited the lowest reported LOD for GLY in the EC, and as this is a non-enzymatic method, it upholds the merit of the present study. Our study show that the EC sensing is more meritorious over the other sensing approachs in terms of LOD, LDR. The AuCuNC@N-GQD exhibited an LOD of 10 nM through EC sensing pathway with the LDR from 0.01–1000 μM. This we attribute to the general mechanism involved in the sensing of each category where EC sensing has an edge as one of the components, the electrode, is fixed, which makes the interaction easier.

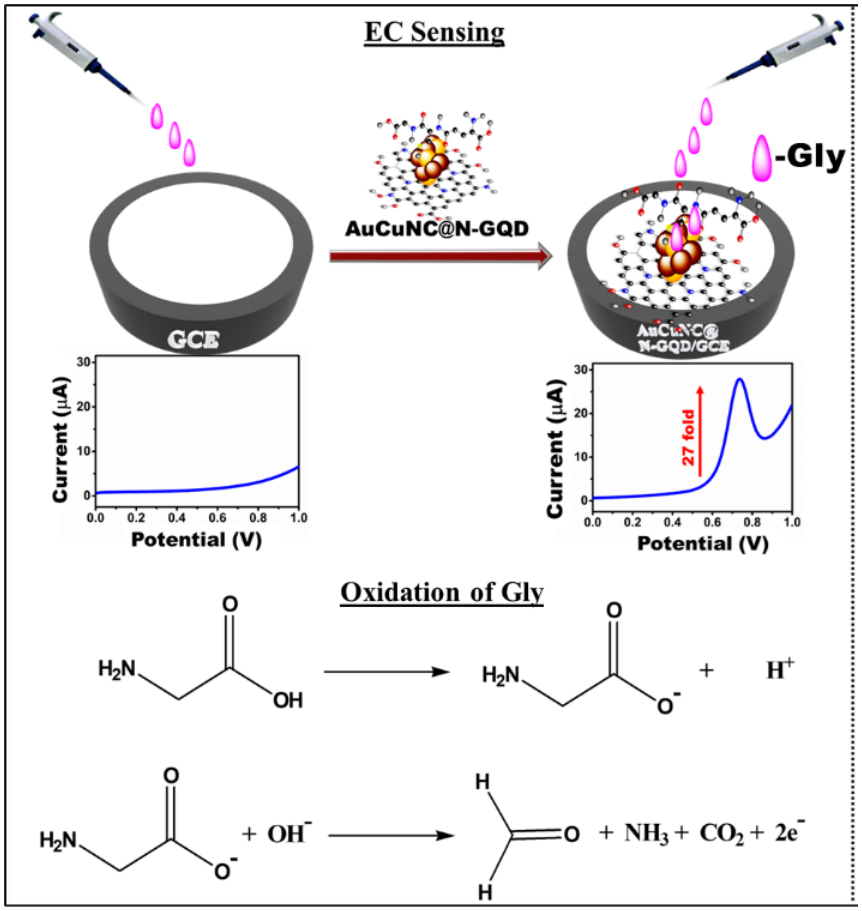

Figure 6.8. The schematic diagram shows the dual-sensing capability of AuCuNC@N-GQD through EC sensing pathway

Table 6.1 Comparison of the LOD of AuCuNC@N-GQD/GCE with that of the literature reports of GLY sensors.

Materials/ Electrodes	**Detection Method**	**LOD (μM)**	**LDR (μM)**	**Sensitivity**	**Reference**
NiO NPs/GCE	EC	0.9	1~ 200	0.0243 $\mu A \mu M^{-1}$	(Roushani, Shamsipur, and Pourmortazavi 2012)
$Ni(OH)_2$ NPs/GCE	EC	30	100~1200	0.92 $\mu A m M^{-1}$	(Vidotti, Torresi, and

					Kubota 2008)
AuCuNC	Fluorescence	5.8	600 – 5000	Nil	(Z. Chen et al. 2020)
	Isotopic dilution mass spectrometry	130	130-10600	Nil	(Culea et al. 2011)
1,2,4,5-benzoltetracarbonic acid, 4,4'-diaminodiphenyloxide.	Piezo resonance sensor	900	Nil	Nil	(Zyablov et al. 2010)
	HPLC	2660	2660-5328	Nil	(Marrubini, Caccialanza, and Massolini 2008)
AuCuNC@N-GQD/GCE	EC	0.01	0.01–1000	0.377 $\mu A \mu M^{-1}$	Our Result

6.3.5 Reusability, Reproducibility and Stability Studies

The reusability of the AuCuNC@N-GQD/GCE electrode was scrutinized by comparing the peak currents of GLY (1 mM) on AuCuNC@N-GQD/GCE (Figure 6.9A) before and after 30 times of washings, and the results showed it had ~ 98% retention. For the reproducibility studies, the current responses of five different electrodes toward 1 mM GLY were examined. The relative standard deviation (RSD) of the peak currents of these individually prepared electrodes was found to be 1.72%, which showed its excellent reproducibility (Figure 6.9B). The current values after one- and two-months were ~ 96% and ~ 93% of its initial current response (Figure 6.9C), respectively.

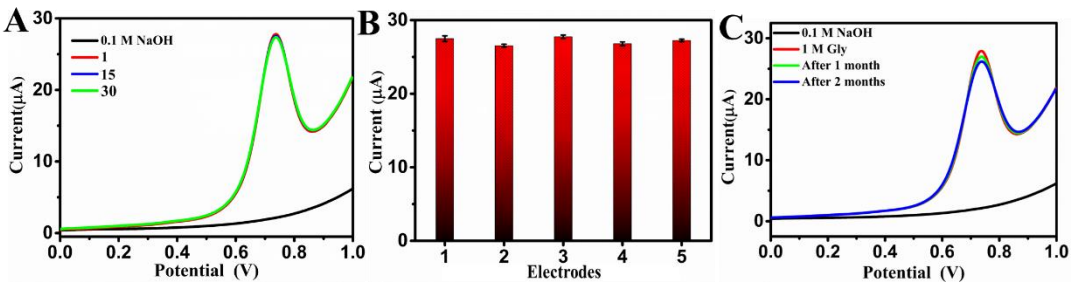

Figure 6.9 (A) The DPV curves after immediate washing for three times showing the reusability of the sensor; (B) The peak currents of five independently coated electrodes showing the reproducibility of AuCuNC@N-GQD/GCE; (C) DPV profiles obtained for GLY (1 mM) on AuCuNC@N-GQD/GCE showing the stability of the sensor for 1 month and 2 months.

6.3.6 Real Sample Studies

The AuCuNC@N-GQD/GCE was further utilized for the detection of GLY in real human blood and urine sample environment via the standard addition method, where known amounts of GLY were added to the diluted (1000x) blood, and urine samples and the recovery amounts were measured from the obtained current response. The measurements are summarized in Table 1, and the DPV profiles are given in Figure 6.10. The recovery calculated was found to be in the range of 100.2-100.75 %. The recovery values of ~100 % in all the samples indicate the successful applicability of the proposed electrode to determine GLY in actual biological samples.

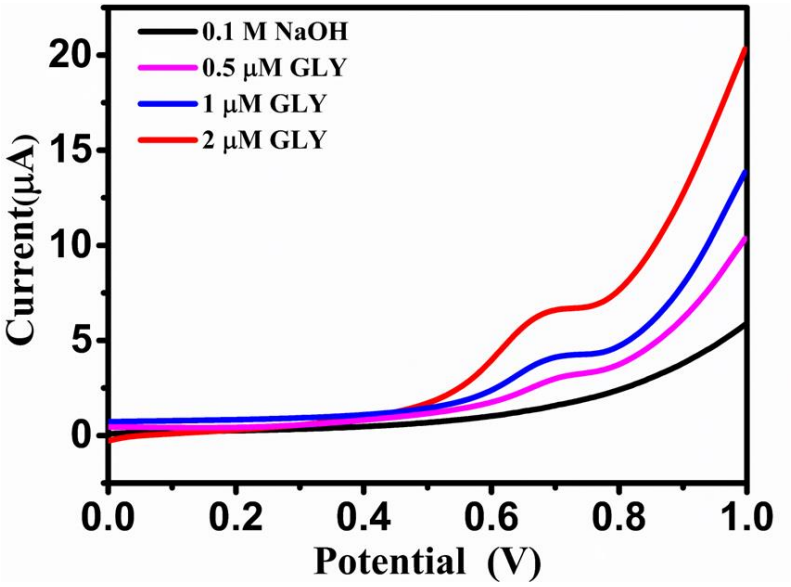

Figure 6.10. The DPV responses of 0.5, 1, and 2 μM of GLY in blood samples.

Table 6.2. The recovery test results of GLY in human blood and urine samples

Sample No.	GLY Spiked (μM)		Found* (μM)	Recovery (%)
1	0.5	Blood	0.503	100. 6
		Urine	0.501	100.20
2	1	Blood	1.007	100.70
		Urine	1.005	100.50
3	2	Blood	2.015	100.75
		Urine	2.008	100.40

* All the recovery values fall within the RSD of 1%

6.4 Conclusion

In this work, a stable bimetallic NC, AuCuNC@N-GQD, with ~1 year of stability that exhibited solid-state and solution-state fluorescence in the NIR region without any synthetic macrocycles such as pillarenes and dual sensing property towards GLY was made by a GE process. The NC exhibited enhanced selective EC sensing towards GLY. The preferential interaction of Au with GLY amongst the amino acids was attributed to the selectivity of AuCuNC@N-GQD towards GLY. This is the first non-enzymatic EC sensing report towards GLY. The ~ 4-fold higher current response of AuCuNC@N-GQD to that of the controls in EC sensing is ascribed to the enhancement in the conductivity and electronic properties of AuCuNC@N-GQD due to the presence of N-GQD. The LOD obtained in the EC sensing was 0.01 μM, which remains the lowest than the so far reported sensors. The good reproducibility, reusability, and stability of AuCuNC@N-GQD-modified electrode, along with the admirable recovery percentages in the real sample study, with ~ 100% in all the tested blood and urine samples, with the recovery values falling within the relative standard deviation of 1%, show the potential applicability of the developed sensor in real-time monitoring.

CHAPTER 7

Picomolar level Ultra-Selective Electrochemical sensing of Lead Ions by a Gold-Copper Nanocluster on Nitrogen-Doped Graphene Quantum Dot

The EC sensing capabilities of AuCuNC@N-GQD were investigated towards the heavy metal ions and observed a highly selective sensing property towards Pb(II) with almost nil current response for all other interfering metal ions studied. The Pb(II) is included in the top ten list of chemicals of major public health concern by the World Health Organization, and its prevalent usage in batteries and other industry makes the detection of Pb(II) in environmental samples decidedly significant. The selective interaction between Au(I) and Pb(II) is responsible for the selective sensing of Pb(II) by AuCuNC@N-GQD. The LOD value obtained was 1 pM , the lowest reported hitherto for Pb(II) by any other material. Such a low LOD value implies the potential of the sensor material.

7.1 Introduction

Lead ion, Pb(II), is one of the top ten toxic heavy metal ions according to the World Health Organization's (WHO) list of 10 chemicals of major public health concern(Sayyad et al. 2021) and has a specified maximum acceptable concentration of ≤10 ppb Pb(II) in drinking water. Due to the widespread use of Pb(II) in rechargeable batteries, electroplating, bullets, constituent of solder, protective shielding around nuclear reactors, particle accelerators, X-ray equipment, containers used for transporting and storing radioactive materials and their non-proper disposal has led to the contamination of land and majority of water sources around the globe. Pb(II) being non-biodegradable makes the possibility of its presence in higher water sources and causes greater risks to human health(Bian et al. 2016). The exposure of Pb(II) affects all living systems including plants and animals through food chain and the adverse effect to humans include damage to liver, kidney, skin, skeletal system,

nervous and haematological systems, and can reside up to ≤ 12 years in human body due to bio-accumulation(Needleman 2004). Thus, an appropriate trace level detection of Pb(II) in water or other environmental samples has become crucial and highly essential. Presently, methods such as mass spectroscopy, X-ray fluorescence spectroscopy, laser-induced breakdown spectroscopy, and atomic absorption spectroscopy, have been used for the determination of heavy metal ions which involves highly expensive and complex instruments, expert personnel, pre-sampling, time-consuming steps and are non-portable(Cheng 2003). In this context, the EC sensing holds remarkable advantages such as simplicity, portability, cost-effectiveness, and instant results with superior selectivity and sensitivity, which can fulfil the growing demand for the on-site environmental monitoring of trace heavy metal ions.

The selective EC sensing of Pb(II) has been reported by various materials, including L-Cysteine peptide-functionalized PEDOT-PSS/rGO nanocomposite with a LOD of 0.43 nM(Sayyad et al. 2021), an α-Fe_2O_3/NiO heterostructure with LOD of 0.02 μM(J. Wei et al. 2021), a silver (Ag)–gold (Au) alloy nanoparticle (NP)–aptamer conjugate with a minimum detectable concentration of 0.8 μM(Yadav et al. 2020), zinc/cobalt co-centered MOF derived carbon–MWCNTs which displayed a detection limit of 3.3 nM(Zhao et al. 2020) and a zinc oxide-decorated MWCNT with a detection limit of 2.3 μM(Malik et al. 2022). It can be noted that most of the materials include toxic organic or metal components and have utilised multi-step synthesis, which holds the main demerits of these reported sensors. Sensor materials which can be achieved through simple and environmentally benign procedures, of low cost, non-toxic along with excellent sensitivity and selectivity are of much interest in the application point of view. Here in this work, we have utilized a bimetallic gold-copper nanocluster (AuCuNC), for the EC sensing of Pb(II). The AuCuNC, co-protected by thiolate and nitrogen-doped graphene quantum dots (N-GQD), AuCuNC@N-GQD, has been successfully synthesized through a simple galvanic exchange (GE) strategy using an earlier reported procedure from our group. In the typical synthesis, we have achieved a AuCuNC@N-GQD through a simple replacement reaction between CuNC@N-GQD and $AuCl_3$. A temporal stability of

≥365 days is one of the significant characteristics of the AuCuNC@N-GQD, considering the low stability issues of Cu containing NCs.

The NCs containing Cu, either mono or bimetallic have begun to attract the attention, now-a-days to the researchers because of the abundance, cost-effectiveness, and easy availability of Cu. But regardless of these advantages, synthesis and applicatio0n of Cu containing NCs are challenging because of their low oxidation stability(Lin et al. 2021). In order to make stable Cu based NCs, larger molecules such as polymers(Barik et al. 2020), DNA(Z. Zhou, Du, and Dong 2011), and proteins(Goswami et al. 2011) were used as steric capping agents, which causes complexity to the characterisation of the NC leading to less understanding of the structure and hinder its application properties due to the lesser accessibility of the NC. There were reports on the synthesis of CuNCs by the utilisation of smaller thiolated ligands as capping agents, but the average stability of the nanoclusters is ~1 month, lower than that of the CuNCs prepared using larger capping agents which are of ~ 6 months. Recently, a CuNC@N-GQD with ≥ 1 year stability was reported by our group(Saisree, Arya Nair, and Sandhya 2022) using N-GQDs as reducing agent and glutathione as a capping agent, where N-GQD plays a major role in the ultra-high stability of the NC by supplying electrons thus lowering the susceptibility of Cu to oxidation. the AuCuNC@N-GQD exhibited highly selective sensing towards one of the top ten toxic metal ion, Pb(II) and expressed an excellent sensitivity of 1.39 $\mu A \mu M^{-1} cm^{-2}$ and lowest detection value of 10^{-12} M, i.e. 1 pM (0.0002 ppb), which is well below the maximum acceptable concentration level (≤ 50 nM). It possesses the higher selectivity for Pb(II), with no interference from a range of metal ions, including Fe(III), Fe(II), Cr(VI), Ag(I), Cd(II), Hg(II), Zn(II), Ni(II), Co(II), Li(I), Mg(II), Cu(II), Mn(II), and Sn(II) and was explained in detail in the latter sections. The higher percentage recovery (~ 100%) in all the tested real samples show the developed sensor's potential applicability in real-time monitoring.

7.2 Experimental Section

7.2.1 Synthesis of AuCuNC@N-GQD

The procedure for the synthesis of the AuCuNC@N-GQD is detailed elsewhere in chapter 6, section 6.2.1. The procedure includes a GE method between $AuCl_3$ and, CuNC@N-GQD.

7.2.2 Preparation of electrodes for EC sensing

The pre-treatment and modification of GCE were done according to the procedure given in the experimental chapter. The samples (AuCuNC@N-GQD, CuNC@N-GQD, AuNC@N-GQD and N-GQD) were drop cast over separate GCEs with care and then allowed to dry for 24 hours at RT to achieve the modified electrodes.

The procedure for the preparation of the AuCuNC@N-GQD-Pb sample for the characterization is as described. The AuCuNC@N-GQD were mixed with $Pb(NO_3)_2$ solution and the product formed was washed well and dried.

7.2.3 Electrochemical methods

The EC behavior of various metal ions (Pb(II), Hg(II), Ag(I), Cd(II), Fe(II), Co(II), Ni(II), Zn(II), Sn(II), Mn(II), Mg(II), Cu(II), and Cr(VI)) on the surface of the AuCuNC@N-GQD/GCE was investigated using CV, differential pulse DPV and chronoamperometry at RT. A 20 µL of AuCuNC@N-GQDs, was drop cast on to a GCE for making the working electrodes. The electrolyte used was 0.1 M NaOH for the studies, unless otherwise mentioned.

7.3 Results and Discussions

7.3.1 Synthesis and characterisations of AuCuNC@N-GQD

The AuCuNC@N-GQD was characterized by various techniques such as TEM, Mass, XPS, UV and Fluorescence spectroscopic analyses, and it is discussed in detail in chapter 6, section 6.3.1. A schematic of the synthesis of AuCuNC@N-GQD is represented in Figure 7.1.

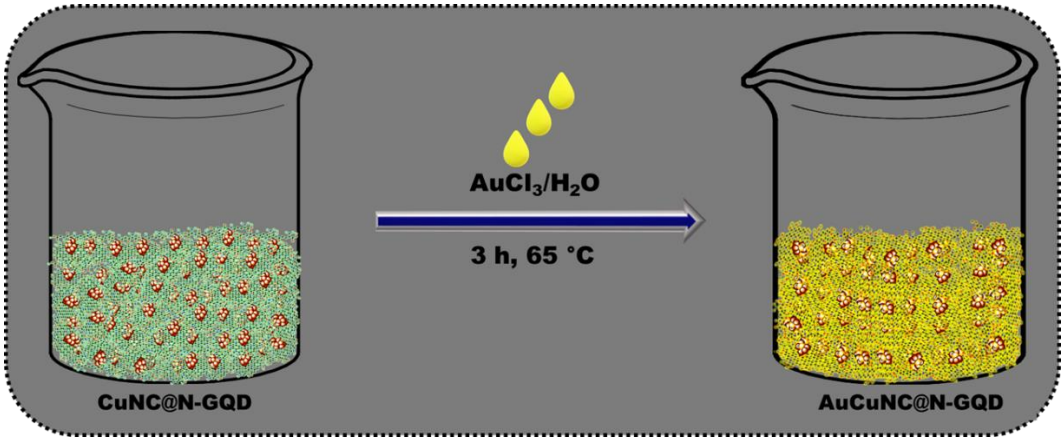

Figure 7.1. Schematic of the synthesis of AuCuNC@N-GQD from the CuNC@N-GQD

7.3.2 EC sensing studies of AuCuNC@N-GQD towards heavy metal ions

The preliminary screening of the EC sensing property of AuCuNC@N-GQD/GCE was done using the heavy metal ions: Cd(II), Hg(II), Ag(I), Pb(II), Fe(II), Co(II), Ni(II), Zn(II), Sn(II), Cu(II), and Cr(VI), and the result showed a current response for only Pb(II). The DPV profiles of Pb(II) on the bare GCE, N-GQD/GCE, AuNC/GCE, CuNC@N-GQD/GCE, AuNC@N-GQD/GCE, and AuCuNC@N-GQD/GCE (Figure 7.2A) showed that only AuNC@N-GQD and AuCuNC@N-GQD/GCE showed sensing property towards Pb(II) and the current response of the latter was ~2 times that of the former . The result point to the fact that the sensing is shown only by the NCs containing both the Au and N-GQD. This may be ascribed to the combination of Au(I)-Pb(II) interaction(López-De-Luzuriaga et al. 2021) and the spontaneous reduction of Pb(II) on the surface of the material, due to the electron-rich N-GQD in the NC. The oxidation of Au metal in basic electrolyte solutions is reported(Lien et al. 2013) and thus we assume some of the surface Au atoms were oxidized in the basic electrolyte solution (dilute NaOH) used, this is supported by the fact that Pb(II) sensing was not observed in other electrolytes such as PBS, and dilute HCl. The spontaneous reduction of metal ions, which has specific interactions with the electrode material, by N-GQD is explained in our earlier reports(Saisree et al. 2021a).

The enhancement (2-fold) in the current response of AuCuNC@N-GQD to that of AuNC@N-GQD may be due to the enhanced conductivity of the former due to the lower number of Au atoms compared to that of the former. It is well-known that Au has a higher reduction potential value and hence has a tendency to attract more electron density towards it which may reduce the availiability of electron in the N-GQD. To prove this hypothesis, the bandgap analysis and electrochemical impedance spectroscopy results were analysed. The bandgap analysis (Figure 7.2B) showed that the AuCuNC@N-GQD has the lowest bandgap value of all the three with a value of 1.32 eV, whereas it is 1.35 and 1.41 eV for CuNC@N-GQD and AuNC@N-GQD, respectively. Further, the impedance spectroscopy (EIS) (Figure 7.2C) shows that the diameter of the semicircle was in the order of: bare GCE (2.4 kΩ) > AuNC@N-GQD/GCE (1.9 kΩ) > CuNC@N-GQD/GCE (1.7 kΩ)>AuCuNC@N-GQD (0.6 kΩ), which suggest that the charge-transfer resistance (R_{ct}) was the lowest for AuCuNC@N-GQD/GCE of all. Thus, these results indicated the better charge-transfer and higher conductivity due to the lower number of Au atoms or due to the presence of Cu atoms are the reason for the higher sensing property of AuCuNC@N-GQD to that of AuNC@N-GQD. The result is an indication of the merit or property changes due to a bimetallic NC.

7.3.3 Sensitivity, LDR, and LOD

In order to investigate the efficiency of the AuCuNC@N-GQD as a quantitative sensing electrode for Pb(II), the current response with the increasing concentration was examined by varying the concentration of Pb(II) from 10^{-12} to 10^{-3} M. The DPV curves (Figure 7.2D) showed an increase in the current response with an increase in the concentration of Pb(II) and the corresponding linear response towards Pb(II) (Figure 7.2E) falls in the concentration range of 10^{-12} to 10^{-3} M. Two separate linear dynamic ranges were obtained: from 10^{-12} to 10^{-5} M (R^2=0.9744, N=20) and 2×10^{-5} to 10^{-3} M (R^2=0.9789, N=14). The corresponding linear regression equations were [I_{pa} (μA)] = 0.0988x (μM)+0.0563 (R^2 = 0.9744) and I_{pa} (μA) = 0.0524x (μM)+99.201 (R^2 = 0.9789) and the sensitivity values were 1.39 and 0.742 $\mu A \mu M^{-1} cm^{-2}$, respectively. The corresponding LOD value (Figure 7.2F) obtained was 10^{-12} M (1 pM). The calculated LOD from the lowest concentration range of the

linear dynamic range plot was 1.2×10^{-12} M (1.2 pM) which is in good agreement with the experimental LOD.

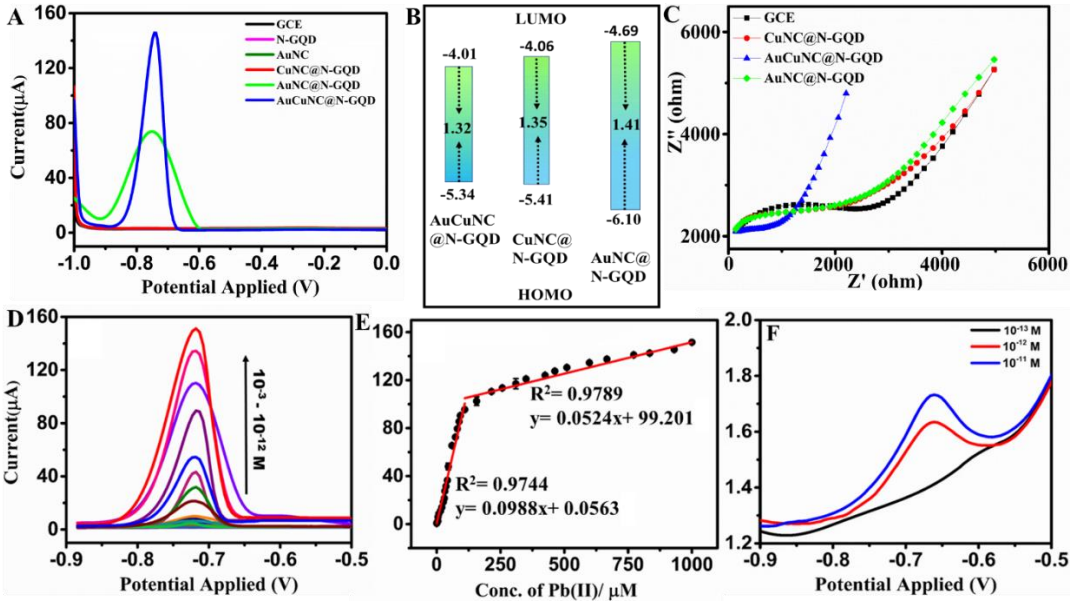

Figure 7.2. The DPV responses of 1 mM each of Pb(II) in 0.1 M NaOH on Bare GCE, N-GQD/GCE, AuNC/GCE, CuNC@N-GQD/GCE, AuNC@N-GQD/GCE, and AuCuNC@N-GQD/GCE; (B) The HOMO and LUMO levels and bandgaps of AuCuNC@N-GQD, CuNC@N-GQD and AuNC@N-GQD obtained experimentally; (C) Electrochemical impedance spectra of bare GCE, CuNC@N-GQD, AuCuNC@N-GQD and AuNC@N-GQD; (D) The DPV responses of Pb(II) in 0.1 M NaOH on AuCuNC@N-GQD/GCE for the concentration range of 10^{-12} to 10^{-3} M; (E) The linear dynamic ranges obtained for the concentration range of 10^{-12} to 10^{-3} M; (F) The DPV responses showing the LOD of Pb(II) as 10^{-12} M.

Table 7.1 compares the analytical performances of the AuCuNC@N-GQD/GCE with the various reported EC Pb(II) sensors. The reports of Au nanoparticle on carbon nanofibers (AuNP-CNF)(B. Zhang et al. 2016), Graphene/PANI/Polystyrene composite(Promphet et al. 2015), ZnO@Graphene nanocomposite(Yukird et al. 2018), and 1-dodecanoyl-3-phenylthiourea (DPT)(Shah et al. 2019), multiwalled carbon nanotube-β cyclodextrin (MWCNT-βCD)(Alam et al. n.d.) and Bi_2O_3 /Graphite-carbon inks(Kadara and Tothill 2008) had employed the stripping technique which employs a time-consuming pre-reduction step to facilitate the sensing itself in case there is no spontaneous reduction or to enhance the sensitivity and the detection limit, which creates experimental complexity, and can be a drawback for its real-time applicability. However, our AuCuNC@N-GQD did not require a pre-reduction step and even without the step

exhibited an LOD value of 1 pM which is the lowest detection limits reported so far. The selectivity and sensitivity of AuCuNC@N-GQD towards Pb(II) is particularly due to the combination of Au, Cu, and N-GQD in the NC which imparted selectivity and enhanced sensitivity, respectively, as explained in previous sections. Further, the n electrons mainly from the N-atom (doped) and the aromatic π electrons of N-GQD could reduce Pb(II) to Pb(0). Thus, the reducing capability of the electron rich N-GQD played a major role to spontaneously reduce Pb(II) on AuCuNC@N-GQD and that facilitated the sensing of Pb(II) without pre-reduction step in the oxidation sweep.

Table 7.1. Comparison of the LOD and linear dynamic ranges of AuCuNC@N-GQD/GCE with that of the literature reports of electrochemical sensors of Pb(II).

Materials	**Method**	**Pre-reduction**	**LOD (nM)**	**Linear Dynamic Range(nM)**	**References**
AuNP-CNF	SWASV	Yes	99	99-1000	(B. Zhang et al. 2016)
Graphene/PANI/Polystyrene	SWASV	Yes	16	48–2413	(Promphet et al. 2015)
Bi_2O_3 /Graphite-carbon inks	CCSCP	Yes	38	96–1447	(Kadara and Tothill 2008)
MWCNT- βCD	DPASV	Yes	4	14-498	(Alam et al. n.d.)
DPT	SWASV	Yes	3	53–217	(Shah et al. 2019)
ZnO@Graphene nanocomposite	SWASV	Yes	3	48–965	(Yukird et al. 2018)
MWCNT-Ion Imprinted polymer/Pt	DPV	No	20	4-24	(Sebastian and Mathew 2018)
AuCuNC@N-GQD	DPV	No	0.001	0.001-1000000	This Work

7.3.4 Mechanism of the sensing of Pb(II) by the AuCuNC@N-GQD with Evidence

The higher selectivity of AuCuNC@N-GQD towards Pb(II) could be primarily assigned to the Au(I)- Pb(II) interaction and is vividly understandable from the lack of the sensing by CuNC@N-GQD and N-GQD. As explained earlier in detail in section 3.2, the basic electrolyte solution can facilitate the oxidation of Au atoms to Au(I) state, which is further interacting with the Pb(II) ions, the interaction is well-established in ref.(Echeverría et al. 2015), this proposal is also augmented by the fact that the sensing does not work in acidic or neutral electrolytes. Further the presence of oxidation peak for Pb(II) without any pre-reduction step indicating spontaneous reduction of Pb(II) on AuCuNC@N-GQD. The spontaneous reduction of Pb(II) on AuCuNC@N-GQD is due to the reducing capability of N-GQD and it can be mainly attributed to the electron rich graphene sheets and N-doping(Saisree et al. 2021a).

In order to understand the interaction between Au(I) the XPS of AuCuNC@N-GQD-Pb and AuCuNC@N-GQD were compared, while the survey scan spectrum of the AuCuNC@N-GQD (Figure 7.3A) revealed the Au 4f peak at 86 eV, C 1s peak at ~284.5 eV, O 1s peak at ~ 530.5 eV, and N 1s peak at ~ 400.5 eV that of AuCuNC@N-GQD-Pb, exhibited an additional pronounced Pb 4f peak at ~ 140 eV. The comparative high resolution XPS Au 4f spectra of AuCuNC@N-GQD and AuCuNC@N-GQD-Pb (Figure 7.3B), displayed a shift in Au 4f peak towards the higher binding energy region indicating an increase in the Au oxidation state from 0 to 1. In addition, a decrease in the intensity Au 4f peaks were observed for the AuCuNC@N-GQD-Pb indicating interaction of Pb(II) with Au (Au(I)). The high-resolution XPS Pb 4f (Figure 7.3C) spectrum displayed two characteristic peaks of Pb $4f_{7/2}$ and Pb $4f_{5/2}$, at 136.9 and 141.9 eV, respectively, which showed a shift from the standard values of 137.3 and 142.3 eV corresponding to Pb 4f7/2 and Pb 4f5/2 of the Pb(II) state, a shift towards the lower binding energy values is an indication of decrease in the oxidation state (or reduction). The resultconfirm the spontaneous reduction of the Pb(II) to a lower oxidation state as suggested in the mechanism which due to the spontaneous reduction of Pb(II) by the N-GQDs via

Au(I). The reducing capability of N-GQDs was due to the graphene structure and effective N doping and was explained elsewhere in detail(Saisree et al. 2021a). Thus, the results confirm the effective interaction between AuCuNC@N-GQD via Au(I) and Pb(II) and the reduction of Pb(II).

A schematic of the sensing of Pb(II) on modification of GCE with AuCuNC@N-GQD with a remarkable enhancement in the current response without any pre-reduction step is illustrated in Figure 7.4. The Au(I)-Pb(II) interaction and N-GQD facilitated the enhanced and selective sensing of Pb(II) on AuCuNC@N-GQD.

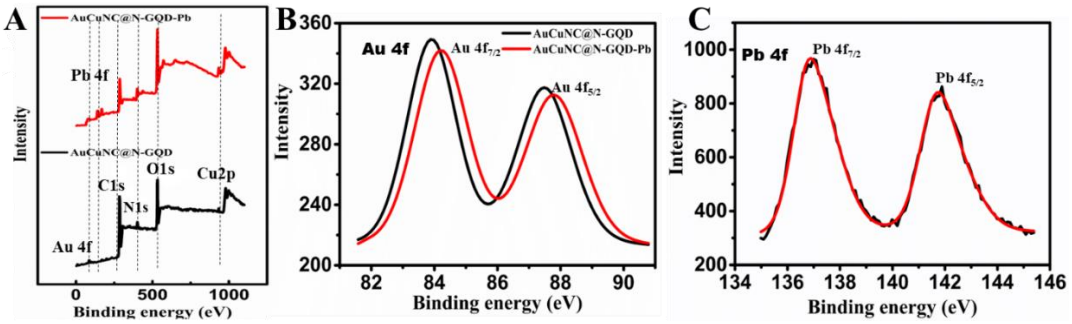

Figure 7.3. The XPS (survey) spectra of AuCuNC@N-GQD and AuCuNC@N-GQD–Pb; (B) The high-resolution Au 4f peaks in AuCuNC@N-GQD and AuCuNC@N-GQD–Pb; (C) The high-resolution Pb 4f peaks in AuCuNC@N-GQD–Pb.

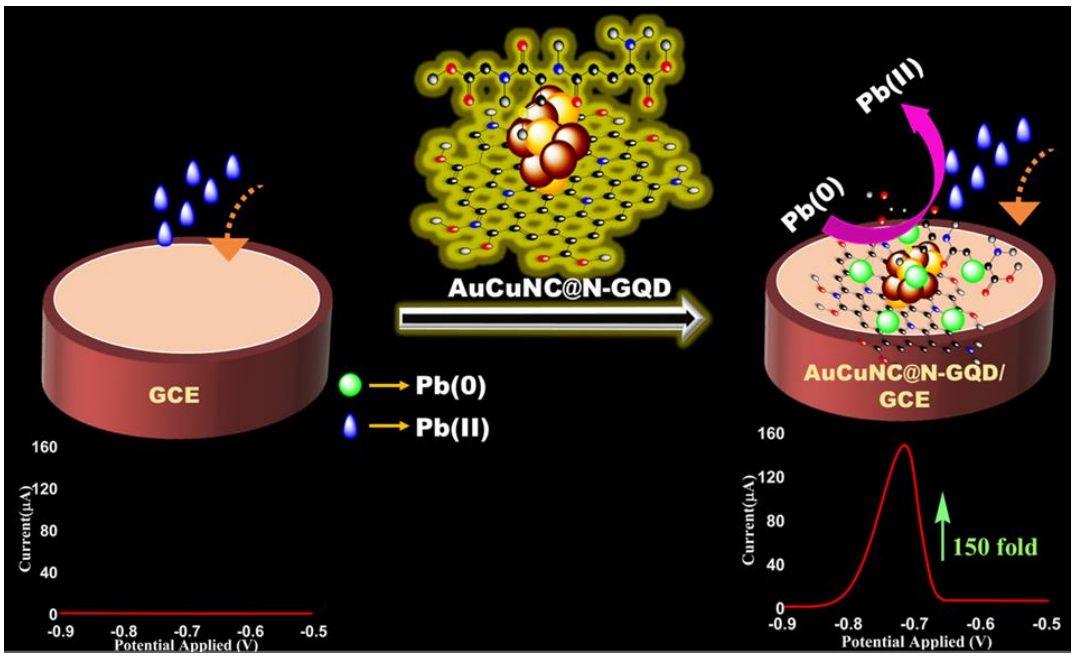

Figure 7.4. Schematic diagram showing the modification of the GCE with the AuCuNC@N-GQD and the resulting enhanced EC sensing of Pb(II) by DPV

7.3.5 Selectivity and interference studies

The selectivity and sensitivity are two of the most significant parameters for ensuring the practical applicability of a sensor. The AuCuNC@N-GQD/GCE exhibited a sensitivity of 1.39 $\mu A \mu M^{-1} cm^{-2}$, and hence exploring its selectivity towards Pb(II) became essential. The DPV profiles obtained for a mixture containing the metal ions [Pb(II) Fe(III), Fe(II), Cr(VI), Ag(I), Cd(II), Hg(II), Zn(II), Ni(II), Co(II), Li(I), Mg(II), Cu(II), Mn(II), and Sn(II)] where [Pb(II)] was 1 nM and all the other metal ions were at 10^6xof [Pb(II)](Figure 7.5A) showed that the current response was of same value (22 μA) to that obtained in the absence of the metal ions, suggesting the non-interference from the ions and the selective interaction and sensing of Pb(II) by the AuCuNC@N-GQD and is depicted in the bar diagram (Figure 7.5B). Further, the interference studies carried out by the chrono-amperometric technique at a fixed operational potential of -0.75 V (Figure 7.5C) showed nil current responses for the other metal ions at 10^6x concentration to that of Pb(II) which was at 1 nM confirms the non-interference from the other metal ions and the radical selectivity of AuCuNC@N-GQD towards Pb(II).

7.3.6 Reusability, reproducibility and stability studies

Reusability, reproducibility and stability studies are other essential parameters to be explored further in detail. The reusability of the AuCuNC@N-GQD/GCE electrode was validated by comparing the peak currents for 1 mM of Pb(II) on AuCuNC@N-GQD/GCE (Figure 7.5D) before and after multiple washings and the results showed it had 97% retention after 50 cycles of washing. For the reproducibility studies, the current responses of five different electrodes toward 1 mM of Pb(II) was scrutinized (Figure 7.5E). The relative standard deviation (RSD) of the peak currents of these individually prepared electrodes was found to be 1.72%, which showed excellent reproducibility of the sensor. Further, the stability studies of the AuCuNC@N-GQDs were conducted for a period of one, three and six months. The results (Figure 7.5F) show that the percentage retention of the current response with respect to the initial current responses were ~99, 96 and 93% after one, three and six months, which shows the higher temporal stability of the developed sensor.

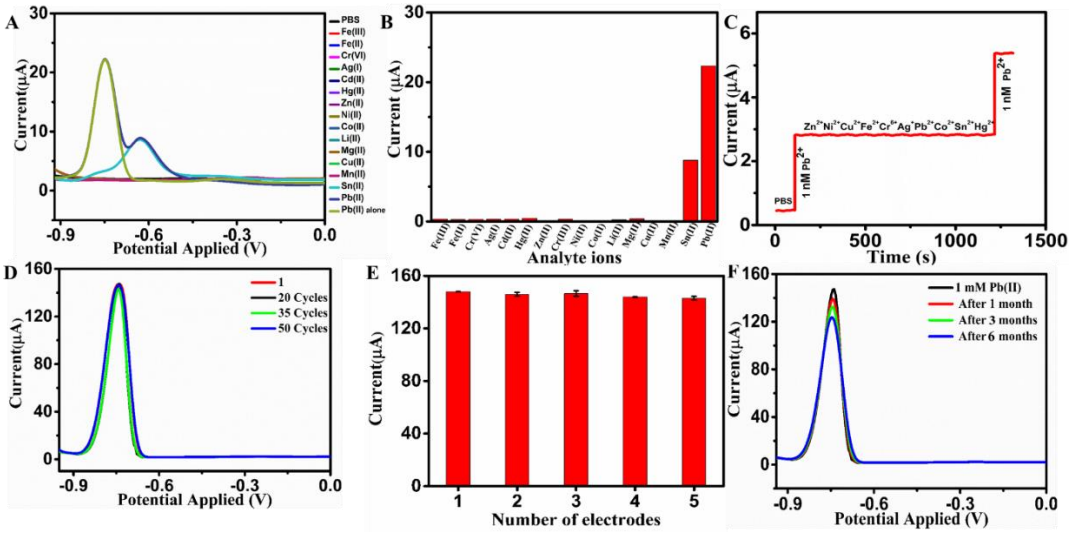

Figure 7.5. (A) and (B) Selectivity studies of AuCuNC@N-GQD/GCE towards 1 nM of Pb(II) in the presence 10^6x concentration of various analyte species; (C) Interference studies of AuCuNC@N-GQD/GCE for the detection of 1 nM of Pb(II) in the presence of other metal ions of 10^6x concentration each by chronoamperometry; (D) The DPV curves after immediate washing for 50 cycles showing the reusability of the sensor; (E) The peak currents of five independently coated electrodes showing the reproducibility of AuCuNC@N-GQD/GCE; (F) The DPV profiles obtained for Pb(II) (1 mM) on AuCuNC@N-GQD/GCE showing the stability of the sensor for 1, 3 months and 6 months.

7.3.7 Environmental sample studies

The AuCuNC@N-GQD/GCE was further utilized for the detection of Pb(II) in real environment samples such as ground water, sea water and waste water, via the standard addition method, where known amounts of Pb(II) were added to the real environment samples and the recovery amounts were measured. The corresponding differential pulse voltammetry profiles are given in Figure 7.6, and the equivalent measurements are summarized in Table 2. The recovery calculated was found to be in the range of 99–101.8%. The corresponding inductively coupled plasma mass spectrometry analysis further validated the recovery values. The inductively coupled plasma mass spectrometry results were in good agreement with the recovery value obtained by AuCuNC@N-GQD, showing the successful applicability of the proposed electrode for the determination of Pb(II) in real environmental samples.

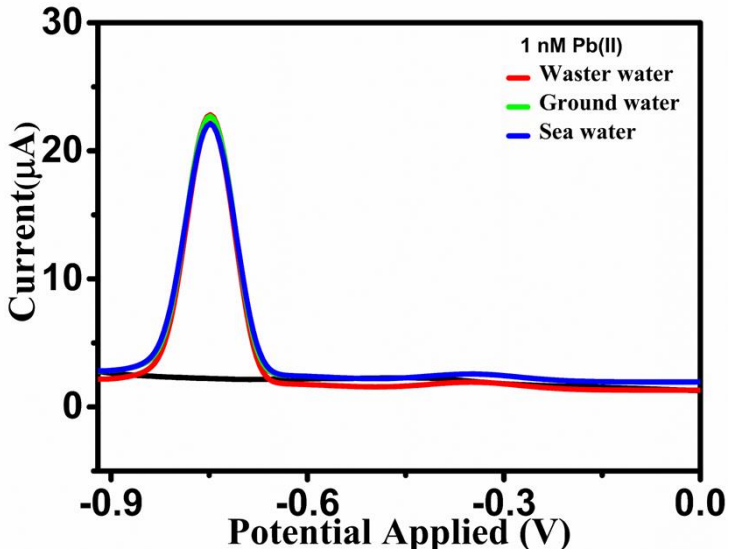

Figure 7.6. The DPV responses of 1 nM of Pb(II) in waste water, ground water, and sea water.

Table 7.2. The recovery test results of Pb(II) in real environmental samples

Sample No.	**Pb(II) Spiked (ppb)**	**Environmental samples**	**Found Quantity (ppb)**	**ICP-MS (ppb)**	**Recovery (%)**
1	0.2	Groundwater	0.200	0.200±0.12	100.0
		Seawater	0.198	0.199±0.09	99
		Wastewater	0.201	0.201±0.16	100.5
2	0.5	Groundwater	0.501	0.501±0.13	100.2
		Seawater	0.499	0.500±0.14	99.8
		Wastewater	0.502	0.501±0.11	100.4
3	1	Groundwater	1.002	1.000±0.19	100.2
		Seawater	1.005	1.001±0.13	100.5
		Wastewater	1.008	1.002±0.15	100.8

* All the recovery values fall within the RSD of 0.5%

7.4 Conclusion

In the present work, we successfully demonstrated the a cu containing bimetallic NC AuCuNC@N-GQD which is stable up to ≥ 1 year which exhibited ultra-selective EC sensing of Pb(II) with the lowest LOD reported hitherto. The LOD obtained was 1 pM with a sensitivity of 1.39 $\mu A \mu M^{-1} cm^{-2}$, without any pre-reduction step. While

it was proved that the Au(I)-Pb(II) interaction played a significant role in the selective sensing performance of AuCuNC@N-GQD towards Pb(II), the enhancement in the sensing properties were attributed to the electron-rich N-GQD in the NC which facilitated the spontaneous reduction of Pb(II) via Au(I). While the combination of Au(I) and N-GQD in the NC enabled the selective enhanced sensing of Pb(II), the presence of Cu along with the Au enhanced the current response further as can be witnessed from the sensing properties of the AuNC@N-GQD. Thus, it is evident that the unique combination of Au, Cu and N-GQD in the NC is responsible for the superior sensing observed. Along with this, the reproducibility (RSD=1.7%), reusability (97%), and stability (93%), along with the admirable recovery percentages (≤100%) in the real sample study, with the recovery values falling within the relative standard deviation of 0.5%, in all the tested environmental samples demonstrate the merit of the Pb(II) sensor.

CHAPTER - 8

SUMMARY AND HIGHLIGHTS

8.1. Summary

EC sensors are the largest and the oldest group of chemical sensors due to the simplicity of the procedures and instrumentation and are easy to miniaturize and integrate into automatic systems without compromising analytical characteristics (Antuña-Jiménez et al., 2012). However, for an EC sensor to hyphenate its possibilities to the advanced clinical and environmental monitoring devices: sensitivity, selectivity, stability, and reproducibility characteristics are of immense importance. It can be achieved by modifying sensors with materials possessing potential electronic and catalytic properties suitable for EC sensing applications. Hence, in this work, we have designed and developed four different EC sensor electrode materials based on N-GQD and various MNC with enhanced structural and functional properties to tune their conductive and catalytic properties, which in turn exhibited unique sensing characteristics either selective or simultaneous with superior sensitivities and LODs compared to the literature reports of the sensors. The mechanism underlined in each sensing system was analyzed meticulously, and confirmed by the aid of various characterization techniques, explained in detail, and a few conclusions were drawn.

To give an overall view and summary of our work, a schematic representation of the EC sensors with emphasis on the correlation between different sensors and the analytes sensed with corresponding LOD values is shown in Figure 8.1. The developed systems include the following, (i) N-GQD/GCE, where N-GQD was synthesized from PANI as a precursor and in situ N doping agent, for the ultra-selective ultra-trace level (0.1 pM) detection of Cd(II); (ii) S,N-GQD, an S codoping was done for N-GQD, using H_2SO_4 as a doping agent and acid catalyst, exhibited miraculous enhancement in properties and further, it was utilized for the simultaneous picomolar level detection of Cd(II), Pb(II) and Hg(II); (iii) The CuNC@N-GQD was synthesized by utilizing N-GQD as reducing agent and

capping agent, which enabled ultra- selectivity for the NC, and it exhibited the simultaneous sensing capability towards functionally correlated neurofunctional molecules DA, SER, and NIC; (iv) Further, AuCuNC@N-GQD was developed from CuNC@N-GQD through a GE process, for the selective and nanomolar detection of GLY non-enzymatically and also (v) for the selective picomolar level detection of Pb(II). The major findings and contributions of the study are listed in the latter section of this chapter.

Here in this chapter, we are listing out the highlights, summary and future perspectives of the work.

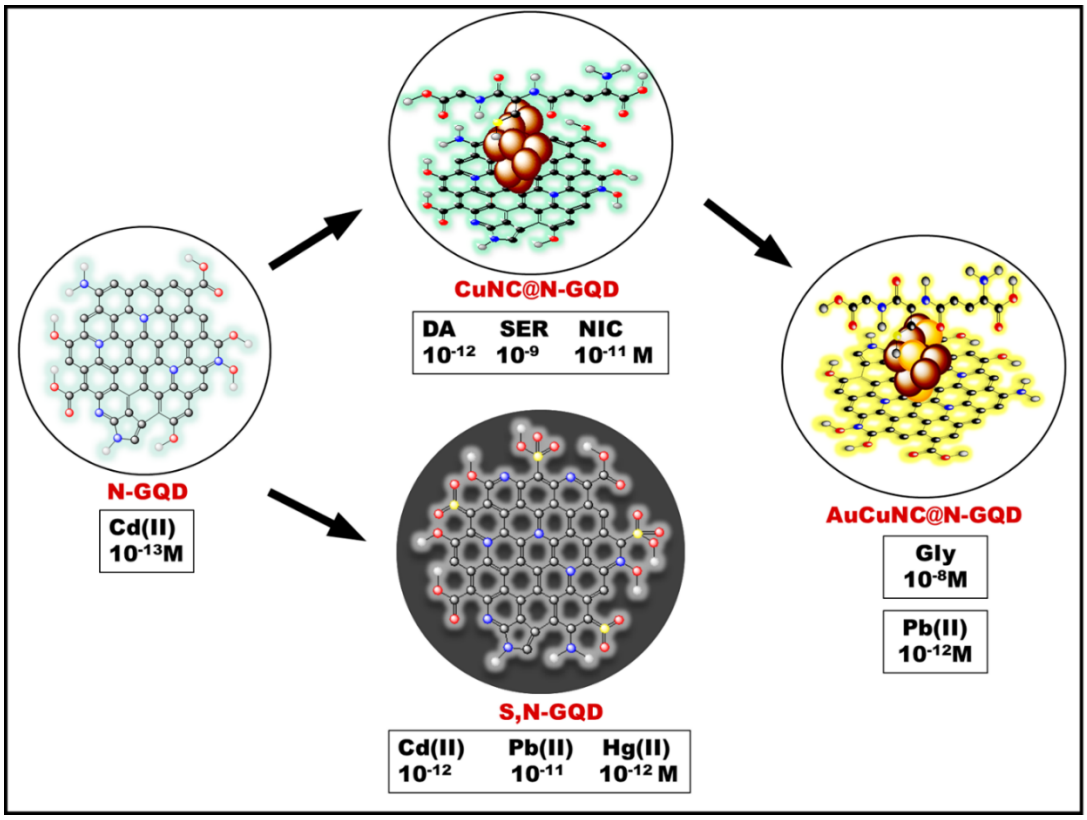

Figure 8.1. The schematic representation showing the relation among the developed systems N-GQD, S,N-GQD, CuNC@N-GQD, and AuCuNC@N-GQD and the analytes sensed with corresponding LOD values.

8.2. Major outcomes of the Thesis

- For the first time, N-GQD was utilized for the selective EC sensing of Cd(II) and exhibited ultra-high sensitivity and lowest LOD reported yet. The LOD were 0.1 pM (without pre-reduction) and 1 fM after pre-reduction. The selective and enhanced Cd(II) sensing was attributed to the interaction between the Cd(II) and N-functionalities, and the graphene structure which spontaneously reduced Cd(II) to Cd(0).
- A stable CuNC@N-GQD was developed using N-GQD as the reducing agent and N-GQD and GSH as the stabilizing agent which exhibited highest stability of ≥1 year. The NC exhibited sensing towards the three functionally correlated neurofunctional molecules DA, SER, and NIC with~ 4, ~ 4, and ~ 2-fold higher sensitivity of the CuNC@N-GQD compared to the controls and was attributed to the synergistic effect of the N-GQD and the CuNC. The LOD values obtained were 1×10^{-3}, 1, and 1×10^{-2} nM for DA, SER, and NIC, which are hitherto the lowest reported so far.
- A bimetallic AuCuNC@N-GQD was prepared by a galvanic exchange process from the stable CuNC@N-GQD which exhibited non-enzymatic EC sensing of Gly, for the first time, with a LOD of 10^{-8} M and is the lowest LOD obtained so far. The enhanced sensitivity and selectivity were explained based on the better the Au-Gly interaction.
- A S and N co-doped GQDwas synthesised through a hydrothermal route from PANI, which exhibited white light emissive properties. The introduction of 'S' lead to the simultaneous EC sensing of Cd(II), Pb(II) and Hg(II) with the LOD values 1 pM, 10 pM and 1 pM. The simultaneous sensing of S,N-GQD/GCE towards Cd(II), Pb(II) and Hg(II) was observed to be due to the interaction between Cd(II), Pb(II) and Hg(II) with the N and S based functionalities
- The selective EC sensing of Pb(II) by AuCuNC@N-GQD was reported for the first time. The NC exhibited good sensitivity towards Pb(II) with a LOD of 10^{-12} M and is capable of sensing in real water samples. The enhanced sensitivity and selective sensing capability was explained by the presence of N-GQD and Au(I)-Pb(II) interaction respectively.

8.3. Future Perspectives

- Sensor fabrication using the synthesized materials
- Synthesis of MNC@S,N-GQD
- EC sensing studies of MNC@S,N-GQD
- EC sensing studies of S,N-GQD towards biomolecules

REFERENCES

1 Abdel-Haleem, A. S., A. Sroor, S. M. El-Bahi, and E. Zohny. 2001. "Heavy Metals and Rare Earth Elements in Phosphate Fertilizer Components Using Instrumental Neutron Activation Analysis." *Applied Radiation and Isotopes* 55(4): 569–73.

2 Adarakatti, Prashanth Shivappa, and Pandurangappa Malingappa. 2016. "Amino-Calixarene-Modified Graphitic Carbon as a Novel Electrochemical Interface for Simultaneous Measurement of Lead and Cadmium Ions at Picomolar Level." *Journal of Solid State Electrochemistry*. http://dx.doi.org/10.1007/s10008-016-3306-4.

3 Al-Tamrah, S. A. 1999. "Spectrophotometric Determination of Nicotine." *Analytica Chimica Acta* 379(1–2): 75–80.

4 Alam, Arif Ul, Matiar M R Howlader, Nan-xing Hu, and M Jamal Deen. "Electrochemical Sensing of Lead in Drinking Water Using MWCNTs and β -Cyclodextrin." : 1–26.

5 Anh, Nguyen Thi Ngoc, and Ruey An Doong. 2018. "One-Step Synthesis of Size-Tunable Gold@Sulfur-Doped Graphene Quantum Dot Nanocomposites for Highly Selective and Sensitive Detection of Nanomolar 4-Nitrophenol in Aqueous Solutions with Complex Matrix." *ACS Applied Nano Materials* 1(5): 2153–63.

6 Arcudi, Francesca, Luka Đorđević, and Maurizio Prato. 2017. "Rationally Designed Carbon Nanodots towards Pure White-Light Emission." *Angewandte Chemie - International Edition* 56(15): 4170–73.

7 Arshad, Muhammad Nadeem et al. 2017. "Fabrication of Cadmium Ionic Sensor Based on (E)-4-Methyl-N′-(1-(Pyridin-2-Yl)Ethylidene)Benzenesulfonohydrazide (MPEBSH) by Electrochemical Approach." *Journal of Organometallic Chemistry* 827: 49–55. http://dx.doi.org/10.1016/j.jorganchem.2016.11.009.

8 Arya Nair, J. S., S. Saisree, R. Aswathi, and K. Y. Sandhya. 2022. "Ultra-Selective and Real-Time Detection of Dopamine Using Molybdenum Disulphide Decorated Graphene-Based Electrochemical Biosensor." *Sensors and Actuators B: Chemical* 354(November 2021): 131254. https://doi.org/10.1016/j.snb.2021.131254.

9 Arya Nair, J. S., S. Saisree, and K. Y. Sandhya. 2022. " Ultra-Rapid Removal of Pb(II) Ions by a Nano-MoS 2 Decorated Graphene Aided by the Unique Combination of Affinity and Electrochemistry (Adv. Sustainable Syst. 7/2022) ." *Advanced Sustainable Systems* 6(7): 2270018.

10 Ashraf, Ghazala et al. 2021. “Rice-Spikelet-like Copper Oxide Decorated with Platinum Stranded in the CNT Network for Electrochemical in Vitro Detection of Serotonin.” *ACS Applied Materials and Interfaces* 13(5): 6023–33.

11 Aswathi, R., Mohamed Mukthar Ali, Anurudha Shukla, and K. Y. Sandhya. 2015. “A Green Method to Gold-Graphene Nanocomposite from Cyclodextrin Functionalized Graphene for Efficient Non-Enzymatic Electrochemical Sensing Applications.” *RSC Advances* 5(40): 32027–33.

12 Aswathi, R., and K. Y. Sandhya. 2018. “Ultrasensitive and Selective Electrochemical Sensing of Hg(II) Ions in Normal and Sea Water Using Solvent Exfoliated MoS2: Affinity Matters.” *Journal of Materials Chemistry A* 6(30): 14602–13.

13 Baghayeri, Mehdi et al. 2018. “A Simple Approach for Simultaneous Detection of Cadmium(II) and Lead(II) Based on Glutathione Coated Magnetic Nanoparticles as a Highly Selective Electrochemical Probe.” *Sensors and Actuators, B: Chemical* 273(April): 1442–50. https://doi.org/10.1016/j.snb.2018.07.063.

14 Bai, Hanyu et al. 2020. “Dual-Emission Carbon Dots-Stabilized Copper Nanoclusters for Ratiometric and Visual Detection of Cr2O72- Ions and Cd2+ Ions.” *Journal of Hazardous Materials* 386(August): 121654. https://doi.org/10.1016/j.jhazmat.2019.121654.

15 Barik, Subrat Kumar et al. 2020. “Polyhydrido Copper Nanoclusters with a Hollow Icosahedral Core: [Cu30H18{E2P(OR)2}12] (E=S or Se; R=nPr, IPr or IBu).” *Chemistry - A European Journal* 26(46): 10471–79.

16 Bhanjana, Gaurav et al. 2015. “Sno2 Quantum Dots as Novel Platform for Electrochemical Sensing of Cadmium.” *Electrochimica Acta* 169: 97–102. http://dx.doi.org/10.1016/j.electacta.2015.04.045.

17 Bian, Shiyue et al. 2016. “One-Pot Synthesis of Sulfur-Doped Graphene Quantum Dots as a Novel Fluorescent Probe for Highly Selective and Sensitive Detection of Lead(II).” *RSC Advances* 6(74): 69977–83.

18 Borghei, Yasaman-sadat, Morteza Hosseini, Mohammad Reza Ganjali, and Saman Hosseinkhani. 2017. “Ac Ce p Te Us T.” *Sensors & Actuators: B. Chemical*. http://dx.doi.org/10.1016/j.snb.2017.03.148.

19 Brett, Christopher M A, and Ana Maria Oliveira-brett. 2011. “Electrochemical Sensing in Solution — Origins , Applications and Future Perspectives.” : 1487–94.

20 Cai, Yuanyuan et al. 2020. “Histidine-Triggered Turning-on of Gold/Copper Nanocluster Fluorescence for the Sensitive and Selective Detection of Histidine.” *Chemical*

Communications 56(78): 11637–40.

21 Chamjangali, M. Arab, H. Kouhestani, F. Masdarolomoor, and H. Daneshinejad. 2015. "A Voltammetric Sensor Based on the Glassy Carbon Electrode Modified with Multi-Walled Carbon Nanotube/Poly(Pyrocatechol Violet)/Bismuth Film for Determination of Cadmium and Lead as Environmental Pollutants." *Sensors and Actuators, B: Chemical* 216(January 2019): 384–93. http://dx.doi.org/10.1016/j.snb.2015.04.058.

22 Chen, Chung An, Chun Chi Wang, Yuh Jyh Jong, and Shou Mei Wu. 2015. "Label-Free Fluorescent Copper Nanoclusters for Genotyping of Deletion and Duplication of Duchenne Muscular Dystrophy." *Analytical Chemistry* 87(12): 6228–32.

23 Chen, Tong Bin et al. 2005. "Assessment of Heavy Metal Pollution in Surface Soils of Urban Parks in Beijing, China." *Chemosphere* 60(4): 542–51.

24 Chen, Yuxiang et al. 2018. "DNA Templated Metal Nanoclusters : From Emergent Properties to Unique Applications Published as Part of the Accounts of Chemical Research Special Issue ' Toward Atomic Precision in Nanoscience ' ."

25 Chen, Zhichuan et al. 2020. "Dopamine-Modified AuCu Bimetallic Nanoclusters as Charge Transfer-Based Biosensors for Highly Sensitive Glycine Detection." *Langmuir* 36(46): 13928–36.

26 Cheng, Shuiping. 2003. "Heavy Metal Pollution in China: Origin, Pattern and Control." *Environmental Science and Pollution Research* 10(3): 192–98.

27 Chhabra, Varun A. et al. 2018. "Synthesis and Spectroscopic Studies of Functionalized Graphene Quantum Dots with Diverse Fluorescence Characteristics." *RSC Advances* 8(21): 11446–53.

28 Culea, M., E. Horj, A. Iordache, and O. Cozar. 2011. "Determination of Glycine in Biological Fluids by Isotopic Dilution Mass Spectrometry." *Asian Journal of Chemistry* 23(10): 4279–81.

29 Dai, Hongxiu et al. 2016. "An Electrochemical Sensor Based on Phytic Acid Functionalized Polypyrrole/Graphene Oxide Nanocomposites for Simultaneous Determination of Cd(II) and Pb(II)." *Chemical Engineering Journal* 299: 150–55. http://dx.doi.org/10.1016/j.cej.2016.04.083.

30 Das, Nirmal Kumar et al. 2015. "Luminescent Copper Nanoclusters as a Speci Fi c Cell-Imaging Probe and a Selective Metal Ion Sensor."

31 Díez, Isabel, and Robin H.A. Ras. 2011. "Fluorescent Silver Nanoclusters." *Nanoscale* 3(5): 1963–70.

32 Echeverría, Raquel, José M. López-De-Luzuriaga, Miguel Monge, and M. Elena Olmos. 2015. "The Gold(I)···lead(II) Interaction: A Relativistic Connection." *Chemical Science* 6(3): 2022–26.

33 Ene, Antoaneta, Alina Boşneagă, and L. Georgescu. 2010. "Determination of Heavy Metals in Soils Using XRF Technique." *Romanian Reports of Physics* 55(7–8): 815–20.

34 Eranjaneya, H. et al. 2018. "Citric Acid Assisted Synthesis of Manganese Tungstate Nanoparticles for Simultaneous Electrochemical Sensing of Heavy Metal Ions." *Materials Science in Semiconductor Processing* 86(June): 85–92. https://doi.org/10.1016/j.mssp.2018.06.020.

35 Facure, Murilo H.M., Rodrigo Schneider, Luiza A. Mercante, and Daniel S. Correa. 2020. "A Review on Graphene Quantum Dots and Their Nanocomposites: From Laboratory Synthesis towards Agricultural and Environmental Applications." *Environmental Science: Nano* 7(12): 3710–34.

36 Faridbod, Farnoush, and Afsaneh L. Sanati. 2018. "Graphene Quantum Dots in Electrochemical Sensors/Biosensors." *Current Analytical Chemistry* 15(2): 103–23.

37 Fu, Yang, Guanyue Gao, and Jinfang Zhi. 2019. "Electrochemical Synthesis of Multicolor Fluorescent N-Doped Graphene Quantum Dots as a Ferric Ion Sensor and Their Application in Bioimaging." *Journal of Materials Chemistry B* 7(9): 1494–1502.

38 Ganjali, Mohammad Reza, and Mehdi Asgari. 2010. "Thiomorpholine-Functionalized Nanoporous Mesopore as a Sensing Material for Cd 2 + Carbon Paste Electrode." : 1359–66.

39 Gao, Xiao Hui et al. 2016. "Single Crystal Sub-Nanometer Sized Cu6 (SR)6clusters: Structure, Photophysical Properties, and Electrochemical Sensing." *Advanced Science* 3(12): 1–7.

40 Gao, Xiaohui, Hancheng Lin, Ping Li, and Wei Chen. 2018. "Self-Assembly of Ag6 Clusters into Nanowires for Nonenzymatic Electrochemical Sensing of Glucose." *Particle and Particle Systems Characterization* 35(6): 1–6.

41 Ge, Shuyan et al. 2019. "One-Step Synthesis of Boron-Doped Graphene Quantum Dots for Fluorescent Sensors and Biosensor." *Talanta* 199: 581–89. https://doi.org/10.1016/j.talanta.2019.02.098.

42 Ghosh, Rama et al. 2014. "Blue-Emitting Copper Nanoclusters Synthesized in the Presence of Lysozyme as Candidates for Cell Labeling." *ACS Applied Materials and Interfaces* 6(6): 3822–28.

43 Godoy-Reyes, T. M., Llopis-Lorente, A., Costero, A. M., Sancenón, F., Gavina, P., & Martínez-Máñez, R. (2018). Selective and sensitive colorimetric detection of the neurotransmitter serotonin based on the aggregation of bifunctionalised gold nanoparticles. S*ensors and Actuators B: Chemical*, 258, 829-835.

44 Goswami, Nirmal et al. 2011. "Copper Quantum Clusters in Protein Matrix: Potential Sensor of Pb 2+ Ion." *Analytical Chemistry* 83(24): 9676–80.

45 Govindhan, Raman, and Balakrishnan Karthikeyan. 2017. "Nano Cu Interaction with Single Amino Acid Tyrosine Derived Self-Assemblies; Study through XRD, AFM, Confocal Raman Microscopy, SERS and DFT Methods." *Journal of Physics and Chemistry of Solids* 111: 123–34.

46 Gu, Siyong et al. 2019. "Sulfur and Nitrogen Co-Doped Graphene Quantum Dots as a Fluorescent Quenching Probe for Highly Sensitive Detection toward Mercury Ions." *ACS Applied Nano Materials* 2(2): 790–98.

47 Gui, Rijun et al. 2014. "Multidentate Polymers Stabilized Water-Dispersed Copper Nanoclusters: Facile Photoreduction Synthesis and Selective Fluorescence Turn-on Response." *RSC Advances* 4(55): 29083–88.

48 Gumpu, Manju Bhargavi, Murugan Veerapandian, Uma Maheswari Krishnan, and John Bosco Balaguru Rayappan. 2017. "Simultaneous Electrochemical Detection of Cd(II), Pb(II), As(III) and Hg(II) Ions Using Ruthenium(II)-Textured Graphene Oxide Nanocomposite." *Talanta* 162(Ii): 574–82. http://dx.doi.org/10.1016/j.talanta.2016.10.076.

49 Han, Ailing et al. 2018. "Highly Bright Self-Assembled Copper Nanoclusters: A Novel Photoluminescent Probe for Sensitive Detection of Histamine." *Analytical Chemistry* 90(15): 9060–67.

50 Hassan, Mahbub et al. 2014. "Edge-Enriched Graphene Quantum Dots for Enhanced Photo-Luminescence and Supercapacitance." *Nanoscale* 6(20): 11988–94. http://dx.doi.org/10.1039/C4NR02365J.

51 He, Yu Sheng et al. 2018. "Highly Sensitive and Selective Dual-Emission Ratiometric Fluorescence Detection of Dopamine Based on Carbon Dots-Gold Nanoclusters Hybrid." *Sensors and Actuators, B: Chemical* 265: 371–77. https://doi.org/10.1016/j.snb.2018.03.080.

52 Heidarieh, Marzieh et al. 2013. "Evaluate of Heavy Metal Concentration in Shrimp (Penaeus Semisulcatus) and Crab (Portunus Pelagicus) with INAA Method." *SpringerPlus*

2(1): 1–5.

53 Hu, Xue et al. 2016. “Recent Advances in the Analytical Applications of Copper Nanoclusters.” http://dx.doi.org/10.1016/j.trac.2015.12.013.

54 Hu, Xue, Wei Wang, and Yuming Huang. 2016. “Copper Nanocluster-Based Fluorescent Probe for Sensitive and Selective Detection of Hg2+ in Water and Food Stuff.” *Talanta* 154: 409–15.

55 Huang, Su Su et al. 2016. “Electrochemical Sensor for Nitrite Using a Glassy Carbon Electrode Modified with Gold-Copper Nanochain Networks.” *Microchimica Acta* 183(2): 791–97.

56 Hutton, Laura A et al. 2014. “By Four Orders of Magnitude.”

57 Inoue, Michiko B. et al. 1990. “Complexation of Electroconducting Polypyrrole with Copper.” *Synthetic Metals* 38(2): 205–12.

58 Intarakamhang, Sireerat, Wolfgang Schuhmann, and Albert Schulte. 2018. “Robotic Heavy Metal Anodic Stripping Voltammetry : Ease and Efficacy for Trace Lead and Cadmium Electroanalysis.”

59 Jayadharan Salini, Arya Nair, Aswathi Ramachandran, Saisree Sadasivakurup, and Sandhya Karunakaran Yesodha. 2020. “Versatile MoS2 Hollow Nanoroses for a Quick-Witted Removal of Hg (II), Pb (II) and Ag (I) from Water and the Mechanism: Affinity or Electrochemistry?” *Applied Materials Today* 20: 100642. https://doi.org/10.1016/j.apmt.2020.100642.

60 Jia, Xiaofang et al. 2012. “DNA-Hosted Copper Nanoclusters for Fluorescent Identi Fi Cation of Single.” (4): 3311–17.

61 Jiloha, R C. 2010. “Biological Basis of Tobacco Addiction : Implications for Smoking-Cessation Treatment.” 52(4).

62 Joseph, Julin, and Aji A. Anappara. 2016. “White Light Emission of Carbon Dots by Creating Different Emissive Traps.” *Journal of Luminescence* 178: 128–33. http://dx.doi.org/10.1016/j.jlumin.2016.05.051.

63 Joshi, Preeti Nigam, Subir Kundu, Sunil K. Sanghi, and Dhiman Sarkar. 2016. “Graphene Quantum Dots - From Emergence to Nanotheranostic Applications.” *Smart Drug Delivery System*.

64 Kadara, Rashid O., Norman Jenkinson, and Craig E. Banks. 2009. “Characterisation of Commercially Available Electrochemical Sensing Platforms.” *Sensors and Actuators, B: Chemical* 138(2): 556–62.

65 Kadara, Rashid O., and Ibtisam E. Tothill. 2008. “Development of Disposable Bulk-Modified Screen-Printed Electrode Based on Bismuth Oxide for Stripping Chronopotentiometric Analysis of Lead (II) and Cadmium (II) in Soil and Water Samples.” *Analytica Chimica Acta* 623(1): 76–81.

66 Karimi-maleh, Hassan, Fatemeh Karimi, and Marzieh Alizadeh. 2020. “Electrochemical Sensors , a Bright Future in the Fabrication of Portable Kits in Analytical Systems.” : 1–12.

67 Karthika, A. et al. 2019. “Electrochemical Sensing of Nicotine Using CuWO4 Decorated Reduced Graphene Oxide Immobilized Glassy Carbon Electrode.” *Ultrasonics Sonochemistry* 55(December 2018): 196–206. https://doi.org/10.1016/j.ultsonch.2019.01.038.

68 Keskin, Semra Yilmazer, and Can Serkan Keskin. 2014. “Quantitative Determination of Glycine in Aqueous Solution Using Glutamate Dehydrogenase-Immobilized Glyoxal Agarose Beads.” *Applied Biochemistry and Biotechnology* 172(1): 289–97.

69 Knight, John, Yamni Nigam, and Aled Jones. 2019. “Cronfa - Swansea University Open Access Repository.” *Nursing Times* 115(5): 56–59. http://dx.doi.org/10.1108/JSBED-07-2018-0215.

70 Koninti, Raj Kumar, Sagar Satpathi, and Partha Hazra. 2018. “Ultrafast Fluorescence Dynamics of Highly Stable Copper Nanoclusters Synthesized Inside the Aqueous Nano-Pool of Reverse Micelles Ultrafast Fluorescence Dynamics of Highly Stable Copper Nanoclusters Synthesized Inside the Aqueous Nano-Pool of Reverse Mice.”

71 Kumar, Sumeet et al. 2017. “Tunable (Violet to Green) Emission by High-Yield Graphene Quantum Dots and Exploiting Its Unique Properties towards Sun-Light-Driven Photocatalysis and Supercapacitor Electrode Materials.” *Materials Today Communications* 11(October): 76–86.

72 Lai, Wing Fu, Wing Tak Wong, and Andrey L. Rogach. 2020. “Development of Copper Nanoclusters for In Vitro and In Vivo Theranostic Applications.” *Advanced Materials* 32(9): 1–21.

73 Length, Full. 2007. “Heavy Metal Pollution and Human Biotoxic Effects.” *International Journal of Physical Sciences* 2(5): 112–18.

74 Li, Bingyang et al. 2021. “Review of Performance Improvement Strategies for Doped Graphene Quantum Dots for Fluorescence-Based Sensing.” *Synthetic Metals* 276(October 2020): 116758. https://doi.org/10.1016/j.synthmet.2021.116758.

75 Li, Jing, Shaojum Guo, Yueming Zhai, and Erkang Wang. 2009. “Nafion-Graphene Nanocomposite Film as Enhanced Sensing Platform for Ultrasensitive Determination of Cadmium.” *Electrochemistry Communications* 11(5): 1085–88. http://dx.doi.org/10.1016/j.elecom.2009.03.025.

76 Li, Libo, Dong Liu, Aiping Shi, and Tianyan You. 2018. “Simultaneous Stripping Determination of Cadmium and Lead Ions Based on the N-Doped Carbon Quantum Dots-Graphene Oxide Hybrid.” *Sensors and Actuators, B: Chemical* 255: 1762–70. http://dx.doi.org/10.1016/j.snb.2017.08.190.

77 Li, Meixiu, Tao Chen, J. Justin Gooding, and Jingquan Liu. 2019. “Review of Carbon and Graphene Quantum Dots for Sensing.” *ACS Sensors* 4(7): 1732–48.

78 Li, Xiaoqing et al. 2017. “Electrochemical Sensing of Nicotine Using Screen-Printed Carbon Electrodes Modified with Nitrogen-Doped Graphene Sheets.” *Journal of Electroanalytical Chemistry* 784: 77–84. http://dx.doi.org/10.1016/j.jelechem.2016.12.009.

79 Liang, Wenting et al. 2019. “Simultaneous Electrochemical Sensing of Serotonin , Dopamine and Ascorbic Acid by Using a Nanocomposite Prepared from Reduced Graphene Oxide , Fe 3 O 4 and Hydroxypropyl- β -Cyclodextrin.”

80 Lien, Chia Wen, Ying Chieh Chen, Huan Tsung Chang, and Chih Ching Huang. 2013. “Logical Regulation of the Enzyme-like Activity of Gold Nanoparticles by Using Heavy Metal Ions.” *Nanoscale* 5(17): 8227–34.

81 Lim, Joanna, Wee Ling, and Sulaiman Ab Ghani. 2013. “Poly (4-Vinylpyridine- Co - Aniline) -Modified Electrode — Synthesis , Characterization , and Application as Cadmium (II) Ion Sensor.” : 681–90.

82 Lin, Yu-Syuan et al. 2021. “A Critical Review of Copper Nanoclusters for Monitoring of Water Quality.” *Sensors and Actuators Reports* 3(January): 100026. https://doi.org/10.1016/j.snr.2021.100026.

83 Liu, Ke et al. 2019. “Film-Based Fluorescence Sensing: A ‘Chemical Nose’ for Nicotine.” *Chemical Communications* 55(84): 12679–82.

84 Liu, Mingyang et al. 2016. “High Performance Au-Cu Alloy for Enhanced Visible-Light Water Splitting Driven by Coinage Metals.” *Chemical Communications* 52(25): 4694–97.

85 López-De-Luzuriaga, José M. et al. 2021. “Computational Prediction of Au(i)-Pb(Ii) Bonding in Coordination Complexes and Study of the Factors Affecting the Formation of Au(i)-E(Ii) (E = Ge, Sn, Pb) Covalent Bonds.” *Physical Chemistry Chemical Physics*

23(17): 10174–83.

86 Lou, Xin Yue, Nan Song, and Ying Wei Yang. 2019. “Enhanced Solution and Solid-State Emission and Tunable White-Light Emission Harvested by Supramolecular Approaches.” *Chemistry - A European Journal* 25(51): 11975–82.

87 Lu, Zhiwei et al. 2018. “Facile One-Step Fabrication of a Novel 3D Honeycomb-like Bismuth Nanoparticles Decorated N-Doped Carbon Nanosheet Frameworks: Ultrasensitive Electrochemical Sensing of Heavy Metal Ions.” *Electrochimica Acta* 266: 94–102. https://doi.org/10.1016/j.electacta.2018.01.188.

88 Luo, Yi et al. 2017. “Tuning the Photoluminescence of Graphene Quantum Dots by Fluorination.” *Journal of Nanomaterials* 2017.

89 Madhu, Rajesh, Kalimuthu Vijaya Sankar, Shen Ming Chen, and Ramakrishnan Kalai Selvan. 2014. “Eco-Friendly Synthesis of Activated Carbon from Dead Mango Leaves for the Ultrahigh Sensitive Detection of Toxic Heavy Metal Ions and Energy Storage Applications.” *RSC Advances* 4(3): 1225–33.

90 Mahmoud, Ashraf M., Mater H. Mahnashi, Saad A. Alkahtani, and Mohamed M. El-Wekil. 2020. “Nitrogen and Sulfur Co-Doped Graphene Quantum Dots/Nanocellulose Nanohybrid for Electrochemical Sensing of Anti-Schizophrenic Drug Olanzapine in Pharmaceuticals and Human Biological Fluids.” *International Journal of Biological Macromolecules* 165: 2030–37. https://doi.org/10.1016/j.ijbiomac.2020.10.084.

91 Maity, Subarna, Dipankar Bain, and Amitava Patra. 2019. “Engineering Atomically Precise Copper Nanoclusters with Aggregation Induced Emission.” *Journal of Physical Chemistry C* 123(4): 2506–15.

92 Malik, Lateef Ahmad, Altaf Hussain Pandith, Arshid Bashir, and Aaliya Qureashi. 2022. “Zinc Oxide-Decorated Multiwalled Carbon Nanotubes: A Selective Electrochemical Sensor for the Detection of Pb(II) Ion in Aqueous Media.” *Journal of Materials Science: Materials in Electronics* 33(9): 6178–89. https://doi.org/10.1007/s10854-022-07793-x.

93 Manuscript, Accepted. 2021. “**可注射水凝胶作**为糖尿病创面修复的动态黏附敷料 Materials Chemistry B.”

94 Marrubini, G., G. Caccialanza, and G. Massolini. 2008. “Determination of Glycine and Threonine in Topical Dermatological Preparations.” *Journal of Pharmaceutical and Biomedical Analysis* 47(4–5): 716–22.

95 Mathew, Meegle S., Kiran Sukumaran, and Kuruvilla Joseph. 2018. “Graphene Carbon

Dot Assisted Sustainable Synthesis of Gold Quantum Cluster for Bio-Friendly White Light Emitting Material and Ratiometric Sensing of Mercury (Hg2+)." *ChemistrySelect* 3(33): 9545–54.

96 Mhammedi, M. A.El et al. 2009. "Electrochemical Determination of Cadmium(II) at Platinum Electrode Modified with Kaolin by Square Wave Voltammetry." *Journal of Hazardous Materials* 170(2–3): 590–94.

97 Mondal, Tapas Kumar, Diptiman Dinda, and Shyamal Kumar Saha. 2018. "Nitrogen, Sulphur Co-Doped Graphene Quantum Dot: An Excellent Sensor for Nitroexplosives." *Sensors and Actuators, B: Chemical* 257: 586–93. http://dx.doi.org/10.1016/j.snb.2017.11.012.

98 Mukthar Ali, Mohamed, and K. Y. Sandhya. 2016. "Selective Photodegradation and Enhanced Photo Electrochemical Properties of Titanium Dioxide-Graphene Composite with Exposed (001) Facets Made by Photochemical Method." *Solar Energy Materials and Solar Cells* 144: 748–57. http://dx.doi.org/10.1016/j.solmat.2015.10.025.

99 Nair J.S, Arya, S. Saisree, and K. Y. Sandhya. 2022. "Picomolar Level Electrochemical Detection of Hydroquinone, Catechol and Resorcinol Simultaneously Using a MoS2 Nano-Flower Decorated Graphene." *Analyst* 147(13): 2966–79.

100 Nasaruddin, Ricca Rahman, Tiankai Chen, Ning Yan, and Jianping Xie. 2018. "Roles of Thiolate Ligands in the Synthesis , Properties and Catalytic Application of Gold Nanoclusters." *Coordination Chemistry Reviews* 368: 60–79. https://doi.org/10.1016/j.ccr.2018.04.016.

101 Needleman, Herbert. 2004. "Lead Poisoning." *Annual Review of Medicine* 55(1): 209–22.

102 Nishan, Umar et al. 2020. "Colorimetric Based Sensing of Dopamine Using Ionic Liquid Functionalized Drug Mediated Silver Nanostructures." *Microchemical Journal* 159.

103 Nordic Council of Ministers. 2003. "Cadmium Review." *UNEP Governing Council* (4): 26.

104 Osmond, Glen et al. 1994. "Ionic-Strength and PH Effects on the Sorption of Cadmium and the Surface Charge of Soils." (2): 419–29.

105 Ouyang, Zhong et al. 2019. "Preparation and Specific Capacitance Properties of Sulfur, Nitrogen Co-Doped Graphene Quantum Dots." *Nanoscale Research Letters* 14(1).

106 Pakhomova, O. A., Ya I. Korenman, N. Ya Mokshina, and S. I. Niftaliev. 2010. "Extraction Separation and Electrophoretic Determination of Tyrosine and Glycine." *Russian Journal of Applied Chemistry* 83(11): 1940–43.

107 Pakiari, A. H., and Z. Jamshidi. 2007. “Interaction of Amino Acids with Gold and Silver Clusters.” *Journal of Physical Chemistry A* 111(20): 4391–96.

108 Panneer Selvam, Sathish, and Kyusik Yun. 2020. “A Self-Assembled Silver Chalcogenide Electrochemical Sensor Based on RGO-Ag2Se for Highly Selective Detection of Serotonin.” *Sensors and Actuators, B: Chemical* 302(September 2019): 127161. https://doi.org/10.1016/j.snb.2019.127161.

109 Pei, Yong, and Xiao Cheng Zeng. 2012. “Investigating the Structural Evolution of Thiolate Protected Gold Clusters from First-Principles.”

110 Promphet, Nadtinan et al. 2015. “An Electrochemical Sensor Based on Graphene/Polyaniline/Polystyrene Nanoporous Fibers Modified Electrode for Simultaneous Determination of Lead and Cadmium.” *Sensors and Actuators, B: Chemical* (PartA): 526–34. http://dx.doi.org/10.1016/j.snb.2014.10.126.

111 Publication, Advance, Cover Page, Kankan Bhattacharyya, and Saptarshi Mukherjee. 2017. “Fluorescent Metal Nano-Clusters as Next Generation Fluorescent Probes for Cell Imaging and Drug Delivery.”

112 Qiao, Yunyun et al. 2015. “Green Synthesis of Fluorescent Copper Nanoclusters for Reversible PH-Sensors.” *Sensors and Actuators, B: Chemical* 220: 1064–69. http://dx.doi.org/10.1016/j.snb.2015.06.073.

113 Qu, Dan et al. 2013. “Highly Luminescent S, N Co-Doped Graphene Quantum Dots with Broad Visible Absorption Bands for Visible Light Photocatalysts.” *Nanoscale* 5(24): 12272–77.

114 ———. 2015. “Tailoring Color Emissions from N-Doped Graphene Quantum Dots for Bioimaging Applications.” *Light: Science & Applications* 4(12): e364–e364.

115 Raghu, Gunigollahalli Kempegowda. 2012. “Chemically Functionalized Glassy Carbon Spheres : A New Covalent Bulk Modified Composite Electrode for the Simultaneous Determination of Lead and Cadmium.” : 1953–63.

116 Rajawat, Deepak Singh, Nitin Kumar, and Soami Piara Satsangee. 2014. “Trace Determination of Cadmium in Water Using Anodic Stripping Voltammetry at a Carbon Paste Electrode Modified with Coconut Shell Powder.” *Journal of Analytical Science and Technology* 5(1): 1–8.

117 Ramachandran, Aswathi, J. S. Arya Nair, and Sandhya Karunakaran Yesodha. 2019a. “Polyaniline-Derived Nitrogen-Doped Graphene Quantum Dots for the Ultratrace Level Electrochemical Detection of Trinitrophenol and the Effective Differentiation of

Nitroaromatics: Structure Matters." *ACS Sustainable Chemistry and Engineering* 7(7): 6732–43.

118 ———. 2019b. "Polyaniline-Derived Nitrogen-Doped Graphene Quantum Dots for the Ultratrace Level Electrochemical Detection of Trinitrophenol and the Effective Differentiation of Nitroaromatics: Structure Matters." *ACS Sustainable Chemistry and Engineering* 7(7): 6732–43.

119 Ramachandran, Aswathi, Sriniwas Panda, and Sandhya Karunakaran Yesodha. 2018. "Physiological Level and Selective Electrochemical Sensing of Dopamine by a Solution Processable Graphene and Its Enhanced Sensing Property in General." *Sensors and Actuators, B: Chemical* 256: 488–97. http://dx.doi.org/10.1016/j.snb.2017.10.094.

120 Ran, Gu, Yang Li, and Ying Xia. 2020. "Graphene Oxide and Electropolymerized P-Aminobenzenesulfonic Acid Mixed Film Used as Dopamine and Serotonin Electrochemical Sensor." *Monatshefte fur Chemie* 151(3): 293–99. https://doi.org/10.1007/s00706-020-02559-9.

121 Rasdi, Fairuz Liyana Mohd, Nor Kartini Abu Bakar, and Sharifah Mohamad. 2013. "A Comparative Study of Selected Trace Element Content in Malay and Chinese Traditional Herbal Medicine (THM) Using an Inductively Coupled Plasma-Mass Spectrometer (ICP-MS)." *International Journal of Molecular Sciences* 14(2): 3078–93.

122 Razak, Meerza Abdul, Pathan Shajahan Begum, Buddolla Viswanath, and Senthilkumar Rajagopal. 2017. "Multifarious Beneficial Effect of Nonessential Amino Acid, Glycine: A Review." *Oxidative Medicine and Cellular Longevity* 2017.

123 Reddy, S. Lokeswara et al. 2020. "A Novel Electrochemical Sensor Based on Fe-Doped MgNi2O3 Nanoparticles for Simultaneous Determination of Dopamine, Uric Acid, Nicotine and Caffeine over Very Wide Linear Ranges." *Journal of Electroanalytical Chemistry* 878: 114648. https://doi.org/10.1016/j.jelechem.2020.114648.

124 Rosini, Elena et al. 2014. "Novel Biosensors Based on Optimized Glycine Oxidase." *FEBS Journal* 281(15): 3460–72.

125 Rotaru, Alexandru et al. 2010. "Selective DsDNA-Templated Formation of Copper Nanoparticles in Solution." *Angewandte Chemie - International Edition* 49(33): 5665–67.

126 Roushani, Mahmoud, Mojtaba Shamsipur, and Seied Mahdi Pourmortazavi. 2012. "Amprometric Detection of Glycine, L-Serine, and L-Alanine Using Glassy Carbon Electrode Modified by NiO Nanoparticles." *Journal of Applied Electrochemistry* 42(12): 1005–11.

127 Roy, Prathik et al. 2014. “Plant Leaf-Derived Graphene Quantum Dots and Applications for White LEDs.” *New Journal of Chemistry* 38(10): 4946–51.

128 S., Saisree, Arya Nair Arya, and Sandhya K. Y. 2022a. “A Highly Stable Copper Nano Cluster on Nitrogen-Doped Graphene Quantum Dots for the Simultaneous Electrochemical Sensing of Dopamine, Serotonin, and Nicotine: A Possible Addiction Scrutinizing Strategy.” *Journal of Materials Chemistry B* 10(21): 3974–88.

129 Saied, Sumayya, Erum Zahir, and Azhar Siddique. 2010. “Heavy Metal Levels in Commonly Used Traditional Medicinal Plants.” *Journal of the Chemical Society of Pakistan* 32(6): 737–43.

130 Saisree, J. S. Arya Nair, and K. Y. Sandhya. 2022. “A Highly Stable Copper Nano Cluster on Nitrogen-Doped Graphene Quantum Dots for the Simultaneous Electrochemical Sensing of Dopamine, Serotonin, and Nicotine: A Possible Addiction Scrutinizing Strategy.” *Journal of Materials Chemistry B* 10(21): 3974–88. http://dx.doi.org/10.1039/d1tb02368c.

131 Saisree, S., R. Aswathi, J. S. Arya Nair, and K. Y. Sandhya. 2021a. “Radical Sensitivity and Selectivity in the Electrochemical Sensing of Cadmium Ions in Water by Polyaniline-Derived Nitrogen-Doped Graphene Quantum Dots.” *New Journal of Chemistry* 45(1): 110–22.

132 ———. 2021b. “Radical Sensitivity and Selectivity in the Electrochemical Sensing of Cadmium Ions in Water by Polyaniline-Derived Nitrogen-Doped Graphene Quantum Dots.” *New Journal of Chemistry* 45(1): 110–22.

133 Saisree, S., J. S. Arya Nair, and K. Y. Sandhya. 2022. “Variant Solvothermal Synthesis of N-GQD for Colour Tuning Emissions and Naked Eye Reversible Shade Tweaking PH Sensing Ability.” *Chemical Papers* (August). https://doi.org/10.1007/s11696-022-02376-w.

134 Sayyad, Pasha W. et al. 2021. “L-Cysteine Peptide-Functionalized PEDOT-PSS/RGO Nanocomposite for Selective Electrochemical Detection of Lead Pb(II) Ions.” *Applied Physics A: Materials Science and Processing* 127(5): 1–13. https://doi.org/10.1007/s00339-021-04511-y.

135 Sebastian, Maria, and Beena Mathew. 2018. “Ion Imprinting Approach for the Fabrication of an Electrochemical Sensor and Sorbent for Lead Ions in Real Samples Using Modified Multiwalled Carbon Nanotubes.” *Journal of Materials Science* 53(5): 3557–72.

136 Shah, Afzal et al. 2019. “Development of a Highly Sensitive Electrochemical Sensing

Platform for the Trace Level Detection of Lead Ions JES F OCUS I SSUE ON 4D M ATERIALS AND S YSTEMS Development of a Highly Sensitive Electrochemical Sensing Platform for the Trace Level Detection ."

137 Sharma, R. K., M. Agrawal, and F. Marshall. 2006. "Heavy Metal Contamination in Vegetables Grown in Wastewater Irrigated Areas of Varanasi, India." *Bulletin of Environmental Contamination and Toxicology* 77(2): 312–18.

138 Shellaiah, Muthaiah et al. 2019. "Cysteamine-Capped Gold-Copper Nanoclusters for Fluorometric Determination and Imaging of Chromium(VI) and Dopamine." *Microchimica Acta* 186(12).

139 Shellaiah, Muthaiah, and Kien Wen Sun. 2017. "Luminescent Metal Nanoclusters for Potential Chemosensor Applications." *Chemosensors* 5(4).

140 Shi, Yu-e et al. 2017. "Synthesis of Ultra – Stable Copper Nanoclusters and Their Potential Application as a Reversible Thermometer." (3): 14251–55.

141 Shtepliuk, Ivan et al. 2017. "On the Interaction of Toxic Heavy Metals (Cd, Hg, Pb) with Graphene Quantum Dots and Infinite Grapheme." *Scientific Reports* 7(1): 1–17.

142 Simões, F R, and M G Xavier. 2017. Micro and Nano Technologies *Chapter 6 - Electrochemical Sensors*. Elsevier Inc. http://dx.doi.org/10.1016/B978-0-323-49780-0/00006-5.

143 Singh, Namrata et al. 2020. "Highly Stable Pyrimidine Based Luminescent Copper Nanoclusters with Superoxide Dismutase Mimetic and Nitric Oxide Releasing Activity."

144 Sohal, Neeraj, Banibrata Maity, and Soumen Basu. 2021. "Recent Advances in Heteroatom-Doped Graphene Quantum Dots for Sensing Applications." *RSC Advances* 11(41): 25586–615.

145 Su, Xuxian, and Jinbin Liu. 2017. "PH-Guided Self-Assembly of Copper Nanoclusters with Aggregation-Induced Emission." *ACS Applied Materials and Interfaces* 9(4): 3902–10.

146 Sun, Danfeng et al. 2018. "Electrodeposition Synthesis of a NiO/CNT/PEDOT Composite for Simultaneous Detection of Dopamine, Serotonin, and Tryptophan." *Sensors and Actuators, B: Chemical* 259: 433–42. http://dx.doi.org/10.1016/j.snb.2017.12.037.

147 Tao, Yu, Mingqiang Li, Jinsong Ren, and Xiaogang Qu. 2015. "Chem Soc Rev Metal Nanoclusters : Novel Probes for Diagnostic and Therapeutic Applications." : 8636–63.

148 Thukral, Kanika et al. 2014. "Synthesis and Single Crystal Growth of L-Proline Cadmium Chloride Monohydrate and Its Characterization for Higher Order Harmonic Generation

Applications.” *CrystEngComm* 16(13): 2802–9.

149 Toshima, Naoki, Yukihide Shiraishi, Toshiharu Teranishi, and Mikio Miyake. 2001. “Various Ligand-Stabilized Metal Nanoclusters as Homogeneous and Heterogeneous Catalysts in the Liquid Phase.” 5: 178–96.

150 Tůma, Petr et al. 2013. “Large-Volume Sample Stacking for in Vivo Monitoring of Trace Levels of γ-Aminobutyric Acid, Glycine and Glutamate in Microdialysates of Periaqueductal Gray Matter by Capillary Electrophoresis with Contactless Conductivity Detection.” *Journal of Chromatography A* 1303: 94–99.

151 Veeralingam, Sushmitha, and Sushmee Badhulika. 2020. “Biconcave Bi 2 WO 6 Nanoparticles for UV Light-Activated Detection of Nicotine in Human Sweat and Cigarette Samples.”

152 Vidotti, Marcio, Susana I.Córdoba de Torresi, and Lauro T. Kubota. 2008. “Electrochemical Oxidation of Glycine by Doped Nickel Hydroxide Modified Electrode.” *Sensors and Actuators, B: Chemical* 135(1): 245–49.

153 Wang, Changxing et al. 2021. “Synthesis of Multi-Color Fluorine and Nitrogen Co-Doped Graphene Quantum Dots for Use in Tetracycline Detection, Colorful Solid Fluorescent Ink, and Film.” *Journal of Colloid and Interface Science* 602: 689–98. https://doi.org/10.1016/j.jcis.2021.06.062.

154 Wang, Gang et al. 2018. “Facile and Highly Effective Synthesis of Controllable Lattice Sulfur-Doped Graphene Quantum Dots via Hydrothermal Treatment of Durian.” *ACS Applied Materials and Interfaces* 10(6): 5750–59.

155 Wang, Qianyu et al. 2021. “Electrochemical Biosensor for Glycine Detection in Biological Fluids.” *Biosensors and Bioelectronics* 182(January).

156 ———. 2022. “Intradermal Glycine Detection with a Wearable Microneedle Biosensor: The First In Vivo Assay.” *Analytical Chemistry* 94(34): 11856–64.

157 Wang, Wei et al. 2014. “One-Step Prepared Fluorescent Copper Nanoclusters for Reversible PH-Sensing.” *Analyst* 139(12): 2990–93.

158 Wang, Xiao Fei et al. 2019. “Direct White Emissive Cl-Doped Graphene Quantum Dots-Based Flexible Film as a Single Luminophore for Remote Tunable UV-WLEDs.” *Chemical Engineering Journal* 361: 773–82. https://doi.org/10.1016/j.cej.2018.12.131.

159 Wang, Yang et al. 2017. “A Metal-Organic Framework and Conducting Polymer Based Electrochemical Sensor for High Performance Cadmium Ion Detection.” *Journal of Materials Chemistry A* 5(18): 8385–93.

160 Wang, Zhenguang et al. 2016. “All-Copper Nanocluster Based Down-Conversion White Light-Emitting Devices.”

161 Wang, Zhenguang, Bingkun Chen, and Andrey L. Rogach. 2017. “Synthesis, Optical Properties and Applications of Light-Emitting Copper Nanoclusters.” *Nanoscale Horizons* 2(3): 135–46. http://dx.doi.org/10.1039/C7NH00013H.

162 Wang, Zihao et al. 2020. “Biomass-Derived Nitrogen Doped Graphene Quantum Dots with Color-Tunable Emission for Sensing, Fluorescence Ink and Multicolor Cell Imaging.” *Spectrochimica Acta - Part A: Molecular and Biomolecular Spectroscopy* 227: 117671. https://doi.org/10.1016/j.saa.2019.117671.

163 Wei, Juan et al. 2021. “Highly Sensitive and Selective Electrochemical Detection of Pb(II) in Serum via an α-Fe2O3/NiO Heterostructure: Evidence from Theoretical Calculations and Adsorption Investigation.” *Sensors and Actuators, B: Chemical* 344(February): 130295. https://doi.org/10.1016/j.snb.2021.130295.

164 Wei, Yan et al. 2012. “SnO 2/Reduced Graphene Oxide Nanocomposite for the Simultaneous Electrochemical Detection of Cadmium(II), Lead(II), Copper(II), and Mercury(II): An Interesting Favorable Mutual Interference.” *Journal of Physical Chemistry C* 116(1): 1034–41.

165 Xie, Hu Jun, Qun Fang Lei, and Wen Jun Fang. 2012. “Intermolecular Interactions between Gold Clusters and Selected Amino Acids Cysteine and Glycine: A DFT Study.” *Journal of Molecular Modeling* 18(2): 645–52.

166 Xing, Huakun et al. 2015. “SC.” *JEAC* (Ii). http://dx.doi.org/10.1016/j.jelechem.2015.11.043.

167 Xuan, Xing, and Jae Y. Park. 2018. “A Miniaturized and Flexible Cadmium and Lead Ion Detection Sensor Based on Micro-Patterned Reduced Graphene Oxide/Carbon Nanotube/Bismuth Composite Electrodes.” *Sensors and Actuators, B: Chemical* 255: 1220–27. http://dx.doi.org/10.1016/j.snb.2017.08.046.

168 Yadav, Reetu et al. 2020. “Rapid and Selective Electrochemical Detection of Pb2+ Ions Using Aptamer-Conjugated Alloy Nanoparticles.” *SN Applied Sciences* 2(12): 1–11. https://doi.org/10.1007/s42452-020-03840-6.

169 Yang, Sha et al. 2016. “Crystal Structures of Two New Gold − Copper Bimetallic Nanoclusters: Cu.” 10: 4–7.

170 Yao, Xianzhi et al. 2014. “Exploiting Differential Electrochemical Stripping Behaviors of Octahedral Fe3O4 Nanocrystals toward Heavy Metal Ions by Crystal Cutting.”

171 Yuan, Xun, Xinyue Dou, Kaiyuan Zheng, and Jianping Xie. 2015. “Recent Advances in the Synthesis and Applications of Ultrasmall Bimetallic Nanoclusters.”

172 Yukird, Jutiporn et al. 2018. “ZnO@graphene Nanocomposite Modified Electrode for Sensitive and Simultaneous Detection of Cd (II) and Pb (II).” *Synthetic Metals* 245(September): 251–59. https://doi.org/10.1016/j.synthmet.2018.09.012.

173 Zazoua, Ali et al. 2018. “Polyphenolic Natural Products for the Electrochemical Determination of Cadmium.” *Analytical Letters* 51(3): 359–70. https://doi.org/10.1080/00032719.2017.1306068.

174 Zhang, Ben Xing, Hui Gao, and Xiao Long Li. 2014. “Synthesis and Optical Properties of Nitrogen and Sulfur Co-Doped Graphene Quantum Dots.” *New Journal of Chemistry* 38(9): 4615–21.

175 Zhang, Bin et al. 2016. “Facile and Green Fabrication of Size-Controlled AuNPs/CNFs Hybrids for the Highly Sensitive Simultaneous Detection of Heavy Metal Ions.” *Electrochimica Acta* 196: 422–30. http://dx.doi.org/10.1016/j.electacta.2016.02.163.

176 Zhang, Hui et al. 2012. “Photoreductive Synthesis of Water-Soluble Fluorescent Metal Nanoclusters.” *Chemical Communications* 48(4): 567–69.

177 Zhao, Rui et al. 2020. “A Unique Bimetallic MOF Derived Carbon–MWCNTs Hybrid Structure for Selective Electrochemical Determination of Lead Ion in Aqueous Solution.” *Microchemical Journal* 158(July): 105271. https://doi.org/10.1016/j.microc.2020.105271.

178 Zhenguang Wang,a Andrei S. Susha,a Bingkun Chen,a, b Claas Reckmeier,a Ondrej Tomanec,c Radek Zboril,c Haizheng Zhong, b and Andrey L. Rogacha Accepted. 2016. “Nanoscale.” *Nanoscale* 8: 7197–7202.

179 Zhou, Jun et al. 2018. “A Galvanic Exchange Process Visualized on Single Silver Nanoparticles: Via Dark-Field Microscopy Imaging.” *Nanoscale* 10(26): 12805–12.

180 Zhou, Ying, Tianshu Zhou, Min Zhang, and Guoyue Shi. 2014. “A DNA–Scaffolded Silver Nanocluster/Cu2+ Ensemble as a Turn-on Fluorescent Probe for Histidine.” *Analyst* 139(12): 3122–26.

181 Zhou, Zhixue, Yan Du, and Shaojun Dong. 2011. “Double-Strand DNA-Templated Formation of Copper Nanoparticles as Fluorescent Probe for Label-Free Aptamer Sensor.” *Analytical Chemistry* 83(13): 5122–27.

182 Zhu, Xiaolei et al. 2017. 248 Electrochimica Acta *Alkaline Intercalation of Ti3C2 MXene for Simultaneous Electrochemical Detection of Cd(II), Pb(II), Cu(II) and Hg(II)*. Elsevier.

183 http://dx.doi.org/10.1016/j.electacta.2017.07.084.

184 Zyablov, A. N. et al. 2010. “Determination of Glycine in Aqueous Solutions Using a Molecularly Imprinted Polymer-Modified Piezosensor.” *Journal of Analytical Chemistry* 65(1): 91–93.

LIST OF PUBLICATIONS

PUBLISHED

1. Saisree S., Arya Nair J. S. and Sandhya K. Y. White Emissive Sulfur Co-Doped Polyaniline Derived Nitrogen- Graphene Quantum Dots as a Versatile Electrochemical Sensor for Toxic Heavy Metal Ions Cadmium, Lead, and Mercury, *ACS Applied Nano Materials*, (2023)
2. Saisree, S., JS Arya Nair., & Sandhya, K. Y, 'Highly Stable Copper Nano Cluster on Nitrogen-Doped Graphene Quantum Dots for the Simultaneous Electrochemical Sensing of Dopamine, Serotonin, and Nicotine; a Possible Addiction Scrutinizing Strategy'. *Journal of Materials Chemistry B,* (2022). **(Featured as Journal Front Cover)**
3. Saisree, S., Aswathi, R., JS Arya Nair., & Sandhya, K. Y, 'Radical sensitivity and selectivity in the electrochemical sensing of cadmium ions in water by polyaniline-derived nitrogen-doped graphene quantum dots'. *New Journal of Chemistry*, *45*(1), 110-122, (2021).
4. Saisree.S, JS Arya Nair, SK Yesodha,'Variant solvothermal synthesis of N-GQD for colour tuning emissions and naked eye reversible shade tweaking pH sensing ability'. *Chemical Papers, 76,* 6953–6962 (2022)
5. JS Arya Nair, Saisree.S, and SK Yesodha, 'Trace Level Detection of Pb(II) and Cd(II) aided by the MoS2 Nano flowers and Graphene Nanosheet combination and the Mechanism', *ACS Applied Engineering Materials*, 2023
6. JS Arya Nair., Ramachandran A., Sadasivakurup, S., & Yesodha, S. K, 'Versatile MoS_2 hollow nanoroses for a quick-witted removal of Hg (II), Pb (II) and Ag (I) from water and the mechanism: Affinity or Electrochemistry'? *Applied Materials Today, 20*, 100642, (2020).
7. JS Arya Nair., Saisree, S., Aswathi, R., & Sandhya, K. Y, 'Ultra-selective and real-time detection of dopamine using molybdenum disulphide decorated graphene-based electrochemical biosensor'. *Sensors and Actuators B: Chemical, 354*, 131254, (2022).

8. JS Arya Nair, Saisree.S, & SK Yesodha, 'Ultra-Rapid Removal of Pb (II) Ions by a Nano-MoS_2 Decorated Graphene Aided by the Unique Combination of Affinity and Electrochemistry'. *Advanced Sustainable Systems, 6,* 2200039, (2022)
9. JS Arya Nair, Saisree.S, SK Yesodha, 'Picomolar Level Electrochemical Detection of Hydroquinone, Catechol and Resorcinol Simultaneously Using a MoS_2 Nano-Flower Decorated Graphene attributed to the structural aspects.' *Analyst, 147,* 2966-2979, (2022)

UNDER REVIEW

1. Saisree S, Dhrishya V, Sandhya K.Y, 'Selective Electrochemical and Fluorescence Sensing of Glycine by an Ultra-stable Gold-Copper Nano Cluster on Nitrogen-Doped Graphene Quantum Dot'. *(ACS Applied Nano Materials)*

UNDER PREPARATION

1. Saisree S, Sandhya K.Y, 'Picomolar level Ultra-Selective Electrochemical sensing of Lead Ions by a Gold-Copper Nanocluster on Nitrogen-Doped Graphene Quantum Dot.'
2. Saisree S, Sandhya K.Y, 'Green synthesis of Graphene Quantum Dots from Cassia Fistula Flowers for the Selective EC sensing of Histidine.'

CONFERENCE PRESENTATIONS

ORAL PRESENTATIONS

1. International Conference on Energy and Environment "ICEE 2k19", organized by the 'Department of Chemistry, Physics and Mathematics of TKM College of Arts and Science, Kollam.
2. Materials research society of India, Trivandrum chapter annual technical meeting – SCIMST, March 7, 2020.
3. International conference on Advances in Material sciences and Chemistry (ICAMSC), 10^{th} – 12^{th} August 2020 organized by Dept. of Chemistry, Amrita Vishwa Vidyapeetham, Kochi. (**Best Oral Presentation Award**)
4. First International Online Conference on Blends, Composites, Bio-Composites and Nanocomposites (ICNC–2020) 9^{th} - 11^{th} October 2020, M.G. University, Kottayam (**Best Oral Presentation Award**)
5. International conference on Sustainable Technologies for Water Treatment and Desalination (STWTD), 8 - 10^{th} December 2020, Dept. of Chemical engineering, National Institute of Technology (NIT), Calicut
6. International Conference on Emerging Trends in Advanced Functional Materials, (ETAFM 2022), 11-12 August 2022, Postgraduate Department of Chemistry, Catholicate College, Pathanamthitta. (**Best Oral Presentation Award**)

POSTER PRESENTATIONS

1. International Conference on Energy and Environment "ICEE 2k19", organized by the 'Department of Chemistry, Physics and Mathematics of TKM College of Arts and Science, Kollam
2. National Conference on Materials Science and Technology, organized by Indian Institute of Space Science and Technology, IIST, December, 2019.
3. International Conference on Functional Materials (ICFM) 2020, January 6 - 8, 2020 organized by Indian Institute of Technology (IIT), Kharagpur.
4. National Online Quiz and Poster competition: 'Chemistry in managing Corona Virus and Chemistry Against COVID-19". Organized by Madhav Science PG college UJJAIN and IPS academy Indore catalyzed by Association of Chemistry Teachers (ACT) C/o Homi Bhabha Centre for Science Education (TIFR), 2020. **(Best Poster Presentation Award)**
5. National Conference on Materials Science and Technology, organized by Indian Institute of Space Science and Technology, IIST, December, 2021.
6. Thirty fifth Kerala Science Congress, held at Mar Baselios Christian College, Kuttikanam on 10-14 February 2023
7. National Conference on New Developments in Polymeric Materials. Organized by "The Society for Polymer Science" Thiruvananthapuram Chapter on 2-3 March 2023, Thiruvananthapuram.